Nature and geodynamics of Grenville-age orogens in Norway and Dronning Maud Land (East Antarctica) during the assembly of Rodinia: insights into the lateral terminations of the greater Grenville Orogen

Chengcheng Wang

Thesis for the degree of Philosophiae Doctor (PhD)
University of Bergen, Norway
2021

UNIVERSITY OF BERGEN

Nature and geodynamics of Grenville-age orogens in Norway and Dronning Maud Land (East Antarctica) during the assembly of Rodinia: insights into the lateral terminations of the greater Grenville Orogen

Chengcheng Wang

Thesis for the degree of Philosophiae Doctor (PhD)
at the University of Bergen

Date of defense: 14.09.2021

Year: 2021

Title: Nature and geodynamics of Grenville-age orogens in Norway and Dronning Maud Land (East Antarctica) during the assembly of Rodinia: insights into the lateral terminations of the greater Grenville Orogen

Name: Chengcheng Wang

Print: Skipnes Kommunikasjon / University of Bergen

博观而约取，厚积而薄发

——苏轼

A saying by my favorite Chinese poet and writer Su Shi (1037–1101), which means ‘to have a profound knowledge accumulation and cream off the best part as the basis before attempting to make new advances’.

Scientific environment

This dissertation was conducted in the group of Geodynamics and Basin Studies at the Department of Earth Science, University of Bergen, between January 2018 and June 2021, under the supervision of Prof. Joachim Jacobs (UiB), with co-supervision by Dr. Robert J. Thomas (Council for Geoscience, South Africa) and Dr. Bernard Bingen (Geological Survey of Norway). Geochronological and isotopic analyses were carried out at the NordSIM laboratory of the Swedish Museum of Natural History (Sweden), IBERSIMS laboratory of the University of Granada (Spain) and the University of Johannesburg (South Africa). The candidate was supported by the China Scholarship Council and received research and travel support from the faculty-specific funds and endowments of the Faculty of Mathematics and Natural Sciences, University of Bergen (No. 812378 and 814220), the Meltzer Research Fund (No. 102737111), and additional funding from the Norwegian Research School for Dynamics and Evolution of Earth and Planets (DEEP) (No. 249040/F60).

Acknowledgements

"I love to travel, but hate to arrive", said by Albert Einstein. At the end of PhD, I am grateful for so much help I have received along the way, which makes this journey rewarding and enjoyable.

It would not have been possible for me to complete the thesis without the guidance and help from my main supervisor Joachim. Thank you Joachim for providing me with this 'grand' but interesting project, for sharing your knowledge and research experience unreservedly, for always being approachable to every meeting and giving effective and helpful feedback on scientific questions and writing, for reminding me of academic rigor and frankly pointing out my mistakes, for pushing me forward to be more extroversive and social, for encouraging me when I lost my confidence and raising me up when I felt down, for taking the role also as a friend and a father who wants nothing but the best for me. I am also indebted to my co-supervisors. Bernard, thank you for joining the field work in Norway, for sharing your knowledge about the Sveconorwegian orogen and for encouraging me to open my mind to have a fair and critical thinking. Thank you Bob for correcting my writings, answering emails promptly with a detailed reply to my questions, and being so positive to introduce and propose geological questions.

I am grateful to all the co-authors for their excellent contribution to my publications. In particular, I thank Marlina Elburg for helping to analyze Lu–Hf isotopes and giving critical feedback on data interpretation and quality control, Johannes Wiest for introducing the Caledonian geology and sharing his samples and dating data, Martin Whitehouse and Heejin Jeon for their help with zircon U–Pb dating and O isotope analyses as well as data processing. I feel fortunate to have received fair and constructive comments and suggestions from a number of reviewers. A huge thanks to Nick Roberts, as I benefited a lot from his reviews on the Sveconorwegian paper and more personal communication.

To all the researchers I have connected on ResearchGate, Twitter, by email or at a conference, I appreciate their positive responses to share research findings. I thank

Graham Hagen-Peter for introducing his work on isotopic modelling and geology of the Ross Orogen (East Antarctica), Paul Macey for sharing his knowledge about the Namaqua belt, Åke Johansson for his proposal for a joint review paper and advice on processing a large dataset, Ibanez-Mejia Mauricio for providing private documents, etc. By taking part in the external courses and annual assemblies organized by the DEEP research school, I have got additional opportunities to meet more geologists and learned how to use Gplates (from Grace Shephard).

Many thanks go to the academic, technological and administrative staff at the Department of Earth Science, UiB, who created a friendly and supportive environment for my PhD work. In particular, I would like to express my gratitude to Irina Dumitru and Andreas Viken for preparing zircon mounts and thin sections, Irene Heggstad for helping with the SEM, Leif-Erik Pedersen for helping with mineral separation and LA-ICP-MS analyses. I have had many wonderful memories with my fellow students and colleagues from lunch times, GEO-talks and seminars. My special thanks go to Zhiyuan and Gang for the advice on surviving PhD and preparing future career, to Hongliang and Edose for helping with improving presentation skills, to Åse for always being enthusiastic to have a chat.

Outside of research, the happy hours spent with a group of new friends to play board games, cook, hike and travel together made my stay in Bergen memorable. A huge thanks to Sisi for many tries to get me out of sitting in front of the computer. I thank my old friends in China for their great concern for me during the Covid-19 outbreak and sending me medical supplies.

I would also like to take the opportunity to thank all the people who have helped me in the last ten years to pursue my study and career interest. I am fortunate all along the way to receive much trust and support, which made it possible for me to get the opportunity to change my major from Mechanical Design to Geology in the freshman year at the China University of Petroleum, get the examination-exemption admission to be enrolled in the University of Science and Technology of China for master studies, and then to get the funding from the China Scholarship Council to support my PhD studies. All of these are essential to make the thesis available and make what I am today.

I owe a great deal of gratitude to my parents, who raised me with considerable effort and love, created a relaxing family environment with much respect and freedom, supported me in all my pursuits, and influenced me with positive and optimistic attitudes to every challenge in life. (爸爸妈妈, 我爱你们!). Thanks to my sister for a great sense of humor, which has brought a lot of cheer and laughter. Finally, I must thank Pengfei for his enduring love and for always being there in my ups and occasional downs during the entire journey.

Abstract

The Grenville Orogeny represents a globally pervasive tectonothermal event resulting in the amalgamation of the supercontinent Rodinia between ca. 1.3 and 1.0 Ga. The Grenville Orogen appears to be a continuous collisional orogen connecting Laurentia, Amazonia, Baltica and Kalahari and is generally compared to the modern Himalaya-Alpine orogenic system. Its eastern lateral termination is seen in the Sveconorwegian orogen in Baltica, while on the extreme other end, the Namaqua–Natal–Maud orogenic system, on the periphery of the Proto-Kalahari Craton, represents the western lateral termination along the conjugate Kalahari-Laurentia margin. This study focuses on the Grenville-age orogenic history of the Maud Belt, East Antarctica, and the Sveconorwegian orogen exposed in Caledonian nappe windows, West Norway, with an aim to provide a potentially comprehensive understanding of spatial terminations of the Grenville Orogen with comparison to its modern analogues. The specific goals are (1) to figure out the tectonic evolution and develop a refined tectonic model of the Maud Belt, and thus shed light on the orogenic style of the Grenville-age orogenic system along the margin of the Proto-Kalahari Craton; (2) to determine the extent and distribution of the Sveconorwegian crust, and to test a continental collision vs. accretionary model for the formation and evolution of the Sveconorwegian orogen. These aims are addressed by conducting large-scale regional investigations on geochronology and isotopic (radiogenic and stable) compositions of magmatism and high-grade metamorphism.

It has been proposed that the formation of the Namaqua-Natal belt is related to the process of continental collision between Laurentia and the Proto-Kalahari Craton, however, the tectonics of the Maud Belt, which is located perpendicular to the Namaqua-Natal belt, were poorly understood so far. In this study, new zircon U–Pb–Hf–O isotopic data along a regional profile from western to eastern Dronning Maud Land (DML) and the comparison to the Natal belt provide new insights into the tectonic interpretation of the Maud Belt and the geodynamics of the western termination of the Grenville Orogen. Isotopic results indicate that older crustal components were involved

in the generation of Grenville-age magmas and the spatial variation of Nd–Hf isotopes indicates an increasing juvenile input from west to east, i.e. away from the interior of the craton. The Maud Belt is interpreted to have developed on the substrate of the Proto-Kalahari Craton as a long-lived continental arc, and periodic magmatic influx is attributed to the switching between advancing and retreating subduction zone systems. The Maud and Natal belts differ clearly in their subduction polarity, geochronology and spatial-temporal trend of isotopic compositions. It is thus speculated that the Namaqua-Natal to Maud Belt may represent a changed tectonic environment from arc/continent-continent collision to slightly younger continental margin orogenesis at the westernmost termination of this part of the global Grenville Orogen. The Kalahari-Laurentia collision may have caused tectonic extrusions of a number of blocks including the Coats Land block, Tasmania and the Southern Tasman Ridge, which were detached from Laurentia and subsequently joined Kalahari and Australo-Antarctica respectively during Rodinia break-up.

The Maud Belt appears to be the temporal starting point for a protracted accretionary tectonic cycle along the eastern margin of Kalahari, and Grenville-age arc magmatism probably evolved to form island arc chains (Tonian Oceanic Arc Super Terrane, TOAST) at ca. 1000–900 Ma. Subsequent to a period of quiescence during the stabilization of Rodinia between ca. 900–800 Ma, this continental margin of Kalahari was reactivated during ca. 780–630 Ma, following the break-up of Rodinia and subduction of the Mozambique Ocean, which is recorded by voluminous arc magmatism and high-grade metamorphism in central DML. The subduction process terminated when a series of terranes/blocks including Indo-Antarctica, TOAST, and Kalahari were welded together during Gondwana assembly at ca. 570–550 Ma, followed by post-collisional delamination during ca. 530–485 Ma.

The Sveconorwegian orogenic evolution remains a hot topic for debate, and the debate centers on whether the Sveconorwegian orogen represents an accretionary orogen with long-term subduction, or a continental collision orogen that can be regarded as an extension of the Grenville Orogen in Laurentia. Our study traces the Sveconorwegian records from the well-established Sveconorwegian Province in southwest Norway into basement windows underneath the Caledonian nappes, by combining zircon U–Pb

geochronology and Hf–O isotopes. Samples along a N-S trending profile reveal multiple magmatic episodes during Gothian (ca. 1650 Ma), Telemarkian (ca. 1500 Ma) and Sveconorwegian (1050–1020 Ma vs. 980–930 Ma) orogenesis as well as Sveconorwegian migmatization (1050–950 Ma). Newly documented 1050–1020 Ma magmatism and migmatization extend the Sirdal Magmatic Belt to a 300 km-long, NNW-SSE trending crustal domain, with the northern boundary corresponding with the gradual transition from Telemarkian to Gothian crust. The Hf–O isotopic patterns show that ca. 1050–950 Ma Sveconorwegian magmas are different from the typical arc magmas and Gothian-Telemarkian magmas by much less addition of juvenile material and sedimentary components, which makes the 1050–930 Ma magmatism incompatible with a long-term subduction setting. The southwest margin of Baltica was most likely transformed from a long-lived Mesoproterozoic accretionary margin into the collisional Sveconorwegian orogen by collisional interactions of Baltica with Laurentia and Amazonia in the context of Rodinia.

Based on combined geological, isotopic and paleomagnetic results from the present and previous studies, it is suggested that the Grenville Orogen probably terminated on its western end by a tectonic transition from collisional orogeny in the Namaqua-Natal belt to accretionary orogeny in the Maud Belt, and Kalahari-Laurentia collision probably caused lateral extrusions of a number of crustal terranes. On its eastern side, the Sveconorwegian Orogen most likely formed by collisional interactions of Baltica with Amazonia, and represented the extension of the Grenville Orogen into southwest Baltica.

List of publications

Paper I

Wang, C-C., Jacobs, J., Elburg, M.A., Läufer, A., Thomas, R.J., Elvevold, S., 2020. Grenville-age continental arc magmatism and crustal evolution in central Dronning Maud Land (East Antarctica): Zircon geochronological and Hf–O isotopic evidence. Gondwana Research 82, 108–127. doi: 10.1016/j.gr.2019.12.004

Paper II

Wang, C-C., Wiest, J.D., Jacobs, J., Bingen, B., Whitehouse, M.J., Elburg, M.A., Sørstrand, T.S., Mikkelsen, L., Hestnes, Å., 2021. Tracing the Sveconorwegian orogen into the Caledonides of West Norway: geochronological and isotopic studies on magmatism and migmatization. Accepted for publication, Precambrian Research, 106301.

Paper III

Jacobs, J., Mikhalsky, E., Henjes-Kunst, F., Läufer, A., Thomas, R.J., Elburg, M.A., **Wang, C-C.**, Estrada, S., Skublov, S., 2020. Neoproterozoic geodynamic evolution of easternmost Kalahari: Constraints from U-Pb-Hf-O zircon, Sm-Nd isotope and geochemical data from the Schirmacher Oasis, East Antarctica. Precambrian Research 342, 105553. doi: 10.1016/j.precamres.2019.105553

Paper IV

Wang, C-C., Jacobs, J., Elburg, M.A., Läufer, A., Elvevold, S., 2020. Late Neoproterozoic–Cambrian magmatism in Dronning Maud Land (East Antarctica): U–Pb zircon geochronology, isotope geochemistry and implications for Gondwana assembly. Precambrian Research 350, 105880. doi: 10.1016/j.precamres.2020.105880

Contents

1 Introduction

1.1 Collisional vs. accretionary orogenic system and lateral terminations

The present is (probably) the key to the past.

Orogenic belts provide a long-term geological archive of continental assembly, crustal growth and recycling during supercontinent assembly and break-up (Windley, 1992; Collins, 2002; Cawood et al., 2009, 2016). The understanding of orogenesis during the history of plate tectonics largely builds on the features and processes of modern orogens, as the margins of the Pacific Ocean and the Alpine–Himalayan orogenic system clearly mark two very different orogenic styles, i.e. accretionary (exterior) and collisional (interior) orogens (Murphy and Nance, 1991; Cawood et al., 2009, 2016). Accretionary orogens form in an environment with continuing subduction of oceanic lithosphere and accretion, while collision orogens mark the end of a cycle of ocean opening and closure (Wilson Cycle) and record the termination of subduction (Cawood et al., 2009). During a supercontinent cycle, final supercontinent assembly is recorded by collisional belts that could have formed during multiple continental collisions, which are usually preceded by subduction-accretion processes with the formation of continental arcs and island arcs during the closure of ocean basins, while break-up of a supercontinent is generally associated with the development of exterior accretionary orogens (Cawood et al., 2016). The evolution and growth of orogens can for example be represented by the temperature-magnitude (T-M) diagram, in which orogens are classified after their T-M relationship (Beaumont et al., 2006, 2010). The evolution of orogens can be represented by the evolution array defined by two fundamental end members, small cold and large hot orogens. In this context, small cold orogens can be small accretionary wedges and collision orogens, which generally lack the levels of crustal thickening and associated thermal relaxation necessary to achieve high temperatures. In contrast, (super)giant hot orogens, with the collisional Grenville and Himalaya-Tibet orogens as two archetypal examples, are characterized by long-duration high thermal influx due to the development of substantial orogenic plateaus and subsequent gravitationally driven channel flows (Beaumont et al., 2006, 2010).

Orogenic evolution during continuous continental convergence usually involves the

development of large, lithosphere-scale, strike-slip fault systems with associated basins and exhumed crystalline massifs, which commonly facilitates orogen-parallel transport of continental material. This is referred to as lateral extrusion (Molnar and Tapponier, 1975), which describes the processes of tectonic escape that crustal blocks move from the collisional site to lateral margins and orogen collapse due to crustal thickening (Tapponnier et al., 1982, 1986; Ratschbacher et al., 1991a, b). These processes are especially common when a relatively stiff plate moves as an indenter to impinge on a weaker and larger continent. Indenter tectonics and lateral extrusions have been widely documented in Phanerozoic orogenic belts particularly in the Himalaya-Alpine system (Fig. 1a), where crustal blocks extruded along conjugate strike-slip faults that were orthogonal to or were oriented at a high angle to the convergence direction. The Himalaya-Tibetan Plateau, the Eastern Alps, and the Anatolian Plateau in eastern Mediterranean, are examples of this process (Fig. 1a). Collision between the Indian (indenter) and Eurasian continents resulted in major deformation of the Eurasian crust, leading to >700 km of southward extrusion of the Indochina Peninsula along the Ailaoshan–Red River shear zone (Fig. 1b; Tapponnier et al., 1982; Searle, 2006). This process also moved south China hundreds of kilometers to the east (Fig. 1b; Tapponnier et al., 1982). In the Mediterranean region, the convergence between the Arabian and Eurasian–Anatolian plates produced westward extrusion of the Anatolian plate towards the Hellenic subduction zone, and northward indentation of the Eastern Alps lithosphere by the Adriatic microplate has driven the extrusion in the Eastern Alps (Fig. 1c, d; Ratschbacher et al., 1991a, b; Schattner, 2010).

As shown in the classical extrusion model proposed by Ratschbacher et al (1991), a weak lateral boundary is required for the establishment of lateral extrusion. A subduction zone and especially subduction retreat is one of the plate tectonic processes providing such a weak lateral boundary for the movement of crustal material. Within the Himalaya-Alpine system, indenter tectonics and continental convergence that caused lateral extrusions are generally accompanied by the development of subduction systems (Fig.1). Processes of continental collision in Himalaya-Tibet are synchronous with subduction retreat/roll-back of the Pacific and Sunda slabs (Fig. 1b). In the Mediterranean region, the western extrusion of the Anatolian plate and the eastern

extrusion of Eastern Alps are closely associated with the Hellenic arc system and the subduction of the Carpathian slab respectively (Fig. 1c, d). Thus, lateral extrusion with associated tectonic escape and orogen collapse is widely considered as a result of the combined effects of collision and subduction processes (e.g., Ratschbacher et al., 1991a; Sperner et al., 2002; Schellart et al., 2019).

Lateral extrusion act as a common plate tectonic process during continental collision, and Himalaya-style escape tectonics have been recognized in a number of ancient orogens, such as the East African-Antarctic Orogen (Jacobs and Thomas, 2004) and the Caledonides-Appalachian orogen (Burke and Sengör, 1986). The development of extruding blocks is associated with crustal thinning and basin formation in the indented plate, which generally has a weaker lithosphere in comparison to the indenting plate, and the displaced extruded blocks are more prone to break off and detach from the parental plate during subsequent continental break-up. These displaced crustal blocks thus have a good potential to be used as piercing points in plate reconstructions. To identify escaped blocks in ancient orogens is important to restore their paleogeographic positions and thus reconstruct their former place in preceding supercontinents.

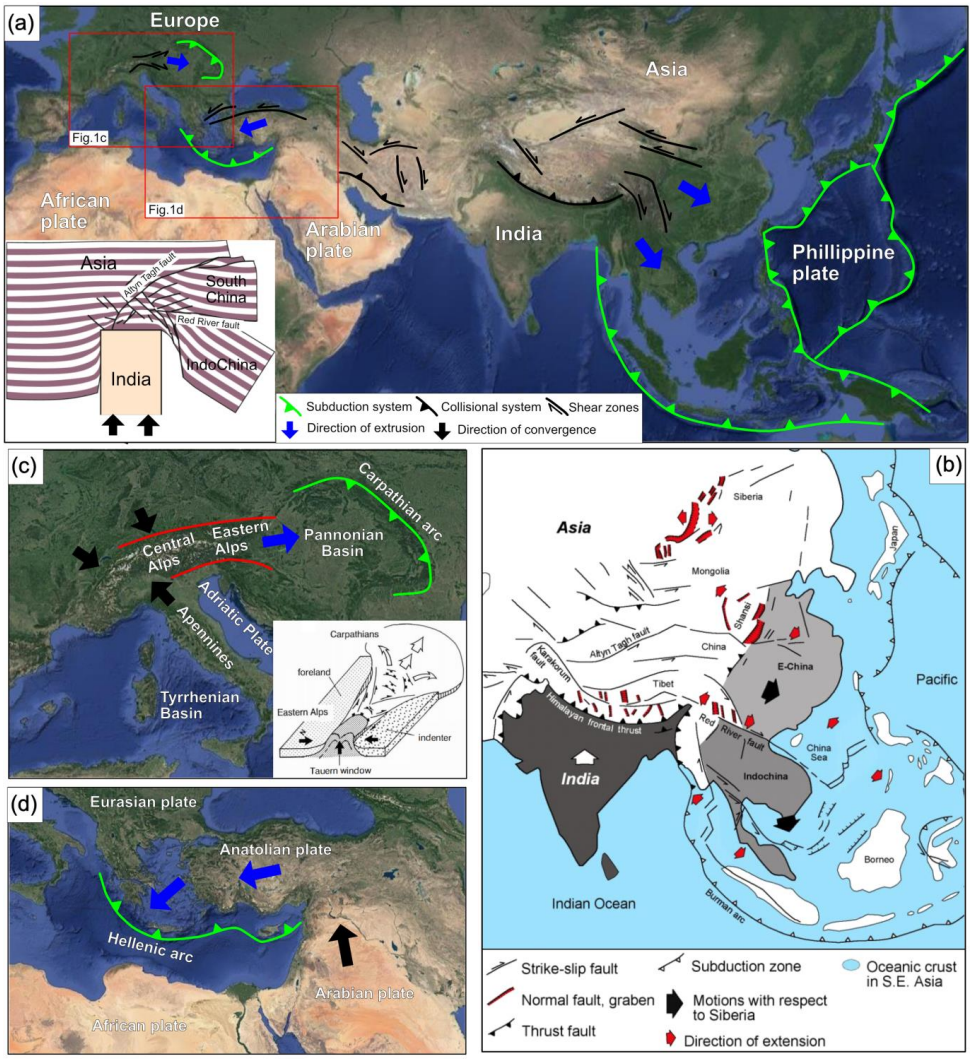

Fig. 1: (a) Google map showing the regions that are affected by lateral extrusion in the Himalaya-Alpine system. The bottom inset shows the simplified indenter and extrusions in Himalaya (modified from Tapponier et al., 1986, in Fossen 2016). The red boxes outline the areas shown in Fig.1c and d; (b) Sketch map of India-Asia collision causing lateral extrusions of South China and Indochina; (c-d) Google maps of the Alps-Apennines and Anatolian regions respectively, showing the directions of the main collision, extrusion and subduction. The inset in Fig. 1c shows the simplified extrusions in the Eastern Alps (from Ratschbacher et al., 1991b)

1.2 Rodinia reconstructions and Grenville orogeny

The supercontinent Rodinia was assembled through a series of accretionary and collisional events during ca. 1250–950 Ma, and broke apart at around ca. 800–700 Ma to form the next 'half-supercontinent' Gondwana. It has been thirty years since the supercontinent model of Rodinia was firstly proposed in the early 1990s, by integrating a large set of geological and paleomagnetic data (Dalziel, 1991; Hoffman, 1991; Moores, 1991). Early reconstructions of Rodinia largely inherited the configuration of Gondwana, which placed Laurentia in the center with East Gondwana (Australia, India, East Antarctica) to the west and Baltica and Amazonia in the eastern part of Rodinia (Fig. 2b). Specifically, East Antarctica was so far regarded as a united landmass and its east coast (Transantarctic Mountains) along with the east coast of Australia was matched with the west coast of Laurentia (present coordinates), called SWEAT (Southwest U.S.–East Antarctica) configuration (Fig. 2c, Moores, 1991). Alternatively, only the eastern margin of Australia was placed against southwestern Laurentia whereas East Antarctica was facing towards the ocean in the so-called AUSWUS fit – Australia–Western United States (Fig. 2d, Burrett and Berry, 2000). A similar reconstruction placed northwest Australia adjacent to southern Laurentia in Mexico (AUSMEX, Australia – Mexico) (Wingate et al., 2002). However, these models have been disproved later as significant geological mismatches exist between the eastern margin of East Gondwana and the western margin of Laurentia and some of the connections are not supported by paleomagnetic data (e.g. Li et al., 2008). Particularly, it has been realized that East Antarctica was not a united craton during the construction of Rodinia, instead, it is composed of a collage of different terranes with geological affinities to India, Australia and Kalahari (Fitzsimons, 2000a, b; Harley, 2003). In subsequent Rodinia reconstructions (Pisarevsky et al., 2003; Li et al., 2008; Merdith et al., 2017), East Gondwana and Kalahari were divided into Indo-Antarctic, Australo-Antarctic and Afro-Antarctic (Kalahari-Dronning Maud Land) parts (Fig. 2e-g). Baltica, Amazonia, Kalahari-Dronning Maud Land (DML) and Rio de la Plata were placed to the south of Laurentia, while Australo-Antarctica was restored adjacent to the west of Laurentia. Four continental blocks, Laurentia, Amazonia, Baltica and Kalahari,

were considered to have constituted the core of the supercontinent Rodinia (Martin et al., 2020) (Fig. 2f, g). Other cratons/plates such as West Africa, Congo, São Francisco and Indo-Antarctica were positioned at the periphery of, or isolated from the supercontinent.

The amalgamation of Rodinia is recorded in a series of orogenic belts of which the Grenville Orogen in SE Laurentia (present co-ordinates) is considered as a key collisional feature (Fig. 2a, e.g. Rivers, 2015). The Grenville Orogen represents a large hot orogen, which resulted from protracted collisional interaction between Laurentia and Amazonia during ca. 1080–980 Ma (Ottawan-Rigolet phases). The long-term continental collision resulted in large volumes of anorthosite–mangerite–charnockite–granite magmatism and granulite-facies metamorphism (e.g. Indares, 2020). The major exposed part of the Grenville Orogen occurs in eastern North America (the Grenville Province in eastern Canada), as well as in a series of smaller fragments preserved as inliers in the Appalachian orogen. These Grenville inliers show both Laurentian and Amazonian affinities in terms of Pb isotopic compositions, which thus provides direct evidence for Laurentia-Amazonia collision with the Sunsas orogen in Amazonia considered as the collisional counterpart of the Grenville Orogen (Tohver et al., 2004; Martin et al., 2020). The Grenville Orogen extends westwards to the southwest US with main exposures in the Llano Uplift in Taxas, but the main continental collision there is interpreted to have happened at ca. 1150–1120 Ma, prior to the emplacement of voluminous granites during 1120–1070 Ma (Mosher et al., 2008). The Grenville Orogen is commonly compared to the Himalayan-Tibetan system in their broad width of oceanic plateaus and a protracted history of high-grade metamorphism and partial melting (Hynes and Rivers, 2010; Indares, 2020). Besides, they also show many similarities in tectonic architecture with coeval development of large thrust systems and detachment faults above, which has led to the upward tectonic exhumation of high-grade metamorphic rocks (Hynes and Rivers, 2010). Prior to continental collision, SE Laurentia was characterized by extensive anorthosite–mangerite–charnockite–granite (AMCG) magmatism during ca. 1250–1140 Ma (Elzevirian and Shawinigan phases), and traditional views interpreted the AMCG magmatism and the major collisional period of ca. 1080–980 Ma to represent the Grenville orogenic cycle (McLelland et al.,

1996), following subduction polarity reversal (from inboard- to outboard-dipping) during ca. 1250–1220 Ma (Hynes and Rivers, 2010). Thus, the term ‘Grenville-age’ in the thesis broadly refers to the orogenic events that happened during ca. 1250–950 Ma.

Multiple paleomagnetic and geological evidence indicates that the four core constituents of Rodinia had been in place and actively involved in collisional orogenesis by ca. 1100–1050 Ma (e.g. Li et al., 2008; Merdith et al., 2017), and the collisional processes were recorded by the Grenville Orogen, the Namaqua-Natal belt in Kalahari, the Sunsas and Putumayo orogens in Amazonia and the Sveconorwegian orogen in Baltica. In contrast, Grenville-age belts in cratons/continental blocks that were placed outboard or at the periphery of Rodinia, such as the South Irumide Belt in Congo-São Francisco Craton, the Rayner/Eastern Ghats complex in India, the Jiangnan Orogen in South China, and the Valhalla Orogen in northeast Laurentia etc., are mostly younger accretionary orogens formed during ca. 1050–850 Ma (Johnson et al., 2006, 2007; Cawood et al., 2016; Yao et al., 2019).

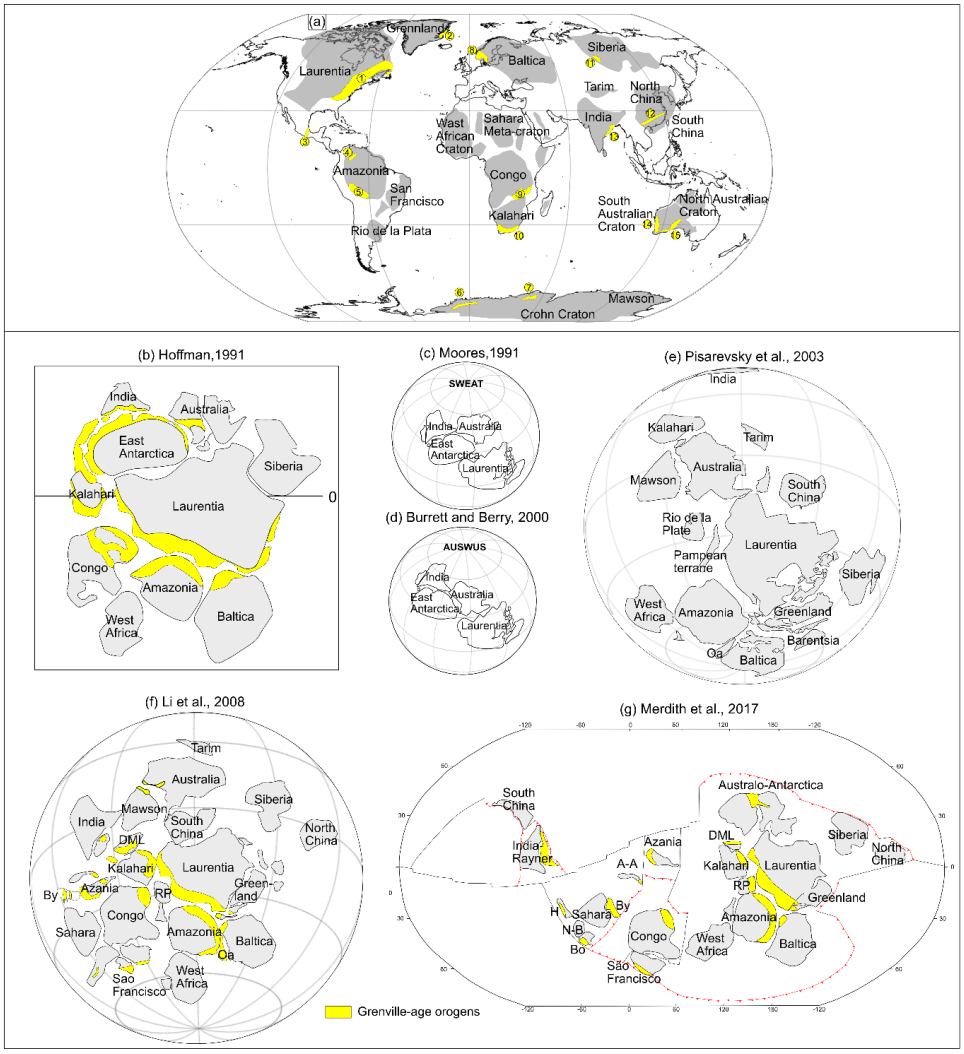

Fig. 2: (a) Current world map with main cratons and Grenville-age orogens in Rodinia (modified after Liu et al., 2019) (1, Grenville Orogen; 2, Valhalla Orogen; 3, Oaxaquia; 4, Putumayo orogen; 5, Sunsas orogen; 6, Maud Belt; 7, Rayner Belt; 8, Sveconorwegian orogen; 9, Irumide and Southern Irumide belts; 10, Namaqua-Natal belt; 11, Yenesei Ridge; 12, Jiangnan orogen; 13, Eastern Ghats; 14, Pinjarra Orogen; 15, Albany-Fraser Belt); (b-g) Various paleogeographic reconstructions of supercontinent Rodinia with Grenville-age orogens marked. A-A, Afif-Abas Terrane; Bo, Borborema; By, Bayuda; DML, Dronning Maud Land; H, Hoggar; N-B, Nigeria-Benin; Oa, Oaxaquia; RP, Rio de la Plata.

1.3 Mesoproterozoic reconstructions of the core constituents of Rodinia

It has been proposed that supercontinents mainly form by two end member mechanisms: extroversion and introversion (Murphy and Nance, 2003, 2013; Murphy et al., 2009). During extroversion, oceanic lithosphere formed and subducted surrounding the predecessor supercontinent and these subduction systems were transformed into internal collisional orogens in the subsequent supercontinent. Introversion on the other hand indicates that the formation and spreading of the oceanic lithosphere mainly occurred in the interior of the supercontinent and the formation of the successor supercontinent resulted from the closure of this interior ocean. The transition from Rodinia to Gondwana (and Pangea) is considered as a well-established example of supercontinent extroversion (e.g. Murphy and Nance, 2003; Li et al., 2019). The break-up of Rodinia was characterized by turning its outside-in (or 'inside-out'), during which Rodinia dispersed into various continental fragments and then its exterior oceans and subduction systems were transformed into the internal collisional belts of Gondwana (Hoffman, 1991; Murphy and Nance, 2005; Li et al., 2008). In contrast, the supercontinent cycle from Columbia/Nuna (hereafter Columbia) to Rodinia featured an incomplete break-up of Columbia and a much less dramatic modification in plate configurations (Evans and Mitchell, 2011; Roberts, 2013). Thus, compared with the assembly of Pangea, which involved nearly all continents on the Earth with the formation of a number of Pan-African/Brasiliano and Caledonian orogens, the Rodinia amalgamation would have probably involved fewer continental blocks into continental collision and produced less collisional orogens (Li et al., 2019). As noted above, the remnants of collisional orogens associated with the amalgamation of Rodinia were mainly preserved in the core of Rodinia, which was defined by the Laurentia–Baltica–Amazonia–Kalahari connection.

Although it has been discussed that the transition from Columbia to Rodinia was mainly achieved by opening and closing of the interior oceans (e.g. Li et al., 2019), southern Columbia developed an exterior accretionary margin that turned into collisional orogens in Rodinia. The configuration and connection of Laurentia, Baltica and Amazonia in Rodinia was transformed from their close juxtaposition in Columbia.

Laurentia and Baltica had a long-lasting juxtaposition (Fig. 3a, i.e. NENA, Northern Europe - North America; Gower et al., 1990) from ca. 1800 Ma to ca. 1250 Ma, which has been well established by paleomagnetic data and their comparable records of Paleo-Mesoproterozoic geological events (Condie, 2013; Pisarevsky et al., 2014). Moreover, the connection of Amazonia with Laurentia-Baltica during this time interval was also proposed (SAMBA, South America-Baltica-West Africa, Johansson, 2009) and agreed by most Paleoproterozoic reconstructions, although there exist different interpretations of paleomagnetic data, which placed Amazonia at a distant position from the mainland of Columbia (Fig.3a, Pisarevsky et al., 2014). The southeastern margin of Laurentia (present coordinates hereafter), the southwest margin of Baltica and the northern margin of Amazonia developed as a large accretionary margin associated with the inboard subduction of the ocean exterior to Columbia (Condie, 2013; Roberts, 2013). During the transition from Columbia to Rodinia, Baltica and Amzonia rotated clockwise relative to Laurentia (Evans, 2013; Cawood and Pisarevsky, 2017), resulting in the closure of the exterior ocean and this accretionary margin was turned 'outside in' and transformed into Grenville-age continental collision along the Grenville/ Sveconorwegian/Sunsas belts (Fig.3, Martin et al., 2020).

In contrast to Laurentia, Baltica and Amazonia that were interpreted as the core constituents of Columbia in most reconstructions, the position of the Proto-Kalahari Craton in Columbia is poorly constrained due to a lack of well-defined paleomagnetic data (e.g. de Kock et al., 2019). In Columbia reconstructions, it is either placed in a position isolated from Columbia or along the distant supercontinent's periphery (Fig.3a, e.g. Pesonen et al., 2012; Pisarevsky et al., 2014; Pehrsson et al., 2016). However, paleomagnetic data show that from Columbia break-up to Rodinia assembly, the Proto-Kalahari Craton travelled northwards from a high latitude at ca. 1350 Ma until arriving at an equatorial position at ca. 1110 Ma (de Kock et al., 2019). During this time interval, the Kalahari margin along the Namaqua-Natal side witnessed multiple periods of arc/back-arc magmatic activities and accretion of oceanic arcs. Thus, in contrast to Laurentia, Baltica and Amazonia with a long-term juxtaposition from Columbia to Rodinia, the Proto-Kalahari Craton appears as an exotic continental block that was incorporated into this 'family' during the amalgamation of Rodinia (Fig. 3b). It finally

collided with Laurentia along the Namaqua-Natal margin after rapid southward drift of Laurentia at ca. 1110–1080 Ma (Loewy et al., 2011; Swanson-Hysell et al., 2015, 2019).

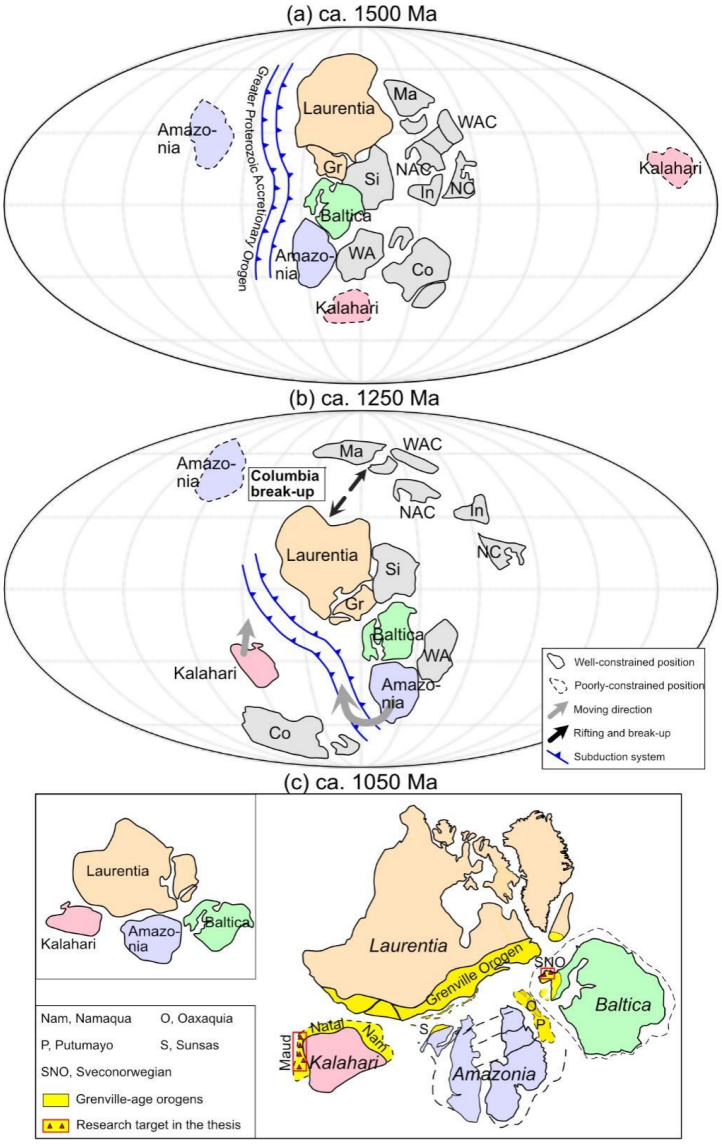

Fig. 3: Tectonic geography at (a) 1500 Ma and (b) 1250 Ma showing the configuration of Columbia supercontinent and its limited break-up respectively (modified from Li et al., 2019). In Columbia, Laurentia, Amazonia and Baltica had a close proximity and they experienced (regional) extroversion during and after Columbia break-up, while Kalahari originated from a

distant position. The Greater Proterozoic Accretionary Orogen was transformed into the collisional Grenville Orogen from Columbia to Rodinia. (c) shows the configuration of four core constituents in Rodinia with Grenville-age orogens and researched areas in this study marked. Co, Congo-São Francisco; Gr, Greenland; In, India; Ma, Mawson; NAC, North Australian Craton; NC, North China; Si, Siberia; WA, West Africa; WAC, West Australia.

1.4 Research aims and methods

As introduced above, Kalahari and Baltica preserve an extensive Grenville-age geological record that is related to a long-lived accretionary and collisional orogenesis during Rodinia assembly. It has been established that Kalahari and Baltica were actively involved in processes of continental collision, and associated orogens may represent the orogenic relics of the Grenville Orogen and its terminations. Modern collisional orogens often feature tectonic escape where crust is translated around the motion of an indenter. However, this has not been discussed in detail in the literature for one of the largest collisional orogens in Precambrian times, the Grenville Orogen. The availability to Grenville-age rocks along the margins of the Proto-Kalahari Craton and Baltica provides a good opportunity to examine, compare and link their orogenic history during Rodinia assembly, and further to explore the signatures and mechanisms of the spatial terminations of the Grenville orogenic system. Under the broad research topic, this study focuses on understanding the Grenville-age orogenic history of the Maud Belt in East Antarctica, and the Sveconorwegian orogen exposed in the Caledonian nappe windows of West Norway (Fig. 3c). The specific aims are:

(1) Western termination: to figure out the tectonic evolution and develop a refined tectonic model of the Maud Belt, and compare it with the Natal Belt, and thus shed light on the orogenic style of the Grenville-age orogenic system along the margin of the Proto-Kalahari Craton;

(2) Eastern termination: to determine the extent and distribution of the Sveconorwegian crust in the basement windows under the Caledonian nappes, and test continental collision vs. accretionary models for the formation and evolution of the Sveconorwegian orogen.

The DML region was largely reworked during the late Neoproterozoic to Cambrian (Pan-African) orogeny associated with Rodinia break-up and Gondwana assembly. A

detailed investigation on the Pan-African magmatic and metamorphic events across western to eastern DML allow for a better understanding of a long-lived evolution of the Kalahari margin during closure of the Mozambique Ocean and subsequent continental collision, which has been included as an additional research task of the thesis beyond the scope of Grenville-age orogeny.

The topic of this study involves orogenic evolution and supercontinent reconstructions, and a comprehensive understanding obviously relies on the results from various analytical methods. This study primarily builds on large-scale regional investigations on geochronology and isotopic (radiogenic and stable) compositions of magmatic rocks, mainly combining zircon U–Pb geochronology, Lu–Hf and O isotopes. Zircon is a common and refractory accessory mineral of continental rocks and contains a wealth of temporal (U–Pb) and isotopic (Lu–Hf, O) information about the magma from which it crystallized. Zircon Lu–Hf and O isotopic analyses are well established to identify the juvenile and reworked components in magmatic systems, and thus have been widely used in studies of magma petrogenesis and source composition. The Hf isotopic signature reflects the relative contributions of depleted mantle and recycled continental crust, which have different Lu/Hf ratios and thereby develop distinct $^{176}Hf/^{177}Hf$ ratios over time. The O isotopic composition of zircons crystallized from mantle and mantle-derived magmas is assumed to be uniform (5.3 ± 0.6‰, 2σ, Valley, 2003), and a positive deviation of $\delta^{18}O$ values from this benchmark is interpreted to be caused by contamination by supracrustal material, which tends to have enriched heavy O isotope values. The most pertinent use of zircon Hf–O isotopes is when they are combined with U–Pb geochronology, and are ideally measured from the same growth zone of zircons with concordat ages. In this way, combined zircon U–Pb–Hf–O isotopic analyses are able to provide reliable information on crystallization time and origin of their host rocks. The general analyzing sequence is that U–Pb isotopes are firstly measured with SHRIMP or Camaca SIMS since they require a relative smaller beam spot and shallower ablation depth than LA-ICP-MS, and then O isotopes are analyzed with SHRIMP/SIMS on those spots with high-quality U–Pb data that yield concordant ages, and Lu–Hf isotopic analyses are finally conducted with MC-LA-ICP-MS.

In regional geological studies, combined U–Pb–Hf–O isotopes are effectively used to show long-term isotopic changes through time on the one hand, which can be associated with the switch of tectonic settings. On the other hand, systematic changes in the isotopic signatures could also be related to the locations, such as from an outboard to inboard position in a subduction-related setting, then it could provide valuable information of spatial variations in crustal architecture and geological history. As such, through geochronological and isotopic investigations along large profiles, this study pays attention to not only general isotopic information of the analyzed samples, but also their temporal and spatial variation of isotopic compositions. Regional investigations on magmatism have been combined with associated metamorphic information, including the new and compiled metamorphic and anatectic ages. In addition, published paleomagnetic interpretations are used when discussing paleogeographic reconstructions.

1.5 Thesis structure and summary of the scientific papers

This dissertation is article-based and the main body consists of four published papers (Paper II is to be published). The first two research aims, which are closely related to the research topic of the thesis, are addressed by the first two papers listed below, while the latter two papers are extensional studies on the Kalahari margin during Rodinia break-up and Gondwana assembly. A summary of the publications and their relevance to the overall research aims of this study are as follows:

Wang, C-C., Jacobs, J., Elburg, M.A., Läufer, A., Thomas, R.J., Elvevold, S., 2020. Grenville-age continental arc magmatism and crustal evolution in central Dronning Maud Land (East Antarctica): Zircon geochronological and Hf–O isotopic evidence. Gondwana Research 82, 108–127.

The goal of this paper is to better understand the orogenic evolution and geodynamic setting of Maud Belt in the context of the wide development of Grenville-age orogens along the margin of Proto-Kalahari Craton during Rodinia assembly. The paper presents, for the first time, an integrated zircon U–Pb–Hf–O isotopic data of the mafic and granitic basement rocks across the central DML. Based on these new and published data, this paper compiles magmatic ages and radioactive Hf–Nd isotopic data from various parts of the Maud Belt, discusses spatial variation in geochronology and

isotopic signatures from the west to east (away from the interior of the craton), and shows that the Maud Belt differs from the Natal Belt in age spectra of Grenville-age thermal events, isotopic compositions and subduction polarity. It is concluded that the formation and evolution of the Maud Belt is different from that of the Natal Belt. The former developed on a long-time active continental margin of the Proto-Kalahari Craton, while the latter witnessed accretion of island arcs and subsequent continental convergence (collision). The Maud and Natal belts thus mark a significant geodynamic transition along the margin of the Proto-Kalahari Carton during Rodinia assembly.

Wang, C-C., Wiest, J.D., Jacobs, J., Bingen, B., Whitehouse, M.J., Elburg, M.A., Sørstrand, T. S., Mikkelsen, L., Hestnes, Å., 2021. Tracing the Sveconorwegian orogen into the Caledonides of West Norway: geochronological and isotopic studies on magmatism and migmatization. Accepted, Precambrian Research, 106301.

This paper explores the Precambrian crustal composition and evolution along a north-south trending profile from the well-defined Sveconorwegian Province to the Scandinavian Caledonides in West Norway by conducting an integrated investigation of field relationships, zircon U–Pb geochronology and Hf–O isotopic studies. This study shows that the region is composed of early Mesoproterozoic (Gothian and Telemarkian) and Grenville-age crust (Sveconorwegian), and correlates the newly discovered Sveconorwegian rocks to the Sveconorwegian crust in SW Norway, and provides the northern limit of the region affected by Sveconorwegian magmatism, high-grade metamorphism and migmatisation. The ca. 1050–930 Ma granitic and mafic magmas differ from typical arc magmas in their Hf–O isotopic pattern, reflecting much less involvement of juvenile material and sedimentary components in magma genesis, which makes the Sveconorwegian magmatism incompatible with a long-term subduction setting. A long-term crustal growth and evolution from Paleo- to Neoproterozoic times along the western margin of Baltica is discussed based on compiled zircon Hf–O isotopic data. These data support the interpretation that the southwest margin of Baltica evolved as a long-lived active continental margin in Paleo-Mesoproterozoic times and subsequently experienced continental collision during Rodinia assembly.

Jacobs, J., Mikhalsky, E., Henjes-Kunst, F., Läufer, A., Thomas, R.J., Elburg, M.A., Wang, C-C., Estrada, S., Skublov, S., 2020. Neoproterozoic geodynamic evolution of easternmost Kalahari: Constraints from U-Pb-Hf-O zircon, Sm-Nd isotope and geochemical data from the Schirmacher Oasis, East Antarctica. Precambrian Research 342, 105553.

This paper focuses on the Schirmacher Oasis region located close to the DML coastline, which is mainly composed of 780–750 Ma and ca. 630 Ma granitic rocks. Although limitedly exposed, the aerogeophysical data show that this region probably represents a significant tectonic province on the edge of Kalahari. This paper presents new, combined zircon U–Pb–Hf–O and whole-rock Nd isotopic data as well as whole-rock geochemical data, which contribute to a better understanding of the tectonic setting in late Neoproterozoic times. The relatively juvenile Hf–Nd isotopic compositions, addition of sedimentary material revealed by highly elevated O isotopes and arc-like whole-rock geochemistry are consistent with rocks that formed under a subduction-related environment. Thus, the eastern Kalahari margin in the late Neoproterozoic was interpreted as an Andean-style continental arc, which was re-activated after a period of relative tectonic quiescence of the Kalahari margin during ca. 900–800 Ma.

Wang, C-C., Jacobs, J., Elburg, M.A., Läufer, A., Elvevold, S., 2020. Late Neoproterozoic–Cambrian magmatism in Dronning Maud Land (East Antarctica): U–Pb zircon geochronology, isotope geochemistry and implications for Gondwana assembly. Precambrian Research 350, 105880.

This study traces source variations of the late Neoproterozoic–Cambrian (650–485 Ma) igneous rocks from western-central to eastern DML, by combining multiple-proxy isotopic methods including zircon Hf–O and whole-rock Sm–Nd isotopes with whole-rock geochemistry. The spatial-temporal variations in source compositions are related to crustal composition and tectonic evolution during Gondwana assembly. Spatially distinctly different isotopic compositions between western-central DML and eastern DML reflect that they are composed of different Precambrian basement, i.e. the continental crust along the Kalahari margin and the Tonian Oceanic Arc Super Terrane (TOAST). Temporally, isotopic signatures varied from relatively juvenile to significantly evolved from Ediacaran to Cambrian times, which is interpreted to have marked a change from subduction-related to a collisional setting. These results,

combined with the compiled geochronology information of regional high-grade metamorphism, provide important implications for the timing and amalgamation processes of discrete cratons/crustal blocks (Kahahari, TOAST and Indo-Antarctica) during Gondwana assembly.

2. Synthesis and outlook

2.1 Crustal evolution and orogenic style indicated by zircon Hf–O isotopes

Zircon Lu–Hf isotopic system is able to identify the relative proportion of mantle and crustal inputs to magma systems, and, when coupled with U–Pb geochronology, it is a powerful and widely used approach for understanding crustal growth and evolution at a regional and global scale. In the recent decade, much research has focused on the topic to investigate secular Hf isotopic patterns in different orogenic systems (external vs. internal, accretionary vs. collisional), which provides a better understanding of crustal growth and recycling under subduction- and collision-related compressional and extensional settings. For instance, Collins et al. (2011) evaluated global Phanerozoic Hf evolution patterns and demonstrated that external orogenic systems (i.e. circum-Pacific margin) were characterized by a Hf isotopic evolution towards more radiogenic through geological time, due to a progressive removal of the ancient lower crust and lithospheric mantle during subduction processes. In contrast, internal orogenic systems, as represented by the Alpine–Himalayan orogenic chain, differ from exterior accretionary orogens by significantly more reworked continental crust with variable Hf signatures. The correlation between juvenile Hf isotopes and accretionary orogens/evolved Hf isotopes and collisional systems is also supported by the Hf isotopic patterns of a global database. The distribution of a global zircon isotope data within εHf(t)-time space show significant troughs during supercontinent assembly, during which a series of continent–continent collision orogens formed, while more juvenile Hf isotopes are seen in supercontinent intervals, which witnessed more accretionary processes (e.g., Roberts, 2012; Gardiner et al., 2016). However, Condie and Aster (2013) suggested that external and internal orogens produced both juvenile and reworked components with similar proportions, as a global dataset shows that these

two types of orogens have similar Nd and Hf isotopic variation patterns. But a greater proportion of juvenile crust was produced during retreating than during advancing subduction. Spencer et al. (2019) made an effort to differentiate Hf isotopic evolution in collisional and accretionary orogens by comparing Hf-time arrays of the Grenville, Sveconorwegian, and Valhalla orogens. The Grenville Orogen yields a lower Lu/Hf ratio than the other two orogens implying that crustal reworking played a dominant role during continental collision while subduction-accretion processes witnessed more juvenile inputs. Overall, these studies indicate that the Hf isotopic trend towards more enriched compositions can be linked to a compressional setting, like continental collision or advancing subduction, while the variation towards more radiogenic Hf isotopic composition most likely happens under an extensional setting like arc-type settings especially associated with retreating subduction.

Coupled analysis of O and Hf isotopes has been proposed as an effective way to identify whether the magma was contaminated by supracrustal material, which generally have highly elevated $\delta^{18}O$ values than common igneous rocks and mantle-derived magmas (Valley et al., 2005). The combined Hf–O isotopes in the study of magma petrogenesis was first used by Hawkesworth and Kemp (2006) and Kemp et al. (2007) on the granitic rocks from the Lachlan Fold Belt, southeastern Australia. The moderately elevated $\delta^{18}O$ values indicate that a considerable amount of sedimentary material was involved in the granitic magmas, rather than the traditional thought based on whole-rock geochemical signatures that these granites were derived from metamorphosed igneous rocks. Since then, zircon combined Hf–O isotopes have been widely used in the studies of magma petrogenesis and source composition, and Hf–O isotopic modelling provide a good potential to give a quantitative constraint on the proportion of two or multiple crustal and mantle endmember components during zircon crystallization. However, regional investigations of O isotopes in well-defined tectonic settings are scarce, so the potential to link coupled Hf–O isotopes with distinct tectonic settings needs to be explored further.

In this thesis, available zircon isotopic data from several accretionary and collisional orogenic systems provide an opportunity to compare their isotopic signatures and to

test the potential to use combined Hf–O isotopes as a tectonic tracer. These data cover a relatively large regional profile in a certain orogen, and thus they are regarded to have to a large degree reflected the compositions of the orogenic crust. Zircon Hf–O isotopic data from our current studies on four orogenic systems are compiled in Fig. 4, including two accretionary orogens (the 1650–1500 Ma Gothian and Telemarkian orogeny in western Fennoscandia and the Grenville-age Maud Belt in East Antarctica), and two orogens that formed related to continental collision (ca. 550–480 Ma East African-Antarctic and the Sveconorwegian mobile belts). Their Hf–O isotopic patterns are compared with those of the Permo-Triassic arc magmas from the Paleo-Pacific margin and with syn- and post-collisional magmas from Tibet, which are considered as typical accretionary and collisional settings, respectively. As mentioned above, a compressional environment is generally associated with magma production from crustal sources, whereas extension is commonly correlated with greater amounts of juvenile inputs. Thus, arc magmas, especially those generated during a long-term subduction process with tectonic switch between compression and extension (such as subduction retreating and advancing), are expected to have various Hf and O isotopic compositions. As shown in Fig. 4, zircon εHf(t) and $\delta^{18}O$ values of magmas from accretionary orogens are overall coupled showing a clear negative correlation, and Hf isotopic compositions are mostly juvenile with εHf(t) values close to that of the new crust. The most straightforward interpretation is the involvement of at least two sources, a juvenile (mantle-derived) source with radiogenic Hf and mantle-like O isotope values and an older supracrustal source with evolved Hf and elevated O values. Particularly, the addition of older crustal/sedimentary material appears to be common during arc magmatism in these Proterozoic to Paleozoic accretionary orogens.

In contrast to subduction-related magmas displaying similar Hf–O isotopic patterns, syn- and post-collisional magmas in different collisional orogenic systems appear to have various isotopic patterns (Fig. 4). In the East African-Antarctic Orogen (the part in East Antarctica) and the Sveconorwegian orogen, related granitic magmas have a wide spread of Hf isotopic values that are associated with relatively homogeneous O isotopic compositions ($\delta^{18}O$ =5.5–7.5‰), and their evolved Hf isotopes reflect that they

were mostly derived from older pre-existing crust with insignificant juvenile and supracrustal inputs. In the Himalaya, recycling of sedimentary material is revealed by high O isotopic values of post-collisional leucogranites (ca. 20 Ma), and these older (Paleoproterozoic) sediments were deposited along the Indian margin (Greater and Lower Himalayan Sequence) and remelted during the India–Asia collision. In contrast, other syn-collisional magmas have more radiogenic isotopic compositions associated with moderate $\delta^{18}O$ values. Since the formation of continent-continent collision orogens may have experienced preceding subduction-accretion processes and many of the features of the collisional orogens may be produced by pre-collisional accretionary orogenesis, syn- and post-collisional magmas largely inherited the isotopic signatures from pre-existing crustal components, such as older crust and sedimentary material from the colliding continents, intervening island arcs, etc. It is therefore indicated that subduction-related magmas during the evolution of accretionary orogens have broadly similar isotopic patterns while for collision-related magmas, their Hf and O isotopic relations, which are largely controlled by the pre-existing crust, could vary significantly.

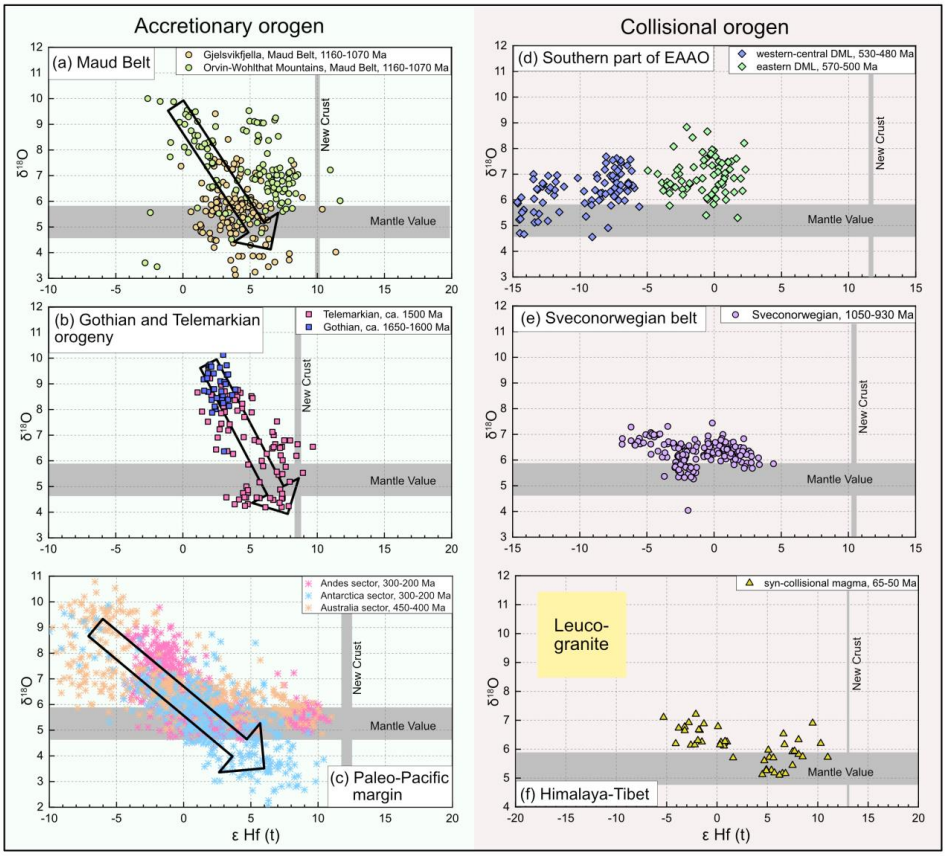

Fig. 4: Epsilon Hf(t) versus $\delta^{18}O$ diagrams showing distinct Hf–O patterns between accretionary and collisional orogenic systems; (a) the 1170–1060 Ma Maud Belt (this study); (b) 1650–1500 Ma Gothian and Telemarkian crust in west Baltica (this study and Roberts et al., 2012); (c) The Phanerozoic Paleo-Pacific accretionary margin, including ca. 300–200 Ma Andes sector (data from Deckart et al., 2014; Hervé et al., 2014; Jones et al., 2015; del Rey et al., 2016; Poole et al., 2020), Antarctic sector (data from Castillo et al., 2015; Elliot et al., 2019), and ca. 450–400 Ma Australia sector (data from Waltenberg et al., 2018); (d) the part of East African-Antarctic Orogen (EAAO) in DML, ca. 550–480 Ma (this study); (e) the 1050–930 Ma Sveconorwegian orogen (this study); (f) ca. 65–15 Ma Himalaya-Tibet collisional belt (data from Mahar et al., 2014; Wang et al., 2015; Hopkinson et al., 2017; Ma et al., 2018). The Hf isotopic value of new crust is calculated using the formula from Dhuime et al. (2012).

2.2 Lateral terminations of the Grenville orogenic system

2.2.1 Western termination: from collisional orogeny with escape tectonics to accretionary orogeny

During the last decades, a number of geological and paleomagnetic studies have improved the understanding of the Mesoproterozoic configuration of the Proto-Kalahari Craton and its collision with Laurentia. It was firstly proposed by Jacobs et al. (1993) and Jacobs and Thomas (1994) that the Proto-Kalahari Craton was probably involved in collisional processes during Rodinia assembly. The Proto-Kalahari Craton was interpreted as a southwest-directed (present direction) indenter during the formation of the Namaqua-Natal belt, based on structural analyses in the Namaqua-Natal belt that reveal changing shear geometries from dextral in Namaqua to sinistral in Natal (Fig. 5b). Dalziel et al. (2000) compared the Grenville-age history in the Namaqua belt and the Llano Uplift in SW Laurentia, and considered the latter as a Laurentian counterpart of the Namaqua sector and suggested that continental collision between Laurentia and Kalahari probably happened no later than ca. 1110 Ma. However, subsequent paleomagnetic results disproved a close proximity between the two continental landmasses at ca. 1100 Ma, as paleomagnetic data of the Umkondo intrusions (1112–1108 Ma) and the synchronous Midcontinent Rift in Laurentia indicated that they were separated by >30° of latitude at that time (Powell et al., 2001; Hanson et al., 2004; Gose et al., 2006). Recent paleomagnetic studies on 1100–1080 Ma rocks from the Midcontinent Rift showed that Laurentia witnessed a rapid motion from a high to low latitude during this time interval and thus it becomes highly possible that the final Laurentia-Kalahari assembly happened during or after this period (Swanson-Hysell et al., 2015, 2019). This is consistent with the geology of the Namaqua-Natal belt. By then, discrete terranes in the Namaqua-Natal belt had finally juxtaposed and accreted onto the Kalahari continental margin. Subsequently, in Natal, widespread A-type granites (Oribi Gorge Suite) were emplaced in the Mzumbe and Margate terranes at ca. 1050–1030 Ma, accompanied by a low-pressure, (ultra)high temperature granulite-facies metamorphic event (peak conditions at 900–1100°C/5–7kbar) followed by isobaric cooling (Spencer et al., 2015 and references therein). This is interpreted as a result of post-collisional extension or a tectonic transition from

convergence to transcurrent deformation (Spencer et al., 2015). During ca. 1080–1030 Ma, the western and southern Namaqua sector in the Bushmanland Subprovince similarly record a prolonged period of granitic and mafic (Koperberg Suite) magmatism associated with low-pressure, (ultra)high temperature (850–900°C/5–5.5kbar) during ca. 1080–1030 Ma (Macey et al., 2018; Schorn et al., 2020).

Our study (paper I), combined with previous studies, indicates that the Maud Belt differs significantly from the Natal belt in terms of geochronological records of magmatic-metamorphic activities, isotopic compositions and subduction polarity. Firstly, in contrast to the Natal belt where the island arcs terranes were interpreted to have formed during 1250–1200 Ma, no >1200 Ma geochronology record has been reported in the Maud Belt, which indicates that preceding arc formation was diachronous in the two belts. Moreover, compiled zircon U–Pb data show that various parts of the Maud Belt appear to have similar magmatic histories with two main periods at 1150–1125 Ma and 1110–1090 Ma, while <1070 Ma magmatic activities are relatively scarce in the Maud Belt, and no <1050 Ma granitic suite comparable to the Oribi Gorge Suite in Natal and Koperberg Suite in Namaqua has been discovered so far. This suggests that the continental convergence and subsequent geological activities related to post-collision/transcurrent deformation appear to be lacking in the Maud Belt. In addition, the ca. 1180–1030 Ma granitic rocks in the Natal belt generally have juvenile isotopic signatures and are interpreted to have derived from >1200 Ma island arcs (Spencer et al., 2015). In the Maud Belt, however, the variation in Nd–Hf isotopic composition of Grenville-age magmas indicates an increasing juvenile input towards the east (i.e. towards the margin of the craton) and significantly evolved isotopic compositions in the westernmost part indicate a large reworking of old Archean-Paleoproterozoic continental crust, which suggests that the Maud Belt was established on older continental lithosphere of the Proto-Kalahari Craton associated with a continent-ward subduction. Similar aged arc magmatism has also been proposed for the Nampula Complex, Mozambique (Macey et al., 2010). Therefore, the Natal belt formed by the accretion of island arcs associated with subduction away from the craton and following continental collision between Kalahari and Laurentia. The Maud-

Mozambique side of the Proto-Kalahari Craton, in contrast, developed as a long-term active continental margin, which probably represents a branch of an exterior accretionary orogen flanking the margin of Rodinia.

The Coats Land block located to the south of the Maud Belt represents a critical block to reconstruct the Mesoproterozoic connection between Laurentia and Kalahari (Loewy et al., 2011). Rock exposures are very limited in Coats Land, but accessible exposures are composed of undeformed felsic volcanic rocks that were dated at 1112 ± 4 Ma (Gose et al., 1997). These rocks cannot be correlated to the coeval Umkondo Large Igneous Province as they have strikingly distinct paleomagnetic data, Pb isotopic composition and magnetic anomaly pattern, which thus indicates that the Coats Land block was unlikely a part of Kalahari (Gose et al., 1997; Lowey et al. 2011; Mieth and Jokat, 2014). Instead, these ca. 1100 Ma rocks in the Coats Land block correlate well with the Franklin Mountains of western Texas in terms of their consistent geochronology and Pb isotopes, where ca. 1120 Ma granitic and basaltic rocks generally have much lower metamorphic grade and lower degree of deformation than the synchronous orogenic granitic rocks in the Llano Uplift and are thus interpreted as rift-related magmatism (Bickford et al., 2000). The formation of a rift-basin is attributed to a major transcurrent shear system that formed across the southern margin of Laurentia (Bickford et al., 2000). Coeval 1100 Ma rocks from Coats Land, the Franklin Mountains and the Midcontinent Rift with consistent Pb isotopic compositions suggest that Coats Land could have originally been a part of Laurentia, which thus leads to a strong argument for a continental collision between Kalahari and Laurentia. Coats Land itself, may have extruded and detached from Laurentia by tectonic translation when Kalahari collided with Laurentia, which resulted in indenter-escape tectonics in the western part of the Grenville Orogen.

In addition to the Coats Land block, other fragments such as the Tasmania and South Tasman Rise preserve a comparable geologic information to SW Laurentia and are thus also placed in a close proximity to SW Laurentia in Rodinia reconstructions (Fioretti et al., 2005; Merdith et al., 2017). In the southern Tasman Rise, undeformed 1119 ± 8 Ma granites have similar Pb isotopic compositions with coeval rocks in the Coats Land block and the Franklin Mountains, which possibly represents another fragment that

separated from Laurentia (Fioretti et al., 2005). Late Mesoproterozoic (1.25–1.10 Ga) sedimentary rocks in Tasmania have a similar zircon geochronology spectrum and Hf isotopic compositions as contemporaneous sedimentary rocks in SW Laurentia, which positions Tasmania adjacent to SW Laurentia in Rodinia (Mulder et al., 2018). The Coats Land block, together with Tasmania and the South Tasman Rise, probably represent displaced fragments from Laurentia, and they subsequently joined Kalahari and Australo-Antarctica respectively during Neoproterozoic rifting (Merdith et al., 2019). It is envisaged that they formed by lateral extrusion in the wake of the Kalahari-Laurentia collision (Fig. 5b).

The recognition of the 1020–980 Ma island arc terranes (TOAST) to the east of the Maud Belt inspires further thoughts on the position and origin of the TOAST in Rodinia. The origin and position of the TOAST in Rodinia is unclear. It is thought to have collided with Kalahari and welded onto the Maud Belt during Gondwana assembly (Jacobs et al., 2015). If the TOAST originally formed close to the Kalahari margin in Rodinia, the part of the Kalahari margin in the Maud Belt probably marks the evolution from an Andean-type continental arc to a Western Pacific-type margin with subduction retreating of oceanic slab and development of island arcs (Fig. 5a). Similar aged (ca. 1080–980 Ma) juvenile rocks have also been reported in Madagascar and Sri Lanka (Archibald et al., 2017), which probably together comprised a connected arc chain in the exterior ocean (Fig. 5a). In Rodinia reconstructions, the TOAST may represent one of voluminous micro-plates/island arc in the exterior ocean on the periphery of Rodinia, comparable to the arc chains along the west-pacific margin.

Therefore, Grenville-age Namaqua-Natal-Maud orogenic system during Kalahari-Laurentia convergence appears to have marked a transition from Himalaya-type collisional orogeny in the Namaqua-Natal belt to a long-term (ca. 1170–900 Ma) subduction-accretion process at the side of the Maud Belt that is comparable to Indonesian-type ocean-continent convergence zone. Both continental collision and subduction processes have probably facilitated the lateral extrusions of a number of crustal blocks.

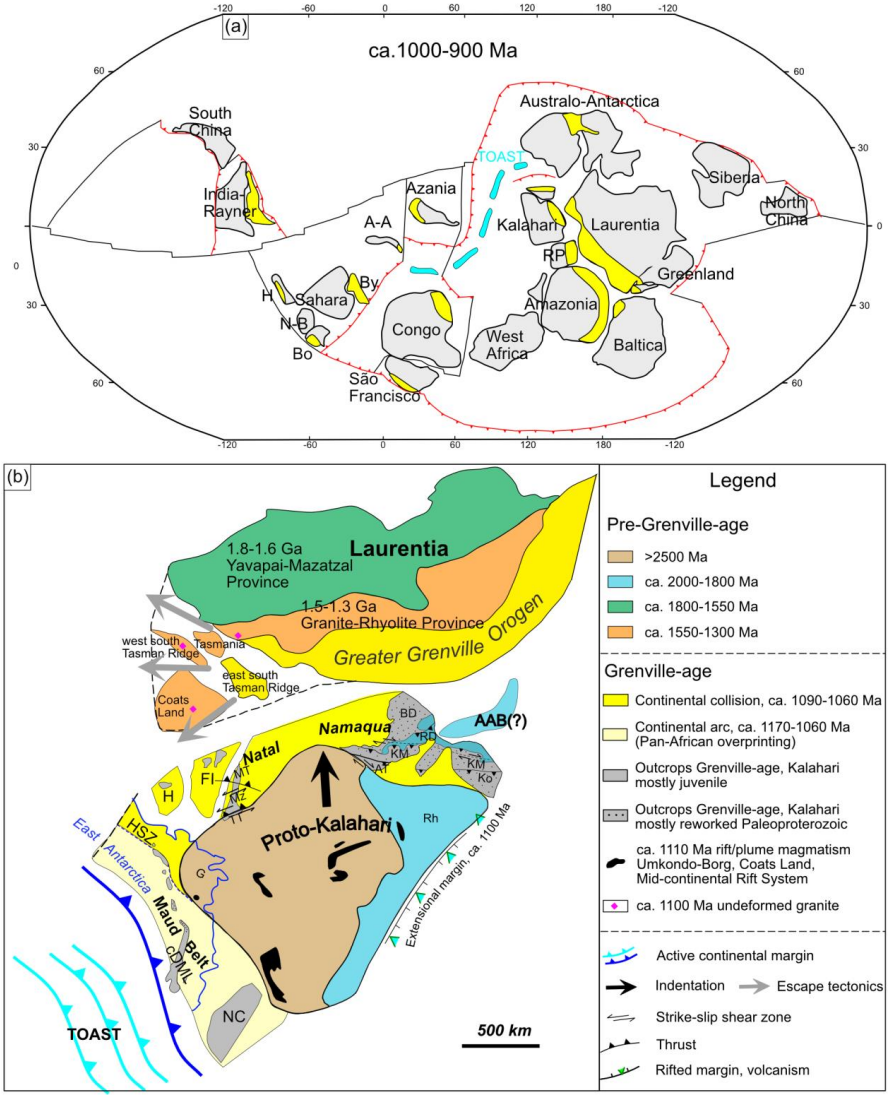

Fig.5: (a) Paleogeographic reconstructions of Rodinia at ca. 1000–900 Ma, with ca. 1080–900 Ma island arcs around Kalahari and Congo (modified after Archibald et al., 2017; Merdith et al., 2017); (b) Configuration of the Proto-Kalahari Craton and Laurentia during Rodinia assembly (modified after Jacobs et al., 2003). The Proto-Kalahari Craton is interpreted as an indenter into Laurentia to form the Namaqua-Natal belt with collision probably happening during 1100–1050 Ma, causing escaped tectonics. The side of the Maud-Mozambique belts, in contrast, witnessed long-term Grenville-age accretionary orogenesis. The Coats Land block is interpreted as a part of Laurentia but was left behind during subsequent separation between

Laurentia and Kalahari. Abbreviations: AT, Areachap Terrane, AAB, Arequipa-Antofalla Basement; BD, Bushmanland Domain; cDML, central Dronning Maud Land; FI, Falkland Islands; G, Grunehogna Craton (Antarctica); H, Haag Nunatak; HSZ, Heimefront Shear Zone; KM, Kakamas Terrane; Ko, Konkiep Terrane; MT, Margate Terrane; Mz, Mzumbe Terrane, NC, Nampula Complex; RD, Richtersveld Domain; Rh, Rehoboth Province; TOAST, Tonian Oceanic Arc Superterrane; TT, Tugela Terrane; other abbreviations in (a) refer to Fig. 2.

2.2.2 Eastern termination: the Sveconorwegian orogen as a continuation of the Grenville Orogen in SW Baltica

It has been well constrained by paleomagnetic data that Baltica had rotated >90° clockwise from ca. 1250 Ma to 990 Ma with its western margin (present-day coordinates) broadly facing the margin of Laurentia-Greenland (Cawood and Pisarevsky, 2017). However, as the exact position of Baltica relative to Laurentia and Amazonia in Rodinia has been poorly constrained plus complicated magmatic and metamorphic events in various litho-tectonic units of the Sveconorwegian orogen, a number of orogenic models have been proposed (see reviews in Bingen et al., 2021). The classical collisional model places the Sveconorwegian orogen facing the northern margin of Amazonia and considers the orogen as the product of continental collision between Baltica and Amazonia with the Putumayo orogen and Oaxaquia in between (Park, 1992; Karlstrom et al., 2001; Bogdanova et al., 2008; Weber et al., 2010; Ibanez-Mejia et al., 2011; Cawood and Pisarevsky, 2017; Ibanez-Mejia, 2020; Bingen et al., 2021), but controversy exists on the collision timing, whether prior to ca. 1050 Ma or at ca. 990 Ma. An alternative view correlates the Sveconorwegian orogen as the opposing collisional margin of the northern Grenville Province in Labrador, mainly based on their comparable ca. 1050 Ma and ca. 950 Ma granitic rocks (Johansson, 2009, 2014). Another model interprets the four western Sveconorwegian lithotectonic units as one plate (exotic to Baltica) that collided with the Eastern Segment (endemic to Baltica) at ca. 990 Ma (Möller et al., 2015; Möller and Andersson, 2018). Alternatively, an accretionary model places Baltica at a position that is relatively distant from Laurentia and Amazonia, and considers southwest Baltica as a long-term accretionary margin with continuous eastward subduction of an oceanic plate beneath southwestern

Baltica from ca. 1280 Ma to ca. 900 Ma (e.g. Slagstad et al., 2013, 2017). In a recent version of the acccretionary model (Slagstad et al., 2020), the southwestern margin of Baltica is proposed to have been fragmented into micro-blocks/continents by extension and rifting during ca. 1340–1100 Ma and re-amalgamated during the Sveconorwegian orogeny between ca. 1150 and 980 Ma.

In the accretionary model, the ca. 1060–1020 Ma and ca. 980–930 Ma Sveconorwegian magmatic activities are compared to periodic arc magmatism that was produced along an Andean-type active continental margin, and specifically the former is correlated to subduction advancing while the latter are interpreted to have emplaced under an extensional setting associated with subduction retreating (Coint et al., 2015; Granseth et al., 2020; Slagstad et al., 2020). However, as discussed in Paper II and the last chapter, the isotopic signatures of ca. 1060–930 Ma magmatic rocks in the Sveconorwegian orogen and a long-term Mesoproterozoic isotopic evolution of the southwestern margin of Fennoscandia are not compatible with a continuous subduction setting. In the Andean-type margin of South America and West Antarctica, isotopic compositions and variations of periodic arc magmatic activities are well coupled with a tectonic switch between advancing and retreating subduction (Nelson and Cottle, 2018), whereas similar isotopic variation is not revealed by the Sveconorwegian magmas, as ca. 950 Ma magmas are expected to have more juvenile radiogenic (such as Hf, Nd) isotopes than ca. 1050 Ma magmas. The Hf isotopic trend during the Telemarkian to Sveconorwegian orogenic evolution is comparable to that of the southeast margin of Laurentia, which shows that Grenville-age magmas in the Sveconorwegian and Grenville Orogen were mainly derived from the reworking of pre-existing crust due to progressive crustal thickening while juvenile inputs (mantle-derived magmas) were relatively insignificant. In addition, homogeneous, moderate O isotopes of ca. 1060–930 Ma samples indicate that the addition of sedimentary material was also insignificant during the genesis of Sveconorwegian magmas, which is inconsistent with the typical Andean-type continental margin where arc magmatism usually witnessed a large involvement of supracrustal material, reflected by high $\delta^{18}O$ isotopic values (Fig. 4). Overall, the ca. 1060–930 Ma Sveconorwegian magmas were generated largely by remelting of pre-existing continental crust with little subduction-related components,

which is incompatible with an active continental margin associated with a long-term subduction process. Therefore, from the isotopic perspective, we prefer the traditional interpretation that these magmas are related to continental collision rather than to subduction-accretion, although the direct evidence for continental collision between Baltica and the other continent, such as the identification of exotic crust from geological and isotopic records, is scarce.

Following the classical collisional model, it is preferred that the Sveconorwegian orogen most likely formed by collisional interactions of Baltica with Amazonia, and thus represents the extension of the Grenville Orogen into southwest Baltica (Fig. 6) (although our study of paper II fails to give new information and constraints on the collisional interactions between Baltica and Amazonia/Laurentia). The Baltica-Amazonia collision probably happened at ca. 1065 Ma, and subsequent 1050–900 Ma syn- and post-collisional magmatism and migmatization were probably a result of lithosphere foundering and asthenosphere upwelling (Bingen et al., 2021).

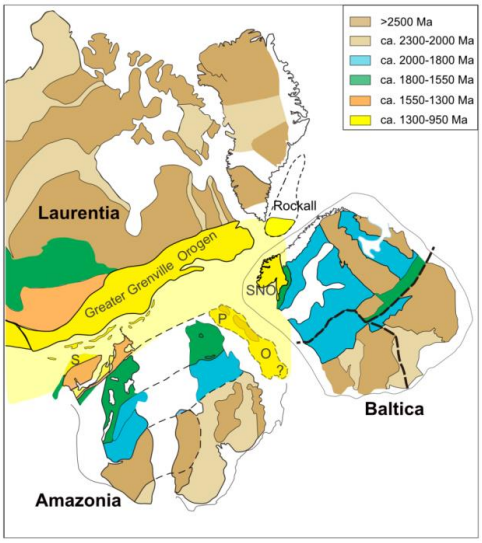

Fig.6: Tectonic reconstructions for Laurentia–Amazonia–Baltica interactions in Rodinia (modified after Ibañez-Mejia, 2020, age domains of Baltica are from Terentiev and Santosh, 2020), showing the Grenville Orogen and Grenville-age Sunsas orogen, Putumayo orogen (P), Oaxaquia (O) and the Sveconorwegian orogen (SNO).

2.3 Questions for future work

Our understanding and interpretation of the tectonic evolution of the Namaqua-Natal-Maud orogenic system and the Sveconorwegian orogen, the lateral termination model of the greater Grenville orogen and the configuration of the Proto-Kalahari Craton and Baltica and their link with Laurentia in supercontinent Rodinia are established on the presently available studies. However, some issues that are closely related to the research topic have not been addressed properly so far and require future work.

(1) Our study (Paper I) shows that the ca. 1160–1070 Ma magmas in the Maud Belt have both juvenile and evolved Hf isotopic compositions, but the presently available Hf isotopic data do not show a clear spatial variation in this time interval. A more detailed investigation on Grenville-age Hf isotopic evolution of the Maud Belt, from both magmatic and detrital zircons, is important for a better understanding of the switch in tectonic setting (convergence vs. extension; subduction advancing vs. retreating).

(2) The inferred collisional conjugate margin of the Namaqua-Natal belt was thought to be preserved in the Llano Uplift in Texas, yet both paleomagnetic data and the geological history failed to lead to a consistent conclusion when the continental collision happened. As noted above, both paleomagnetism and the magmatic-metamorphic history in the Natal Belt support that Kalahari and Laurentia were juxtaposed at ca. 1080 Ma. However, in the Llano Uplift, according to the tectonic model of Mosher et al. (2008), continent-continent collision inferred from high-grade metamorphism happened at 1150–1120 Ma, while subsequent 1120–1070 Ma granitic intrusions were attributed to post-collisional slab detachment and upwelling of asthenospheric mantle. On the other hand, the tectonic history of the Llano Uplift correlate well with the Namaqua belt (Dalziel et al., 2000), but an earlier collision at ca. 1150 Ma appears to be less likely in terms of paleomagnetism as available paleomagnetic data show that the Proto-Kalahari Craton and Laurentia were separated over large distances by ca. 1110 Ma. A better understanding of the Namaqua-Natal-Llano Uplift connections requires more geological work to better compare the geological history between SW Grenville and the Namaqua-Natal belt.

(3) To figure out the basement composition and geological history of the Coats Land block is crucial to understand its origin and paleogeographic location in Rodinia, and its drifting history during the transition from Rodinia to Gondwana. A better understanding of its link with SW Laurentia requires more geological investigations and solid evidence from geochronology, geochemistry and paleomagnetism studies. For example, the early-middle Mesoproterozoic rocks that are comparable to 1.5–1.3 Ga Granite–Rhyolite Provinces and 1.8–1.6 Ga Yavapai-Mazatzal Province in SW Laurentia are expected to exist in Coats Land.

(4) Paleoproterozoic crust (2.1–1.8 Ga) comprises a large part of the Namaqua sector and provides material for the formation of late Mesoproterozoic rocks. However, the formation and origin of these Paleoproterozoic terranes, specifically whether they represent continental arc magmatism along the margin of the Proto-Kalahari Craton or exotic terranes that were accreted onto the Kalahari continental margin during late Mesoproterozoic times, remain debated. This Paleoproterozoic crust has been correlated to the Arequipa-Antofalla Basement (now exposed along the Andean margin to the southwest of Amazonia) based on their consistent geochronological and isotopic records, the latter of which has been interpreted as a single block that was accreted to Amazonia during the Sunsas orogeny (Loewy et al., 2004; Ramos, 2008). In this regard, the Paleoproterozoic crust in the Namaqua and the Arequipa-Antofalla Basement probably represents a united terrane between Amazonia and the Proto-Kalahari Craton in Rodinia, which would be a strong argument for the Amazonia-Kalahari (Namaqua side) collision during Grenville-age orogeny. Further evidence, like Nd–Hf–Pb isotopic comparison, is required to prove or disprove their connection.

References

Archibald, D.B., Collins, A.S., Foden, J.D., Razakamanana, T., 2017. Tonian arc magmatism in central Madagascar: the petrogenesis of the Imorona-Itsindro Suite. The Journal of Geology 125, 271–297.

Beaumont, C., Nguyen, M., Jamieson, R. A., S. Ellis., 2006. Crustal flflow modes in large hot orogens, Geological Society, London, Special Publication 268, 91–145.

Beaumont, C., Jamieson, R., Nguyen, M., 2010. Models of large, hot orogens containing a collage of reworked and accreted terranes. Canadian Journal of Earth Sciences 47, 485–515.

Bingen, B., Viola, G., Möller, C., Vander Auwera, J., Laurent, A., Yi, K., 2021. The Sveconorwegian orogeny. Gondwana Research 90, 273–313.

Bickford, M.E., Soegaard, K., Nielsen, K.C., McLelland, J.M., 2000. Geology and geochronology of Grenville-age rocks in the Van Horn and Franklin Mountains area, west Texas: Implications for the tectonic evolution of Laurentia during the Grenville. Geological Society of America Bulletin 112, 1134–1148.

Bogdanova, S.V., Bingen, B., Gorbatschev, R., Kheraskova, T.N., Kozlov, V.I., Puchkov, V.N., Volozh, Y.A., 2008. The East European Craton (Baltica) before and during the assembly of Rodinia. Precambrian Research 160, 23–45.

Burke, K., Sengör, C., 1986. Tectonic escape in the evolution of the continental crust. Reflection seismology: the continental crust 14, 41–53.

Burrett, C., Berry, R., 2000. Proterozoic Australia–Western United States (AUSWUS) fit between Laurentia and Australia. Geology 28, 103–106.

Castillo, P., Fanning, C.M., Hervé, F., Lacassie, J.P., 2016. Characterisation and tracing of Permian magmatism in the south-western segment of the Gondwanan margin; U–Pb age, Lu–Hf and O isotopic compositions of detrital zircons from metasedimentary complexes of northern Antarctic Peninsula and western Patagonia. Gondwana Research 36, 1–13.

Castillo, P., Fanning, C.M., Riley, T.R., 2020. Zircon O and Hf isotopic constraints on the genesis of Permian–Triassic magmatic and metamorphic rocks in the Antarctic Peninsula and correlations with Patagonia. Journal of South American Earth Sciences 104, 102848.

Cawood, P.A., Kröner, A., Collins, W.J., Kusky, T.M., Mooney, W.D., Windley, B.F., 2009. Accretionary orogens through Earth history. Geological Society, London, Special Publication 318, 1–36.

Cawood, P.A., Strachan, R.A., Pisarevsky, S.A., Gladkochub, D.P., Murphy, J.B., 2016. Linking collisional and accretionary orogens during Rodinia assembly and breakup: Implications for models of supercontinent cycles. Earth and Planetary Science Letters 449, 118–126.

Cawood, P.A., Pisarevsky, S.A., 2017. Laurentia-Baltica-Amazonia relations during Rodinia assembly. Precambrian Research 292, 386–397.

Collins, W.J., 2002. Hot orogens, tectonic switching, and creation of continental crust. Geology 30, 535–538.

Collins, W.J., Belousova, E.A., Kemp, A.I., Murphy, J.B., 2011. Two contrasting Phanerozoic orogenic systems revealed by hafnium isotope data. Nature Geoscience 4, 333–337.

Condie, K.C., Aster, R.C., 2013. Refinement of the supercontinent cycle with Hf, Nd and Sr isotopes. Geoscience Frontiers 4, 667–680.

Condie, K.C., 2013. Preservation and recycling of crust during accretionary and collisional phases of Proterozoic orogens: A bumpy road from Nuna to Rodinia. Geosciences 3, 240–261.

Dalziel, I.W., 1991. Pacific margins of Laurentia and East Antarctica-Australia as a conjugate rift pair: Evidence and implications for an Eocambrian supercontinent. Geology 19, 598–601.

Dalziel, I.W., Mosher, S., Gahagan, L.M., 2000. Laurentia-Kalahari collision and the assembly of Rodinia. The Journal of Geology 108, 499–513.

Deckart, K., Hervé Allamand, F., Fanning, M., Ramírez, V., Calderón, M., Godoy, E., 2014. U-Pb geochronology and Hf-O isotopes of zircons from the Pennsylvanian Coastal Batholith, south-central Chile. Andean Geology 41, 49–82.

De Kock, M.O., Gumsley, A.P., Klausen, M.B., Söderlund, U., Djeutchou, C., 2019. The Precambrian mafic magmatic record, including large igneous provinces of the Kalahari craton and its constituents: A paleogeographic review. Dyke Swarms of the World: A Modern Perspective, 155–214.

del Rey, A., Deckart, K., Arriagada, C., Martínez, F., 2016. Resolving the paradigm of the late Paleozoic–Triassic Chilean magmatism: Isotopic approach. Gondwana Research 37, 172–181.

Dhuime, B., Hawkesworth, C.J., Cawood, P.A., Storey, C.D., 2012. A change in the geodynamics of continental growth 3 billion years ago. Science 335, 1334–1336.

Evans, D.A., Mitchell, R.N., 2011. Assembly and breakup of the core of Paleoproterozoic–Mesoproterozoic supercontinent Nuna. Geology 39, 443–446.

Evans, D.A., 2013. Reconstructing pre-Pangean supercontinents. Bulletin 125, 1735–1751.

Fioretti, A.M., Black, L.P., Foden, J., Visonà, D., 2005. Grenville-age magmatism at the South Tasman Rise (Australia): A new piercing point for the reconstruction of Rodinia. Geology 33, 769–772.

Fitzsimons, I.C.W., 2000a. A review of tectonic events in the East Antarctic Shield and their implications for Gondwana and earlier supercontinents. Journal of African Earth Sciences 31, 3–23.

Fitzsimons, I.C.W., 2000b. Grenville-age basement provinces in East Antarctica: evidence for three separate collisional orogens. Geology 28, 879–882.

Fossen, H., 2016. Structural geology. Cambridge University Press, London. https://doi.org/10.1017/ CBO9780511777806, 510 p.

Gardiner, N.J., Kirkland, C.L., Van Kranendonk, M.J., 2016. The juvenile hafnium isotope signal as a record of supercontinent cycles. Scientific reports 6, 1–10.

Gose, W.A., Helper, M.A., Connelly, J.N., Hutson, F.E., Dalziel, I.W., 1997. Paleomagnetic data and U-Pb isotopic age determinations from Coats Land, Antarctica: Implications for late Proterozoic plate reconstructions. Journal of Geophysical Research: Solid Earth 102, 7887–7902.

Gose, W.A., Hanson, R.E., Dalziel, I.W., Pancake, J.A., Seidel, E.K., 2006. Paleomagnetism of the 1.1 Ga Umkondo large igneous province in southern Africa. Journal of Geophysical Research: Solid Earth, 111(B9).

Gower, C.F., Rivers, T., Ryan, A.B. eds., 1990. Mid-Proterozoic Laurentia-Baltica. Geological Association of Canada, Department of Earth Sciences.

Hanson, R.E., Crowley, J.L., Bowring, S.A., Ramezani, J., Gose, W.A., Dalziel, I.W., Pancake, J.A., Seidel, E.K., Blenkinsop, T.G., Mukwakwami, J., 2004. Coeval large-scale magmatism in the Kalahari and Laurentian cratons during Rodinia assembly. Science 304, 1126–1129.

Harley, S.L., 2003. Archaean-Cambrian crustal development of East Antarctica: metamorphic characteristics and tectonic implications. Geological Society, London, Special Publication 206, 203–230.

Hawkesworth, C.J., Kemp, A.I.S., 2006. Using hafnium and oxygen isotopes in zircons to unravel the record of crustal evolution. Chemical Geology 226, 144–162.

Hervé, F., Fanning, C.M., Calderón, M., Mpodozis, C., 2014. Early Permian to Late Triassic batholiths of the Chilean Frontal Cordillera (28°-31°S): SHRIMP U–Pb zircon ages and Lu-Hf and O isotope systematics. Lithos 184–187, 436–446.

Hoffman, P.F., 1991. Did the breakout of Laurentia turn Gondwanaland inside-out?. Science 252, 1409–1412.

Hopkinson, T.N., Harris, N.B., Warren, C.J., Spencer, C.J., Roberts, N.M., Horstwood, M.S., Parrish, R.R., 2017. The identification and significance of pure sediment-derived granites. Earth and Planetary Science Letters 467, 57–63.

Hynes, A., Rivers, T., 2010. Protracted continental collision—Evidence from the Grenville orogen. Canadian Journal of Earth Sciences 47, 591–620.

Ibanez-Mejia, M., Ruiz, J., Valencia, V.A., Cardona, A., Gehrels, G.E., Mora, A.R., 2011. The Putumayo Orogen of Amazonia and its implications for Rodinia reconstructions: New U–Pb geochronological insights into the Proterozoic tectonic evolution of northwestern South America. Precambrian Research 191, 58–77.

Ibañez-Mejia, M., 2020. The Putumayo Orogen of Amazonia: A synthesis. In: Gómez, J. & Mateus–Zabala, D. (editors), The Geology of Colombia, Volume 1 Proterozoic–

Paleozoic. Servicio Geológico Colombiano, Publicaciones Geológicas Especiales 35, 101–131. Bogotá.

Indares, A., 2020. Deciphering the metamorphic architecture and magmatic patterns of large hot orogens: Insights from the central Grenville Province. Gondwana Research 80, 385–409.

Jacobs, J., Thomas, R.J. and Weber, K., 1993. Accretion and indentation tectonics at the southern edge of the Kaapvaal craton during the Kibaran (Grenville) orogeny. Geology 21, 203–206.

Jacobs, J., Thomas, R.J., 1994. Oblique collision at about 1.1 Ga along the southern margin of the Kaapvaal continent, south-east Africa. Geologische Rundschau 83, 322–333.

Jacobs, J., Bauer, W., Fanning, C.M., 2003. New age constraints for Grenville-age metamorphism in western central Dronning Maud Land (East Antarctica), and implications for the palaeogeography of Kalahari in Rodinia. International Journal of Earth Sciences 92, 301–315.

Jacobs, J., Thomas, R.J., 2004. Himalayan-type indenter-escape tectonics model for the southern part of the late Neoproterozoic–early Paleozoic East African–Antarctic orogen. Geology 32, 721–724.

Jacobs, J., Elburg, M., Läufer, A., Kleinhanns, I.C., Henjes-Kunst, F., Estrada, S., Ruppel, A.S., Damaske, D., Montero, P., Bea, F., 2015. Two distinct late Mesoproterozoic/early Neoproterozoic basement provinces in central/eastern Dronning Maud Land, East Antarctica: The missing link, 15–21 E. Precambrian Research 265, 249–272.

Johansson, Å., 2009. Baltica, Amazonia and the SAMBA connection—1000 million years of neighbourhood during the Proterozoic? Precambrian Research 175, 221–234.

Johansson, Å., 2014. From Rodinia to Gondwana with the 'SAMBA' model—a distant view from Baltica towards Amazonia and beyond. Precambrian Research 244, 226–235.

Johnson, S.P., De Waele, B., Liyungu, K.A., 2006. U–Pb sensitive high-resolution ion microprobe (SHRIMP) zircon geochronology of granitoid rocks in eastern Zambia: Terrane subdivision of the Mesoproterozoic Southern Irumide Belt. Tectonics, 25(6).

Johnson, S.P., De Waele, B., Tembo, F., Katongo, C., Tani, K., Chang, Q., Iizuka, T., Dunkley, D., 2007. Geochemistry, geochronology and isotopic evolution of the Chewore–Rufunsa Terrane, Southern Irumide Belt: a Mesoproterozoic continental margin arc. Journal of Petrology 48, 1411–1441.

Jones, R.E., Kirstein, L.A., Kasemann, S.A., Dhuime, B., Elliott, T., Litvak, V.D., Alonso, R., Hinton, R., Facility, E.I.M., 2015. Geodynamic controls on the contamination of Cenozoic arc magmas in the southern Central Andes: Insights from the O and Hf isotopic composition of zircon. Geochimica et Cosmochimica Acta 164, 386–402.

Karlstrom, K.E., Åhäll, K.I., Harlan, S.S., Williams, M.L., McLelland, J., Geissman, J.W., 2001. Long-lived (1.8–1.0 Ga) convergent orogen in southern Laurentia, its extensions to Australia and Baltica, and implications for refining Rodinia. Precambrian Research 111, 5–30.

Kemp, A.I.S., Hawkesworth, C.J., Foster, G.L., Paterson, B.A., Woodhead, J.D., Hergt, J.M., Gray, C.M., Whitehouse, M.J., 2007. Magmatic and crustal differentiation history of granitic rocks from Hf-O isotopes in zircon. Science 315, 980–983.

Li, Z.X., Bogdanova, S.V., Collins, A.S., Davidson, A., De Waele, B., Ernst, R.E., Fitzsimons, I.C.W., Fuck, R.A., Gladkochub, D.P., Jacobs, J., Karlstrom, K.E., 2008. Assembly, configuration, and break-up history of Rodinia: a synthesis. Precambrian research 160, 179–210.

Li, Z.X., Mitchell, R.N., Spencer, C.J., Ernst, R., Pisarevsky, S., Kirscher, U., Murphy, J.B., 2019. Decoding Earth's rhythms: modulation of supercontinent cycles by longer superocean episodes. Precambrian Research 323, 1–5.

Liu, C., Runyon, S.E., Knoll, A.H., Hazen, R.M., 2019. The same and not the same: Ore geology, mineralogy and geochemistry of Rodinia assembly versus other supercontinents. Earth-Science Reviews 196, 102860.

Loewy, S.L., Connelly, J.N., Dalziel, I.W., 2004. An orphaned basement block: The Arequipa-Antofalla Basement of the central Andean margin of South America. GSA Bulletin 116, 171–187.

Loewy, S.L., Dalziel, I.W.D., Pisarevsky, S., Connelly, J.N., Tait, J., Hanson, R.E., Bullen, D., 2011. Coats Land crustal block, East Antarctica: A tectonic tracer for Laurentia? Geology 39, 859–862.

Ma, L., Wang, Q., Kerr, A.C., Yang, J.H., Xia, X.P., Ou, Q., Yang, Z.Y., Sun, P., 2017. Paleocene (c. 62 Ma) leucogranites in southern Lhasa, Tibet: Products of syn-collisional crustal anatexis during slab roll-back?. Journal of Petrology 58, 2089–2114.

Macey, P.H., Thomas, R.J., Grantham, G.H., Ingram, B.A., Jacobs, J., Armstrong, R.A., Roberts, M.P., Bingen, B., Hollick, L., De Kock, G.S., Viola, G., 2010. Mesoproterozoic geology of the Nampula Block, northern Mozambique: Tracing fragments of Mesoproterozoic crust in the heart of Gondwana. Precambrian Research 182, 124–148.

Macey, P.H., Bailie, R.H., Miller, J.A., Thomas, R.J., De Beer, C., Frei, D., Le Roux, P.J., 2018. Implications of the distribution, age and origins of the granites of the Mesoproterozoic Spektakel Suite for the timing of the Namaqua Orogeny in the Bushmanland Subprovince of the Namaqua-Natal Metamorphic Province, South Africa. Precambrian Research 312, 68–98.

Mahar, M.A., Mahéo, G., Goodell, P.C., Pavlis, T.L., 2014. Age and origin of post collision Baltoro granites, south Karakoram, North Pakistan: Insights from in-situ U–Pb, Hf and oxygen isotopic record of zircons. Lithos 205, 341–358.

Martin, E.L., Spencer, C.J., Collins, W.J., Thomas, R.J., Macey, P.H., Roberts, N.M.W., 2020. The core of Rodinia formed by the juxtaposition of opposed retreating and advancing accretionary orogens. Earth-Science Reviews 211, 103413.

McLelland, J., Daly, J.S., McLelland, J.M., 1996. The Grenville orogenic cycle (ca. 1350–1000 Ma): an Adirondack perspective. Tectonophysics 265, 1–28.

Merdith, A.S., Collins, A.S., Williams, S.E., Pisarevsky, S., Foden, J.D., Archibald, D.B., Blades, M.L., Alessio, B.L., Armistead, S., Plavsa, D., Clark, C., 2017. A full-plate global reconstruction of the Neoproterozoic. Gondwana Research 50, 84–134.

Merdith, A.S., Williams, S.E., Brune, S., Collins, A.S., Müller, R.D., 2019. Rift and plate boundary evolution across two supercontinent cycles. Global and planetary change 173, 1–14.

Mieth, M., Jokat, W., 2014. New aeromagnetic view of the geological fabric of southern Dronning Maud Land and Coats Land, East Antarctica. Gondwana Research 25, 358–367.

Molnar, P., Tapponier. P., 1975. Cenozoic tectonics of Asia: Effects of a continental collision, Science, 189, 419–426.

Moores, E.M., 1991. Southwest US-East Antarctic (SWEAT) connection: a hypothesis. Geology 19, 425–428.

Mosher, S., Levine, J.S.F., Carlson, W.D., 2008. Mesoproterozoic plate tectonics: A collisional model for the Grenville-aged orogenic belt in the Llano uplift, central Texas. Geology 36, 55–58.

Möller, C., Andersson, J., Dyck, B., Antal Lundin, I., 2015. Exhumation of an eclogite terrane as a hot migmatitic nappe, Sveconorwegian orogen. Lithos, 226, 147–168.

Möller, C., Andersson, J., 2018. Metamorphic zoning and behaviour of an underthrusting continental plate. Journal of metamorphic geology 36, 567–589.

Mulder, J.A., Karlstrom, K.E., Halpin, J.A., Merdith, A.S., Spencer, C.J., Berry, R.F., McDonald, B., 2018. Rodinian devil in disguise: Correlation of 1.25–1.10 Ga strata between Tasmania and Grand Canyon. Geology 46, 991–994.

Murphy, J.B., Nance, R.D., 2003. Do supercontinents introvert or extrovert? Sm-Nd isotope evidence. Geology 31, 873–876.

Murphy, J.B., Damian Nance, R., 2005. Do supercontinents turn inside-in or inside-out? International Geology Review 47, 591–619.

Murphy, J.B., Nance, R.D., Cawood, P.J., 2009. Contrasting modes of supercontinent formation and the conundrum of Pangea. Gondwana Research 15, 408–420.

Murphy, J.B., Nance, R.D., 2013. Speculations on the mechanisms for the formation and breakup of supercontinents. Geoscience Frontiers 4, 185–194.

Nelson, D.A., Cottle, J.M., 2018. The secular development of accretionary orogens: linking the Gondwana magmatic arc record of West Antarctica, Australia and South America. Gondwana Research 63, 15–33.

Park, R.G., 1992. Plate kinematic history of Baltica during the Middle to Late Proterozoic: a model. Geology 20, 725–728.

Pehrsson, S.J., Eglington, B.M., Evans, D.A., Huston, D., Reddy, S.M., 2016. Metallogeny and its link to orogenic style during the Nuna supercontinent cycle. Geological Society, London, Special Publications 424, 83–94.

Pesonen, L.J., Mertanen, S., Veikkolainen, T., 2012. Paleo-Mesoproterozoic supercontinents–a paleomagnetic view. Geophysica 48, 5–47.

Pisarevsky, S.A., Wingate, M.T., Powell, C.M., Johnson, S., Evans, D.A., 2003. Models of Rodinia assembly and fragmentation. Geological Society, London, Special Publication 206, 35–55.

Pisarevsky, S.A., Elming, S.Å., Pesonen, L.J., Li, Z.X., 2014. Mesoproterozoic paleogeography: Supercontinent and beyond. Precambrian Research 244, 207–225.

Poole, G.H., Kemp, A.I., Hagemann, S.G., Fiorentini, M.L., Jeon, H., Williams, I.S., Zappettini, E.O. and Rubinstein, N.A., 2020. The petrogenesis of back-arc magmas, constrained by zircon O and Hf isotopes, in the Frontal Cordillera and Precordillera, Argentina. Contributions to Mineralogy and Petrology 175, 1–21.

Powell, C.M., Jones, D.L., Pisarevsky, S., Wingate, M.T.D., 2001. Palaeomagnetic constraints on the position of the Kalahari craton in Rodinia. Precambrian Research 110, 33–46.

Ramos, V.A., 2008. The basement of the Central Andes: the Arequipa and related terranes. Annual Review of Earth and Planetary Sciences 36, 289–324.

Ratschbacher, L., Merle, O., Davy, P., Cobbold, P., 1991a. Lateral extrusion in the Eastern Alps, Part 1: Boundary conditions and experiments scaled for gravity. Tectonics 10, 245–256.

Ratschbacher, L., Frisch, W., Linzer, H.G., Merle, O., 1991b. Lateral extrusion in the Eastern Alps, part 2: structural analysis. Tectonics 10, 257–271.

Rivers, T., 2015. Tectonic setting and evolution of the Grenville Orogen: An assessment of progress over the last 40 years. Geoscience Canada, pp.77–124.

Roberts, N.M., 2012. Increased loss of continental crust during supercontinent amalgamation. Gondwana Research 21, 994–1000.

Roberts, N.M., 2013. The boring billion?–Lid tectonics, continental growth and environmental change associated with the Columbia supercontinent. Geoscience Frontiers 4, 681–691.

Schattner, U., 2010. What triggered the early-to-mid Pleistocene tectonic transition across the entire eastern Mediterranean? Earth and Planetary Science Letters 289, 539–548.

Schellart, W.P., Chen, Z., Strak, V., Duarte, J.C., Rosas, F.M., 2019. Pacific subduction control on Asian continental deformation including Tibetan extension and eastward extrusion tectonics. Nature communications 10, 1–15.

Schorn, S., Diener, J.F., Sorger, D., Clark, C., 2020. The contribution of charnockite magmatism to achieve near-ultrahigh temperatures in the Namaqua–Natal Metamorphic Province, South Africa. Lithos 368, 105585.

Searle, M.P., 2006. Role of the Red River Shear zone, Yunnan and Vietnam, in the continental extrusion of SE Asia. Journal of the Geological Society 163, 1025–1036.

Slagstad, T., Roberts, N.M., Marker, M., Røhr, T.S., Schiellerup, H., 2013. A non-collisional, accretionary Sveconorwegian orogen. Terra Nova 25, 30–37.

Slagstad, T., Roberts, N.M., Kulakov, E., 2017. Linking orogenesis across a supercontinent; the Grenvillian and Sveconorwegian margins on Rodinia. Gondwana Research 44, 109–115.

Slagstad, T., Marker, M., Roberts, N.M., Saalmann, K., Kirkland, C.L., Kulakov, E., Ganerød, M., Røhr, T.S., Møkkelgjerd, S.H., Granseth, A., Sørensen, B.E., 2020. The Sveconorwegian orogeny–reamalgamation of the fragmented southwestern margin of Fennoscandia. Precambrian Research, 105877.

Spencer, C.J., Thomas, R.J., Roberts, N.M., Cawood, P.A., Millar, I., Tapster, S., 2015. Crustal growth during island arc accretion and transcurrent deformation, Natal Metamorphic Province, South Africa: new isotopic constraints. Precambrian Research 265, 203–217.

Spencer, C.J., Kirkland, C.L., Prave, A.R., Strachan, R.A., Pease, V., 2019. Crustal reworking and orogenic styles inferred from zircon Hf isotopes: Proterozoic examples from the North Atlantic region. Geoscience Frontiers 10, 417–424.

Sperner, B., Ratschbacher, L., Nemčok, M., 2002. Interplay between subduction retreat and lateral extrusion: Tectonics of the Western Carpathians. Tectonics 21, 1–1.

Swanson-Hysell, N.L., Kilian, T.M., Hanson, R.E., 2015. A new grand mean palaeomagnetic pole for the 1.11 Ga Umkondo large igneous province with implications for palaeogeography and the geomagnetic field. Geophysical Supplements to the Monthly Notices of the Royal Astronomical Society 203, 2237–2247.

Swanson-Hysell, N.L., Ramezani, J., Fairchild, L.M., Rose, I.R., 2019. Failed rifting and fast drifting: Midcontinent rift development, Laurentia's rapid motion and the driver of Grenvillian orogenesis. Bulletin 131, 913–940.

Tapponnier, P., Peltzer, G.L.D.A.Y., Le Dain, A.Y., Armijo, R., Cobbold, P., 1982. Propagating extrusion tectonics in Asia: New insights from simple experiments with plasticine. Geology 10, 611–616.

Tapponnier, P., Peltzer, G., Armijo, R., 1986. On the mechanics of the collision between India and Asia. Geological Society, London, Special Publication 19, 113–157.

Terentiev, R.A., Santosh, M., 2020. Baltica (East European Craton) and Atlantica (Amazonian and West African Cratons) in the Proterozoic: The pre-Columbia connection. Earth-Science Reviews, 103378.

Tohver, E., Bettencourt, J.S., Tosdal, R., Mezger, K., Leite, W.B., Payolla, B.L., 2004. Terrane transfer during the Grenville orogeny: tracing the Amazonian ancestry of southern Appalachian basement through Pb and Nd isotopes. Earth and Planetary

Science Letters 228, 161–176.

Valley, J.W., 2003. Oxygen isotopes in zircon. Reviews in mineralogy and geochemistry 53, 343–385.

Valley, J.W., Lackey, J.S., Cavosie, A.J., Clechenko, C.C., Spicuzza, M.J., Basei, M.A.S., Bindeman, I.N., Ferreira, V.P., Sial, A.N., King, E.M., Peck, W.H., 2005. 4.4 billion years of crustal maturation: oxygen isotope ratios of magmatic zircon. Contributions to Mineralogy and Petrology 150, 561–580.

Waltenberg, K., Bodorkos, S., Armstrong, R., Fu, B., 2018. Mid-to lower-crustal architecture of the northern Lachlan and southern Thomson orogens: evidence from O–Hf isotopes. Australian Journal of Earth Sciences 65, 1009–1034.

Wang, R., Richards, J.P., Hou, Z.Q., An, F., Creaser, R.A., 2015. Zircon U–Pb age and Sr–Nd–Hf–O isotope geochemistry of the Paleocene–Eocene igneous rocks in western Gangdese: Evidence for the timing of Neo-Tethyan slab breakoff. Lithos 224, 179–194.

Wingate, M.T., Pisarevsky, S.A., Evans, D.A., 2002. Rodinia connections between Australia and Laurentia: no SWEAT, no AUSWUS? Terra Nova 14, 121–128.

Yao, J., Cawood, P.A., Shu, L., Zhao, G., 2019. Jiangnan Orogen, South China: A~ 970–820 Ma Rodinia margin accretionary belt. Earth-Science Reviews 196, 102872.

Scientific papers

Paper I

***Wang, C-C.**, Jacobs, J., Elburg, M.A., Läufer, A., Thomas, R.J., Elvevold, S., 2020. Grenville-age continental arc magmatism and crustal evolution in central Dronning Maud Land (East Antarctica): Zircon geochronological and Hf–O isotopic evidence. Gondwana Research 82, 108–127.*

Gondwana Research 82 (2020) 108–127

Contents lists available at ScienceDirect

Gondwana Research

journal homepage: www.elsevier.com/locate/gr

Grenville-age continental arc magmatism and crustal evolution in central Dronning Maud Land (East Antarctica): Zircon geochronological and Hf–O isotopic evidence

Cheng-Cheng Wang [a,*], Joachim Jacobs [a], Marlina A. Elburg [b], Andreas Läufer [c], Robert J. Thomas [d], Synnøve Elvevold [e]

[a] Department of Earth Science, University of Bergen, PB7803, N-5020 Bergen, Norway
[b] Department of Geology, University of Johannesburg, Auckland Park 2006, Johannesburg, South Africa
[c] Federal Institute for Geosciences and Natural Resources (BGR), Stilleweg 2, 30655 Hannover, Germany
[d] Council for Geoscience, 3 Oos Street, Bellville, 7535 Cape Town, South Africa
[e] Norwegian Polar Institute, N-9296 Tromsø, Norway

ARTICLE INFO

Article history:
Received 21 July 2019
Received in revised form 6 November 2019
Accepted 3 December 2019
Available online 10 January 2020

Handling Editor: T. Tsunogae

Keywords:
U-Pb-Hf-O
Maud Belt
Crustal evolution
Rodinia
Mesoproterozoic

ABSTRACT

This study focusses on the Grenville-age Maud Belt in Dronning Maud Land (DML), East Antarctica, which was located at the margin of the Proto-Kalahari Craton during the assembly of Rodinia. We present new U–Pb zircon ages and Hf–O isotope analyses of mafic and granitic gneisses exposed in the Orvin-Wohlthat Mountains and Gjelsvikfjella, central DML (cDML). The geochronological data indicate continuous magmatic activity from 1160 to 1070 Ma which culminated at 1110–1090 Ma, followed by high-grade metamorphism between 1080 and 1030 Ma. The majority of zircons from the Orvin-Wohlthat Mountains exhibit radiogenic Hf isotopic compositions corresponding to suprachondritic $\varepsilon_{Hf}(t)$ values and Mesoproterozoic model ages, indicating crystallization from predominantly juvenile magmas. However, the involvement of ancient sedimentary material, which were most likely derived from the adjacent Proto-Kalahari Craton, is revealed by a few samples with negative to neutral $\varepsilon_{Hf}(t)$ and significantly elevated $\delta^{18}O$ values (8–10‰). Samples from further west, in Gjelsvikfjella have more mantle-like zircon O isotopic compositions and late Paleoproterozoic Hf model ages, indicating the incorporation of ancient, previously mantle-derived continental crust. The rocks in cDML, thus define part of an extensive Mesoproterozoic magmatic arc with subduction under the Proto-Kalahari margin. This involved significant growth of new continental crust, possibly related to slab retreat, accompanied by subordinate recycling of older crustal components. The Maud Belt has previously been correlated with the 1250–1030 Ma Natal Belt in southern Africa, which lay to the west in the context of Gondwana, although this assertion has recently been questioned. Our study supports the latter view in demonstrating that the continental arc magmatism in the Maud Belt appears to be temporally and tectonically unconnected to the accretion of (slightly older) juvenile oceanic islands in the Natal Belt, which, in contrast to the Maud Belt, show subduction polarity away from the craton. We thus speculate that the Namaqua-Natal to Maud Belt contact (exposed in the Heimefront Shear Zone) may represent a changed tectonic environment from arc/continent-continent collision to slightly younger continental margin orogenesis at the westernmost termination of this part of the global Grenville Orogen. The Maud Belt marks the beginning of a major, long-lived accretionary Andean-type tectonic regime on the eastern margin of Proto-Kalahari in the Meso-Neoproterozoic during Rodinia assembly and break-up until the formation of Gondwana.

1. Introduction

Earth's Grenville-age orogenic belts record the assembly of the supercontinent Rodinia at the end of the Mesoproterozoic. This involved major accretionary and collisional events from 1245 Ma to 980 Ma and eventual tectonic stabilization of Rodinia after 1090 Ma (e.g. Li et al., 2008; Rivers, 2009; Hynes and Rivers, 2010; McLelland et al., 2010). The Grenville Orogen itself represents a major Himalaya-type collisional belt, mainly exposed along the eastern margin of North America (Laurentia). Although there is no consensus as to the restoration of the continental fragments enveloping Laurentia in reconstructed configurations of Rodinia (e.g. Weil et al., 1998; Dalziel et al., 2000; Pisarevsky et al., 2003; Torsvik, 2003; Li et al., 2008; Johansson, 2009;

* Corresponding author.
E-mail address: Cheng-Cheng.Wang@uib.no (C.-C. Wang).

https://doi.org/10.1016/j.gr.2019.12.004
1342-937X/

Merdith et al., 2017), combined geological and paleomagnetic data show that the collision counterparts of Laurentia may include Amazonia (Cawood and Pisarevsky, 2017), Rio de la Plata (Gaucher et al., 2011), Baltica (Bingen et al., 2008; Bingen and Viola, 2018) and Proto-Kalahari (Dalziel et al., 2000; Jacobs et al., 2003a, 2008b; Loewy et al., 2011; Swanson-Hysell et al., 2015). Whatever configuration holds true, following amalgamation, exterior ocean basins locally evolved into accretionary orogens around parts of the periphery of Rodinia (Murphy and Nance, 2005). The subduction and convergence of these encircling orogens may have triggered the development of rifting and break-up of Rodinia at 800–750 Ma (Cawood et al., 2016). Some of the rifted continental fragments subsequently collided along the East Africa-Antarctic Orogen (EAAO) to form Gondwana during Pan-African times between ~650 and 500 Ma (Stern, 1994; Jacobs and Thomas, 2004).

During the assembly of Rodinia, subduction zones with different subduction polarities developed at the periphery of the Proto-Kalahari Craton, giving rise to several tectonic subdomains within the larger Grenville Orogen (e.g. Thomas et al., 1994; Jacobs et al., 2008a; Oriolo and Becker, 2018), including the Namaqua-Natal Belt in southern Africa and the Maud Belt in East Antarctica (Fig. 1). The Natal Belt was formed by a long-term accretion of island arcs and final indentation of Proto-Kalahari into Laurentia (Jacobs et al., 1993, 2003a; Mendonidis and Thomas, 2019). The Maud Belt was initially regarded as the lateral continuation of the Namaqua-Natal Belt (Fig. 1a; e.g., Groenewald et al., 1995; Jacobs et al., 2003a). However, recent studies proposed that they appear to be distinct with respect to subduction polarity and the timing of tectono-thermal events (Bisnath et al., 2006; Grantham et al., 2011; Mendonidis et al., 2015). Thus, the orogenic history of the Maud Belt and its correlation with the Natal Belt, remains uncertain (Groenewald et al., 1995; Bauer et al., 2003a; Paulsson and Austrheim, 2003; Grosch et al., 2007, 2015; Marschall et al., 2013).

The nature and geodynamic evolution of an orogenic belt is reflected in its history of crustal growth and recycling. During continent-continent collisional orogenesis the dominant magmatism generally reworks older crust with only minor amounts of juvenile crust produced. By contrast, subduction-related orogenic systems (island arc accretion and continental arc) usually involve progressive addition of mantle-derived (juvenile) magmas during continuous subduction of oceanic slabs (Condie, 2005; Cawood et al., 2009; Collins et al., 2011; Ducea et al., 2015; Hagen-Peter and Cottle, 2017; Spencer et al., 2019). Lu–Hf and O isotopic tracing of zircon is a well-established and powerful tool to identify the juvenile and reworked components in magmatic systems (Valley, 2003; Hawkesworth and Kemp, 2006; Kemp et al., 2007). The Hf isotopic signature reflects the relative contributions of depleted mantle and recycled continental crust, which have differing Lu/Hf ratios, and thereby develop distinct $^{176}Hf/^{177}Hf$ ratios over time. The O isotopic composition of zircons crystallized from mantle and mantle-derived magmas is assumed to be uniform ($5.3 \pm 0.6‰$, 2σ; Valley et al., 1998). Any positive deviation of $\delta^{18}O$ value from this benchmark is interpreted to be caused by contamination by supracrustal material, which tends to have enriched heavy O isotope values. Accordingly, along with U–Pb dating, the Hf–O isotopic composition in zircon provides valuable information on crustal and mantle processes involved in the generation of source rocks and parent magmas.

The unravelling of the Grenville-age history of the Maud Belt is rendered extremely difficult due to later intense high-grade tectono-metamorphic overprinting in late Neoproterozoic/early Paleozoic ("Pan-African") times during Gondwana assembly (Fig. 1b). Because of this, previous studies have mainly focussed on this aspect of the Maud Belt. Consequently, geochronological and isotopic investigations that target the Grenville-age history are currently sparse and it is this gap in our knowledge that this paper seeks to redress, by focussing on a portion of the Maud Belt in central Dronning Maud Land (cDML, Fig. 2). In order to constrain the timing and source composition of Mesoproterozoic magmatism in cDML, an integrated zircon U–Pb dating and Hf–O isotopic study was conducted on a series of samples from the Orvin-Wohlthat Mountains and Gjelsvikfjella. The results allow us to evaluate the role of crustal growth and recycling, recognize and characterize the main Grenville-age orogenic events, and arrive at a better understanding of the geodynamic evolution of orogenic belts along the margin of the Proto-Kalahari Craton during the assembly of Rodinia.

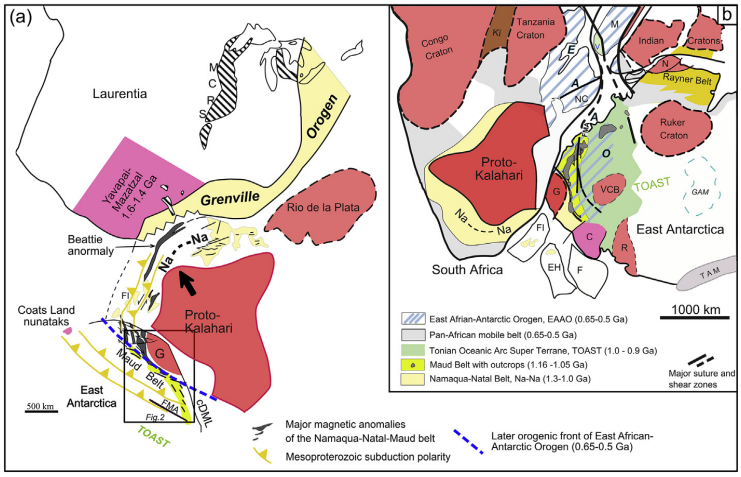

Fig. 1. (a) Reconstruction of the Maud and Namaqua-Natal belts along the Proto-Kalahari Craton with Laurentia in Rodinia, after Jacobs et al. (2003a). The Proto-Kalahari Craton is interpreted as an indenter into Laurentia to form the Namaqua-Natal Belt at ca. 1050 Ma. The Maud Belt was traditionally regarded as the natural continuation of the Namaqua-Natal Belt into East Antarctica (e.g., Groenewald et al., 1995; Bauer et al., 2003a, 2003b), but has later been interpreted as a slightly younger accreted arc terrane (e.g. Mendonidis et al., 2015). Location of Rio de la Plata is from Li et al. (2008). (b) Location of Dronning Maud Land (DML) in East Antarctica and the Namaqua-Natal Belt in South Africa in Gondwana (after Jacobs et al., 2015). Abbreviations: C, Coats Land; cDML, central Dronning Maud Land; EH, Ellsworth-Haag; F, Filchner Block; FI, Falkland Islands; FMA, Forster Magnetic Anomaly; G, Grunehogna Craton; GAM, Gamburtsev Mts.; Ki, Kibaran; M, Madagascar; MCRS, Mid Continental Rift System; N, Napier Complex; NC, Nampula Complex; NC, Na–Na, Namaqua-Natal Belt; R, Read Block; TAM, Transantarctic Mts.; V, Vohibori; VCB, Valkyrie Cratonic Block.

2. Geological background: the Maud Belt

DML in the South Atlantic-Indian Ocean sector of East Antarctica comprises three main geological domains: a) the Grunehogna Craton, which represents an Archaean fragment of the Proto-Kalahari Craton (Groenewald et al., 1995; Jones et al., 2003); b) the approximately 1000 km long Grenville-age (ca. 1100 Ma) Maud Belt that relates to the amalgamation of the supercontinent Rodinia, and c) the Tonian Oceanic Arc Super Terrane (TOAST) in south-eastern and eastern DML that probably evolved outside Rodinia and was only later amalgamated to East Antarctica during Gondwana assembly (Elburg et al., 2015; Jacobs et al., 2015, 2017) (Fig. 2). The use of the term "Proto-Kalahari Craton" in this paper follows the definition proposed by Jacobs et al. (2008a), referring to the Archean-Paleoproterozoic core before Mesoproterozoic accretion produced the (full) Kalahari Craton. The Maud Belt was first described by Groenewald et al. (1995), referring to a Mesoproterozoic orogenic mobile belt recognized at H.U. Sverdrupfjella, Kirwanveggen and Heimefrontfjella in western DML (Fig. 2). Similar Grenville-age rocks were subsequently identified across large parts of western and central DML including Gjelsvikfjella, the Mühlig-Hofmann-Gebirge and the Orvin-Wohlthat Mountains (Jacobs et al., 1998, 2003a, 2003b; Paulsson and Austrheim, 2003; Bisnath et al., 2006; Baba et al., 2015) (Fig. 2). The Ulvetanna Lineament separates Gjelsvikfella and the Mühlig-Hofmann-Gebirge in the west from the Orvin-Wohlthat mountains in the east (Fig. 2). The eastern extent of the Maud Belt (and easternmost Kalahari) coincides with the Forster Magnetic Anomaly (Fig. 2), east of which younger rocks (990–900 Ma) of the Tonian Oceanic Arc Super Terrane (TOAST) are juxtaposed (Jacobs et al., 2015, 2019).

The Maud Belt, together with the Namaqua-Natal Belt in southern Africa, the Nampula Complex in northern Mozambique, the Falkland microplate and the Haag Nunatak block, has been restored along the margin of the Kalahari Craton in Rodinia and Gondwana reconstructions (Fig. 1, Groenewald et al., 1995; Grantham et al., 1997; Thomas et al., 2000; Jacobs and Thomas, 2004; Manhica et al., 2001). The Namaqua-Natal-Maud belt was initially considered as a single continuous orogen, formed by the accretion of island arcs on to the margin of Proto-Kalahari during the assembly of Rodinia. Recently, however, the Natal-Maud correlation has been questioned. Bisnath et al. (2006) pointed out that the two areas appear to have different subduction polarities and independent tectonic histories until high-grade metamorphism affected both belts at 1090–1070 Ma. Mendonidis and Armstrong (2016) noted that the Natal Belt has a significantly older history (>ca. 1200 Ma) than most of the Maud Belt (ca. 1150 Ma). The exception to this is the granulite facies Vardeklettane Terrane in Heimefrontfjella, westernmost DML (Fig. 2, Bauer et al., 2003c, 2009), which, alone in East Antarctica, probably correlates with the Margate Terrane in Natal.

The tectonic boundary between the Vardeklettane Terrane (i.e. the Natal Belt) and the rest of the Maud Belt has been identified as the major Heimefront Shear Zone (Fig. 2, Jacobs et al., 1996; Golynsky and Jacobs, 2001). Furthermore, this structure forms the boundary between essentially pristine Mesoproterozoic crust in the west (Natal) and crust in the east (Maud) that was pervasively reworked in late Neoproterozoic-Cambrian times during the assembly of Gondwana. Thus, the Maud Belt can be defined as Stenian crust in DML with extensive late-Neoproterozoic/early Paleozoic reworking (Jacobs and Thomas, 2004), bounded in the west by the Heimefront Shear Zone and in the east by the major structure associated with the Forster Magnetic Anomaly (Fig. 2).

The basement rocks in the Maud Belt are dominated by Grenville-age (meta-) supracrustal and intrusive rocks formed from 1170 to 1090 Ma, followed by 1090–1050 Ma A-type granitic sheets and plutons (Arndt et al., 1991; Harris, 1999; Jackson, 1999; Bauer et al., 2003a, 2003b; Jacobs et al., 2003a, 2003b; Paulsson and Austrheim, 2003; Board et al., 2005; Bisnath et al., 2006; Grantham et al., 2011). The emplacement of these A-type intrusions was accompanied by amphibolite- to granulite-facies metamorphism, which has been recognized from various parts of the Maud Belt (Arndt et al., 1991; Harris, 1999; Jackson, 1999; Jacobs et al., 1998, 2003a; Board et al., 2005; Bisnath et al., 2006; Marschall et al., 2013). Syn-tectonic magmatism and metamorphism were linked to convergent tectonics related either to continent-continent and/or arc-continent collision. Pre-tectonic magmatic rocks emplaced between 1170 and 1120 Ma are composed of granitic gneisses and subordinate mafic rocks with a common geochemical affinity to subduction-related volcanic arc rocks (Jacobs et al., 1999; Paulsson and Austrheim, 2003; Bisnath et al., 2006; Grantham et al., 2011), of which 1140–1130 Ma banded felsic and mafic gneisses were interpreted as bimodal metavolcanic rocks (Grantham, 1992; Jacobs et al., 1998; Mikhalsky and Jacobs, 2004). Most of these rocks in

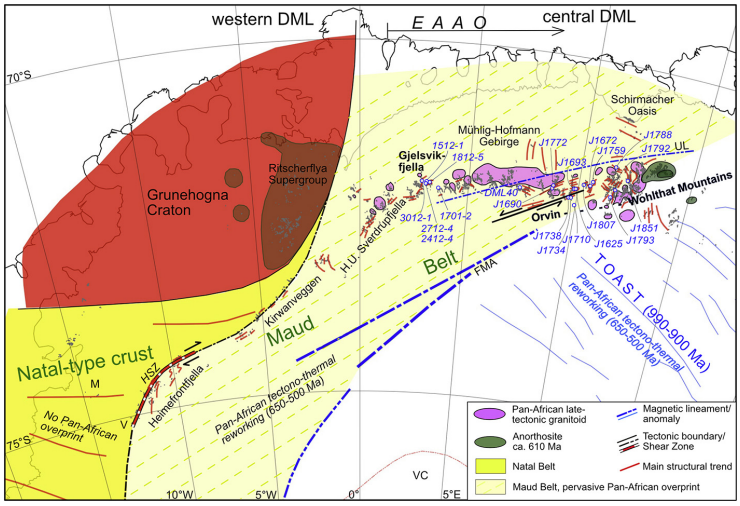

Fig. 2. Geological overview map of the study area and sample localities in the Orvin-Wohlthat Mountains and Gjelsvikfjella, cDML (cDML: from Gjelsvikfjella to Wohlthat mountains in this study). Abbreviations: FMA, Forster magnetic anomaly; HSZ, Heimefront Shear Zone; M, Mannefallknausane; TOAST, Tonian Oceanic Arc Super Terrane; UL, Ulvetanna Lineament; V, Vardeklettane Terrane.

Heimefrontfjella, Kirwanveggen and cDML have depleted Nd isotopic compositions with Mesoproterozoic to late Paleoproterozoic model ages (1.7–1.4 Ga), indicating a relatively juvenile source composition (Arndt et al., 1991; Moyes, 1993; Jacobs et al., 1998; Wareham et al., 1998; Harris, 1999; Grantham et al., 2001). However, Paleoproterozoic-Archaean Nd model ages from H.U. Sverdrupfjella and Heimefrontfjella imply the involvement of older crust in parts of the Maud Belt (Arndt et al., 1991; Wareham et al., 1998; Grosch et al., 2007). Whether these magmas were formed along the continental margin of Proto-Kalahari or in a Rodinia-distant oceanic arc, remains ambiguous and controversial (Arndt et al., 1991; Jacobs et al., 1993, 2008a; Groenewald et al., 1995; Bauer et al., 2003a; Paulsson and Austrheim, 2003; Mikhalsky and Jacobs, 2004; Grosch et al., 2007, 2015; Grantham et al., 2011). Some studies opine that the parts of the Maud Belt represent juvenile island arcs that accreted onto the Proto-Kalahari Craton margin (Groenewald et al., 1995; Bauer et al., 2003a; Grantham et al., 2011). In contrast, a continental arc setting has been supported by other studies (Frimmel, 2004; Bisnath et al., 2006; Grosch et al., 2007; Marschall et al., 2013).

Crustal components of 1.2–1.0 Ga are also preserved in the Grunehogna Craton in western DML to the northwest of the Maud Belt (Fig. 2). The late Mesoproterozoic Ritscherflya Supergroup comprises a sedimentary sequence recording the erosional remnants of Grenville-age rocks close-by (e.g. Marschall et al., 2013). The sedimentary rocks are intruded by (ultra-) mafic and felsic intrusions (Wolmarans and Kent, 1982; Krynauw et al., 1988), which were dated at ca. 1.1 Ga (Peters et al., 1991; Moyes et al., 1995; Hanson et al., 2004).

3. Samples and analytical methods

The samples for the present study were collected during three field seasons between 1995 and 2002 with the aim of elucidating the Mesoproterozoic history of this part of cDML. Because the rocks were subject to pervasive intense Neoproterozoic-Cambrian ("Pan-African") tectono-thermal reworking and magmatism, the sampling was focused on a variety of specific lithotypes (mainly orthogneisses of various compositions). Detailed structural and intrusive relations between the lithotypes cannot be ascertained because the original relationships are totally obscured by the intense, polyphase tectonism to which they were subjected some 500 Ma after their formation. The localities for the analysed samples are marked on Fig. 2. Fifteen samples from the Orvin-Wohlthat Mountains, including granitic and mafic gneisses as well as one paragneiss, were selected for SHRIMP U–Pb dating, Lu–Hf and O isotopic investigations. In addition, six samples from Gjelsvikfjella, some 200 km west of the Orvin-Wohlthat Mountains, which had previously been U–Pb zircon dated (Jacobs et al., 2003a, 2008b), were analysed for their Hf–O isotopic composition for comparison. Zircon concentrates, mount preparation, optical (reflected and transmitted light) and cathodoluminescence (CL) imaging were completed before analysis and guided the selection of the analysed spots. U–Pb, Lu–Hf and O isotopic analyses were performed on the same spot or from the same growth domain. In some cases, Lu–Hf analyses were not possible due to the necessity to use a large beam size (50 μm).

3.1. SHRIMP U–Pb dating

Twelve samples were analysed using the Sensitive High Resolution Ion Microprobe (SHRIMP) at the IBERSIMS laboratory, University of Granada, Spain and three samples (J1759, J1772, J1792) were analysed at the John de Laeter Centre, Curtin University, Australia. For details of methodology and analytical conditions see Supplementary file B of Jacobs et al. (2017) and Jacobs et al. (2008b), respectively. If common lead concentrations are low, we report uncorrected ages, otherwise we report common lead-corrected ages. Weighted mean ages and group concordant ages are calculated with Isoplot (Version 4.15; Ludwig, 2011). All errors are reported at the 2σ-level.

3.2. O-isotope system determination

Oxygen isotope ratios of zircon grains that were previously analysed for their U–Pb ages were measured using a CAMECA IMS-1280 instrument at the Swedish Museum of Natural History, Stockholm (Sweden), as well as at the IBERSIMS SHRIMP-IIe/mc facility in Granada (Spain). Prior to ion microprobe analysis, the U–Pb analysis spots were removed from the zircons by polishing followed by recoating with ~30 nm gold.

On the CAMECA IMS-1280, a Cs^+ primary ion beam of 5–7 nA was focused on a 20 μm diameter area. Analytical procedures and parameters follow the scheme of Nemchin et al. (2006). Each analysis involved a pre-sputtering time of 40 s to remove the Au layer, followed by automatic secondary beam alignment, entrance slit centring, and then 20 cycles of oxygen isotope analysis using a ca. 10 μm × 10 μm spot. A total of about 250 unknowns were analysed in six sessions. In each session, every set of six unknowns was bracketed by two analyses of reference material. Most data were normalized to zircon 91500 assuming a $\delta^{18}O$ value of 9.86‰ (SMOW, Wiedenbeck et al., 2004) and Temora-2 was used for data normalization in minor sessions assuming a $\delta^{18}O$ value of 8.20‰ (Black et al., 2004). Small linear-drift corrections were applied to partial data sets. All internal errors and external uncertainty in the standard analyses are propagated.

Three samples (J1690, J1693, J1851) were analysed on the IBERSIMS SHRIMP_IIe/mc, following the procedure as described in Montero et al. (2017): the SHRIMP primary ion optics was set with a 120 μm Kohler aperture to produce a ~18 μm diameter spot on the mount surface. The Cs gun was set to yield a ~8 nA Cs^+ beam. The e-gun to neutralize Cs ions on non-conductive material was set to an intensity of about 1 μA. Spots to be analysed were pre-sputtered for about 5 min before measurements. During this time, the secondary beam and the e-gun were fully optimized to maximize the ^{16}O signal. Measurements were done in 2 sets of 10 scans each. The scans were of 10 s each so that the total data collection time was 200 s per spot. The electron-induced secondary ion emission background was recorded during 10 s before and after each set and subtracted from the ^{18}O and ^{16}O counts. Temora-2 was used as the standard, with zircon measured every four unknowns and cross-checked against the 91,500 zircon every 20 unknowns. The reproducibility of the standards was excellent: $\delta\ ^{18}O = 8.17 \pm 0.34$ (2SD) for the TEMORA and $\delta\ ^{18}O = 9.98 \pm 0.26$ (2SD) for the 91500 respectively. Data reduction was done with the POXY program developed by P. Lanc and P. Holden at the Australian National University.

3.3. Lu–Hf isotope system determination

Lu–Hf isotopes were measured at the University of Johannesburg, using an ASI Resonetics 193 nm Excimer laser ablation system coupled to a Nu Plasma II multi-collector ICPMS. Ablations were done using a 50–70 μm diameter spot, at an ablation rate of 7 Hz and an energy density of 6 J/cm^2. Prior to ablation the area was cleaned with two laser shots, and after 10 s of decay time, the background was measured for 25 s. The signal was collected for 75 s during ablation. During the analytical session, accuracy and external reproducibility of the method was verified by repeated analyses of reference zircon Mud Tank, Temora2 and LV-11, which yielded $^{176}Hf/^{177}Hf$ of 0.282490 ± 0.000036 (2SD, n = 56), 0.282684 ± 0.000054 (2SD, n = 59), and 0.282845 ± 0.000076 (2SD, n = 46), respectively. These ratios are well within the zircon reference data from Woodhead and Hergt (2005) and Heinonen et al. (2010).

For calculation of the epsilon Hf, the chondritic uniform reservoir (CHUR) was used as recommended by Bouvier et al. (2008); $^{176}Lu/^{177}Hf$ and $^{176}Hf/^{177}Hf$ of 0.0336 and 0.282785, respectively), and a decay constant of 1.867×10^{-11} (Scherer et al., 2001; Söderlund et al., 2004). Calculation of model ages is based on the depleted mantle source values of Griffin et al. (2000) with present-day $^{176}Hf/^{177}Hf = 0.28325$ and $^{176}Lu/^{177}Hf = 0.0384$. For granitic samples, the model

ages are calculated using $^{176}Lu/^{177}Hf = 0.015$ for the average continental crust, while a ratio of 0.022 (Amelin et al., 1999) is used for two mafic samples (J1625, J1759). Initial $^{176}Hf/^{177}Hf$ and epsilon Hf for all analysed zircon domains were calculated using the respective interpreted crystallization age of each sample. The values of average ε_{Hf} (t) and $^{176}Hf/^{177}Hf_{(i)}$ for each sample are reported as mean ± 1SD.

4. Results

All U–Pb data and Hf–O isotopic results are presented in Supplementary files A and B respectively. Following, the (meta-)igneous samples from the Orvin-Wohlthat Mountains are ordered from old to young and the last one is a paragneiss sample.

4.1. U–Pb zircon geochronology and Hf–O isotopic composition of samples from the Orvin-Wohlthat Mountains

4.1.1. J1625 mafic gneiss (location coordinates: −71.859678; 9.905846)

Zircon grains in this sample are subhedral to anhedral, rounded, stubby or irregular, clear to light brown, 100–150 μm in size with aspect ratios of up to 3 (Fig. 3). CL images show frequent core – mantle structures reflected by a medium-CL core with oscillatory or weak sector zoning and a CL-dark mantle. Besides, a few stubby to slightly elongated zircons appear entirely CL-dark and structureless, with U contents up to 20,000 ppm. Thirty-eight analyses were conducted on 34 grains, targeting all zircon domain-types. Zoned cores were analysed on 23 grains, most with typical Th/U ratios of 0.30–0.60. The 9 oldest analyses form an age group with a concordia age of 1152 ± 7 Ma (MSWD = 1.4), which is interpreted as the crystallization age of the igneous protolith. The remaining 14 analyses are discordant possibly due to recent and ancient Pb-loss. Fifteen analyses on rims and structureless domains commonly have high to very high U concentrations (1500–20,000 ppm) with Th/U ratios of 0.07–0.30, typical of metamorphic zircons. A few of them (e.g. 8.1, 9.1, 28.1, 29.1) with high U contents and low Th/U ratios (0.07–0.28) are concordant at ca. 1083 Ma. This age group documents the Grenville-age metamorphism in this area. Seven analyses on high-U zircon areas and rims have $^{206}Pb/^{238}U$ ages ranging from 460 to 540 Ma (Fig. 4a), representing a later early Paleozoic tectono-metamorphic overprint.

Lu–Hf and O isotope analyses were conducted on thirteen Grenville-age igneous grains. Except for one outlier with a significantly high ε_{Hf} (t) value (+15.3), which could represent accidental ablation of a Pan-African-aged domain at depth, the rest show ε_{Hf} (t) values ranging from +2.6 to +7.9 (Fig. 5a) with an average of +4.8 ± 1.8 ($^{176}Hf/^{177}Hf_{(i)} = 0.28218 \pm 0.00005$), corresponding to a two-stage model age of 2.06–1.69 Ga. $\delta^{18}O$ values range from 4.5 to 6.6‰ with an average of 5.5 ± 0.6‰ (Fig. 6a).

4.1.2. J1772 migmatitic biotite gneiss (−71.889882; 8.835805)

Zircon grains are mostly euhedral to subhedral, stubby to long prismatic, clear to light brown with abundant fractures, 50–300 μm in length with aspect ratios up to 5. In CL images, most zircons exhibit core–rim structures, characterized by oscillatory zoning in the cores and thin, weakly or strongly luminescent rims. However, the oscillatory zones in some cores have been thickened, blurred, and even entirely homogenized due to Grenville-aged and/or Pan-African alteration. Sixteen core analyses with varied CL characteristics show U abundances of 170–1500 ppm and Th of 60–350 ppm, with Th/U ratios of 0.06–0.82. One grain (16.1) gives an age of ca. 1800 Ma and one grain (7.1) is excluded because it is strongly reversely discordant. The remaining 14 analyses define a discordia line with an upper intercept at ca. 1140 Ma and a lower intercept at ca. 510 Ma (Fig. 4b). The former is interpreted as an approximate crystallization age of an igneous protolith, whereas the latter represents the timing of Pan-African metamorphism.

Lu–Hf isotopic analyses were completed on fourteen grains with different degrees of Pb-loss, but $^{176}Hf/^{177}Hf$ and Lu/Hf ratios are uncorrelated with Th, U contents and age, indicating a possible resistance of Hf isotopic composition during subsequent metamorphism. Three analyses yield significantly positive ε_{Hf} (t) values between +5.3 and + 9.6 (Fig. 5a), and the remaining 11 analyses define a uniform isotopic composition with ε_{Hf} (t) values from +0.9 to +3.6 ($^{176}Hf/^{177}Hf_{(i)} = 0.28217 \pm 0.00003$) and model ages of 1.89–1.72 Ga.

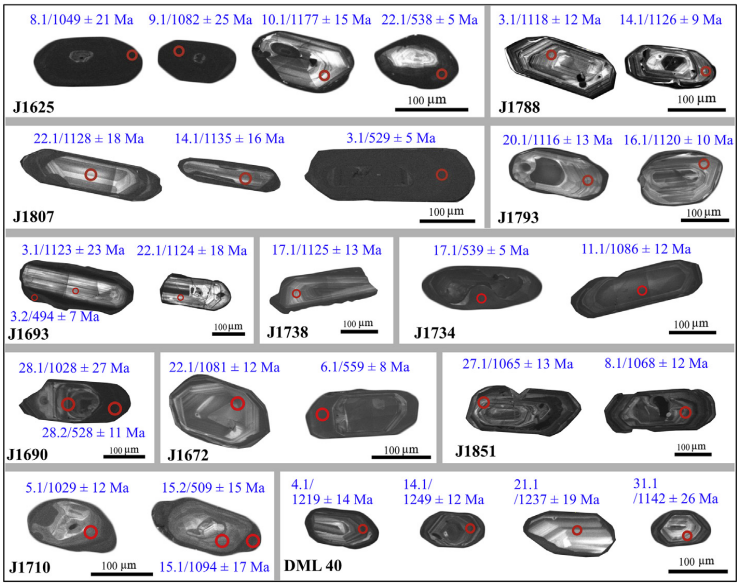

Fig. 3. Representative CL images with $^{206}Pb/^{238}U$ ages of zircons from the Orvin-Wohlthat Mountains.

4.1.3. J1807 granitic orthogneiss (−71.784806, 10.234231)

Zircons are subhedral and elongated, composed of a relatively bright core with oscillatory zoning and structureless rims significantly dark in CL images (Fig. 3). Twenty-eight analyses were obtained on 22 rims and 6 cores. The core and rim domains show distinct difference in U concentration and Th/U ratio; the U content of the cores is generally below 500 ppm and Th/U ratio ranges from 0.19–0.36, while the rims have U contents of several thousand ppm and Th/U ratio between 0.01 and 0.13. ^{208}Pb-corrected isotopic ratios were used to calculate for rim areas while no correction was necessary for the core analyses. Six core analyses show significant scatter due to Pb-loss. The 3 most concordant cores provide a concordia age of 1130 ± 11 Ma (MSWD = 1.03), which is interpreted to represent the crystallization age of the igneous protolith. The rim analyses give two age populations, 20 of which define a well-constrained concordia age of 526 ± 3 Ma (MSWD = 1.17), while the other 2 are (nearly) concordant at ca. 580 Ma (Fig. 4d). They are interpreted to record the timing of multiple high-grade metamorphic overprint.

4.1.4. J1788 granitic orthogneiss (−71.457797; 11.544662)

Zircons in this sample are euhedral to subhedral, slightly rounded, up to 150 μm in length with aspect ratios of 2 to 3. In CL images, the main portions of the zircons appear oscillatory zoned (Fig. 3) and a few grains have metamict cores. Many zircons have thin CL-bright rims, though too thin to be analysed. Twenty analyses were performed on oscillatory- and band-zoned domains, which are characterized by relatively uniform Th/U ratios of 0.3–0.5 with Th = 50–310 ppm and U = 180–800 ppm. Twelve analyses yield a concordia age of 1128 ± 5 Ma (MSWD = 1.4), interpreted as the crystallization age of the igneous protolith. The remaining 9 discordant analyses are affected by recent Pb-loss (Fig. 4c).

Ten ε_{Hf} (t) values range from 5.5 to 6.7 (Fig. 5a) with an average of +6.0 ± 0.4 ($^{176}Hf/^{177}Hf_{(i)}$ = 0.28224 ± 0.00001), corresponding to a two-stage model age of 1.59–1.52 Ga. δ^{18}O values range from 6.3 to 7.4‰ with an average of 7.0 ± 0.3‰ (Fig. 6b).

4.1.5. J1793 tonalitic gneiss (−71.916417; 11.559102)

This sample contains zircon grains that are euhedral to subhedral, transparent, bright and clear, up to 200 μm long with aspect ratios of 2–3. In CL images, zircons show bright to medium oscillatory zoned cores with or without dark unzoned rims which are mostly too thin to be analysed (Fig. 3). Thirty analyses were carried out on 28 cores and 2 rims. The zircons contain very little common Pb. The Th/U ratios of the cores range between 0.29 and 0.68, with Th = 60–250 ppm and U = 150–980 ppm. A concordia age of 1118 ± 3 Ma (MSWD = 1.3) is calculated from 17 core analyses, whilst a few other core analyses showed slight signs of Pb-loss and were excluded from the age calculation (Fig. 4e). One of the analysed rims is discordant but has a similar Mesoproterozoic age as the cores (Th/U = 0.26), and may be of metamorphic origin. The other rim analysis (Th/U = 0.01) plots on the concordia curve at ca. 566 Ma. The core analyses are interpreted as the crystallization age of the igneous protolith, whereas the one younger rim analysis represents metamorphic overprint.

Twelve isotopic analyses on concordant igneous domains define a population with a homogeneous Hf–O isotopic composition. ε_{Hf} (t) values range from +6.3 to +7.9 (Fig. 5a) with an average of +7.1 ± 0.5 ($^{176}Hf/^{177}Hf_{(i)}$ = 0.28228 ± 0.00001), corresponding to two-stage model ages of 1.53–1.43 Ga. Their δ^{18}O values range from 6.1–6.9‰ with an average of 6.5 ± 0.2‰ (Fig. 6c).

4.1.6. J1693 granitic orthogneiss (−71.846046; 9.885719)

Zircon grains are euhedral to subhedral, equant to elongated with aspect ratios of 2–3, clear to light brown and 150–300 μm long. In CL images, many zircons show oscillatory zoned cores that are surrounded by rims (Fig. 3). A few individual zircons are completely CL-dark and structureless. The zircons were analysed in 27 spots, including 20 oscillatory zoned cores and in 7 CL-dark structureless domains. The core analyses show a significant scatter and are in part discordant. The 8 most concordant analyses yield a concordia age of 1108 ± 10 Ma (MSWD = 1.3). Of the 7 rim analyses, two are discordant and the remaining 5 analyses provide a concordia age of 500 ± 4 Ma (MSWD = 0.87) (Fig. 4f). The age of ca. 1108 Ma is the best estimate for the crystallization age of the igneous protolith, whilst the rim analyses of ca. 500 Ma are interpreted as the timing of a metamorphic overprint.

Fourteen Lu–Hf isotopic analyses have been conducted on 14 concordant or nearly concordant igneous domains. Except one with inclusions, the remaining 13 analyses range in ε_{Hf} (t) from 1.1 to 5.5 (Fig. 5a) with an average of +2.7 ± 1.2 ($^{176}Hf/^{177}Hf_{(i)}$ = 0.28216 ± 0.00004), corresponding to two-stage model ages of 1.85–1.58 Ga. O isotope analyses yield δ^{18}O values ranging from 5.7 to 8.0 (mean = 7.1 ± 0.7‰, Fig. 6d).

4.1.7. J1738 garnet-biotite orthogneiss (−71.976795 l; 9.692059)

Zircons are subhedral to anhedral mostly with rounded terminations, clear to bright brown and 150–300 μm in length with aspect ratios up to 3. They are generally medium to dark in CL, with weak oscillatory zoning overprinted by thin dark rims (Fig. 3). Twenty-two analyses were performed on 21 oscillatory zoned cores and one rim. The Th/U ratio of the cores range between 0.04 and 0.54 (Th = 25–180 ppm, U = 90–1660 ppm) and the rim has a Th/U ratio of 0.01. Five of the oscillatory zoned cores give a concordia age of 1107 ± 8 Ma (MSWD = 1.3), whilst the other analyses are discordant due to recent and Pan-African Pb-loss (Fig. 4g). The age of 1107 ± 8 Ma is interpreted to represent the igneous crystallization age of the granite protolith. Metamorphic overprint is evident from one rim analysis at ca. 560 Ma.

4.1.8. J1734 garnet-biotite orthogneiss (−71.972900; 9.765919)

Zircon grains are subhedral to anhedral, with rounded terminations, light brown to clear, 150–450 μm long with aspect ratios generally between 2 and 3 but sometimes up to 7 (Fig. 3). Although many of the grains are dark in CL, oscillatory zoning can be observed. Many of the grains have a thin dark rim, but in most cases, they are too thin to be analysed. Twenty-three zircon grains were analysed, of which 22 are cores and one rim. The core analyses have Th/U ratios ranging from 0.03 to 0.87, with Th and U of 30–290 ppm and 340–2200 ppm respectively, and the rim analysis has a Th/U ratio of 0.01. Twelve of the oscillatory zoned cores give a concordia age of 1102 ± 4 Ma (MSWD = 1.12), whilst the others show signs of recent Pb-loss. The only one rim analysis is nearly concordant and gives an age of ca. 540 Ma (Fig. 4h). The concordia age of 1102 ± 4 Ma is interpreted to represent the crystallization age of the igneous protolith with the younger rim analysis attributed to later metamorphism.

Lu–Hf isotope analyses were conducted on 16 concordant or nearly concordant magmatic domains. ε_{Hf} (t) values are between −0.2–+2.4 (Fig. 5a) with an average of +1.2 ± 0.7 ($^{176}Hf/^{177}Hf_{(i)}$ = 0.28212 ± 0.00002), corresponding to two-stage model ages of 1.92–1.76 Ga. Fifteen δ^{18}O values range from 7.8 to 9.5‰ with an average of 8.5 ± 0.5‰ (Fig. 6h).

4.1.9. J1792 granitic orthogneiss (−71.772930; 11.692213)

Zircon grains are mostly subhedral to anhedral with elongate or equant morphologies, yellowish and small (30–120 μm long) with aspect ratios of 1.5–2. In CL images, most of them are characterized by weakly-luminescent oscillatory zoning. A few grains show resorption and a thin, moderately-strongly luminescent overgrowth. Fifteen analyses were performed on zircon cores. These domains have relatively low U (150–750 ppm) and Th (70–340 ppm) contents, with Th/U ratios of 0.12–0.78. Four analyses have been excluded: two with high common

lead (3.1, 8.1) and two that are significantly reversely discordant (10.1, 13.1). Ten of the remaining 11 analyses define a concordia age of 1100 ± 5 Ma (MSWD = 1.3) (Fig. 4i).

Lu–Hf and O isotope analyses were conducted on twelve igneous zircons. Except one Hf analysis with an unusually high ε_{Hf} (t) value at +11.7, the others range in ε_{Hf} (t) from +6.5 to +8.4 (Fig. 5a) with an average of +7.2 ± 0.9 ($^{176}Hf/^{177}Hf_{(i)}$ = 0.28230 ± 0.00003), corresponding to two-stage model ages of 1.53–1.42 Ga. $\delta^{18}O$ values range from 5.7‰ to 7.2‰ with an average of 6.1 ± 0.4‰ (Fig. 6e).

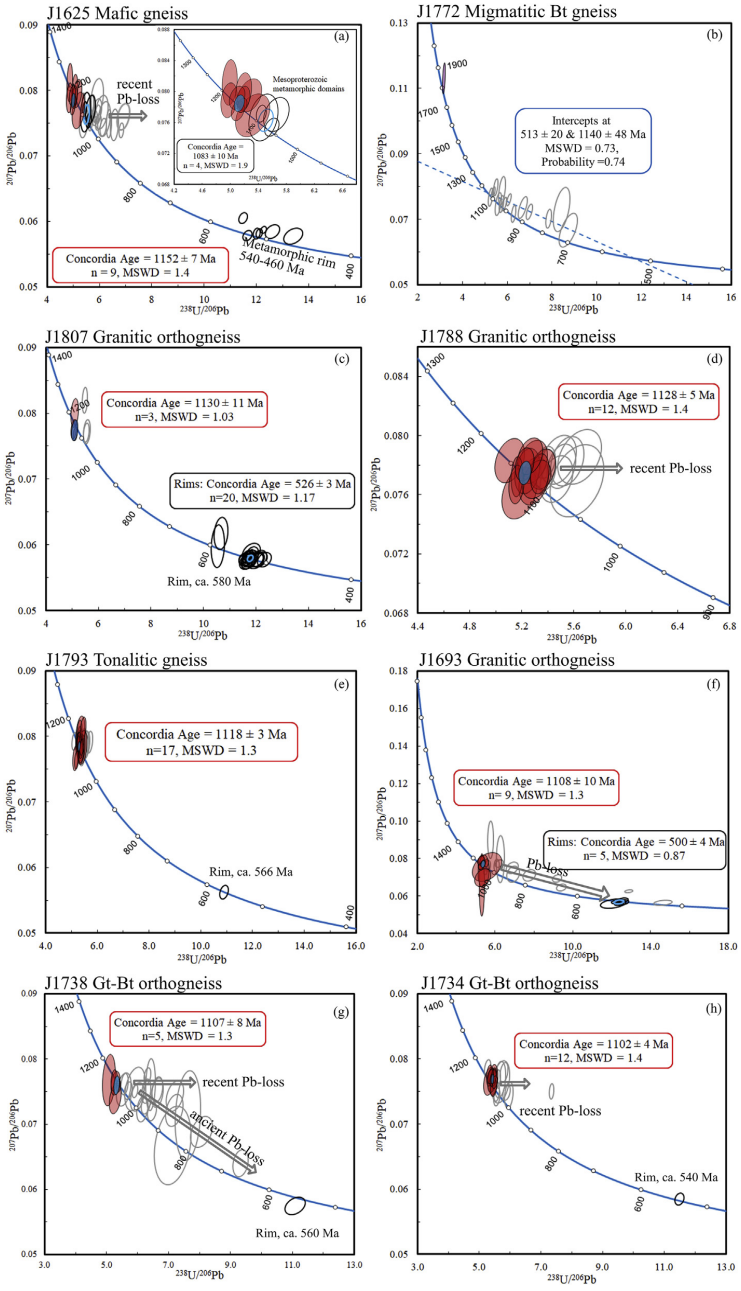

Fig. 4. U–Pb zircon geochronology of samples from Orvin-Wohlthat Mountains. Purple: inherited zircons and detrital zircons in DML 40; Red: Grenville-age concordant igneous zircons with concordia ellipse (blue); Black: Grenville-age and Pan-African metamorphic zircons; Grey: discordant zircon. Error ellipses shown at 2σ level.

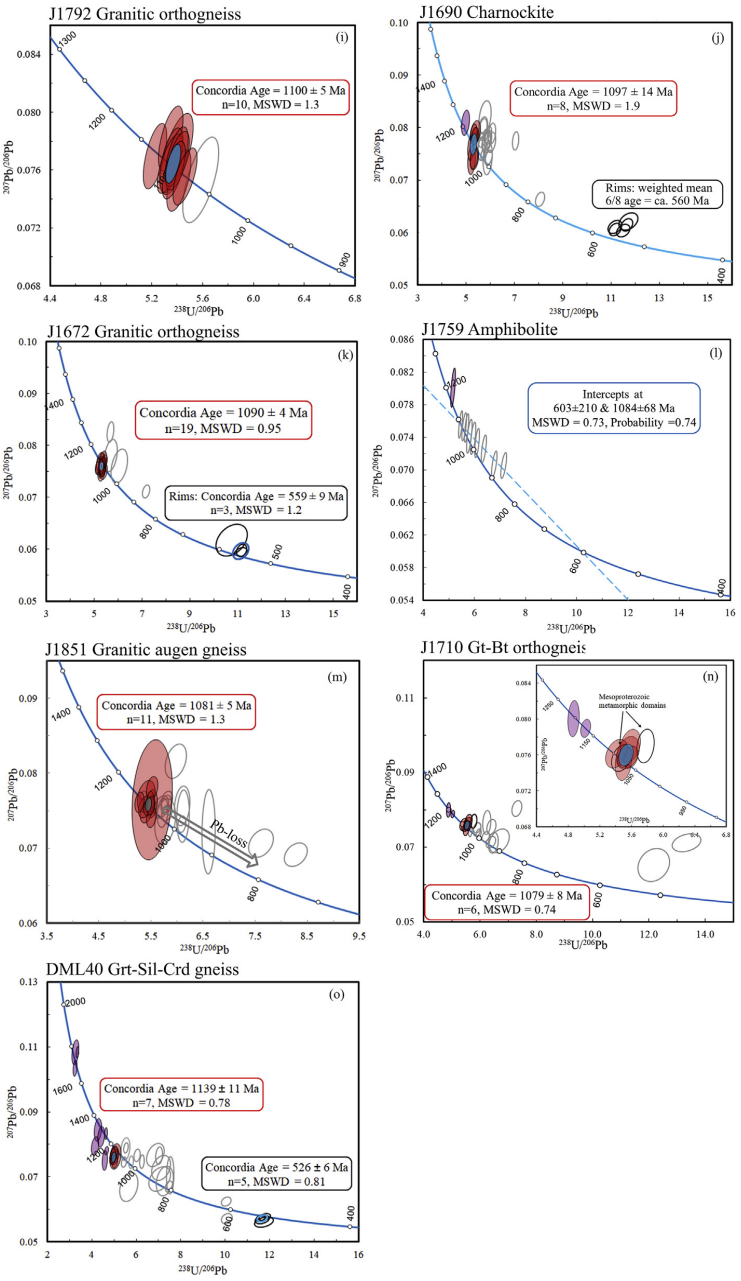

Fig. 4 (*continued*).

4.1.10. J1690 charnockite (−71.922297; 8.768715)

Zircon grains are subhedral, elongated, clear, 200–600 μm long with aspect ratios up to 4. In CL images, zircons show oscillatory zoning of inclusion-rich cores that are surrounded by mostly structureless dark rims (Fig. 3). Twenty-seven cores and 5 rims were analysed. Twenty-seven core analyses, including one potential inherited zircon at ca. 1200 Ma, show a scatter due to Pb-loss in some analyses. The 8 most concordant cores provide a concordia age of 1097 ± 14 Ma (MSWD = 1.9). Five rim analyses are all slightly discordant and have a weighted mean $^{206}Pb/^{238}U$ age of ca. 560 Ma (Fig. 4j). The former age is interpreted as

the crystallization age of the igneous protolith, whilst the latter is interpreted to represent the age of charnockitisation.

Lu–Hf isotopic analyses were conducted on 13 igneous domains. Two analyses with higher ε_{Hf} (t) values, possibly due to a mixture of core and rim domains, have been excluded from the data-averages. The remaining 11 ε_{Hf} (t) values vary from +4.1 to +6.7 (Fig. 5a) with an average of +5.0 ± 0.8 ($^{176}Hf/^{177}Hf_{(i)}$ = 0.28223 ± 0.00002), corresponding to two-stage model ages of 1.67–1.50 Ga. O isotopic analyses have a $\delta^{18}O$ value from 5.3‰ to 7.1‰ with an average value of 6.6 ± 0.5‰ (Fig. 6f).

4.1.11. J1672 granitic orthogneiss (−71.778109; 10.553229)

Zircons are subhedral to anhedral with rounded terminations, up to 300 μm long, with aspect ratios of 2–3. Many of the zircons show oscillatory zoning with thin, dark, structureless rims that were mostly too thin to be analysed (Fig. 3). Twenty-six zircon domains were analysed, including 21 zoned grains and 5 rims. The rims have a Th/U ratio ranging from 0.005 to 0.26, and the cores have Th/U ranging from 0.19 to 0.65 with Th = 35–510 ppm and U = 100–800 ppm. Nineteen analyses of oscillatory zoned cores give a concordia age of 1090 ± 4 Ma (MSWD = 0.95). The other 2 core analyses show Pb-loss, and/or have high analytical error. Three rim analyses yield a concordia age at ca. 560 Ma (Fig. 4k). The age of ca. 1090 Ma is interpreted as the crystallization age of the igneous protolith and the rim analyses of ca. 560 Ma are regarded as the time of metamorphic overprint.

Lu–Hf and O isotope analyses were conducted on fifteen concordant igneous domains. One Hf analysis yielded an aberrantly high ε_{Hf} (t) value at +11.0, whilst the other values range from +6.3 to +8.4 (Fig. 5a) with an average of +7.4 ± 0.6 ($^{176}Hf/^{177}Hf_{(i)}$ = 0.28230 ± 0.00002), corresponding to two-stage model ages of 1.51–1.38 Ga. $\delta^{18}O$ values range from 6.7 to 7.9‰ with an average of 7.1 ± 0.3‰ (Fig. 6g).

4.1.12. J1759 amphibolite (−71.722712; 10.629123)

Zircon grains are stubby to short prismatic, clear to light brown, with lengths of 50–300 μm and aspect ratios of 1.5–3. Most zircons display core-rim structures. The former are CL-dark and either show no zoning, sector zoning or oscillatory zoning and the rims are CL-bright and structureless. A few grains are distinctly highly luminescent with dark thin rims. Eleven grains were analysed, 9 of which are from the low-luminescent domains with high U concentrations (570–1640 ppm) and Th/U ratios of 0.14–0.46. Most analyses are discordant and plot on a discordia line, with a poorly-defined upper intercept at 1084 ± 68 Ma (MSWD = 0.73, Probability = .74) and a lower intercept at ca. 600 Ma (Fig. 4l). The upper intercept at ca. 1084 Ma is interpreted as being close to the crystallization age of the igneous protolith, whilst the lower intercept is probably related to metamorphic overprint and the time of Pb-loss. The remaining two zircon domains with high luminescence (10.1, 11.1) have much lower U-concentrations (250–280 ppm) and higher Th/U ratios of 0.62–0.83. One of them is highly discordant and thus excluded from the calculation. The other one gave an older age of ca. 1.2 Ga, which may represent an inherited domain.

Lu–Hf isotopic analyses have been done on twelve igneous grains with different degrees of Pb-loss. They display a spread in Hf isotopic composition, with ε_{Hf} (t) values ranging from +5.1 to +12.1 (Fig. 5a, $^{176}Hf/^{177}Hf_{(i)}$ = 0.28224–0.28244) and two-stage model ages from 1.79 to 1.17 Ga.

4.1.13. J1851 granitic augen gneiss (−71.574047; 12.146767)

The sample contains euhedral to subhedral, clear to light brown zircons, 200–400 μm long with aspect ratios up to 5. In CL images, most grains appear bright with oscillatory growth zoning (Fig. 3). Some have minor, dark rims that were too thin to be analysed. Twenty-seven spots were analysed, all from the oscillatory zoned cores. The analyses show a significant scatter due to Pb-loss. Two analyses, including one with a large error (15.1) and the other with high discordance (7.1), are excluded from plotting. The most concordant analyses provide a well-constrained concordia age of 1081 ± 5 Ma (MSWD = 1.3, n = 11, Fig. 4m). This age is interpreted as the igneous crystallization age of the igneous protolith.

Fifteen O isotopic analyses on igneous domains have a $\delta^{18}O$ value from 8.3‰ to 9.5‰ with an average value of 8.9 ± 0.4‰ (Fig. 6j). The ε_{Hf} (t) values range from +4.5 to +7.1 (Fig. 5a) with an average of +5.8 ± 0.9 ($^{176}Hf/^{177}Hf_{(i)}$ = 0.28226 ± 0.00002), corresponding to two-stage model ages of 1.62–1.46 Ga.

4.1.14. J1710 garnet-biotite orthogneiss (−72.143052; 10.013868)

Zircon grains are anhedral, stubby to elongate and clear to brownish. Some grains are cracked and many have inclusions. Many zircons have clear core-mantle structures. In CL images, zircons show mostly oscillatory zoned cores with moderate CL response. The cores have CL-dark, structureless rims, often thick enough at their tips to be analysed (Fig. 3). Few zircons are composed of oscillatory zoned cores, CL-moderate mantles and dark rims (Fig. 3). Twenty-five spots were analysed on 18 cores, one mantle and 6 rims. Most core analyses have Th/U ratios ranging from 0.18 to 0.86, whilst most rim domains have very high U concentrations up to 6600 ppm with typical Th/U ratios below 0.1. Of the 18 core analyses two inherited zircon domains plot on the concordia curve at ca. 1200 Ma, and 6 analyses form a uniform age group with a concordia age of 1079 ± 8 Ma (MSWD = 0.74) (Fig. 4n). Some zircon cores appear to have recrystallized to some extent to have a low Th/U ratio (< 0.2). The core analyses of ca. 1079 Ma are interpreted as the best estimate for the crystallization age of the granitic protolith. A mantle and a rim domain yield ages of ca. 1030 Ma and ca. 1080 Ma respectively, which are regarded as the timing of a subsequent metamorphic event. Furthermore, the 1000–900 Ma and 500 Ma discordant zircons may record evidence of multistage metamorphism in early Tonian and Cambrian times.

Lu–Hf and O isotope analyses were performed on eleven concordant or nearly concordant grains. $\delta^{18}O$ values range from 7.7 to 10.0‰ with an average of 9.0 ± 0.8‰ (Fig. 6i), and ε_{Hf} (t) value from −2.8 to +1.1 (Fig. 5a) with an average of −0.4 ± 1.1 ($^{176}Hf/^{177}Hf_{(i)}$ = 0.28209 ± 0.00003), corresponding to two-stage model ages of 2.07–1.82 Ga.

4.1.15. DML 40 garnet-sillimanite-cordierite gneiss (metapelitic paragneiss) (−71.965033, 7.367933)

This is the only meta-sedimentary sample of this study. It is a garnet-sillimanite-cordierite gneiss with melanocratic layers alternating with layers of leucosome. Zircon grains are subhedral, short columnar with a maximum length of ca. 200 μm. CL images of most zircons show oscillatory zoned cores surrounded by dark, unzoned rims (Fig. 3). Twenty-three analyses were conducted on core domains, which have high Th/U ratios ranging from 0.16 to 0.89. Seven of them yield a concordant age at 1139 ± 11 Ma (MSWD = 0.78), 3 grains were dated at ca. 1750 Ma, and 6 have Mesoproterozoic (Ectasian) ages of 1320–1200 Ma. Other analyses on cores are discordant because of Pb-loss (Fig. 4o). Fourteen analyses were performed on rim domains. Low Th/U ratios (0.01–0.16) with Th = 4–161 ppm and U = 344–2193 ppm may indicate a metamorphic origin. The 5 youngest rim analyses form a well-constrained age group with a concordia age of 526 ± 6 Ma (MSWD = 0.81). The other rim analyses are discordant with an age of 850–800 Ma and ca. 610 Ma (Fig. 4o).

The core age spectrum from ca. 1770–1220 Ma represents detrital zircon components from the Paleoproterozoic to Ectasian sources. The youngest concordant detrital ages are ca. 1140 Ma and likely represent the maximum depositional age of the sedimentary protolith, coinciding with the older age spectrum of igneous rocks in this study. The rim age of 526 ± 6 Ma is interpreted to represent crystallization of anatectic melt during cooling from peak temperatures.

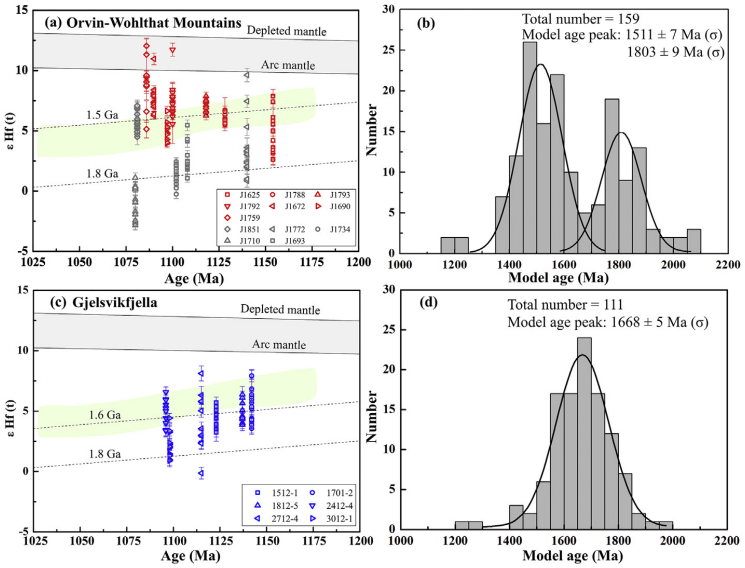

Fig. 5. Time versus $\varepsilon_{Hf}(t)$ plot and histograms of zircon Hf model ages from the Orvin-Wohlthat Mountains (a, b) and Gjelsvikfjella (c, d). The evolution curve of arc mantle is from Dhuime et al. (2011). The light green range is composed of samples from the Natal Belt (Spencer et al., 2015). Samples from the Orvin-Wohlthat Mountains with moderate $\delta^{18}O$ values (5.5–7.1‰) and juvenile Hf isotopic compositions are marked in red; the dark grey samples have evolved Hf and/or elevated O isotopic composition (a). These samples display two model age peaks at the Meso- and Paleoproterozoic times respectively (b). The Gjelsvikfjella samples have more evolved Hf isotopic composition than juvenile samples from the Orvin-Wohlthat Mountains with a cluster of model ages in late Paleoproterozoic times (c, d). Evolution curves of continental crust are calculated by assuming a $^{176}Lu/^{177}Hf$ ratio of 0.015.

4.2. Hf–O isotopic signature of samples from Gjelsvikfjella

Six granitic gneiss samples that had been U–Pb zircon dated previously (Jacobs et al., 2003a, 2008b) were analysed for their Hf–O isotopic compositions (Table 1, Figs. 5c–d and 7). Despite a broad spread in Hf isotopic composition observed in several samples, the two-stage Hf model ages cluster between 1.75 and 1.55 Ga with a peak at 1.67 Ga (Fig. 5d), which are distinct from those of the Orvin-Wohlthat Mountains (Fig. 5b). Zircons dominantly have an oxygen isotopic composition in the range of mantle values (5.3 ± 0.6, 2σ, Valley et al., 1998) but a few (e.g. sample 1701–2) display low $\delta^{18}O$ values (Fig. 7a).

4.3. Summary of zircon geochronological and Hf–O isotopic data

The U–Pb geochronological results of the 15 newly dated samples are summarized in Fig. 8. The igneous ages show a protracted and continuous igneous crystallization from 1160 Ma to 1070 Ma, with an age concentration at ca. 1110–1090 Ma. Some samples also show Mesoproterozoic metamorphic ages, which are recorded by single grains or rim overgrowths, characterized by dark CL and low Th/U at ca. 1080–1030 Ma. Most samples also exhibit a metamorphic overprinting history between 600 and 500 Ma. Zircon inheritance is rare, with ca. 1200 Ma ages recorded by a few samples and ca. 1700 Ma by one sample. No early Paleoproterozoic or Archaean inherited zircons were found. Detrital zircons from the only meta-sedimentary sample (DML 40) yield U–Pb ages clustering around 1750 Ma, 1320–1200 Ma and 1140 Ma, overprinted by Cambrian (ca. 530 Ma) metamorphism. Most samples from the Orvin-Wohlthat Mountains have $\delta^{18}O$ values that are similar to, or slightly higher than, mantle values and have strongly positive $\varepsilon_{Hf}(t)$, while a few samples (e.g. J1710, J1734; Fig. 5) with a mineralogical affinity to S-type granites (garnet-bearing) display distinctly higher $\delta^{18}O$ and lower $\varepsilon_{Hf}(t)$ values. Five of six samples from Gjelsvikfjella have mantle-like O and suprachondritic Hf-isotopic compositions, whereas one sample has a lower $\delta^{18}O$ value (2.9–4.3‰) than mantle value.

5. Discussion

5.1. Mesoproterozoic crustal growth and reworking in cDML

Magmas generated in subduction zones commonly contain components sourced from a number of different reservoirs, such as the subducted oceanic slab and sediments, the mantle wedge, and overlying crustal material of different ages and provenance (Pearce et al., 1999; Elburg et al., 2002; Bindeman et al., 2005). Combined zircon Hf–O isotopic investigations have the potential to constrain variable contributions of juvenile (directly mantle-derived) versus pre-existing continental components in source rocks and parent melts (e.g. Lancaster et al., 2011; Roberts and Spencer, 2015; Payne et al., 2016). Such data allow us to track the magmatic source characteristics of the Grenville-age samples collected from cDML and thus provide important insights into the history of crustal growth and recycling during orogenesis.

5.1.1. Orvin-Wohlthat Mountains

Meta-igneous samples from the Orvin-Wohlthat Mountains predominantly give igneous crystallization ages of 1110–1090 Ma. They show a broad variation in zircon Hf and O isotopic compositions (Fig. 9a), implying the involvement of multiple mantle- and crust-derived components in the source. Most samples show moderately elevated $\delta^{18}O$ values between 6.4 and 7.3‰ (Figs. 6, 9a), compositions typical of I-type arc rocks (Eiler, 2001; Kemp et al., 2007). A large proportion of zircons from these samples (red in Fig. 5a) display suprachrondritic $\varepsilon_{Hf}(t)$ values, with the averages lying slightly below the composition of the arc mantle array presented by Dhuime et al. (2011) and corresponding to Mesoproterozoic model ages (Fig. 5b). This indicates that the parental magmas are rather juvenile with limited contribution from ancient continental components, either in the melt source region

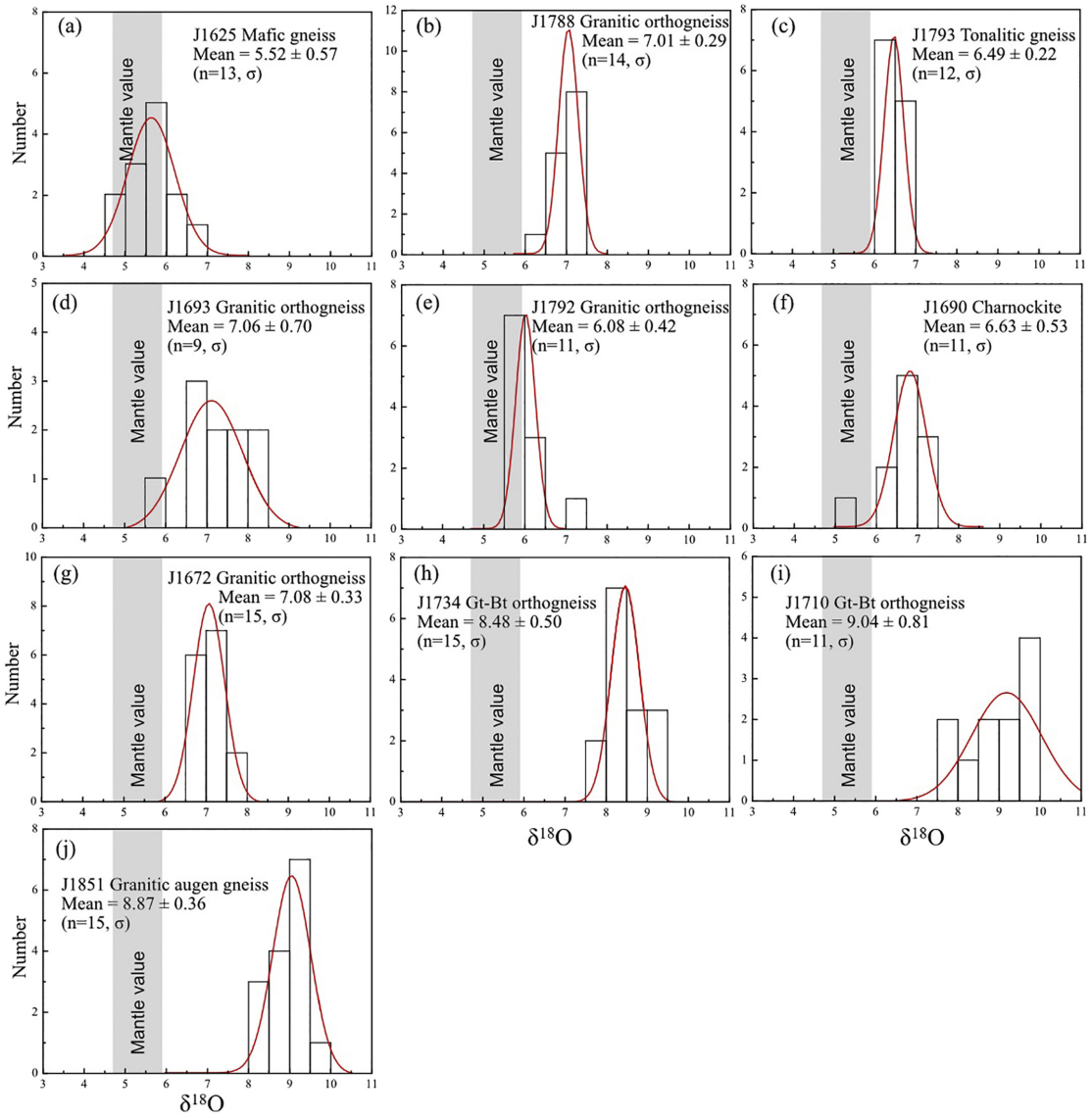

Fig. 6. Histograms of $\delta^{18}O$ values of samples from the Orvin-Wohlthat Mountains.

or by crustal contamination. The absence of any significantly older inherited zircons provides further evidence for minor to negligible interaction of these magmas with old continental crust. Sample J1851 displays an average $\varepsilon_{Hf}(t)$ value of +5 in association with elevated $\delta^{18}O$ values (8–10‰), suggesting a derivation from mixing of juvenile, mantle-derived magma with young supracrustal components, either altered volcanic crust or sedimentary rock.

The addition of ancient crustal material to arc magmas in this region is also revealed by a group of samples with enriched Hf isotope compositions (Fig. 5a, b). Two samples (J1710, J1734) have distinctively elevated $\delta^{18}O$ values at 8.5–9.0‰ (Fig. 6h, i) associated with unradiogenic $\varepsilon_{Hf}(t)$ and Paleoproterozoic model ages (Fig. 5b). The Hf–O isotopic signatures combined with the presence of garnets and whole-rock elemental data comparable to S-type granite (e.g. high A/CNK > 1.0, unpublished data) indicate a significant contribution from ancient sedimentary supracrustal material. The addition of the sedimentary material could be achieved by source contamination, i.e. the inclusion of subducted sediments overlying the oceanic crust, or by assimilation and re-melting of sedimentary components from overlying arc crust. The latter mechanism is preferred here, as previous studies show that in arc magmas, the contribution of heavy $\delta^{18}O$ from the subducted material can be very limited (e.g. Vroon et al., 2001). Whatever explanation, the Hf model ages ranging from 2.1 to 1.8 Ga suggest that the sediments could possibly have a Paleoproterozoic or older age, which then were most likely derived from the Proto-Kalahari Craton. The other two samples (J1693 and J1772) with a more depleted but

Table 1
Zircon Hf–O isotopic data of samples from Gjelsvikfjella.

Sample	Rock types	Igneous age (Ma)	$^{176}Hf/^{177}Hf_{(t)}$	$\varepsilon_{Hf}(t)$	$\varepsilon_{Hf}(t) \pm$ S.D.	$\delta^{18}O$ (‰)
1701–2	Migmatitic gneiss	1142 ± 10	0.28219–0.28230	+3.6–+6.8	5.3 ± 1.5	2.9–4.3
1812–5	Migmatitic augen gneiss	1137 ± 14	0.28217–0.28224	+3.8–+6.4	4.9 ± 0.7	4.5–6.1
1512–1	Augen gneiss	1123 ± 21	0.28216–0.28223	+3.1–+5.7	4.3 ± 0.8	5.0–6.5
2712–4	Migmatitic gneiss	1115 ± 12	0.28207–0.28231	−0.1–+8.3	3.7 ± 2.2	4.3–7.6
2412–4	Migmatitic augen gneiss	1096 ± 8	0.28219–0.28228	+3.4–+6.6	4.8 ± 0.9	4.6–5.9
3012–1	Mylonitic felsic gneiss	1098 ± 25	0.28206–0.28221	−1.1–+4.4	2.0 ± 1.1	4.2–5.6

heterogeneous Hf isotopic composition may be derived from a mixing of old sedimentary material and juvenile magmas.

The oldest sample in this study (mafic gneiss J1625, 1152 ± 7 Ma), which has a relatively homogeneous mantle-like $\delta^{18}O$ value (Fig. 6a), exhibits, however, a spread in Hf isotopic composition (ε_{Hf} (t) = 2.6–7.9, Fig. 5a). This indicates that this sample was most likely derived from juvenile mantle-derived magmas mixed with recycled older continental crust. The post-1110 Ma zircons with a moderate $\delta^{18}O$ value commonly have a more juvenile Hf isotopic composition than the older ones (Fig. 5a), suggesting an overall increasing input of mantle-derived magmas from 1150 Ma to 1090 Ma.

5.1.2. Gjelsvikfjella

In contrast to the Orvin-Wohlthat Mountains samples, which show significant inter-sample variation in Hf–O isotopic composition, the samples from Gjelsvikfjella have broadly similar isotopic signatures (Fig. 9a). The mantle-like $\delta^{18}O$ value (4.5–6.0‰) exhibited by most zircons shows little influence of supracrustal components, such as sediments, in the source. Most zircons display suprachondritic Hf isotopic characteristics, although with lower ε_{Hf} (t) values than zircons crystallized from juvenile magmas in the Orvin-Wohlthat Mountains, and yield a peak of model ages at 1.7–1.6 Ga (Fig. 5c, d). Assuming these rocks were dominantly crust-derived, the model age represents either the real age when the crust was extracted from the depleted mantle, or an average age of the various components contributing to the magma. These crustal component(s) must have resided for an extended period at depth since separation from the mantle reservoir, in order to avoid hydrothermal alteration that would have driven their oxygen isotopic signature to higher values than those measured. The spread of ε_{Hf} (t) values and model ages (2.0–1.4 Ga) may reflect a heterogeneous source composition composed of both older Paleoproterozoic and Mesoproterozoic crustal components. Alternatively, a source consisting of both older components and juvenile additions could also explain the Hf–O isotopic signature of these samples. In this scenario, the reworked crustal components must be older than the calculated model age, and involvement of Paleoproterozoic and/or Archean crust is possible. The mixing of juvenile magmas and older components is indicated by sample 2712–4, which displays both mantle-like and moderate high $\delta^{18}O$ and variable ε_{Hf} (t) values (Figs. 5c, 6d). Therefore, it is evident that ancient crust was involved in the formation of the Grenville-age samples in Gjelsvikfjella.

Some zircons (e.g. all zircons from sample 1701–2) yield an average $\delta^{18}O$ value below the 2σ lower uncertainty of the mantle reference value (<4.7‰, Valley et al., 1998), associated with depleted Hf isotopic compositions. Zircons with low $\delta^{18}O$ values are commonly interpreted to have been crystallized from originally ^{18}O-poor magmas (Zheng et al., 2004; Hiess et al., 2011; Rehman et al., 2018), although post-magmatic hydrothermal alteration has also been proposed to interpret low $\delta^{18}O$ values in metamict zircons (Iizuka et al., 2013). The low-$\delta^{18}O$ zircons in this study most likely inherited the oxygen isotopic

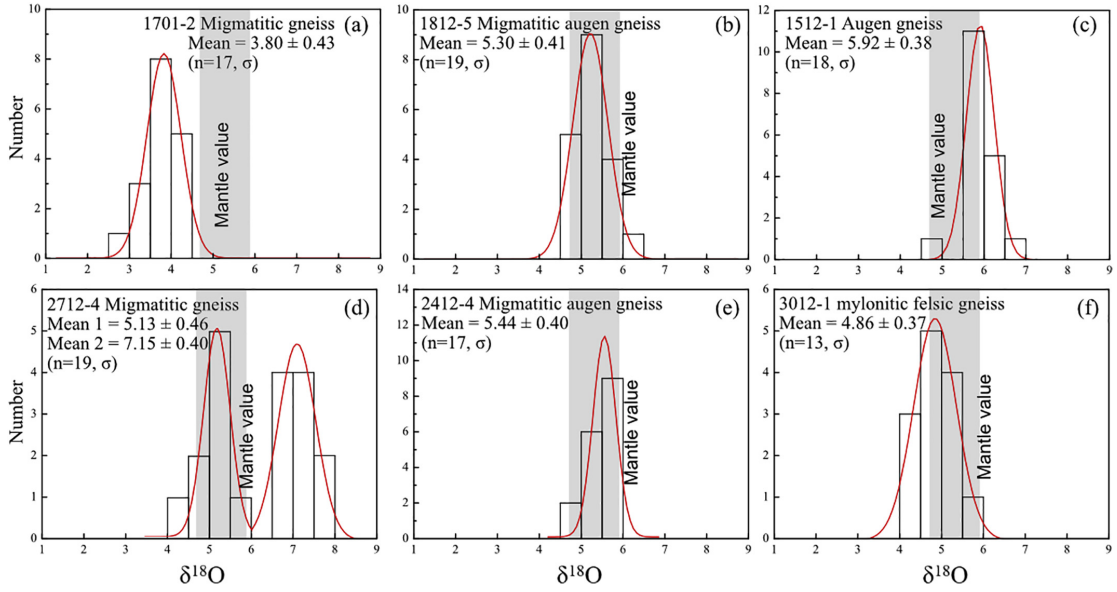

Fig. 7. Histograms of $\delta^{18}O$ values of samples from the Gjelsvikfjella.

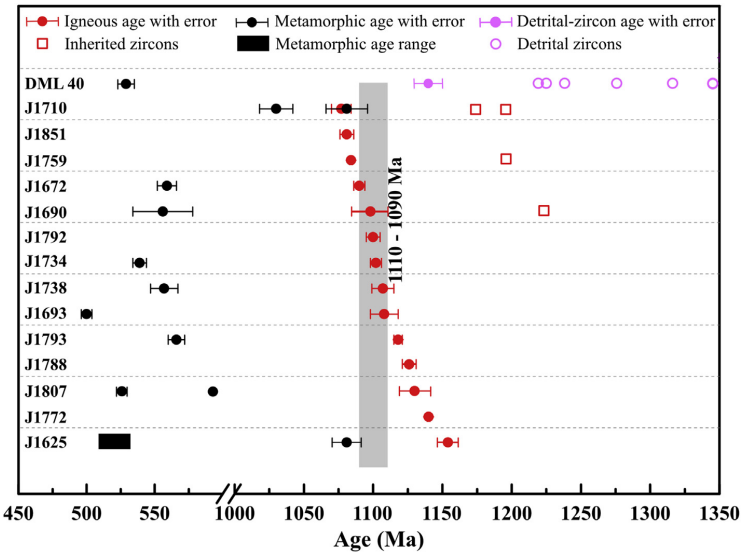

Fig. 8. Summary of Mesoproterozoic ages from igneous and detrital zircons and Pan-African metamorphic time in this study, with an igneous age concentration at 1110–1090 Ma (grey vertical bar). Sample 1772 and 1759 are marked with approximate upper-intercept age without error bars.

compositions from parental magmas, which had probably obtained light oxygen isotopes by fluid-rock interaction at a high temperature in the subduction zone, and/or involving isotopically light meteoric water.

5.1.3. Summary of Grenville-age crustal evolution in cDML

In summary, the zircon Hf–O isotopic data from cDML show apparently contradictory results (Fig. 9a). On the one hand, the paucity of ancient inherited zircons, radiogenic Hf isotopic compositions shown by supra-chondritic $\varepsilon_{Hf}(t)$ values and Mesoproterozoic model ages of most orthogneiss samples from the Orvin-Wohlthat Mountains are compelling evidence that they are of predominantly juvenile character. Conversely, re-melting of sedimentary rocks derived from the erosion of older basement, and of the basement at the edge of the Proto-Kalahari Craton itself is indicated by (meta)granitic rocks from the Orvin-Wohlthat Mountains which are characterized by high $\delta^{18}O$ values (8.0–10.0‰) and evolved Hf isotopic signatures, and from Gjelsvikfjella samples with Paleoproterozoic Hf model ages and mantle-like oxygen isotopic compositions.

The data suggest therefore that both processes, juvenile addition and crustal recycling, were operative in the generation of the granitoids of cDML during Grenville-age orogenesis.

5.2. Grenville-age continental arc magmatism in the Maud Belt

Whether the arc magmatism of the Maud Belt developed on oceanic or continental substrates remains controversial; our data show that a combination of juvenile and reworked crust was instrumental in producing the voluminous granitoids in cDML. Although the Maud Belt is now adjacent to the Archean Grunehogna Craton, where basement outcrops were dated at ~3.1 Ga (Barton et al., 1987; Marschall et al., 2010), there is only sparse evidence of incorporation of the Archean components in its Grenville-age magmas. Instead, previous work reported relatively juvenile Nd isotopic composition in most sections of the Maud Belt with dominant early Mesoproterozoic/late Paleoproterozoic model ages (e.g. Arndt et al., 1991; Jacobs et al., 1998; Wareham et al., 1998; Grantham et al., 2011). The Maud Belt was thus interpreted by some researchers as a number of exotic island arcs that accreted onto the craton margin (e.g. Bauer et al., 2003a; Grosch et al., 2007; Grantham et al., 2011). However, our new zircon Hf–O isotopic data show that the amount of older crust (most likely Paleoproterozoic in age) that was incorporated into the source of Grenville-age magmas is greater than previously recognized (Section 5.1). Moreover, the juvenile input to arc magmas, as recorded in the Orvin-Wohlthat Mountains samples, does not equate with an absence of continental crust overlying the subduction zone. In Andean-type orogens, the overlying continental crust makes a variable contribution to arc magmas during the evolution of the arc system. Juvenile magmas with minor to negligible contamination from older crust are commonly emplaced when subduction retreat and the ocean-ward migration of the arc cause crustal thinning (Cawood et al., 2009; Boekhout et al., 2015). For example, the southern Central Andes experienced a progressive input of mantle-derived melts over several tens of million years with little recycling of pre-existing crustal material (Jones et al., 2015).

Zircon Hf–O isotopic data in this study provide crucial information on the crustal composition along the eastern margin of the Proto-Kalahari Craton, which is important for the better understanding of the nature and geodynamics of the Maud Belt. We speculate that Paleoproterozoic components existed or still exist in this region based on following lines of evidence in addition to our new data. Firstly, detrital zircons from the Mesoproterozoic Ritscherflya Supergroup, which were most likely derived from the Maud Belt, exhibit the growth of ca. 1130 Ma igneous zircons on 1.9–1.7 Ga cores, indicating the development of Grenville-age magmatism on Paleoproterozoic basement (Marschall et al., 2013). Secondly, Paleoproterozoic inherited zircons, although rare, have been discovered in various parts of the Maud Belt (e.g. Baba et al., 2015; Ksienzyk and Jacobs, 2015 and this study) and hints of such sources are even present in the adjacent Natal-aged crust (e.g. Arndt et al., 1991; Mendonidis and Thomas, 2019). Moreover, 1.3–1.2 Ga detrital zircons (sample DML 40 in this study and Baba et al., 2015) and a few 1.2 Ga inherited zircons may imply a more complicated crustal composition in this region with a Mesoproterozoic (Ectasian) component, although the origin of these detrital zircons is enigmatic since much of the southern Kalahari and Laurentia margins preserve similar geochronological records of this period. In view of the above, it

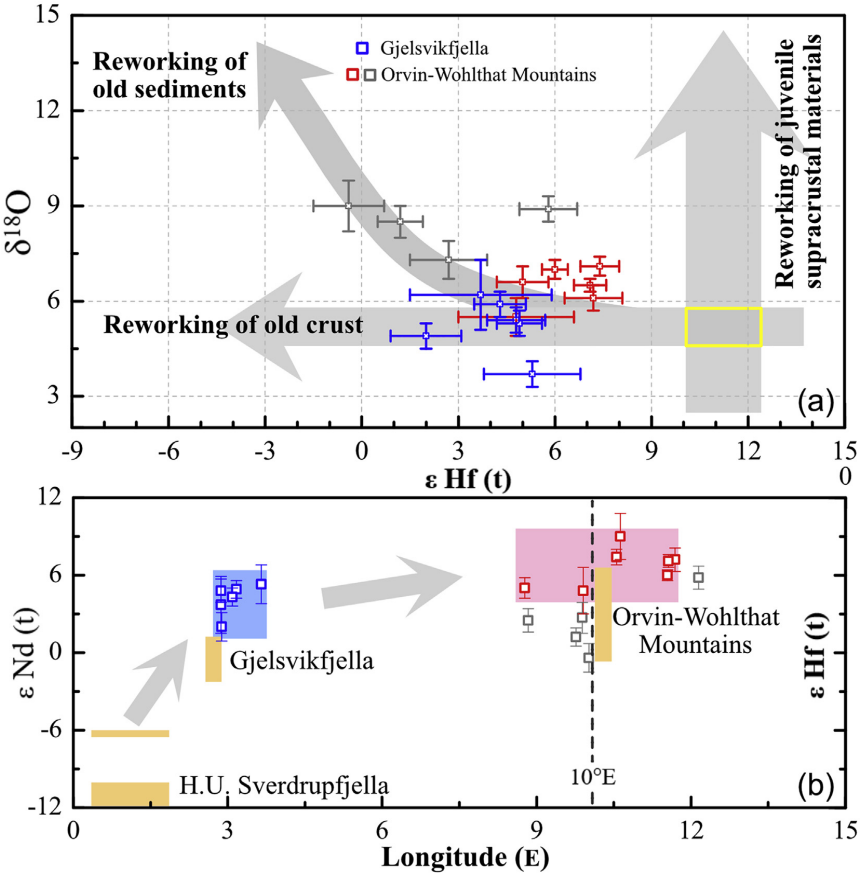

Fig. 9. (a) Plot of $\delta^{18}O$ versus ε_{Hf} (t) for zircons from cDML, showing the difference in source composition of samples between Gjelsvikfjella and the Orvin-Wohlthat Mountains. The yellow rectangles show the theoretical Hf–O isotopic composition of 1.1 Ga arc- and depleted-mantle derived magmas ($\delta^{18}O = 4.7–5.9‰$, ε_{Hf} (t) = +10–+12.5). The old basement and sediments are assumed to be Paleoproterozoic, with similarly evolved Hf isotopic composition but mantle-like and high $\delta^{18}O$ values respectively. Most samples from the Orvin-Wohlthat Mountains (red) are rather juvenile with moderate $\delta^{18}O$ values and high ε_{Hf} (t) values. Some samples (dark grey) display an elevated O isotopic signature associated with much lower ε_{Hf} (t) values, indicating the involvement of older Paleoproterozoic sediments. Mantle-like O and more evolved Hf isotopic compositions of samples from Gjelsvikfjella (blue) indicate the addition of old basements in the source. (b) ε_{Hf} (t) and ε_{Nd} (t) vs. longitude diagram showing the increasingly juvenile isotopic composition towards the east, away from the Grunehogna Craton. The orange rectangles show ε_{Nd} values reported by Jacobs et al. (1998), Wareham et al. (1998), Paulsson and Austrheim (2003) and Grosch et al. (2007).

is therefore not tenable to consider the Maud Belt as a single island arc edifice. It was more likely built upon pre-existing crust along the margin of the Proto-Kalahari Craton.

The Grenville-age magmatism in the Maud Belt shows significant spatial variation, with radiogenic isotopic compositions becoming increasingly juvenile towards the east (Fig. 9b). Samples from the H.U. Svedrupfjella (closest to the Grunehogna Craton) are characterized by negative ε_{Nd} (t) values associated with Paleoproterozoic to Archean model ages (Wareham et al., 1998; Grosch et al., 2007), suggesting a large degree of reworking of older basement crust underlying the Proto-Kalahari Craton (Fig. 2). In Gjelsvikfjella, Hf model ages of zircon grains with mantle-like O isotopic composition yield a peak at late Paleoproterozoic times, which indicates a significant contribution from pre-existing crustal material. In the Orvin-Wohlthat Mountains, east of the Ulvetanna Lineament, the samples with addition of old crustal material are mainly exposed in the western part (W of 10°E), while the Grenville-age component in the eastern part is mainly composed of 1120–1080 Ma juvenile rocks (Fig. 9b). This spatial isotopic trend is consistent with the characteristics of continental-arc magmatism, which commonly incorporates more isotopically evolved continental crust landward (Chapman et al., 2017). The Orvin-Wohlthat Mountains most probably represent the accretionary terrane overlying the inboard subduction zone beneath the Proto-Kalahari Craton, with a transition in source composition of Grenville-age rocks from ancient craton-derived to younger oceanic-crust related material towards the east. In this scenario, the Ulvetanna Lineament (Fig. 2) may represent the boundary between an accretionary complex and the cryptic edge of the continental crust of the Proto-Kalahari Craton.

A group of ~1100 Ma igneous ages in our dataset from cDML indicates a significant magmatic episode between the emplacement of early arc magmas and late-stage tectono-thermal events. In adjacent areas, magmatic activity at this time produced the Borgmassivet mafic/ultramafic sills intruding the Ritscherflya Supergroup in the Grunehogna Craton, which were interpreted as subduction-related magmatism in some studies (Grosch et al., 2015; Hokada et al., 2019). An opposing opinion considers that the mafic intrusions form part of the Umkondo Large

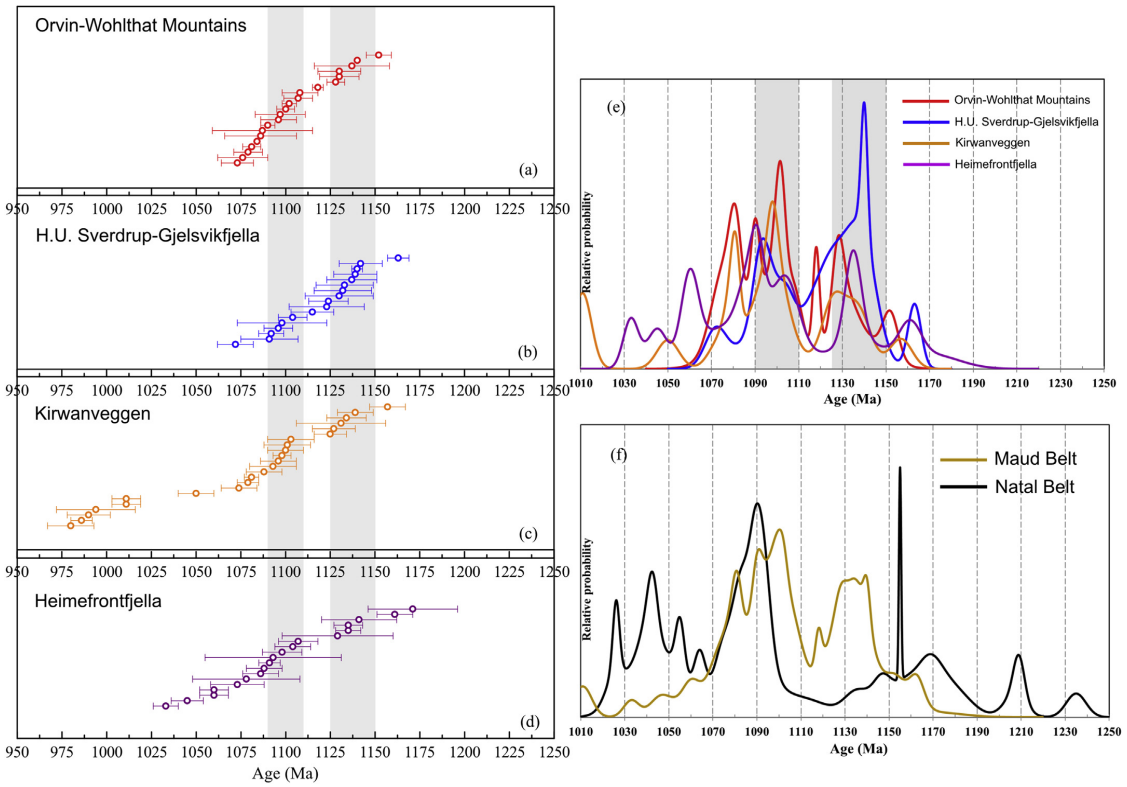

Fig. 10. (a–e) Summary of igneous U–Pb zircon ages from different parts of the Maud Belt. Two main periods of magmatism (1150–1125 Ma, 1110–1090 Ma) are marked with grey bar; (f) Comparison of major times of igneous activity in the Maud and Natal belts. The Natal Belt has an early crustal record that is several tens of million years older than the Maud Belt. The 1150–1120 Ma igneous ages are interpreted as continental-arc magmatism in the Maud Belt, while this time period was almost quiet in Natal.
(Sources for the data of the Orvin-Wohlthat Mountains: Jacobs et al., 1998, Baba et al., 2015; and data in this study; H.U. Sverdrup-Gjelsvikfjella: Paulsson and Austrheim, 2003; Jacobs et al., 2003a, 2003b, 2008a; Board et al., 2005; Bisnath et al., 2006; Grantham et al., 2011; Hokada et al., 2019; Kirwanveggen: Harris et al., 1995; Harris, 1999; Jackson, 1999; Heimefrontfjella: Arndt et al., 1991; Bauer et al., 2003a, 2003b; Jacobs et al., 2003b; Natal: Thomas and Eglington, 1990; Thomas et al., 1993, 1999, 2003; Johnston et al., 2001; Mendonidis and Armstrong, 2009, 2016; Mendonidis et al., 2002, 2009, 2015; Eglington et al., 2003, 2010; Spencer et al., 2015; Hokada et al., 2019).

Igneous Province (LIP) emplaced in the interior of the Proto-Kalahari Craton (e.g. Moabi et al., 2017). From a global perspective, the Umkondo magmatism is coeval with several other LIPs in Laurentia including the Coats Land block, Amazonia, Congo and in the cratons of India (e.g. Davis and Green, 1997; Ernst et al., 2013; De Kock et al., 2014; Teixeira et al., 2015). These large-scale intraplate magmatic events could be a consequence of anomalously high mantle heat flow in the Mesoproterozoic, which might have been independent of the supercontinent cycle (Hanson et al., 2004). The relationship between the synchronous Umkondo LIP and the subduction-related magmatism along the margin of Kalahari remains ambiguous (e.g. Hanson et al., 1998, 2004; Hokada et al., 2019). In the Orvin-Wohlthat Mountains, apparently more juvenile Hf isotopic composition of post-1110 Ma rocks compared to the older orthogneisses argues for a transition in the tectonic setting (Fig. 5a), most likely from an advancing to a retreating accretionary orogenic setting, resulting in the generation of voluminous juvenile magmas. Subsequent granitic magmatism and high-grade metamorphism at 1090–1030 Ma may have taken place under convergence in an overall advancing accretionary tectonic setting. The tectonic switch could be partly related to the changes in mantle convection and global plate reorganisation during eruption and cooling down of plume activities in the Umkondo LIP magmatism.

Grenville-age geochronological records are also preserved in the Nampula Complex in NE Mozambique, lying to the north of the Maud Belt in Gondwana (Fig. 1b). Grenville-age magmatic activity in the Nampula Complex has been well constrained at 1150–1030 Ma (Bingen et al., 2009; Macey et al., 2010; Thomas et al., 2010). The age is comparable to the Maud Belt but distinctly older than other Mesoproterozoic crust to the north (i.e. 1060–950 Ma Marrupa and Unango complexes, Bingen et al., 2009). It is thus envisaged that the Nampula Complex cannot be correlated with these complexes in the north but most likely has a tectonic affinity with the Maud Belt and could possibly be restored to a position along the margin of Proto-Kalahari (Bingen et al., 2009). This is supported by the similarity in Hf isotopic characteristics between these two regions. Thomas et al. (2010) showed that 1.1–1.0 Ga detrital zircons derived from the Nampula Complex yield both juvenile ($\varepsilon_{Hf}(t) = 5–9$) and evolved Hf isotopic compositions with model ages ranging from Mesoproterozoic to Archean times, comparable to the isotopic signature of samples from the Orvin-Wohlthat Mountains in this study. Therefore, the Maud Belt very likely extended northwards into NE Mozambique, constituting a composite Andean-type magmatic arc along the eastern margin of the Proto-Kalahari Craton.

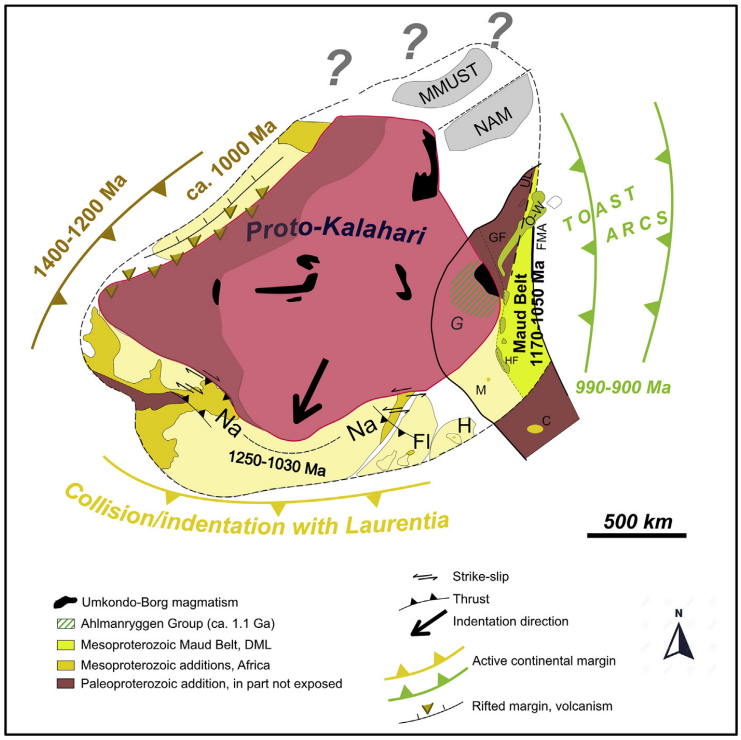

Fig. 11. Time-transgressive tectonic setting along the margin of the Proto-Kalahari Craton, showing the Namaqua-Natal and Maud Belts in late Mesoproterozoic times (modified from Jacobs et al., 2008a). The eastern margin along the Maud Belt is interpreted as an active continental margin with ancient continental crust most likely extending to cDML. The southern margin, in contrast, is characterized by outward subduction with accretion of Proterozoic arcs or microcontinents followed by collision with Laurentia to form the Na–Na Belt. Abbreviations: C, Coats Land Block; O–W, Orvin-Wohlthat Mountains; FMA, Forster Magnetic Anomaly; FI, Falkland Islands; G, Grunehogna Craton; GF, Gjelsvikfjella; H, Haag Nunatak; HF, Heimefrontfjella; M, Mannefallknausane; MMUST, Marupa-Malawi-Unango south Tanzania terrane; NAM, Nampula Complex; UL, Ulvetanna Lineament.

5.3. Implications for the Natal and Maud belts

In Rodinia, the Natal and Maud belts were in relatively close proximity and together formed the western extension of the greater Grenville Orogen. However, although they formed roughly synchronously along the same part of the orogen, their subduction polarity, age and orogen style are distinctly different. Whilst the Natal Belt is best explained as a juvenile arc-continent collision orogen followed by continental collision, the Maud Belt may be better explained as a slightly younger, continental arc with significant (but diminishing eastwards) elements of older (Proto-Kalahari) crust, recorded by spatially-controlled differing zircon U–Pb ages and radiogenic isotope signatures of the evolving igneous rocks.

The Natal Belt is characterized by a subduction polarity away from Proto-Kalahari with a passive margin until arc-continental collision commenced at ca. 1150 Ma (Jacobs et al., 1997; McCourt et al., 2006). Structural, petrological, and paleomagnetic data support the interpretation of continental collision between Proto-Kalahari and Laurentia, with the accreted Natal arcs sandwiched between the two cratonic masses. The changing late shear geometries from dextral in Namaqualand to sinistral in the Natal prompted the hypothesis of the Proto-Kalahari being an indenter into Laurentia (Jacobs et al., 1993, 2003a, 2008a). The widespread A-type charnockitic magmatism at 1050–1030 Ma and simultaneous LP-(U)HT metamorphism, followed by isobaric cooling in the Natal sector has been interpreted to take place in a convergent (transpressional) setting (Thomas et al., 1993; Spencer et al., 2015). The palaeomagnetic data from the Umkondo LIP and DML lead to an interpretation that Proto-Kalahari conjoined with Laurentia in the late Mesoproterozoic with the Namaqua-Natal Belt oriented towards the Grenville margin of Laurentia (Powell et al., 2001; Swanson-Hysell et al., 2015). The collision of Proto-Kalahari and Laurentia is also supported by the position of the Coats Land Block within Rodinia. The Coats Land Block is interpreted as a part of Laurentia (Loewy et al., 2011) or an exotic terrane accreted to Laurentia (Swanson-Hysell et al., 2015), and may represent a rifted block that was incorporated into Greater Kalahari after collision and dispersal of Rodinia (Gose et al., 1997; Jacobs et al., 2003a, 2003b; Loewy et al., 2011). Grenville-age magmas in the Natal Belt predominantly originated from the reworking of lithospheric substrate of pre-Rodinian island arcs with negligible addition of ancient crust or mantle-derived magmas (Eglington et al., 1989; Spencer et al., 2015), indicated by Sr, Nd and Hf isotopic compositions of 1175–1030 Ma granitoids with a similar trend to the evolution curve of continental crust (Fig. 5a, c).

In contrast to the Natal Belt, the Maud Belt shows clear evidence for subduction polarity towards Proto-Kalahari within an overall active continental margin setting (e.g. Bisnath et al., 2006; Marschall et al., 2013). However, our new data acquired in this study, together with published data from other parts of the Maud Belt, necessitate a re-appraisal of this simple model. Our new U–Pb geochronological data combined with published geochronological results from the Orvin-Wohlthat Mountains have identified two major periods of Grenville-age magmatism at 1150–1125 and 1110–1090 Ma, comparable to

other areas in the Maud Belt (Fig. 10a–e). The age spectra from the Maud Belt are clearly distinguishable from that obtained from the Natal Belt, which has distinct records of pre-1200 Ma island arc magmatism, an age component which is missing in the Maud Belt (Fig. 10f). In the Natal Belt, syn-collisional granitic magmatism and high-grade metamorphism is well constrained between 1050 and 1030 Ma (Thomas et al., 1993; Spencer et al., 2015 and references therein), whereas such ages are very rarely reported in the Maud Belt (Fig. 10f). In further contrast to Natal, samples in the Orvin-Wohlthat Mountains with moderate ^{18}O values define an ε_{Hf} – time trajectory nearly parallel to the evolution trend of the arc mantle in cDML (Fig. 5a), which implies progressive juvenile input to arc magmas. This is commonly documented in active continental margins with continuous subduction processes (e.g. Spencer et al., 2019).

It is thus clear that the Maud and Natal belts cannot be correlated in a simple geodynamic model as originally suggested (e.g. Groenewald et al., 1995). The tectonic contact between the Natal and Maud belts may mark the change from final continental collision to outboard-Proto Kalahari accretionary tectonics at the westernmost end of the greater Grenville Orogen (Figs. 1 and 11). The Maud Belt probably marks the start of a long-term active continental margin setting along eastern Kalahari, with periodic, west-facing subduction systems for the subsequent 500 Ma. This tectonic setting may have been reactivated and continued during the extroversion of Rodinia and closure of the exterior ocean in the middle to late Neoproterozoic. The westward subduction of the Mozambique oceanic slab beneath this margin led to the accretion of the TOAST (990–900 Ma) and terminated with the final amalgamation of Gondwana in late Neoproterozoic to Cambrian times (Jacobs and Thomas, 2004).

6. Summary and conclusions

(1) New SHRIMP zircon U–Pb data provide detailed constraints on the temporal framework of Grenville-age tectono-thermal events in a large part of the Maud Belt. Arc magmatism in Orvin-Wohlthat Mountains occurred from 1160 to 1070 Ma with a culmination at 1110–1090 Ma, followed by high-grade metamorphism at ca. 1080–1030 Ma.

(2) Most zircons from the Orvin-Wohlthat Mountains have positive $\varepsilon_{Hf}(t)$ values and Mesoproterozoic model ages, with $\delta^{18}O$ values similar to, or slightly higher than, typical mantle values. This suggests crystallization from juvenile magmas with little recycling of pre-existing continental crust.

(3) In contrast, zircons from Gjelsvikfjella predominantly have mantle-like $\delta^{18}O$ values and more evolved Hf isotopic compositions with Paleoproterozoic model ages, indicating more contribution of older crust components from the Proto-Kalahari Craton. The involvement of ancient sediments is additionally reflected by some zircons from the Orvin-Wohlthat Mountains with distinctively lower ε_{Hf} and highly elevated $\delta^{18}O$ values.

(4) The reworking of ancient continental material indicates that the Maud Belt developed on the lithospheric substrate of the Proto-Kalahari Craton margin. A protracted accretionary process associated with westward subduction beneath the craton involving tectonic switching between advancing and retreating subduction processes may best explain the formation of the cDML part of the Maud Belt during the later stage of Rodinia amalgamation.

(5) A new definition of the younger Maud Belt (as distinct from the older Namaqua-Natal Belt) can be proposed. Continuous continental arc magmatism in the Maud Belt is tectonically unrelated with the accretion of oceanic island arcs and final continent-continent collision in the Natal Belt. The Natal and Maud belts therefore had independent tectonic evolutions although they both reside along the margin of Proto-Kalahari.

(6) The tectonic contact relationship of the Natal and Maud belts is highly speculative, because it is largely unexposed and/or overprinted by later Pan-African tectono-thermal events. The complex and contrasting tectonic evolution of the two belts characterises the lateral western termination of the greater Grenville Orogen. The Maud Belt appears to be the temporal starting point for a protracted accretionary tectonic cycle in the region, which was reactivated and continued in late Tonian to early Ediacaran times during the break-up of Rodinia by extroversion to form Gondwana.

Supplementary data to this article can be found online at https://doi.org/10.1016/j.gr.2019.12.004.

Declaration of competing interest

None.

Acknowledgements

This work was financially supported by faculty-specific funds and endowments of the Faculty of Mathematics and Natural Sciences, University of Bergen (No. 812378). C–C. Wang thanks for support from the China Scholarship Council. J. Jacobs thanks for continued field support of the Alfred-Wegener Institute, Bremerhaven, and the Federal Institute for Geosciences and Natural Resources (BGR). M. Suppersberger Hamre and St. Larsen are thanked for help with mineral preparation. We thank M. Whitehouse, K. Lindén and H. Jeon for their help in SIMS zircon O isotopic analyses, P. Montero and F. Bea for their help with SHRIMP analyses at the IBERSIMS facility, Granada, and M. Wingate for his help with SHRIMP analyses at Curtin. The MC-ICPMS lab at UJ was funded by NRF-NEP grant 93208, and is supported by DSI-NRF CIMERA. M. A. Elburg acknowledges NRF IFRR funding (No. 119297). We thank Prof. T. Tsunogae and two anonymous referees for the editorial handing and helpful comments. This is IBERSIMS publication #66, NordSIMS publication #631, and a contribution to IGCP 648, Supercontinent Cycles & Global Dynamics.

References

Amelin, Y., Lee, D.C., Halliday, A.N., Pidgeon, R.T., 1999. Nature of the Earth's earliest crust from hafnium isotopes in single detrital zircons. Nature 399, 252–255.
Arndt, N.T., Todt, W., Chauvel, C., Tapfer, M., Weber, K., 1991. U-Pb zircon age and Nd isotopic composition of granitoids, charnockites and supracrustal rocks from Heimefrontfjella, Antarctica. Geol. Rundsch. 80, 759–777.
Baba, S., Horie, K., Hokada, T., Owada, M., Adachi, T., Shiraishi, K., 2015. Multiple collisions in the East African–Antarctica Orogen: constraints from timing of metamorphism in the Filchnerfjella and Hochlinfjellet terranes in central Dronning Maud Land. J. Geol. 123, 55–77.
Barton, J.M., Klemd, R., Allsopp, H.L., Auret, S.H., Copperthwaite, Y.E., 1987. The geology and geochronology of the Annandagstoppane granite, western Dronning Maud Land, Antarctica. Contrib. Mineral. Petrol. 97, 488–496.
Bauer, W., Jacobs, J., Fanning, C.M., Schmidt, R., 2003a. Late Mesoproterozoic Arc and Back-arc Volcanism in the Heimefrontfjella (East Antarctica) and Implications for the Palaeogeography at the Southeastern Margin of the Kaapvaal-Grunehogna Craton. Gondwana Res. 6, 449–465.
Bauer, W., Fielitz, W., Jacobs, J., Fanning, C.M., Spaeth, G., 2003b. Mafic dykes from Heimefrontfjella and implications for the post-Grenvillian to pre-Pan-African geological evolution of western Dronning Maud Land, Antarctica. Antarct. Sci. 15, 379–391.
Bauer, W., Thomas, R.J., Jacobs, J., 2003c. Proterozoic-Cambrian history of Dronning Maud Land in the context of Gondwana assembly. Geol. Soc. Lond. Spec. Publ. 206, 247–269.
Bauer, W., Jacobs, J., Thomas, R.J., Spaeth, G., Weber, K., 2009. Geology of the Vardeklettane Terrane, Heimefrontfjella (East Antarctica). Polarforschung 79, 29–32.
Bindeman, I.N., Eiler, J.M., Yogodzinski, G.M., Tatsumi, Y., Stern, C.R., Grove, T.L., Portnyagin, M., Hoernle, K., Danyushevsky, L.V., 2005. Oxygen isotope evidence for slab melting in modern and ancient subduction zones. Earth Planet. Sci. Lett. 235, 480–496.

Bingen, B., Viola, G., 2018. The early-Sveconorwegian orogeny in southern Norway: tectonic model involving delamination of the sub-continental lithospheric mantle. Precambrian Res. 313, 170–204.

Bingen, B., Nordgulen, Ø., Viola, G., 2008. A four-phase model for the Sveconorwegian orogeny, SW Scandinavia. Nor. J. Geol. 88, 43–72.

Bingen, B., Jacobs, J., Viola, G., Henderson, I.H.C., Skår, Ø., Boyd, R., Thomas, R.J., Solli, A., Key, R.M., Daudi, E.X.F., 2009. Geochronology of the Precambrian crust in the Mozambique belt in NE Mozambique, and implications for Gondwana assembly. Precambrian Res. 170, 231–255.

Bisnath, A., Frimmel, H.E., Armstrong, R.A., Board, W.S., 2006. Tectono-thermal evolution of the Maud Belt: New SHRIMP U–Pb zircon data from Gjelsvikfjella, Dronning Maud Land, East Antarctica. Precambrian Res. 150, 95–121.

Black, L.P., Kamo, S.L., Allen, C.M., Davis, D.W., Aleinikoff, J.N., Valley, J.W., Mundil, R., Campbell, I.H., Korsch, R.J., Williams, I.S., Foudoulis, C., 2004. Improved $^{206}Pb/^{238}U$ microprobe geochronology by the monitoring of a trace-element-related matrix effect; SHRIMP, ID–TIMS, ELA–ICP–MS and oxygen isotope documentation for a series of zircon standards. Chem. Geol. 205, 115–140.

Board, W.S., Frimmel, H.E., Armstrong, R.A., 2005. Pan-African Tectonism in the Western Maud Belt: P–T–t Path for high-grade Gneisses in the H.U. Sverdrupfjella, East Antarctica. J. Petrol. 46, 671–699.

Boekhout, F., Roberts, N.M., Gerdes, A., Schaltegger, U., 2015. A Hf-isotope perspective on continent formation in the south Peruvian Andes. Geol. Soc. Lond. Spec. Publ. 389, 305–321.

Bouvier, A., Vervoort, J.D., Patchett, P.J., 2008. The Lu–Hf and Sm–Nd isotopic composition of CHUR: constraints from unequilibrated chondrites and implications for the bulk composition of terrestrial planets. Earth Planet. Sci. Lett. 273, 48–57.

Cawood, P.A., Pisarevsky, S.A., 2017. Laurentia-Baltica-Amazonia relations during Rodinia assembly. Precambrian Res. 292, 386–397.

Cawood, P.A., Kröner, A., Collins, W.J., Kusky, T.M., Mooney, W.D., Windley, B.F., 2009. Accretionary orogens through Earth history. Geol. Soc. Lond. Spec. Publ. 318, 1–36.

Cawood, P.A., Strachan, R.A., Pisarevsky, S.A., Gladkochub, D.P., Murphy, J.B., 2016. Linking collisional and accretionary orogens during Rodinia assembly and breakup: implications for models of supercontinent cycles. Earth Planet. Sci. Lett. 449, 118–126.

Chapman, J.B., Ducea, M.N., Kapp, P., Gehrels, G.E., DeCelles, P.G., 2017. Spatial and temporal radiogenic isotopic trends of magmatism in Cordilleran orogens. Gondwana Res. 48, 189–204.

Collins, W.J., Belousova, E.A., Kemp, A.I., Murphy, J.B., 2011. Two contrasting Phanerozoic orogenic systems revealed by hafnium isotope data. Nat. Geosci. 4, 333–337.

Condie, K.C., 2005. Earth as an Evolving Planetary System. Elsevier, Amsterdam, Netherlands, pp. 90–91.

Dalziel, I.W., Mosher, S., Gahagan, L.M., 2000. Laurentia-Kalahari collision and the assembly of Rodinia. J. Geol. 108, 499–513.

Davis, D.W., Green, J.C., 1997. Geochronology of the North American Midcontinent rift in western Lake Superior and implications for its geodynamic evolution. Can. J. Earth Sci. 34, 476–488.

De Kock, M.O., Ernst, R., Söderlund, U., Jourdan, F., Hofmann, A., Le Gall, B., Bertrand, H., Chisonga, B.C., Beukes, N., Rajesh, H.M., Moseki, L.M., 2014. Dykes of the 1.11 Ga Umkondo LIP, Southern Africa: clues to a complex plumbing system. Precambrian Res. 249, 129–143.

Dhuime, B., Hawkesworth, C., Cawood, P., 2011. When continents formed. Science 331, 154–155.

Ducea, M.N., Saleeby, J.B., Bergantz, G., 2015. The architecture, chemistry, and evolution of continental magmatic arcs. Annu. Rev. Earth Planet. Sci. 43, 299–331.

Eglington, B.M., Harmer, R.E., Kerr, A., 1989. Isotope and geochemical constraints on Proterozoic crustal evolution in south-eastern Africa. Precambrian Res. 45, 159–174.

Eglington, B.M., Thomas, R.J., Armstrong, R.A., Walraven, F., 2003. Zircon geochronology of the Oribi Gorge Suite, KwaZulu-Natal, South Africa: Constraints on the timing of trans-current shearing in the Namaqua–Natal Belt. Precambrian Res. 123, 29–46.

Eglington, B.M., Thomas, R.J., Armstrong, R.A., 2010. U-Pb SHRIMP zircon dating of Mesoproterozoic magmatic rocks from the Scottburgh area, central Mzumbe Terrane, KwaZulu-Natal, South Africa. S. Afr. J. Geol. 113, 229–235.

Eiler, J.M., 2001. Oxygen isotope variations of basaltic lavas and upper mantle rocks. Rev. Mineral. Geochem. 43, 319–364.

Elburg, M.A., van Bergen, M.J., Hoogewerff, J., Foden, J., Vroon, P.Z., Zulkarnain, I., Nasution, A., 2002. Geochemical trends across an arc-continent collision zone: magma sources and slab-wedge transfer processes below the Pantar Strait volcanoes (Indonesia). Geochim. Cosmochim. Acta 66, 2771–2789.

Elburg, M., Jacobs, J., Andersen, T., Clark, C., Läufer, A., Ruppel, A., Krohne, N., Damaske, D., 2015. Early Neoproterozoic metagabbro-tonalite-trondhjemite of Sør Rondane (East Antarctica): Implications for supercontinent assembly. Precambrian Res. 259, 189–206.

Ernst, R.E., Pereira, E., Hamilton, M.A., Pisarevsky, S.A., Rodriques, J., Tassinari, C.C., Teixeira, W., Van-Dunem, V., 2013. Mesoproterozoic intraplate magmatic 'barcode' record of the Angola portion of the Congo Craton: newly dated magmatic events at 1505 and 1110 Ma and implications for Nuna (Columbia) supercontinent reconstructions. Precambrian Res. 230, 103–118.

Frimmel, H.E., 2004. Formation of a late Mesoproterozoic supercontinent: the South Africa–East Antarctica connection. In: Eriksson, P.G., Altermann, W., Nelson, D.R., Mueller, W.U., Catuneanu, O. (Eds.), The Precambrian Earth: Tempos and Events. Developments in Precambrian Geology. 12, pp. 240–255.

Gaucher, C., Frei, R., Chemale, F., Frei, D., Bossi, J., Martínez, G., Chiglino, L., Cernuschi, F., 2011. Mesoproterozoic evolution of the Río de la Plata Craton in Uruguay: at the heart of Rodinia? Int. J. Earth Sci. 100, 273–288.

Golynsky, A., Jacobs, J., 2001. Grenville-age versus pan-african magnetic anomaly imprints in Western Dronning Maud Land, East Antarctica. J. Geol. 109, 136–142.

Gose, W.A., Helper, M.A., Connelly, J.N., Hutson, F.E., Dalziel, I.W., 1997. Paleomagnetic data and U-Pb isotopic age determinations from Coats Land, Antarctica: implications for late Proterozoic plate reconstructions. J. Geophys. Res. Solid Earth 102 (B4), 7887–7902.

Grantham, G.H., 1992. Geological Evolution of Western H.U. Sverdrupfjella, Dronning Maud Land, Antarctica. Doctoral dissertation, University of Natal.

Grantham, G.H., Storey, B.C., Thomas, R.J., Jacobs, J., Ricci, C.A., 1997. The pre-break-up position of Haag Nunataks within Gondwana: possible correlatives in Natal and Dronning Maud Land. The Antarctic Region: Geological Evolution and Processes. Terra Antartica Publication, Siena, pp. 13–20.

Grantham, G.H., Eglington, B.M., Thomas, R.J., Mendonidis, P., 2001. The Nature of the Grenville-age Charnockitic A-type Magmatism from the Natal, Namaqua and Maud Belts of Southern Africa and Western Dronning Maud Land, Antarctica. National Institute of Polar Research, Tokyo, pp. 59–86 Special Issue 55.

Grantham, G.H., Manhica, A.D.S.T., Armstrong, R.A., Kruger, F.J., Loubser, M., 2011. New SHRIMP, Rb/Sr and Sm/Nd isotope and whole rock chemical data from central Mozambique and western Dronning Maud Land, Antarctica: implications for the nature of the eastern margin of the Kalahari Craton and the amalgamation of Gondwana. J. Afr. Earth Sci. 59, 74–100.

Griffin, W.L., Pearson, N.J., Belousova, E., Jackson, S.E., van Achterbergh, E., O'Reilly, S.Y., Shee, S.R., 2000. The Hf isotope composition of cratonic mantle: LAM-MC-ICPMS analysis of zircon megacrysts in kimberlites. Geochim. Cosmochim. Acta 64, 133–147.

Groenewald, P.B., Moyes, A.B., Grantham, G.H., Krynauw, J.R., 1995. East Antarctic crustal evolution: geological constraints and modelling in western Dronning Maud Land, East Antarctica. Precambrian Res. 75, 231–250.

Grosch, E.G., Bisnath, A., Frimmel, H.E., Board, W.S., 2007. Geochemistry and tectonic setting of mafic rocks in western Dronning Maud Land, East Antarctica: implications for the geodynamic evolution of the Proterozoic Maud Belt. J. Geol. Soc. 164, 465–475.

Grosch, E.G., Frimmel, H.E., Abu-Alam, T., Košler, J., 2015. Metamorphic and age constraints on crustal reworking in the western H.U. Sverdrupfjella: implications for the evolution of western Dronning Maud Land, Antarctica. J. Geol. Soc. 172, 499–518.

Hagen-Peter, G., Cottle, J., 2017. Evaluating the relative roles of crustal growth versus reworking through continental arc magmatism: a case study from the Ross orogen, Antarctica. Gondwana Res. 55, 153–156.

Hanson, R.E., Martin, M.W., Bowring, S.A., Munyanyiwa, H., 1998. U-Pb zircon age for the Umkondo dolerites, eastern Zimbabwe: 1.1 Ga large igneous province in southern Africa–East Antarctica and possible Rodinia correlations. Geology 26, 1143–1146.

Hanson, R.E., Crowley, J.L., Bowring, S.A., Ramezani, J., Gose, W.A., Dalziel, I.W., Pancake, J. A., Seidel, E.K., Blenkinsop, T.G., Mukwakwami, J., 2004. Coeval large-scale magmatism in the Kalahari and Laurentian cratons during Rodinia assembly. Science 304, 1126–1129.

Harris, P.D., 1999. The geological evolution of Neumayerskarvet in the northern Kirwanveggen, western Dronning Maud Land, Antarctica. Unpublished. Ph.D. thesis. Rand Afrikaans University.

Harris, P.D., Moyes, A.B., Fanning, C.M., Arimstrong, R.A., 1995. Zircon Ion Microscope Results from the Maudheim High-Grade Gneiss Terrane, Western Dronning Maud Land, Antarctica. Extended AbstractsCentennial Geocongress, Rand Afrikaans University, Johannesburg, pp. 240–243.

Hawkesworth, C.J., Kemp, A.I.S., 2006. Using hafnium and oxygen isotopes in zircons to unravel the record of crustal evolution. Chem. Geol. 226, 144–162.

Heinonen, A.P., Andersen, T., Rämö, O.T., 2010. Re-evaluation of rapakivi petrogenesis: source constraints from the Hf isotope composition of zircon in the rapakivi granites and associated mafic rocks of southern Finland. J. Petrol. 51, 1687–1709.

Hiess, J., Bennett, V.C., Nutman, A.P., Williams, I.S., 2011. Archaean fluid-assisted crustal cannibalism recorded by low $\delta^{18}O$ and negative ε Hf (T) isotopic signatures of West Greenland granite zircon. Contrib. Mineral. Petrol. 161, 1027–1050.

Hokada, T., Grantham, G.H., Arima, M., Saito, S., Shiraishi, K., Armstrong, R.A., Eglington, B., Misawa, K., Kaiden, H., 2019. Stenian A-type granitoids in the Namaqua-Natal Belt, southern Africa, Maud Belt, Antarctica and Nampula Terrane, Mozambique: Rodinia and Gondwana amalgamation implications. Geosci. Front. 10, 2265–2280.

Hynes, A., Rivers, T., 2010. Protracted continental collision—evidence from the Grenville orogen. Can. J. Earth Sci. 47, 591–620.

Iizuka, T., Campbell, I.H., Allen, C.M., Gill, J.B., Maruyama, S., Makoka, F., 2013. Evolution of the African continental crust as recorded by U–Pb, Lu–Hf and O isotopes in detrital zircons from modern rivers. Geochim. Cosmochim. Acta 107, 96–120.

Jackson, C., 1999. Characterization of the Mesoproterozoic to Palaeozoic crustal evolution of western Dronning Maud Land. Study 3: deformational history and thermochronology of the Kirwanveggen. Unpublished report. Council for Geoscience Open File Report 1999–0135.

Jacobs, J., Thomas, R.J., Weber, K., 1993. Accretion and indentation tectonics at the southern edge of the Kaapvaal craton during the Kibaran (Grenville) orogeny. Geology 21, 203–206.

Jacobs, J., Bauer, W., Spaeth, G., Thomas, R.J., Weber, K., 1996. Lithology and structure of the Grenville-aged (~ 1.1 Ga) basement of Heimefrontfjella (East Antarctica). Geol. Rundsch. 85, 800–821.

Jacobs, J., Falter, M., Thomas, R.J., Kunz, J., Jessberger, E.K., 1997. 40Ar/39Ar thermochronological constraints on the structural evolution of the Mesoproterozoic Natal Metamophic Province, SE Africa. Precambrian Res. 86, 71–92.

Jacobs, J., Fanning, C.M., Henjes-Kunst, F., Olesch, M., Paech, H.J., 1998. Continuation of the Mozambique Belt into East Antarctica: Grenville-age metamorphism and polyphase Pan-African high-grade events in central Dronning Maud Land. J. Geol. 106, 385–406.

Jacobs, J., Thomas, R.J., Armstrong, R.A., Henjes-Kunst, F., 1999. Age and thermal evolution of the Mesoproterozoic Cape Meredith Complex, West Falkland. J. Geol. Soc. 156, 917–928.

Jacobs, J., Thomas, R.J., 2004. Himalayan-type indenter-escape tectonics model for the southern part of the late Neoproterozoic–early Paleozoic East African–Antarctic orogen. Geology 32, 721–724.

Jacobs, J., Bauer, W., Fanning, C.M., 2003a. New age constraints for Grenville-age metamorphism in western central Dronning Maud Land (East Antarctica), and implications for the palaeogeography of Kalahari in Rodinia. Int. J. Earth Sci. 92, 301–315.
Jacobs, J., Fanning, C.M., Bauer, W., 2003b. Timing of Grenville-age vs. Pan-African medium- to high grade metamorphism in western Dronning Maud Land (East Antarctica) and significance for correlations in Rodinia and Gondwana. Precambrian Res. 125, 1–20.
Jacobs, J., Pisarevsky, S., Thomas, R.J., Becker, T., 2008a. The Kalahari Craton during the assembly and dispersal of Rodinia. Precambrian Res. 160, 142–158.
Jacobs, J., Bingen, B., Thomas, R.J., Bauer, W., Wingate, M.T., Feitio, P., 2008b. Early Palaeozoic orogenic collapse and voluminous late-tectonic magmatism in Dronning Maud Land and Mozambique: insights into the partially delaminated orogenic root of the East African–Antarctic Orogen? Geol. Soc. Lond. Spec. Publ. 308, 69–90.
Jacobs, J., Elburg, M., Läufer, A., Kleinhanns, I.C., Henjes-Kunst, F., Estrada, S., Ruppel, A.S., Damaske, D., Montero, P., Bea, F., 2015. Two distinct Late Mesoproterozoic/Early Neoproterozoic basement provinces in central/eastern Dronning Maud Land, East Antarctica: the missing link, 15–21°E. Precambrian Res. 265, 249–272.
Jacobs, J., Opås, B., Elburg, M.A., Läufer, A., Estrada, S., Ksienzyk, A.K., Damaske, D., Hofmann, M., 2017. Cryptic sub-ice geology revealed by a U-Pb zircon study of glacial till in Dronning Maud Land, East Antarctica. Precambrian Res. 294, 1–14.
Jacobs, J., Mikhalsky, E., Henjes-Kunst, F., Läufer, A., Thomas, R.J., Elburg, M.A., Wang, C.C., Estrada, S., Skublov, G., 2019. Neoproterozoic geodynamic evolution of easternmost Kalahari: Constraints from U-Pb-Hf-O zircon, Sm-Nd isotope and geochemical data from the Schirmacher Oasis, East Antarctica. Precambrian Res. in press.
Johansson, Å., 2009. Baltica, Amazonia and the SAMBA connection—1000 million years of neighbourhood during the Proterozoic? Precambrian Res. 175, 221–234.
Johnston, S.T., Armstrong, R., Heaman, L., McCourt, S., Mitchell, A., Bisnath, A., Arima, M., 2001. Preliminary U-Pb geochronology of the Tugela terrane, Natal belt, eastern South Africa. National Institute of Polar Research (Japan), pp. 40–58 Special Issue 55.
Jones, D.L., Bates, M.P., Li, Z.X., Corner, B., Hodgkinson, G., 2003. Palaeomagnetic results from the ca. 1130 Ma Borgmassivet intrusions in the Ahlmannryggen region of Dronning Maud Land, Antarctica, and tectonic implications. Tectonophysics 375, 247–260.
Jones, R.E., Kirstein, L.A., Kasemann, S.A., Dhuime, B., Elliott, T., Litvak, V.D., Alonso, R., Hinton, R., Facility, E.I.M., 2015. Geodynamic controls on the contamination of Cenozoic arc magmas in the southern Central Andes: insights from the O and Hf isotopic composition of zircon. Geochim. Cosmochim. Acta 164, 386–402.
Kemp, A.I.S., Hawkesworth, C.J., Foster, G.L., Paterson, B.A., Woodhead, J.D., Hergt, J.M., Gray, C.M., Whitehouse, M.J., 2007. Magmatic and crustal differentiation history of granitic rocks from Hf-O isotopes in zircon. Science 315, 980–983.
Krynauw, J.R., Hunter, D.R., Wilson, A.H., 1988. Emplacement of sills into wet sediments at Grunehogna, western Dronning Maud Land, Antarctica. J. Geol. Soc. 145, 1019–1032.
Ksienzyk, A.K., Jacobs, J., 2015. Western Australia-Kalahari (WAlahari) connection in Rodinia: not supported by U/Pb detrital zircon data from the Maud Belt (East Antarctica) and the Northampton Complex (Western Australia). Precambrian Res. 259, 207–221.
Lancaster, P.J., Storey, C.D., Hawkesworth, C.J., Dhuime, B., 2011. Understanding the roles of crustal growth and preservation in the detrital zircon record. Earth Planet. Sci. Lett. 305, 405–412.
Li, Z.X., Bogdanova, S.V., Collins, A.S., Davidson, A., DeWaele, B., Ernst, R.E., Fitzsimons, I.C. W., Fuck, R.A., Gladkochub, D.P., Jacobs, J., Karlstrom, K.E., Lu, S., Natapov, L.M., Pease, V., Pisarevsky, S.A., Thrane, K., Vernikovsky, V., 2008. Assembly, configuration, and break- up history of Rodinia: a synthesis. Precambrian Res. 160, 179–210.
Loewy, S.L., Dalziel, I.W.D., Pisarevsky, S., Connelly, J.N., Tait, J., Hanson, R.E., Bullen, D., 2011. Coats Land crustal block, East Antarctica: a tectonic tracer for Laurentia? Geology 39, 859–862.
Ludwig, K.R., 2011. A Geochronological Toolkit for Microsoft Excel. Berkeley Geochronology Centre Special Publications, p. 1 Version 4.
Macey, P.H., Thomas, R.J., Grantham, G.H., Ingram, B.A., Jacobs, J., Armstrong, R.A., Roberts, M.P., Bingen, B., Hollick, L., De Kock, G.S., Viola, G., 2010. Mesoproterozoic geology of the Nampula Block, northern Mozambique: Tracing fragments of Mesoproterozoic crust in the heart of Gondwana. Precambrian Res. 182, 124–148.
Manhica, A.D.S.T., Grantham, G.H., Armstrong, R.A., Guise, P.G., Kruger, F.J., 2001. Polyphase deformation and metamorphism at the Kalahari Craton—Mozambique Belt boundary. In: Miller, J.A., Holdsworth, R.E., Buick, I.S., Hand, M. (Eds.), Continental Reactivation and Reworking. 184, pp. 303–322 Geological Society, London, Special Publication.
Marschall, H.R., Hawkesworth, C.J., Storey, C.D., Dhuime, B., Leat, P.T., Meyer, H.P., Tamm-Buckle, S., 2010. The Annandagstoppane Granite, East Antarctica: evidence for Archaean intracrustal recycling in the Kaapvaal–Grunehogna Craton from zircon O and Hf isotopes. J. Petrol. 51, 2277–2301.
Marschall, H.R., Hawkesworth, C.J., Leat, P.T., 2013. Mesoproterozoic subduction under the eastern edge of the Kalahari-Grunehogna Craton preceding Rodinia assembly: the Ritscherflya detrital zircon record, Ahlmannryggen (Dronning Maud Land, Antarctica). Precambrian Res. 236, 31–45.
McCourt, S., Armstrong, R.A., Grantham, G.H., Thomas, R.J., 2006. Geology and evolution of the Natal belt, South Africa. J. Afr. Earth Sci. 46, 71–92.
McLelland, J.M., Selleck, B.W., Bickford, M.E., Tollo, R.P., Bartholomew, M.J., Hibbard, J.P., Karabinos, P.M., 2010. Review of the Proterozoic evolution of the Grenville Province, its Adirondack outlier, and the Mesoproterozoic inliers of the Appalachians. From Rodinia to Pangea: the Lithotectonic Record of the Appalachian Region. 206. Geological Society of America Memoir, pp. 21–49.
Mendonidis, P., Armstrong, R.A., 2009. A new U-Pb zircon age for the Portobello granite from the southern part of the Natal Metamorphic belt. S. Afr. J. Geol. 112, 197–208.
Mendonidis, P., Armstrong, R.A., 2016. U–Pb Zircon (SHRIMP) ages of granite sheets and timing of deformational events in the Natal Metamorphic Belt, southeastern Africa: evidence for deformation partitioning and implications for Rodinia reconstructions. Precambrian Res. 278, 22–33.
Mendonidis, P., Thomas, R.J., 2019. A review of the geochronology of the Margate Terrane reveals a history of diachronous terrane docking and arc accretion across the Mesoproterozoic Natal belt, southeastern Africa. J. Afr. Earth Sci. 150, 532–545.
Mendonidis, P., Armstrong, R.A., Eglington, B.M., Grantham, G.H., Thomas, R.J., 2002. Metamorphic history and U-Pb Zircon (SHRIMP) geochronology of the Glenmore Granite: implications for the tectonic evolution of the Natal Metamorphic Province. S. Afr. J. Geol. 105, 325–336.
Mendonidis, P., Armstrong, R.A., Grantham, G.H., 2009. U–Pb SHRIMP ages and tectonic setting of the Munster Suite of the Margate Terrane of the Natal Metamorphic Belt. Gondwana Res. 15, 28–37.
Mendonidis, P., Thomas, R.J., Grantham, G.H., Armstrong, R.A., 2015. Geochronology of emplacement and charnockite formation of the Margate Granite Suite, Natal Metamorphic Province, South Africa: implications for Natal-Maud belt correlations. Precambrian Res. 265, 189–202.
Merdith, A.S., Collins, A.S., Williams, S.E., Pisarevsky, S., Foden, J.D., Archibald, D.B., Blades, M.L., Alessio, B.L., Armistead, S., Plavsa, D., Clark, C., 2017. A full-plate global reconstruction of the Neoproterozoic. Gondwana Res. 50, 84–134.
Mikhalsky, E., Jacobs, J., 2004. Orthogneisses in central Dronning Maud Land, East Antarctica: Their origin and tectonic setting. In: Paech, H.-J. (Ed.), International GeoMaud Expedition of the BGR to Central Dronning Maud in 1995/96–Geological Results. vol. B96, pp. 49–76 Geologisches Jahrbuch.
Moabi, N.G., Grantham, G.H., Roberts, J., Le Roux, P., 2017. The geology and geochemistry of the Straumsnutane Formation, Straumsnutane, western Dronning Maud Land, Antarctica and its tectonic setting on the western margin of the Kalahari Craton: additional evidence linking it to the Umkondo Large Igneous Province. Geol. Soc. Lond. Spec. Publ. 457, 61–85.
Montero, P., Talavera, C., Bea, F., 2017. Geochemical, isotopic, and zircon (U-Pb, O, Hf isotopes) evidence for the magmatic sources of the volcano-plutonic Ollo de Sapo Formation, Central Iberia. Geol. Acta 15, 245–260.
Moyes, A.B., 1993. The age and origin of the Jutulsessen granitic gneiss, Gjelsvikfjella, Dronning Maud Land. SA J. Antarctic Res. 23, 25–32.
Moyes, A.B., Krynauw, J.R., Barton, J.M., 1995. The age of the Ritscherflya Supergroup and Borgmassivet Intrusions, Dronning Maud Land, Antarctica. Antarct. Sci. 7, 87–97.
Murphy, J.B., Nance, R.D., 2005. Do supercontinents turn inside-in or inside-out? Int. Geol. Rev. 47, 591–619.
Nemchin, A.A., Whitehouse, M.J., Pidgeon, R.T., Meyer, C., 2006. Oxygen isotopic signature of 4.4–3.9 Ga zircons as a monitor of differentiation processes on the Moon. Geochim. Cosmochim. Acta 70, 1864–1872.
Oriolo, S., Becker, T., Siegesmund, S., 2018. In: Stipp Basei, M.A., Oyhantçabal, P., Oriolo, S. (Eds.), The Kalahari Craton, Southern Africa: From Archean Crustal Evolution to Gondwana Amalgamation. Springer International Publishing, Geology of Southwest Gondwana, pp. 133–159.
Paulsson, O., Austrheim, H., 2003. A geochronological and geochemical study of rocks from Gjelsvikfjella, Dronning Maud Land, Antarctica—implications for Mesoproterozoic correlations and assembly of Gondwana. Precambrian Res. 125, 113–138.
Payne, J.L., McInerney, D.J., Barovich, K.M., Kirkland, C.L., Pearson, N.J., Hand, M., 2016. Strengths and limitations of zircon Lu-Hf and O isotopes in modelling crustal growth. Lithos 248, 175–192.
Pearce, J.A., Kempton, P.D., Nowell, G.M., Noble, S.R., 1999. Hf-Nd element and isotope perspective on the nature and provenance of mantle and subduction components in western Pacific arc-basin systems. J. Petrol. 40, 1579–1611.
Peters, M., Haverkamp, B., Emmermann, R., Kohnen, H., Weber, K., 1991. Palaeomagnetism, K-Ar dating and geodynamic setting of igneous rocks in western and central Neuschwabenland, Antarctica. In: Thomson, M.R.A., Crame, J.A., Thomson, J.W. (Eds.), Geological Evolution of Antarctica. Cambridge University Press, Cambridge, pp. 549–555.
Pisarevsky, S.A., Wingate, M.T., Powell, C.M., Johnson, S., Evans, D.A., 2003. Models of Rodinia assembly and fragmentation. Geol. Soc. Lond. Spec. Publ. 206, 35–55.
Powell, C.M., Jones, D.L., Pisarevsky, S., Wingate, M.T.D., 2001. Palaeomagnetic constraints on the position of the Kalahari craton in Rodinia. Precambrian Res. 110, 33–46.
Rehman, H.U., Kitajima, K., Valley, J.W., Chung, S.L., Lee, H.Y., Yamamoto, H., Khan, T., 2018. Low-$\delta^{18}O$ mantle-derived magma in Panjal Traps overprinted by hydrothermal alteration and Himalayan UHP metamorphism: Revealed by SIMS zircon analysis. Gondwana Res. 56, 12–22.
Rivers, T., 2009. The Grenville Province as a large hot long-duration collisional orogen–insights from the spatial and thermal evolution of its orogenic fronts. Geol. Soc. Lond. Spec. Publ. 327, 405–444.
Roberts, N.M., Spencer, C.J., 2015. The zircon archive of continent formation through time. Geol. Soc. Lond. Spec. Publ. 389, 197–225.
Scherer, E., Münker, C., Mezger, K., 2001. Calibration of the lutetium-hafnium clock. Science 293, 683–687.
Söderlund, U., Patchett, P.J., Vervoort, J.D., Isachsen, C.E., 2004. The ^{176}Lu decay constant determined by Lu–Hf and U–Pb isotope systematics of Precambrian mafic intrusions. Earth Planet. Sci. Lett. 219, 311–324.
Spencer, C.J., Thomas, R.J., Roberts, N.M.W., Cawood, P.A., Millar, I., Tapster, S., 2015. Crustal growth during island arc accretion and transcurrent deformation, Natal Metamorphic Province, South Africa: new isotopic constraints. Precambrian Res. 265, 203–217.
Spencer, C.J., Kirkland, C.L., Prave, A.R., Strachan, R.A., Pease, V., 2019. Crustal reworking and orogenic styles inferred from zircon Hf isotopes: Proterozoic examples from the North Atlantic region. Geosci. Front. 10, 417–424.
Stern, R.J., 1994. Arc assembly and continental collision in the Neoproterozoic East African Orogen: implications for the consolidation of Gondwanaland. Annu. Rev. Earth Planet. Sci. 22, 319–351.

Swanson-Hysell, N.L., Kilian, T.M., Hanson, R.E., 2015. A new grand mean palaeomagnetic pole for the 1.11 Ga Umkondo large igneous province with implications for palaeogeography and the geomagnetic field. Geophys. J. Int. 203, 2237–2247.
Teixeira, W., Hamilton, M.A., Lima, G.A., Ruiz, A.S., Matos, R., Ernst, R.E., 2015. Precise ID-TIMS U–Pb baddeleyite ages (1110–1112 Ma) for the Rincón del Tigre–Huanchaca large igneous province (LIP) of the Amazonian Craton: Implications for the Rodinia supercontinent. Precambrian Res. 265, 273–285.
Thomas, R.J., Eglington, B.M., 1990. A Rb–Sr, Sm–Nd and U–Pb zircon isotopic study of the Mzumbe Suite, the oldest intrusive granitoid in southern Natal, South Africa. S. Afr. J. Geol. 93, 761–765.
Thomas, R.J., Eglington, B.M., Bowring, S.A., 1993. Dating the cessation of Kibaran magmatism in Natal, South Africa. J. Afr. Earth Sci. 16, 247–252.
Thomas, R.J., Agenbacht, A.L.D., Cornell, D.H., Moore, J.M., 1994. The Kibaran of southern Africa: tectonic evolution and metallogeny. Ore Geol. Rev. 9, 131–160.
Thomas, R.J., Cornell, D.H., Armstrong, R.A., 1999. Provenance age and metamorphic history of the Quha Formation, Natal Metamorphic Province: a U-Th-Pb zircon SHRIMP study. S. Afr. J. Geol. 102, 83–88.
Thomas, R.J., Jacobs, J., Eglington, B.M., 2000. Geochemistry and isotopic evolution of the Mesoproterozoic Cape Meredith Complex, West Falkland. Geol. Mag. 137, 537–553.
Thomas, R.J., Armstrong, R.A., Eglington, B.M., 2003. Geochronology of the Sikombe Granite, Transkei, Natal Metamorphic Province, South Africa. S. Afr. J. Geol. 106, 403–408.
Thomas, R.J., Jacobs, J., Horstwood, M.S.A., Ueda, K., Bingen, B., Matola, R., 2010. The Mecubúri and Alto Benfica groups, NE Mozambique: aids to unravelling ca. 1 and 0.5 Ga events in the east African orogen. Precambrian Res. 178, 72–90.
Torsvik, T.H., 2003. The Rodinia jigsaw puzzle. Science 300, 1379–1381.
Valley, J.W., 2003. Oxygen isotopes in zircon. Rev. Mineral. Geochem. 53, 343–385.
Valley, J.W., Kinny, P.D., Schulze, D.J., Spicuzza, M.J., 1998. Zircon megacrysts from kimberlite: oxygen isotope variability among mantle melts. Contrib. Mineral. Petrol. 133, 1–11.
Vroon, P.Z., Lowry, D., van Bergen, M.J., Boyce, A.J., Mattey, D.P., 2001. Oxygen isotope systematics of the Banda Arc: low $\delta^{18}O$ despite involvement of subducted continental material in magma genesis. Geochim. Cosmochim. Acta 65, 589–609.
Wareham, C.D., Pankhurst, R.J., Thomas, R.J., Storey, B.C., Grantham, G.H., Jacobs, J., Eglington, B.M., 1998. Pb, Nd, and Sr isotope mapping of Grenville-age crustal provinces in Rodinia. J. Geol. 106, 647–660.
Weil, A.B., Van der Voo, R., Mac Niocaill, C., Meert, J.G., 1998. The Proterozoic supercontinent Rodinia: paleomagnetically derived reconstructions for 1100 to 800 Ma. Earth Planet. Sci. Lett. 154, 13–24.
Wiedenbeck, M., Hanchar, J.M., Peck, W.H., Sylvester, P., Valley, J., Whitehouse, M., Kronz, A., Morishita, Y., Nasdala, L., Fiebig, J., Franchi, I., 2004. Further characterisation of the 91500 zircon crystal. Geostand. Geoanal. Res. 28, 9–39.
Wolmarans, L.G., Kent, K.E., 1982. Geological investigations in western Dronning Maud Land, Antarctica—a synthesis. S. Afr. J. Antarct. Res. 2, 1–93.
Woodhead, J.D., Hergt, J.M., 2005. A preliminary appraisal of seven natural zircon reference materials for in situ Hf isotope determination. Geostand. Geoanal. Res. 29, 183–195.
Zheng, Y.F., Wu, Y.B., Chen, F.K., Gong, B., Li, L., Zhao, Z.F., 2004. Zircon U-Pb and oxygen isotope evidence for a large-scale ^{18}O depletion event in igneous rocks during the Neoproterozoic. Geochim. Cosmochim. Acta 68, 4145–4165.

Paper II

***Wang, C-C.**, Wiest, J.D., Jacobs, J., Bingen, B., Whitehouse, M.J., Elburg, M.A., Sørstrand, T.S., Mikkelsen, L., Hestnes, Å., 2021. Tracing the Sveconorwegian orogen into the Caledonides of West Norway: geochronological and isotopic studies on magmatism and migmatization. Accepted, Precambrian Research, 106301.*

Tracing the Sveconorwegian orogen into the Caledonides of West Norway: geochronological and isotopic studies on magmatism and migmatization

Cheng-Cheng Wang[a*], Johannes D. Wiest[a,b], Joachim Jacobs[a], Bernard Bingen[c], Martin J. Whitehouse[d], Marlina A. Elburg[e], Thea S. Sørstrand[a], Lise Mikkelsen[a], Åse Hestnes[a]

[a] Department of Earth Science, University of Bergen, PB7803, N-5020 Bergen, Norway
[b] Geozentrum Nordbayern, Friedrich-Alexander-Universität Erlangen-Nürnberg, 91054 Erlangen, Germany
[c] Geological Survey of Norway, 7491 Trondheim, Norway
[d] Department of Geosciences, Swedish Museum of Natural History, Stockholm, Sweden
[e] Department of Geology, University of Johannesburg, Auckland Park 2006, Johannesburg, South Africa

Abstract

The Sveconorwegian orogen represents a branch of Grenville-age (~1250–950 Ma) orogenic belts that formed during the construction of the supercontinent Rodinia. This study traces the Sveconorwegian records from its type-area in the Baltic Shield of South Norway into basement windows underneath Caledonian nappes, by combining zircon U–Pb geochronology and Hf–O isotopes. Samples along a N-S trending transect reveal multiple magmatic episodes during Gothian (ca. 1650 Ma), Telemarkian (ca. 1500 Ma) and Sveconorwegian (1050–1020 Ma vs. 980–930 Ma) orogenesis as well as Sveconorwegian migmatization (1050–950 Ma). Newly documented 1050–1020 Ma magmatism and migmatization extend the Sirdal Magmatic Belt to a 300 km-long, NNW-SSE trending crustal domain, with the northern boundary corresponding to the gradual transition from Telemarkian to Gothian crust. These Precambrian crustal heterogeneities largely controlled the development of Caledonian shear zones. Extensive granitic magmas were produced during ca. 1050–1040 Ma, and their slightly positive εHf(t) and moderate $\delta^{18}O$ values (6–7‰) indicate they were most likely products of mixed melts from older Telemarkian crust and juvenile mafic crust. The generation of leucosomes and leucogranites at ca. 1030–1020 Ma, which have a more evolved Hf isotopic composition, probably reflect a higher degree of remelting of older crust. The Hf–O isotopic patterns show that Sveconorwegian magmas differ from typical arc magmas by lower involvement of sedimentary components and juvenile material. This makes the 1050–930 Ma magmatism incompatible with a long-term subduction setting. The ca. 1650–1500 Ma samples, in contrast, generally have juvenile Hf isotopic compositions associated with varying $\delta^{18}O$ values of 4.5–9‰, consistent with subduction-accretion processes involving significant sedimentary recycling. This accretionary margin was most likely transformed into the Sveconorwegian orogen through the collisional interactions of Baltica, Laurentia and Amazonia in the context of Rodinia amalgamation.

Key words

Mesoproterozoic; Baltica; Zircon U–Pb geochronology, Hf–O isotopes; Collisional orogen; Rodinia

1 Introduction

Baltica records a long-lived orogenic history associated with the formation of the supercontinent Columbia/Nuna and its breakup and reassembly into Rodinia. Svetlana Bogdanova, honored in this special volume, made a career-long effort to correlate the geology across continents to give substance to models of assembly and breakup of these supercontinents (Gorbatschev and Bogdanova, 1993; Bogdanova et al., 2008; Bogdanova et al., 2015). The southwestern margin of Baltica has been interpreted as an active continental margin that probably witnessed a continuous process of crustal accretion and growth during the Paleo- and Mesoproterozoic (Gorbatschev and Bogdanova, 1993; Åhäll and Larson, 2000; Andersen et al., 2002; Roberts and Slagstad, 2015), and was subsequently overprinted by the Grenville-age Sveconorwegian orogeny during Rodinia assembly (Fig. 1a, Bogdanova et al., 2008). The Sveconorwegian orogenic evolution remains a hot topic for debate, although much has been published on the many very varied aspects of geology and geochemistry in recent years (e.g. Slagstad et al., 2018a, 2020; Bingen et al., 2018, 2021; Stephens et al., 2020). In archetypal reconstructions of Rodinia, Laurentia is located in the centre of Rodinia, with Baltica to the east and Amazonia to the south and the Sveconorwegian orogen facing the northern margin of Amazonia (present coordinates) (Hoffman, 1991; Torsvik, 1996; Dalziel, 1997; Li et al., 2008; Cawood and Pisarevsky, 2017; Merdith et al., 2017). The Kalahari craton is regarded as another core constituent of the Rodinia landmass on the western side of the supercontinent, as supported by both paleomagnetic and geological studies (Dalziel et al., 2000; Jacobs et al., 2008; Swanson-Hysell et al., 2015, 2019).

During and after Rodinia breakup, the margins of Laurentia, Baltica and Amazonia were affected by two Wilson cycles from the late Neoproterozoic to the Mesozoic. These cycles involved the opening and closing of the Iapetus Ocean, formation of the Caledonian and Appalachian orogens, and opening of the Atlantic Ocean (Torsvik et al., 1996; Bingen et al., 1998; Cawood et al., 2001; Cocks and Torsvik, 2005). Portions of the margins of Laurentia, Baltica and Amazonia, characterized by Mesoproterozoic magmatism and metamorphism, are now located in basement windows (inliers) and in thrust nappes in the Caledonides of Scandinavia, the British Isles and Greenland, and the Appalachian Mountains of Canada and the USA (Bingen et al., 2008c; McLelland et al., 2010; Roffeis and Corfu, 2014). In West Norway, the Baltican basement is largely exposed underneath vast thrust sheets (Fig. 1b), and the intersection between the Caledonian and Sveconorwegian orogens makes it a challenging but interesting issue to clarify the northward extension of the Sveconorwegian Province (e.g. Lorenz et al., 2012; Gee et al., 2015). Investigating these basement windows is crucial to understand the composition and evolution of the continental crust, determine the distribution of the orogenic domains, and reconstruct the Grenville-age orogeny during Rodinia assembly.

In this paper, we address the geology, geochronology and isotope geochemistry of four parts of the Baltican basement in West Norway that represent variable states of Caledonian reworking (Fig. 1).

Corresponding to increasing strain from southeast to northwest, they are the Hardangerfjord area (Fossen and Hurich, 2005), the Øygarden Complex (Wiest et al., 2020a) and the southern and central parts of the Western Gneiss Region (Gulen dome (Wiest et al., 2019) and Nordfjord area (Labrousse et al., 2004)). We report zircon U–Pb, Lu–Hf and O isotopic data on zircons from magmatic rocks and leucosomes from migmatites. By constraining the magmatic and metamorphic events, we explore the relation between the basement windows and the type-area of the Sveconorwegian orogen in southwest Norway, and thereby trace the Sveconorwegian orogeny northwards. Furthermore, the review and comparison of Mesoproterozoic orogenesis along the margins of Baltica, Laurentia and Kalahari allows for a better understanding of the tectonic evolution of Grenville-age orogenic belts in the core of Rodinia.

2 Geological setting

2.1 The Sveconorwegian orogen

The Sveconorwegian orogen (ca. 1150–900 Ma) is a ca. 550 km wide orogenic zone covering south Norway and southwest Sweden (Fig.1a). It can be divided into five main lithotectonic units/terranes separated by N-S-trending crustal-scale shear zones. From the Sveconorwegian front in the east towards the west these are: the Eastern Segment, the Idefjorden, Kongsberg, Bamble and Telemarkia lithotectonic units (Bingen et al., 2008a, 2021). The Sveconorwegian orogen was built on the Paleo-Mesoproterozoic continental lithosphere. In general, the formation of the first lithosphere in these five units occurred progressively later towards the west: in the Eastern Segment as part of the 1710–1660 Ma Transcandinavian Igneous Belt, at 1660–1520 Ma during the Gothian orogeny in the Idefjorden, Bamble and Kongsberg units, and at 1520–1480 Ma during the Telemarkian orogeny in the Telemarkia unit (Bingen et al., 2005; Roberts and Slagstad, 2015). After lithosphere formation, the Eastern Segment was affected by the 1.47–1.38 Ga Hallandian accretionary orogeny, which has been scarcely reported in the remaining of the Sveconorwegian orogen to the west of the Eastern Segment (Ulmius et al., 2015).

The five lithotectonic units are characterized by distinct Sveconorwegian magmatic and metamorphic histories. The Eastern Segment appears to be distinct from the other four units by lacking >1000 Ma Sveconorwegian events. It is characterized by ca. 990 Ma eclogite-facies metamorphism with estimated peak P-T conditions at 860–900°C/1.65–1.8 GPa (Möller et al., 2015; Tual et al., 2017). This metamorphism was interpreted to reflect underthrusting of the Eastern Segment beneath the lithotectonic units to the west (Möller and Andersson, 2018). The Idefjorden unit contains evidence for 1050–1020 Ma granulite-facies metamorphism and several pulses of magmatism between 1040 and 910 Ma (Bingen et al., 2008b; Söderlund et al., 2008; Bergström et al., 2020). In the Kongsberg and Bamble units, high-grade metamorphism is older at 1150–1120 Ma (Cosca et al., 1998; Bingen et al., 2008b; Engvik et al., 2016; Bingen and Viola, 2018). The Telemarkia unit features 1050–930 Ma granitic magmatism, 930–920 Ma anorthosite–mangerite–charnockite magmatism and associated high-grade metamorphism (more details below). Distinct Sveconorwegian magmatic and metamorphic records in

the five lithotectonic units reflect a complex orogenic history. Therefore, there are distinct views in the literature on the formation and evolution of the Sveconorwegian orogen, and contrasting tectonic models have been proposed (see review in Bingen et al., 2021 and references therein). In general, the debate centers on whether the Sveconorwegian orogen represents an accretionary orogen with long-term subduction, or a continental collision orogen that can be regarded as an extension of the Grenville Orogen in Laurentia (e.g. Slagstad et al., 2018a, 2020; Möller and Andersson, 2018; Bingen et al., 2018, 2021).

2.2 The Telemarkia unit

The Telemarkia crust mainly formed during three episodes of magmatic events, at 1520–1480 Ma, 1280–1140 Ma and 1060–930 Ma (Andersen et al., 2001, 2007; Bingen et al., 2005; Pedersen et al., 2009; Roberts et al., 2013; Roberts and Slagstad, 2015). The 1520–1480 Ma event (Telemarkian) is interpreted as a supra-subduction accretionary event, with voluminous volcanic arc lithologies towards the west (the Suldal volcanic arc; Roberts et al., 2013) and back-arc rift lithologies towards the east (the Rjukan rift). The 1280–1140 Ma rocks are mainly bimodal plutonic and volcanic suites as well as associated sedimentary rocks, which formed in the 1280–1240 Ma, 1230–1200 Ma and 1180–1140 Ma time intervals. The 1060–930 Ma Sveconorwegian syn-orogenic magmatic rocks include three main plutonic suites, the 1060–1020 Ma Sirdal Magmatic Belt (SMB), the 980–930 Ma hornblende-biotite granite suite (HBG) and the 930–920 Ma Rogaland anorthosite–mangerite–charnockite suite (Vander Auwera et al., 2011; Granseth et al., 2020) (Fig. 1b). The SMB is a more than 150 km long, NNW-SSE trending batholith exposed from the southern tip of Norway and disappearing northwards under Caledonian nappes (Slagstad et al., 2013). It is mainly composed of porphyritic amphibole-biotite and biotite granitoids, associated with leucogranite and garnet granite (Coint et al., 2015). These rocks have a high-K calc-alkaline geochemical signature (Slagstad et al., 2013a, b; Bingen et al., 2015) that may reflect inheritance from the source rocks, i.e. the 1520–1480 Ma calc-alkaline rocks of the Suldal volcanic arc (Coint et al., 2015). The 980–930 Ma HBG suite occurs as discrete granitoid plutons with a ferroan ‘A-type’ geochemical signature, cropping out in the area defined by the SMB and east of it (Bogaerts et al., 2003; Vander Auwera et al., 2011; Granseth et al., 2020). The 930–920 Ma Rogaland anorthosite–mangerite–charnockite suite, exposed in the westernmost part of the orogen, is a Proterozoic massif-type anorthosite plutonic complex, which is anhydrous with an alkalic ferroan geochemical signature (Fig. 1b; Ashwal, 1993; Schärer et al., 1996; Vander Auwera et al., 2011).

The metamorphic grade increases southwestwards in the Telemarkia unit towards the Rogaland anorthosite–mangerite–charnockite plutonic complex. Three isograds are mapped, the orthopyroxene-in, osumilite-in and pigeonite-in isograds (Tobi et al., 1985). Metamorphic zircon and monazite define a wide range of U–Pb apparent ages ranging from ca. 1050 to 920 Ma (Möller et al., 2002; Tomkins et al., 2005; Bingen et al., 2008a; Drüppel et al., 2013; Blereau et al., 2017; Laurent et al., 2018a, b;

Slagstad et al., 2018), suggesting that this region underwent long-lived high-grade metamorphism. In more detail, two distinct metamorphic events can be recognized, both reaching ultra-high temperature (>900 °C) conditions. The first event is interpreted as part of a long-lived regional metamorphic event, peaking at ca. 0.6 GPa/920 °C and dated between ca. 1045 and 990 Ma, while the second event, peaking at ca. 4.5 GPa/900°C, was closely related to the intrusion of the anorthosite–mangerite–charnockite complex at ca. 930 Ma (Drüppel et al., 2013; Blereau et al., 2017; Laurent et al., 2018a, b).

2.3 The Caledonian orogen

Break-up of Rodinia and the opening of the Iapetus Ocean in the Neoproterozoic formed a segmented passive margin of Baltica (e.g. Jakob et al., 2019). Subsequent closure of the Iapetus in the Paleozoic resulted in the Caledonian orogeny, which culminated with the collision between Laurentia, Avalonia and Baltica in the Silurian–Devonian (Scandian orogeny) (Corfu et al., 2014a). Various parts of the Laurentian margin, the Iapetus oceanic realm and the distal domains of the Baltican margin were thrust onto Baltica, while the western margin of Baltica was subducted below Laurentia down to mantle depths (Brueckner, 2018). Continent-continent collision was swiftly followed by a change from plate convergence to divergence (Fossen, 1992; Rey et al., 1997). Early Devonian transtensional collapse formed an orogen-wide network of extensional detachments and supra-detachment basins (Fossen, 2010) and resulted in the diachronous exhumation of the former orogenic infrastructure in metamorphic core complexes of variable size (Wiest et al., 2021). Later extensional episodes, related to North Sea rifting, took place from the Permian throughout the Mesozoic, reactivating the previously formed crustal template in a brittle fashion (Fossen et al., 2016; Ksienzyk et al., 2016; Peron-Pinvidic and Osmundsen, 2020; Wiest et al., 2020b).

2.4 Geology of the studied areas

Western Gneiss Region (WGR)

The WGR represents a giant (> 30,000 km^2) basement window underneath the Caledonian nappes, exposing the Proterozoic Baltican margin that was subducted to (ultra)high-pressure metamorphism and variably deformed (Milnes et al., 1997; Wain, 1997; Hacker et al., 2010) (Fig. 1b). The WGR mainly consists of migmatitic orthogneisses with dioritic to granitic compositions. The protoliths formed mostly during the Gothian orogeny around 1650 Ma (Bingen et al., 2005) and were intruded by mafic dykes at 1470–1450 and 1260–1250 Ma (Austrheim et al., 2003; Krogh et al., 2011; Beckman et al., 2014). Except for the north-easternmost part of the WGR, there is abundant evidence for Sveconorwegian reworking, including widespread migmatization, granitic magmatism and granulite-facies metamorphism (Tucker et al., 1990; Skar and Pedersen, 2003; Røhr and Corfu, 2004; Glodny et al., 2008). Ages of Sveconorwegian granites and migmatites in the WGR fall exclusively in the range between ca. 980 and 940 Ma (e.g. Skår and Pedersen, 2003; Gordon et al., 2013; Røhr et al., 2013; Kylander-Clark and Hacker, 2014). In contrast to the Sveconorwegian orogen in southwest Norway,

1060–1020 Ma intrusives have not been reported.

This study addresses the Nordfjord and Gulen areas, which constitute a transect from ultra high-pressure to high-pressure conditions of Caledonian reworking in the Baltican basement. The Nordfjord domain represents the southernmost occurrence of ultra high-pressure minerals and furthermore records migmatization and intense shearing during extensional collapse (Labrousse et al., 2002; Labrousse et al., 2004; Kylander-Clark and Hacker, 2014). The Gulen area defines a metamorphic core complex in the southernmost WGR, the Gulen dome, which exhumed strongly deformed, eclogite-bearing crust during Devonian collapse (in the footwall of the extensional Bergen Arcs Shear Zone and the Nordfjord-Sogn detachment) (Wiest et al., 2019). Like other parts of the WGR, eclogites are hosted in migmatites, but based on field observations, Wiest et al. (2019) inferred that Caledonian deformation involved exclusively solid-state shearing and, hence, migmatization must be older. Granulite-facies rocks along the rim of a weakly deformed granite-diorite pluton revealed Tonian U–Pb zircon (ca. 980 Ma) and monazite (ca. 950 Ma) ages (Røhr et al., 2004), while the Caledonian shear zones are associated with Ar-Ar mica ages mostly in the range from 405 to 393 Ma (Wiest at al., 2021).

Øygarden Complex

The Øygarden Complex is the southernmost Devonian metamorphic core complex along the west coast of South Norway (Wiest et al., 2020a). It is separated from the neighbouring Gulen dome by the Bergen Arcs Shear Zone (Fig. 1c) (Wennberg et al., 1998) and in contrast to the former, no eclogites have been documented in this region. The eastern (structurally higher) part of the Øygarden Complex consists of a Sveconorwegian magmatic complex, comprising ca. 1040 Ma granites and gabbros as well as 1020 Ma leucogranites, intruding Telemarkian (1500 Ma) granitic basement (Wiest et al., 2018). The western (structurally lower) part of the Øygarden Complex consists mostly of migmatites with granitic to dioritic compositions and associated leucogranites. The migmatites at the deepest levels of the dome are evidently Caledonian and crystallized at ca. 405 Ma, but preserve also Sveconorwegian ages (Wiest et al., 2021). The entire complex was strongly sheared (Wiest et al., 2020a) during core-complex exhumation between 405 and 398 Ma (Wiest at al., 2021).

Hardangerfjord area

The Hardangerfjord runs along a major Devonian extensional shear zone, the Hardangerfjord shear zone, that juxtaposes Caledonian nappes in the NW, above a Proterozoic basement little affected by Caledonian reworking in the SE (Fig. 1c) (Fossen and Hurich, 2005). As such, the Hardangerfjord shear zone represents the southernmost limit of thick-skinned deformation during Caledonian extensional collapse (Fossen et al., 2014). Towards the SE, this Proterozoic basement is largely covered by Caledonian nappes, called the Hardangervidda-Ryfylke nappe complex, in such a way that the continuity of outcrop between the Proterozoic rocks in the Hardangerfjord area and the Telemarkia lithotectonic unit of the Sveconorwegian orogen is only locally observable (Roffeis et al., 2013). On

geological maps, the Proterozoic basement in the Hardangerfjord area is directly correlated with the Telemarkia lithotectonic unit further south and considered as integral part of it (Bingen et al., 2005; Sigmond, 1998). However, actual data to support this correlation are scant.

The Proterozoic basement in the Hardangerfjord area consists of large NNW-SSE-trending granite plutons, which intrude tracts of tonalitic to gabbroic rocks and supracrustal sequences (Torske, 1982). Metavolcanic rocks within the latter have a Telemarkian (1500 Ma) age (Bingen et al., 2005) similar to gabbros and granites in the Suldal volcanic arc further south (Roberts et al., 2013). Caledonian extensional deformation was highly localized into weak lithologies in the nappes and a narrow shear zone in the basement, leaving most of the Precambrian lithologies in this area virtually undeformed.

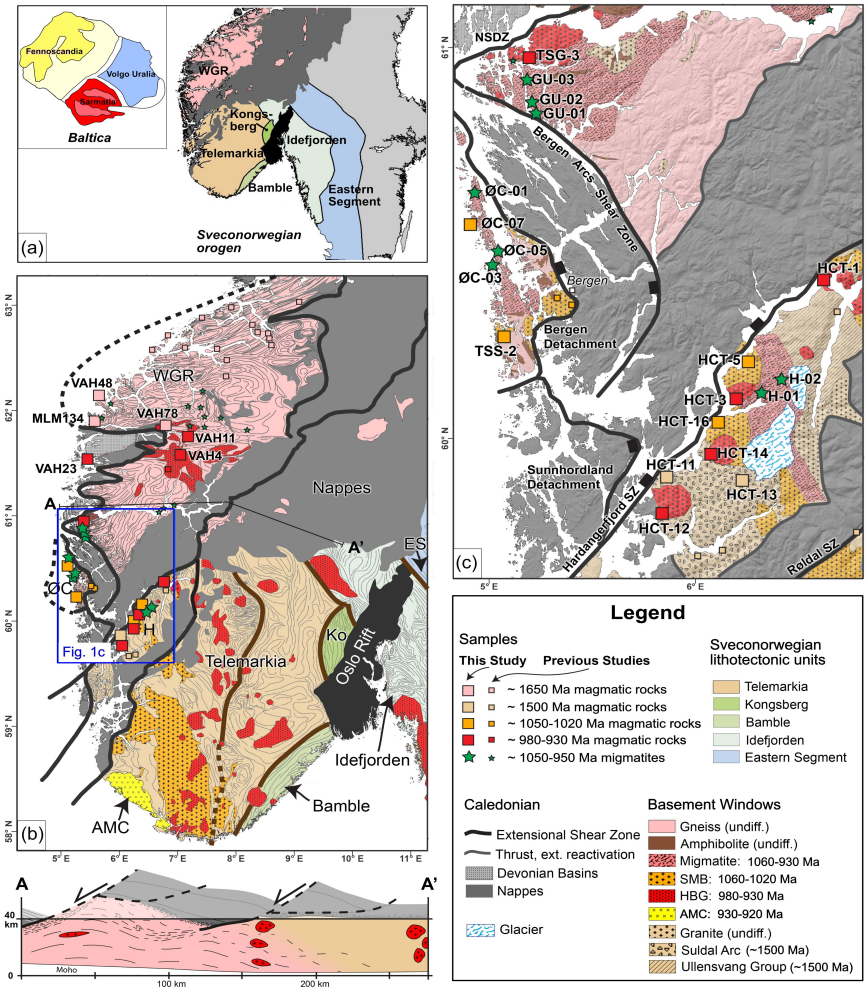

Fig. 1: (a) Tectonic sketch map of Baltica (after Bogdanova et al., 2008) and the Sveconorwegian orogen; (b) Geologic overview map of South Norway, showing the distribution of Sveconorwegian crust, its relation to the Caledonian province (nappes) to the north and location of the study area with samples localities in the WGR; schematic cross section (A-A', modified from Milnes et al., 1997) showing the structural relationship between the undeformed Baltic Shield and variably deformed crust (schematically represented by the shape of granites) exposed in the Caledonian basement windows; (c) Newly compiled geologic map of the study area, with igneous and migmatite samples from the Øygarden Complex and the Hardangerfjord area. The interpreted distribution of Sveconorwegian crustal ages is based on new and previously published U–Pb zircon geochronology. Abbreviations: AMC, Anorthosite–Mangerite–Charnockite suite; ES, Eastern Segment; H, Hardangerfjord area; HBG, hornblende-biotite granite; Ko, Kongsberg unit; NSDZ, Nordfjord-Sogn Detachment Zone; ØC, Øygarden Complex; SMB, Sirdal Magmatic Belt; SZ, shear zone; WGR, Western Gneiss Region.

3 Methods

This study involves twenty-five newly collected igneous and migmatite samples from the Hardangerfjord area, the Øygarden Complex and the WGR as well as six igneous samples dated by Wiest et al. (2018). Selected zircon grains were mounted in epoxy and polished. Prior to U–Pb analyses, images were collected with optical microscopy (reflected and transmitted light) and with a cathodoluminescence (CL) detector in a scanning electron microscope, to reveal the internal textures of zircon and select analytical spots. U–Pb, Lu–Hf and O isotopic analyses were performed as much as possible on the same spot or from the same growth zone. Detailed analytical methods are described in Supplementary File A.

Zircon U–Pb dating was carried out using a CAMECA IMS-1280 instrument at the NordSIM laboratory, Swedish Museum of Natural history, Stockholm. Weighted mean ages and concordia ages are calculated with the program Isoplot (Version 4.15). All errors are reported at the 2σ-level. Oxygen isotope ratios of zircon were measured with the same instrument with a Cs source. Prior to O analysis, the U–Pb analysis pits were removed by polishing. The values of average $\delta^{18}O$ values are reported as mean ± standard deviation (S.D.).

Lu–Hf isotopes were measured at the University of Johannesburg, using an ASI Resonetics 193 nm Excimer laser ablation system coupled to a Nu Plasma II multi-collector ICPMS. Initial epsilon Hf values (εHf(t)) were calculated using a decay constant of 1.867×10^{-11} (Scherer et al., 2001; Söderlund et al., 2004), and CHUR models of Bouvier et al. (2008) ($^{176}Lu/^{177}Hf$ and $^{176}Hf/^{177}Hf$ of 0.0336 and 0.282785, respectively). The calculation of model ages is based on the depleted mantle model of Griffin et al. (2000) with present-day $^{176}Hf/^{177}Hf = 0.28325$ and $^{176}Lu/^{177}Hf = 0.0384$. Initial $^{176}Hf/^{177}Hf$ and epsilon Hf values for analyzed zircons from magmatic rocks were calculated using the respective interpreted crystallization age of each sample. For anatectic zircons from leucosomes in migmatites, the concordia age interpreted as the crystallization age of the melts were used, although some samples may record multiple periods of partial melting and migmatization. The values of average εHf(t) and $^{176}Hf/^{177}Hf_{(i)}$ for each sample are reported as mean ± S.D.

4 Results, (meta)igneous rocks

Key information on the samples, including the lithologies, coordinates, U–Pb, Lu–Hf and O isotopic data, is summarized in Table 1.

4.1 Hardangerfjord area

Telemarkian (ca. 1520 Ma) tonalitic gneisses

Samples HCT-11 and HCT-13 are two grey tonalitic gneisses collected some 15 km apart. The outcrop of HCT-13 is weakly foliated and interlayered with amphibolite (Fig. 2a, b). Zircon crystals from these two samples exhibit broad CL-bright domains with oscillatory or banded zoning frequently surrounded by CL-dark rims, tips or prisms. In sample HCT-11, 16 analyses mostly on CL-bright, zoned domains give a concordia age at 1528 ± 7 Ma (MSWD = 1.6) (Fig. 2a). In sample HCT-13, 20 analyses were conducted on zoned domains, and 11 of them define a concordia age at 1516 ± 6 Ma (MSWD = 1.5) (Fig. 2b). These ages represent the crystallization age of the tonalite protolith.

Their Hf isotopic compositions are rather juvenile with mean εHf(t) values of +6.9 ± 0.7 and +4.8 ± 0.8 for HCT-11 and HCT-13 respectively; $\delta^{18}O$ values are in the range of or slightly lower than mantle value, and the average values are 4.5/4.6 ± 0.2‰.

Sveconorwegian (ca. 1050–930 Ma) granitoids

Sample HCT-16 is a weakly foliated porphyritic granite (Fig. 2c). Zircon crystals are usually subhedral, fractured and rich in inclusions. In CL images, most grains exhibit highly luminescent cores with oscillatory zoning surrounded by darker rims, tips or prisms. Some grains are entirely CL-dark with patchy and mosaic CL emission locally or along the margin, and have high contents of common lead, suggesting possible metamictization and alteration by hydrothermal fluids. Seventeen analyses were conducted on oscillatory zoned cores. One analysis, although slightly discordant (disc. 5.6%), gives a $^{207}Pb/^{206}Pb$ age at ca. 1480 Ma, indicating zircon inheritance. Eight concordant analyses on zoned domains define a concordia age at 1042 ± 9 Ma (MSWD = 1.9) (Fig. 2c), which is interpreted as the crystallization age of the granite. Eight analyses on rims are mostly slightly discordant ranging from 1050 to 460 Ma ($^{206}Pb/^{238}U$ ages), and reflect varying degrees of resetting of U–Th–Pb system. Two concordant analyses give an age at ca. 460 Ma, which may represent the time of metamorphic resetting. The Hf isotopic compositions defined by 8 concordant spots yield εHf(t) values of +0.4 ± 0.5. All analyses have similar O isotopic composition with an average $\delta^{18}O$ value of 6.4 ± 0.3‰.

Sample HCT-5 was collected from a heterogeneous outcrop consisting of a folded sequence of granitic to dioritic gneisses (Fig. 2d), intruded by granitic sheets, mafic dikes and pegmatite veins. It is a mesocratic granite with mafic clusters consisting of amphibole and biotite. Zircons are euhedral to subhedral, and most crystals show oscillatory or banded zones occasionally surrounded by a dark rim (too narrow to be analyzed). Several zircons have homogeneous CL-dark cores; one analysis was slightly discordant at ca. 1270 Ma (disc. 3.9%), probably representing inheritance. Twenty analyses on

297 zoned domains give a concordia age of 1045 ± 5 Ma (MSWD = 1.4) (Fig. 2d), representing the time of
298 igneous crystallization. In this sample, 21 isotopic analyses on zoned domains give an average εHf(t)
299 value of +0.7 ± 0.7, and an average $\delta^{18}O$ values of 6.4 ± 0.2‰.

300 HCT-3 is a foliated granite sample (Fig. 2e). Zircons are euhedral to subhedral, and commonly rich in
301 mineral inclusions. In CL images, most crystals are dominated by oscillatory, banded or sector zones,
302 and few ones have a thin and dark rim. Thirty-two analyses on zoned domains define a concordia age
303 at 978 ± 4 Ma (MSWD = 1.03) (Fig. 2e), representing the time of igneous crystallization. In this sample,
304 16 analyses on zoned cores give an average εHf(t) value of –2.0 ± 0.5, and an average $\delta^{18}O$ value of 5.6
305 ± 0.3‰.

306 HCT-14 is a granite sample. Zircons are mostly euhedral, commonly rich in mineral inclusions, and are
307 finely oscillatory in CL images. Twenty-seven analyses on zoned domains, except one that is excluded
308 from the calculation because of a large uncertainty, define a concordia age at 944 ± 5 Ma (MSWD =
309 1.4) (Fig. 2f). This age represents the crystallization age of the sample. In addition, minor zircon grains
310 are smaller and significantly darker in CL because of high U contents; one analysis yields a $^{206}Pb/^{238}U$
311 age at ca. 1025 Ma, which may represent zircon inheritance. Sixteen analyses on ca. 945 Ma zircon
312 grains give an average εHf(t) value of –0.8 ± 0.6, and an average $\delta^{18}O$ values of 6.4 ± 0.3‰.

313 HCT-12 is a granite with abundant K-feldspar megacrysts up to 5 cm wide. Sampled at the rim of the
314 circular pluton (Fig. 1c), a weak foliation is developed in the homogeneous exposure (Fig. 2g). In CL
315 images, most grains show moderate to high luminosity with oscillatory or banded zones. Twenty-seven
316 of 30 analyses define a concordia age at 944 ± 6 Ma (MSWD = 1.6) (Fig. 2g), recording the
317 crystallization time of the granite. Seventeen analyses have an average εHf(t) value of +2.6 ± 0.6, and
318 an average $\delta^{18}O$ value of 5.9 ± 0.2‰.

319 Sample HCT-1 is collected from an outcrop of grey isotropic equigranular granite, in the northern part
320 of the Hardangerfjord area (Fig. 2h). Most zircon grains consist of a CL-bright core with
321 oscillatory/banded zones surrounded by a CL-dark rim. In several grains, the rim domains or even the
322 whole grain of several zircons show bright and patchy CL images, similar to the characteristics of
323 metamict zircon altered by aqueous fluids. The dating results of 13 analyses on cores show two
324 concordant age populations at 938 ± 11 Ma (n=4, MSWD = 0.82) and 1052 ± 15 Ma (n=3, MSWD =
325 1.7), respectively (Fig. 2h). The former is interpreted as the time of igneous crystallization, while the
326 latter group together with two older analyses at 1.4–1.2 Ga probably represents zircon inheritance. Six
327 analyses on rims are concordant or nearly concordant with $^{206}Pb/^{238}U$ ages ranging from ca. 890 to 450
328 Ma, and the youngest age at ca. 450 Ma is probably approaching the timing of formation of the rim.
329 The Hf isotopic analyses on the four concordant ca. 938 Ma spots yield a εHf(t) value of –3.7 ± 0.7.
330 Oxygen isotopic analyses on both concordant and discordant spots have very a similar O isotopic
331 composition with an average $\delta^{18}O$ value of 6.7 ± 0.4‰.

4.2 Øygarden Complex, Sveconorwegian (ca. 1050–1030 Ma) (meta)igneous rocks

TSS-2 is an augen gneiss sample (Fig. 2i). Zircons are euhedral to subhedral with roundish terminations, and most grains have a dominant oscillatory-zoned domain surrounded by thin, dark, structureless rims. Small, dark cores are observed in a few grains. Twenty-four analyses were performed on domains with oscillatory zones. Ten of them give a concordia age at 1036 ± 5 Ma (MSWD = 1.4) (Fig. 2i), which is interpreted as the crystallization time of the granite. Of the two analyses on rims, one has significantly low Th content and Th/U ratio (0.04) and is nearly concordant at ca. 960 Ma, probably representing the time of subsequent metamorphism. Nine analyses on zoned domains give an average εHf(t) value of +0.5 ± 1.0, and an average $\delta^{18}O$ value of 6.4 ± 0.3‰.

In addition, 6 samples from the mountain Lyderhorn, the Øygarden Complex, dated by Wiest et al. (2018), were also analyzed for Hf and O isotopic compositions, including one ca. 1500 Ma granitic gneiss and five Sveconorwegian 1040–1020 Ma mafic and granitic rocks. The oldest sample (LYD83-1, 1506 ± 5 Ma) is characterized by highly elevated $\delta^{18}O$ values of 8.5 ± 0.3 ‰ and positive εHf(t) values of +3.9 ± 0.9. The two mafic rocks (LYD35-1, 1040 ± 11 Ma; LYD44-1, 1041 ± 3 Ma) have near-chondritic εHf(t) values of –0.2 ± 1.3 and +1.8 ± 0.6 respectively, comparable to the value of coeval granitic rocks (LYD197-1, 1042 ± 3 Ma, εHf(t) = +1.2 ± 0.9). Two leucogranitic rocks (LYD163-1, 1022 ± 11 Ma; LYD169-1, 1027 ± 4 Ma) have more negative εHf(t) values of –2.4 ± 1.0 and –2.6 ± 0.8. The five Sveconorwegian samples have very similar O isotopic compositions with average $\delta^{18}O$ values of 6.2–6.5‰.

4.3 Western Gneiss Region

Gothian (ca. 1650–1620 Ma) granitic gneisses

Samples VAH 78, VAH 48 and MLM 134 (Fig. 3a-c) are augen gneisses collected from the west end of the Nordfjord. In CL images, zircon crystals are mostly subhedral, and dominated by low-luminescent, oscillatory zoned cores surrounded by bright rims, tips or prisms. The cores define concordia ages of 1653 ± 8 Ma (n=6, MSWD = 0.9), 1651 ± 7 Ma (n=9, MSWD = 1.6), 1621 ± 8 Ma (n=5, MSWD = 1.2) respectively (Fig. 3a-c), recording the crystallization time of the granitic protolith. These samples have slightly depleted Hf isotopic compositions with mean εHf(t) values of +2.3 ± 0.8 to +3.1 ± 0.7, and highly elevated mean $\delta^{18}O$ values of 8.4–9.1‰.

Sveconorwegian (ca. 970–940 Ma) granitoids

Sample TSG-3 is taken from a foliated granite pluton in the Gulen dome. The granite grades into dioritic compositions towards the margins of the intrusion. Along the contact between the granite and the host rock, there is a zone of gneissic rocks that partly preserve granulite-facies mineral assemblages (Røhr et al., 2004). It is a weakly sheared biotite-rich granite (Fig. 3d). Zircon crystals are generally subhedral, 150–300 μm long, with aspect ratios of about 2. In CL images, most grains show moderately- to strongly-luminescent oscillatory zones. Twenty-five analyses define a concordia age at 966 ± 4 Ma

(MSWD = 0.99) (Fig. 3d), representing the crystallization age of the sample. Sixteen analyses of zoned domains give an average εHf(t) value of –2.5 ± 0.5, and an average $\delta^{18}O$ value of 5.8 ± 0.2‰.

Two granitic samples (VAH 11, VAH 04) were collected from the inner Nordfjord, and sample VAH23 (Fig. 3e-g) was from the western end of the Nordfjord. Zircons from these samples are euhedral to subhedral, 150–250 μm long, with aspect ratios of about 2. They are dominated by oscillatory, banded or sector zones in CL images. The analyses on VAH 11, VAH 04 and VAH 23 give concordia ages of 961 ± 8 Ma (n=12, MSWD = 1.7), 958 ± 7 Ma (n=11, MSWD = 1.2), and 944 ± 7 Ma (n=14, MSWD = 1.4) respectively (Fig. 3e-g). These ages are interpreted to record the time of crystallization of the granites. The first two samples, VAH 11 and VAH 04, have very similar Hf–O isotopic compositions, with significantly negative εHf(t) values (–5.1 ± 0.6 and –5.3 ± 1.0) and moderately elevated $\delta^{18}O$ values (6.8 ± 0.3‰ and 6.8 ± 0.2‰). Sample VAH 23 has an average εHf(t) value of –3.1 ± 0.7, and an average $\delta^{18}O$ values of 6.4 ± 0.4‰.

4.4 Synopsis of U–Pb, Lu–Hf and O isotope data

The geochronological data in this study include four igneous age groups of Gothian (1650–1620 Ma) and Telemarkian (1520–1500 Ma) metagranitoids and Sveconorwegian (1050–1020 Ma, 980–930 Ma) intrusions (Fig. 5a). The 1650–1620 Ma granitic rocks from the WGR are characterized by highly elevated $\delta^{18}O$ values of 8–9‰ associated with slightly positive Hf isotopic values of +2–+3. In contrast, the 1520–1500 Ma tonalitic and granitic rocks from the Hardangerfjord area and the Øygarden Complex show bimodal O isotopic charateristics; tonalitic rocks yield mantle-like O isotopic values while the granitic sample has a heavy $\delta^{18}O$ value of 8–9‰. They all have significantly positive average εHf(t) values of +4–+7, more radiogenic than the Gothian samples. Six ca. 1050 Ma mafic and granitic rocks have very homogeneous and similar Hf–O isotopic compositions: the average εHf(t) values are –1–+2 and $\delta^{18}O$ values 6–6.5‰, while two ca. 1020 Ma leucogranite samples show a more evolved εHf(t) value of –3 to –2. The 980–930 Ma granites from the Hardangerfjord area and the Øygarden Complex have a relatively wide spread of εHf(t) values of –3–+3 and $\delta^{18}O$ values of 5.5–6.5‰, and 970–940 Ma Ma granites from the WGR commonly have negative εHf(t) values of –5 to –3.

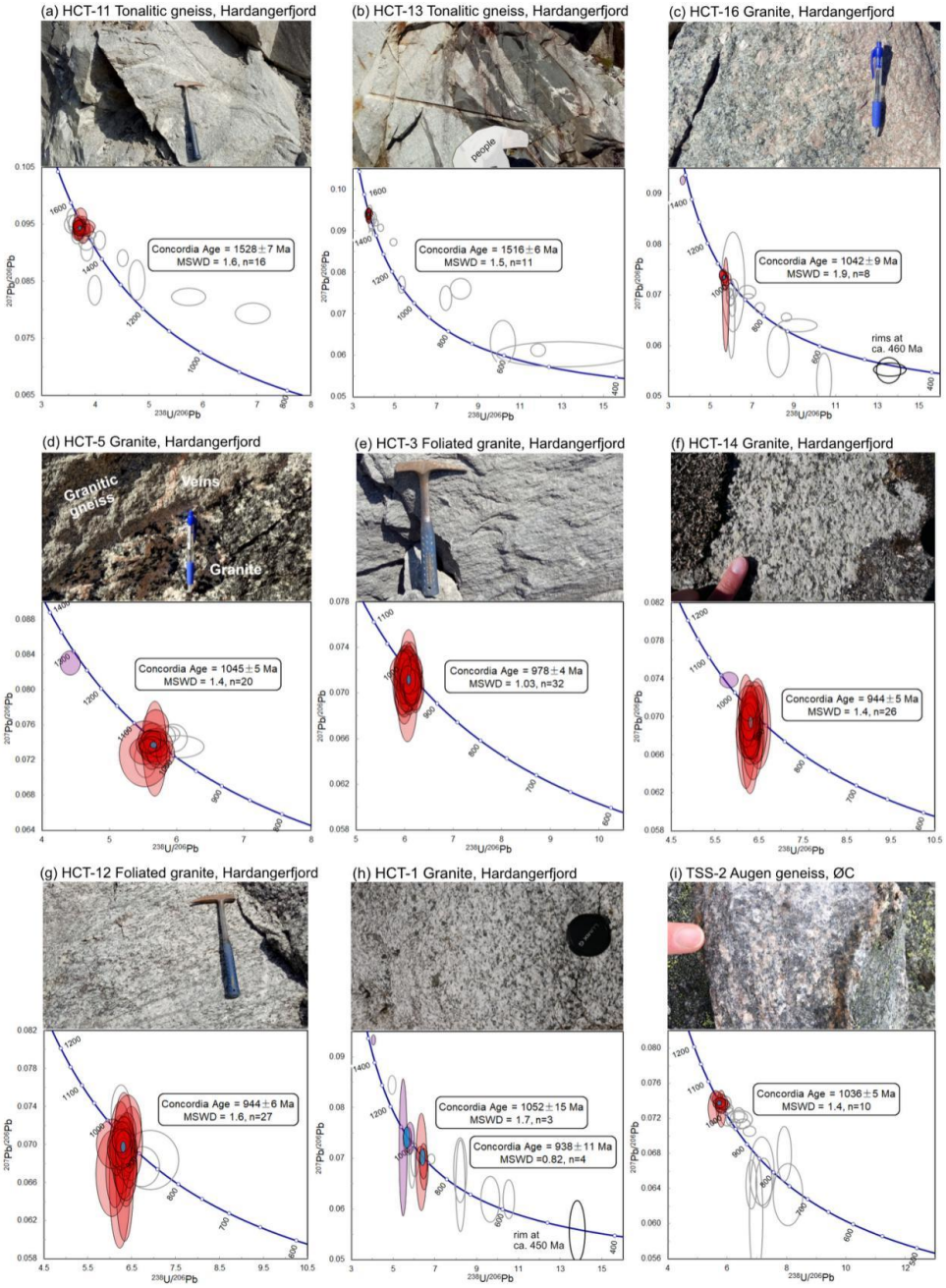

Fig. 2: Field outcrop photographs and zircon U–Pb Tera-Wasserburg diagrams of igneous samples from the Hardangerfjord and Øygarden Complex (ØC); red ellipses: igneous zircons used for calculation of concordia age (turquoise); purple: inherited zircons; grey: (reversely) discordant and Pb-loss analyses; black, Caledonian metamorphic rims. For details of each data-point see Table 1, supplementary file B.

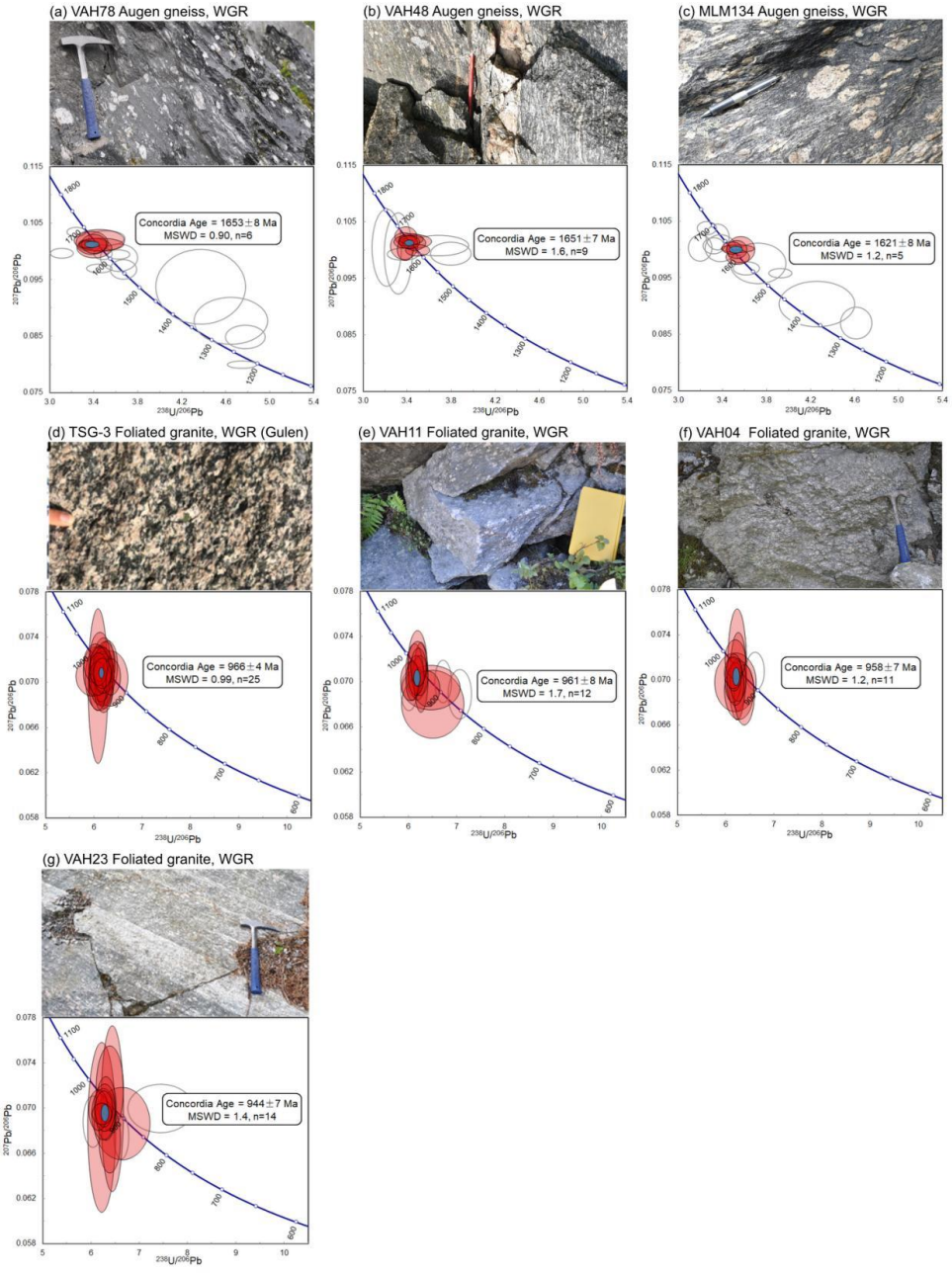

Fig. 3: Field outcrop photographs and zircon U–Pb Tera-Wasserburg diagrams of igneous samples from the WGR; For details of each data-point see Table 1, supplementary file B.

5 Results, migmatites

Key information on the migmatite samples is summarized in Table 2.

5.1 Hardangerfjord area

Two migmatite samples, H-01 and H-02 were taken several kilometers away from the Hardangerfjord shear zone. Sample H-01 is taken from a migmatitic dioritic gneiss with small stromatic and dilatational leucosomes that formed during shear deformation. The sampled domain is a foliation-parallel, medium grained, hornblende-bearing tonalitic leucosome (Fig. 4a). Zircons from this sample are subhedral to rounded with clear oscillatory zoning in dominant domains surrounded by CL-dark, unzoned rims. Seven analyses on cores define a concordia age of 1498 ± 10 Ma (MSWD = 1.8), representing the crystallization age of the dioritic protolith. Seven analyses on rims show a large scatter from ca. 1460 Ma to Cambrian times, and one nearly concordant spot has an age of ca. 1000 Ma (Fig. 4a). It is not possible to extract a reliable age of migmatitization from the data.

Sample H-02 is from the migmatitized part of a metavolcanic sequence in the 1.5 Ga Ullensvang group (Kinnsarvik formation; Sigmond, 1998). The sample is taken from a m-scale, medium- to coarse-grained tonalitic vein that fills a boudin-neck in between boudins of amphibolite (Fig. 4b). Zircons from this sample are elongated with round terminations. Most grains are entirely dark in CL, some have CL-bright cores with oscillatory/banded zones. Three analyses on cores are (nearly) concordant, with two of them yielding $^{207}Pb/^{206}Pb$ ages at ca. 1490–1470 Ma and the third one at ca. 1045 Ma (Fig. 4b). Eleven analyses on CL-dark domains are mostly discordant and show a scatter in apparent ages, ranging from Mesoproterozoic to Cambrian times. Four concordant or nearly concordant analyses yield a $^{206}Pb/^{238}U$ age at 600–570 Ma. The scatter is probably attributed to variable Caledonian lead loss due to metamictization. Collectively, the data suggest formation of the volcanic protolith at ca. 1490–1470 Ma, possible migmatitization and vein formation at ca. 1045 Ma and a final event of Caledonian lead loss.

5.2 Øygarden Complex

Migmatites in the Øygarden Complex contain moderate to high volumes of leucosomes, forming regularly metatexites and sometimes diatexites. They are usually of granitic composition but host abundant mafic bodies. In places, quartzite and mica-schist are associated with the migmatites. This suggests that at least part of the migmatites formed through melting of metasedimentary protoliths. The entire complex experienced strong penetrative shear deformation during late Caledonian collapse (Wiest et al., 2020a). Therefore, pre-Caledonian relationships have been obliterated except for low-strain domains, which represent the targets of this study.

Sample ØC-01 is a granitic diatexite that contains blocks of amphibolite and quartzite (Fig. 4c). The sampled domain is a coarse-grained hornblende-bearing granitic leucosome. In CL images, most grains show cores with fine oscillatory zoning surrounded by CL-bright mantles with faint oscillatory or banded zones and dark, unzoned rims (Fig. 4j). The size of mantle and rim domains varies between

different crystals. Core domains show zircon inheritance from the protolith of the migmatite, with 3 of them yielding a concordia age at 1640 ± 9 Ma (MSWD = 1.4) while others are highly discordant. The age from oscillatory zoned mantles is similar to that of the CL-dark rims. The dark rims are all characterized by a low Th content (3–13 ppm) and therefore a low Th/U ratio (≤ 0.01). Ten analyses in the mantles and rims define a common concordia age at 1043 ± 6 Ma (MSWD = 1.18), which represents the time of crystallization of the leucosomes (Fig. 4c). Two analyses on mantle and rims have distinctly higher Th concentration and Th/U ratio, and are concordant at ca. 925 Ma and ca. 650 Ma respectively, which may be a result of incomplete Pb loss during Caledonian thermal events. The older cores generally have positive εHf(t) values of +2–+4, while the ca. 1043 Ma domains have an average εHf(t) value of –2.2 ± 1.3 (n=8).

Sample ØC-03 is a granitic metatexite with thin and folded stromatic leucosomes and larger patches of melt. The sample is a coarse-grained hornblende-bearing granitic leucosome (Fig. 4d). Zircons show moderate CL luminosity with fine oscillatory zones partly surrounded by CL-darker, unzoned or faintly zoned rims. Eight analyses on oscillatory-zoned domains with typical Th/U ratios of igneous zircons (0.34–0.72) show similar ages and 5 of them give a concordia age at 1491 ± 8 Ma (MSWD = 1.6), representing the single-sourced zircon inheritance from the protolith. By comparison, the rims commonly have higher U (560–2110 ppm), lower Th (10–140 ppm) and Th/U ratios (0.02–0.14). The $^{206}Pb/^{238}U$ ages of 9 analyses range from 1088 Ma to 972 Ma ($^{206}Pb/^{238}U$ ages, Fig. 4d), probably indicating zircon recrystallization/regrowth during a long-term thermal event.

Sample ØC-05 is a granodioritic metatexite with thin, ptygmatically folded leucosomes and locally diffuse, coarser-grained patches (Fig. 4e). The leucosomes are surrounded by thin biotite melanosomes. The sample is a coarse-grained granitic leucosome patch. Zircons are partly small and stubby (< 100 µm) with CL-dark rims around zoned cores, and partly elongated (150–300 µm long) with oscillating/banded zones (Fig. 4k). Four analyses on the cores of the former give a concordia age at 1480 ± 9 Ma (MSWD = 0.61), and the remaining one is older at ca. 1600 Ma (Fig. 4e). A concordia age at 1034 ± 5 Ma (MSWD = 1.5) is defined by 8 concordant analyses on each rim and the zoned domains (Fig. 4e), representing the time of crystallization of the leucocratic vein. The older cores generally have positive εHf(t) values of +2–+6; three analyses on ca. 1034 Ma domains have an average εHf(t) value of –4.0 ± 1.7, while two yield a slightly positive value of 0–+2.

Sample ØC-07 is taken from within a K-feldspar-rich leucogranite body that is unfoliated. The leucogranite itself is very homogeneous and consists almost entirely of feldspar and quartz. However, it contains numerous mafic bodies that occur as m-scale dykes, aligned (but disconnected) patches, up to 20 m long schlieren or isolated irregularly shaped blobs. Granitic veins, rooted in the leucogranite, commonly intrude the mafic bodies. In places, the mafic bodies developed a solid-state foliation parallel to their outer perimeter that is cut by the granitic veins. The contact relationships suggest that the mafic

melt was injected into the granite body while the latter was close to its crystallization temperature. This led to a remobilization of granitic melt that intruded the mafic bodies, which were already solid because of their higher solidus temperature. The sample was taken from coarse-grained granitic veins (Fig. 4f) that cut through foliated amphibolite. Zircons from this sample are euhedral to subhedral, and are weakly to moderately luminescent with clear oscillatory zones in CL images. The crystallization age is determined by the concordia age of 15 analyses at 1030 ± 4 Ma (MSWD = 1.3) (Fig. 4f). Fifteen analyses yield a homogeneous Hf isotopic composition, with an average εHf(t) value of –4.2 ± 0.7.

5.3 Southern Western Gneiss Region, Gulen area

The migmatites from the Gulen area commonly show a high degree of migmatization with a large volume of leucosomes. Like in the Øygarden Complex, quartzites and mica schists are found locally contained within migmatites and witness a metasedimentary protolith. During the Caledonian orogeny, mafic bodies within the migmatites have been transformed to eclogite, while the migmatites themselves appear unaffected by this metamorphism (Wiest et al., 2019). However, large volumes of the migmatites have been strongly deformed during extensional collapse of the Caledonian orogen. The samples were taken from domains that escaped Caledonian shear deformation.

Sample GU-01 is a granitic metatexite preserved in sheared gneisses in the footwall of the Bergen Arcs shear zone. Leucosomes occur as stromatic layers and as diffuse patches (Fig. 4g). The sampled domain is a medium-grained patch of granitic composition. Zircons from this sample are 150–250 μm long with roundish terminations, composed of oscillatory-zoned cores and CL-dark, wide rims. Some crystals also have strongly luminescent mantles (Fig. 4n). The analyses on cores define two groups of concordia ages at 1492 ± 11 Ma (MSWD = 0.81, n=4) and 1419 ± 13 Ma (MSWD=1.5, n=2) respectively, which are interpreted as inherited zircons. Two concordia ages at 1053 ± 12 Ma (MSWD = 1.6, n=3) and 1014 ± 6 Ma (MSWD = 1.9, n=4) are defined by analyses on CL-bright mantles and rims (Fig. 4g). These two ages likely indicate two episodes of zircon recrystallization and/or overgrowth during metamorphism and migmatization, or reflect a protracted thermal event lasting for 40 Ma. An alternative possibility, although not preferred here, is they represent incomplete lead-loss, with the two ages capturing a snapshot of a lead-loss trend to a young Sveconorwegian age. Five analyses on mantle/rim domains yield εHf(t) value of –5–0 with an average εHf(t) value of –2.8 ± 1.5.

Sample GU-02 is a veined granitic metatexite that experienced weak penetrative shear deformation. The sampled domain is a coarse-grained granitic leucosome (Fig. 4h), which is surrounded by a biotite melanosome. Zircons from this sample are subhedral to elliptical with clear core-rim structures. The cores have euhedral to irregular shape and are relatively CL-bright with oscillatory zones, while the broad rims are CL-darker with banded, oscillatory or no zones (Fig. 4m). Three analyses on cores are slightly discordant, ranging in age from 1370 Ma to 1500 Ma ($^{207}Pb/^{206}Pb$ ages). Ten concordant analyses yield concordia ages of ca. 1050–940 Ma ($^{206}Pb/^{238}U$ ages), indicating zircon

recrystallization/regrowth during long-term high-grade metamorphism and migmatization. Five analyses on ca. 1030–950 rims yield εHf(t) values of –8 to –4 with an average εHf(t) value of –6.2 ± 1.4.

Sample GU-03 is a weakly deformed granitic metatexite. Amphibolite layers within the migmatite have been statically transformed into eclogite during the Caledonian orogeny. The migmatite contains stromatic and vein leucosomes that are surrounded by biotite melanosomes (Fig. 4i). The sampled domain is a coarse-grained patch of granitic leucosome. This sample has subhedral to rounded zircons with wide, CL-dark rims around irregular cores (Fig. 4o); some grains are almost entirely oscillatory/banded-zoned with very small cores. Two nearly concordant analyses on cores have ages at ca. 1580 Ma and ca. 1640 Ma, respectively. Ten analyses on zoned grains and rims give very similar ages, suggesting that crystallization of new zircon occurred at the same time that the CL-dark zircon rims grew. Five of them define a concordia age of 1052 ± 6 Ma, MSWD = 1.2) (Fig. 4i). This age is interpreted as the time of crystallization of the leucocratic vein. Six analyses on ca. 1052 Ma domains give an average εHf(t) value of –4.5 ± 1.3.

5.4 Summary of zircon U-Pb geochronology and Hf isotopic composition

In summary, zircon grains from the dated leucosomes generally display two kinds of internal structures in CL images. One has oscillatory- or banded- zoned cores enveloped by CL-bright or -dark rims that are structureless or have faint zoning. The second one shows euhedral prismatic zircons with oscillatory zoning (Fig. 4j-o). The core domains generally have relatively low U concentrations and Th/U ratios > 0.1, which display Gothian and Telemarkian (1650–1500 Ma) ages and represent primary igneous zircons. In contrast, the simply zoned grains and zircon rims mostly have much higher U contents and lower Th/U ratios, which have a wide range of age between 1050 and 950 Ma and yield a peak at ca. 1030 Ma (Fig. 5b, c). This is coeval with the igneous crystallization age of the leucogranite sample (ØC-07) and is interpreted to represent the timing of high-grade metamorphism and migmatization. The zircons from the leucosomes and leucogranite samples commonly have an enriched Hf isotopic composition with εHf(t) values mostly of –6 to –3, in contrast to the ca. 1050 Ma igneous samples, which generally have an averaged positive εHf(t) value.

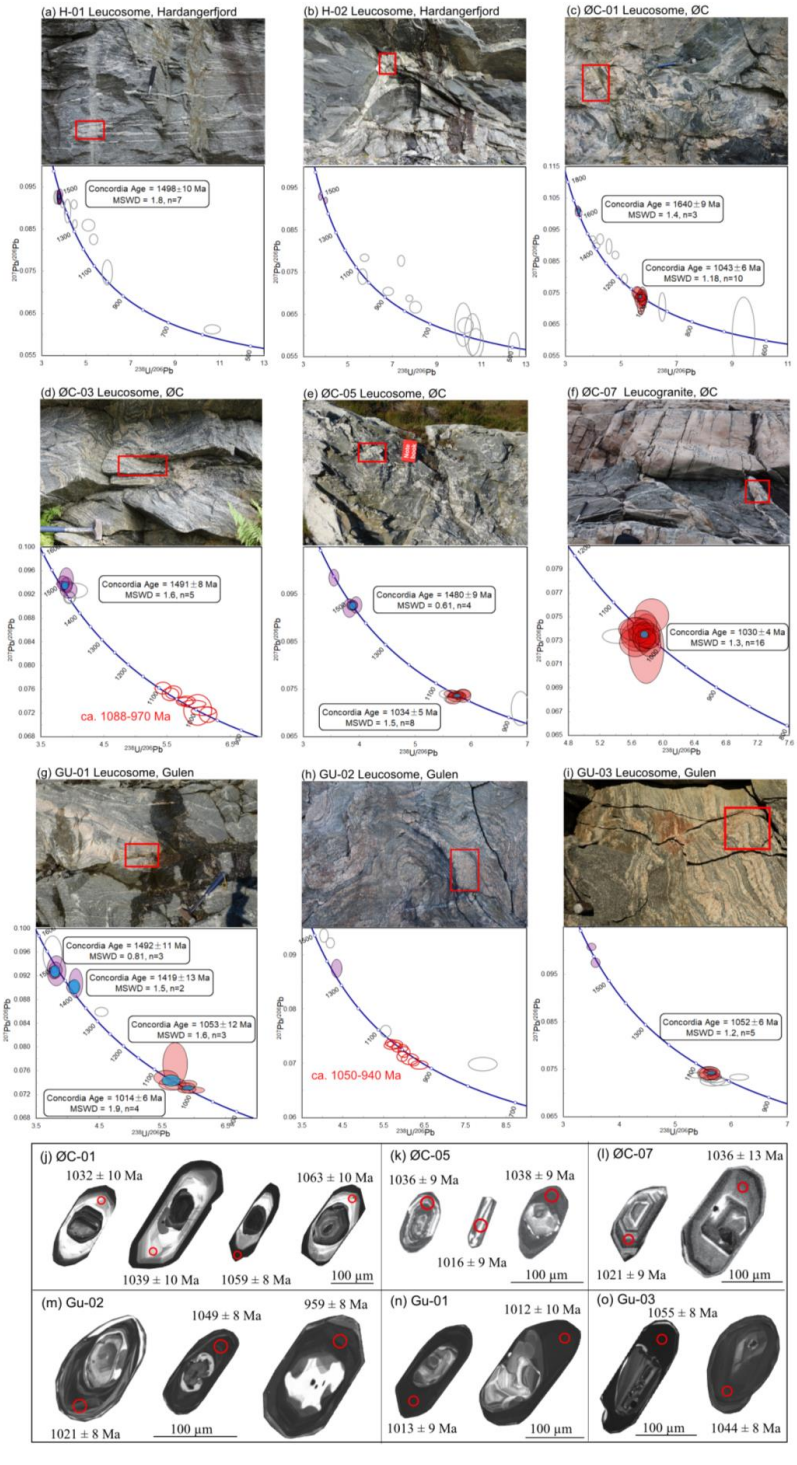
(a) H-01 Leucosome, Hardangerfjord
Concordia Age = 1498±10 Ma
MSWD = 1.8, n=7
(b) H-02 Leucosome, Hardangerfjord
(c) ØC-01 Leucosome, ØC
Concordia Age = 1640±9 Ma
MSWD = 1.4, n=3
Concordia Age = 1043±6 Ma
MSWD = 1.18, n=10
(d) ØC-03 Leucosome, ØC
Concordia Age = 1491±8 Ma
MSWD = 1.6, n=5
ca. 1088-970 Ma
(e) ØC-05 Leucosome, ØC
Concordia Age = 1480±9 Ma
MSWD = 0.61, n=4
Concordia Age = 1034±5 Ma
MSWD = 1.5, n=8
(f) ØC-07 Leucogranite, ØC
Concordia Age = 1030±4 Ma
MSWD = 1.3, n=16
(g) GU-01 Leucosome, Gulen
Concordia Age = 1492±11 Ma
MSWD = 0.81, n=3
Concordia Age = 1419±13 Ma
MSWD = 1.5, n=2
Concordia Age = 1053±12 Ma
MSWD = 1.6, n=3
Concordia Age = 1014±6 Ma
MSWD = 1.9, n=4
(h) GU-02 Leucosome, Gulen
ca. 1050-940 Ma
(i) GU-03 Leucosome, Gulen
Concordia Age = 1052±6 Ma
MSWD = 1.2, n=5
(j) ØC-01
1032 ± 10 Ma
1063 ± 10 Ma
1039 ± 10 Ma
1059 ± 8 Ma
100 µm
(k) ØC-05
1036 ± 9 Ma
1038 ± 9 Ma
1016 ± 9 Ma
100 µm
(l) ØC-07
1036 ± 13 Ma
1021 ± 9 Ma
100 µm
(m) Gu-02
1049 ± 8 Ma
959 ± 8 Ma
1021 ± 8 Ma
100 µm
(n) Gu-01
1012 ± 10 Ma
1013 ± 9 Ma
100 µm
(o) Gu-03
1055 ± 8 Ma
100 µm
1044 ± 8 Ma

534

Fig. 4: Field photographs, zircon U–Pb Tera-Wasserburg diagrams and CL images for for migmatite samples in this study. For details of each data-point see Table 2, supplementary file B. The red rectangles on field photos show sampling location of leucosomes.

6 Discussion

6.1 Geochronology: magmatism and migmatization

The new zircon U–Pb ages obtained in this study range from ca. 1650 to 930 Ma and demonstrate the importance of the Sveconorwegian record in the Baltican basement of the southern Scandinavian Caledonides. These results make it possible to link the 'Caledonized' basement to well-established Sveconorwegian Province in the western Sveconorwegian lithotectonic units.

6.1.1 Gothian (ca. 1650 Ma) vs. Telemarkian (ca. 1500 Ma) crust

As outlined above, the age of the first (oldest) lithosphere formation in each lithotectonic unit of the Sveconorwegian orogen decreases in a stepwise fashion towards the west: Transcandinavian Igneous Belt (1710–1660 Ma) in the Eastern Segment, Gothian (1660–1520 Ma) in the Idefjorden, Bamble and Kongsberg units, and Telemarkian (1520–1480 Ma) in the Telemarkia unit (Bingen et al., 2005). The data from the studied areas can be correlated to the Gothian and Telemarkian crust.

In the Hardangerfjord area, two samples of tonalitic gneiss yield ages of ca. 1520 Ma and three samples of migmatite and granite host have 1490–1470 Ma inherited zircons. These results largely confirm previously reported geochronological data from the Hardangerfjord area (Bingen et al., 2005; Roberts et al., 2013). They support a Telemarkian age of the crust formation in the area and suggest that large parts of the Hardangerfjord area belong to the Telemarkian Suldal volcanic arc (Roberts et al., 2013). In the Øygarden Complex, Telemarkian granitic gneisses (ca. 1506 Ma) are also found (Wiest et al., 2018) as well as inherited zircon cores between ca. 1490 and 1480 Ma in migmatites. Two samples though (ØC-01 and ØC-05), contain Gothian zircon populations (1640–1600 Ma). In the Gulen area of the southern WGR, migmatite samples similarly contain Telemarkian (ca. 1500–1490 Ma) in addition to Gothian (ca. 1640 Ma) inherited zircon populations. Elsewhere in the WGR, the oldest orthogneiss protoliths are Gothian with ages ranging from ca. 1650 to 1620 Ma (3 samples of this study and published data; Austrheim et al., 2003; Corfu et al., 2014b; Krogh et al., 2011; Røhr et al., 2013), while Telemarkian ages are absent.

Collectively, the data suggest that the Øygarden and Gulen areas represent a transition zone between Telemarkian crust in the southwest and Gothian crust in the northeast, with no mappable discrete boundary as proposed by Roffeis et al. (2013).

6.1.2 Sveconorwegian (1060–1020 Ma) magmatism and migmatization

The Sirdal Magmatic Belt (SMB) is a large composite batholith formed between ca. 1060 and 1020 Ma in South Norway (Coint et al., 2015; Slagstad et al., 2013). Its formation was accompanied and followed by regional granulite-facies metamorphism between ca. 1045 and 990 Ma (Bingen et al., 2008a;

Drüppel et al., 2013; Blereau et al., 2017; Laurent et al., 2018a, b; Slagstad et al., 2018). Based on the recognition of 1050–1020 Ma granitic and gabbroic magmatism in the Øygarden Complex, Wiest et al. (2018) concluded that the SMB continues towards the NNW into the Caledonian province. While this has been reaffirmed by additional dating of granites in the Øygarden Complex (sample TSS-2, ca. 1036 Ma) and geophysical correlations with the SMB (Slagstad et al., 2018a), no evidence from the interjacent Hardangerfjord area was previously available. Two of our samples of foliated/gneissic K-feldspar megacrystic granite-granodiorite (HCT-5, 1045 ± 5 Ma and HCT-16, 1042 ± 9 Ma) document 1050–1020 Ma felsic magmatism in the Hardangerfjord area for the first time and thereby establish the missing link between the autochthonous basement windows in the Caledonian province and the Sveconorwegian province. This indicates that 1060–1020 Ma magmatism occurred in a distinctly NNW-trending, ca. 300 km long magmatic belt. Within this domain, it appears that the emplaced magmas decrease in volume from south to north until they disappear in the southern WGR.

Furthermore, our new data document a temporal and spatial association between 1050–1020 Ma magmatism and migmatization in the Hardangerfjord area, the Øygarden Complex and the southern WGR. The ages of migmatization are constrained by dating of zircon grains and rims from leucosomes. Nine samples of migmatite show a wide range of concordant ages, which encompasses almost the entire range of Sveconorwegian magmatism from 1050 to 950 Ma. However, the majority of ages falls between 1050–1020 Ma, which is coeval with SMB-type magmatism (Fig. 5). The relative probability distribution of migmatite ages shows a prominent peak at ca. 1030 Ma, which conforms to the magmatic crystallization age of the leucogranite sample (ØC-07) that apparently represents the climax of high-grade metamorphism and crustal anatexis. This age falls in between two distinct magmatic pulses in the Øygarden Complex, namely a pulse of mafic to intermediate magmatism at ca. 1040 Ma, and a pulse of leucogranite magmatism at ca. 1020 Ma (Wiest et al., 2018). The clear temporal and spatial link between migmatization and magmatism supports the interpretation from the Rogaland area in southwest Norway, that mafic magmatism and underplating were driving migmatization in the crust (Laurent et al., 2018a; Slagstad et al., 2018b).

In contrast to previous studies, our results demonstrate that the southernmost part of the WGR (Gulen area) was affected by migmatization between c. 1054 and 1014 Ma, in a time interval overlapping with intrusion of the SMB. So far, all previously reported ages of Sveconorwegian migmatites and high-grade metamorphism in the WGR are younger than 1000 Ma (Skår and Pedersen 2003; Røhr et al., 2004, 2013; Kylander-Clark and Hacker 2014). While the Proterozoic evolution of most parts of the WGR is still poorly constrained, the currently available data suggest that the Øygarden and Gulen areas represent a gradual western boundary of pre-1000 Ma tectono-magmatic activity in the Sveconorwegian orogen. As mentioned before, this coincides with the gradual transition from Gothian to Telemarkian crust.

6.1.3 Late-Sveconorwegian (980–930 Ma) magmatism and migmatization

Plutons of the hornblende-biotite granite (HBG) suite formed between 980 and 930 Ma over most of the Sveconorwegian orogen in South Norway (Bogaerts et al., 2003; Vander Auwera et al., 2011; Granseth et al., 2020). In the studied areas, late-Sveconorwegian plutons are common: four of them are dated between c. 978 and 938 Ma in the Hardangerfjord area, and another four of them between c. 966 and 943 Ma in the WGR (Table 1). In the Øygarden Complex, sample ØC-03 shows evidence for protracted zircon growth during migmatization until ca. 970 Ma, however, no pluton of this age group is exposed.

In the Hardangerfjord area, the conspicuous feature of the late-Sveconorwegian plutons is an almost perfectly circular shape with little to no deformational fabric. A syn-magmatic foliation is visible at the margin of the plutons (e.g. samples HCT-3 and HCT-12) and a Caledonian fabric may only be locally present. In the WGR, in contrast, these plutons have been variably deformed into elliptical bodies and can thus serve as strain markers. In the Gulen area, sample TSG-3 robustly constrains the age of a ca. 25 x 10 km large pluton at ca. 966 Ma. This pluton is deformed and reworked along several Caledonian shear zones (Wiest et al., 2019). This age of c. 966 Ma is identical within errors to U–Pb zircon and monazite ages of granulite-facies rocks (Røhr et al., 2004), which occur along the rim of the pluton, where the granite grades into monzonitic and dioritic compositions (Wiest et al., 2019). The range of ages in the nearby migmatite samples suggests that the granite intruded a long-lasting migmatite terrane that was around or above solidus conditions for almost 100 Myrs (between ca. 1050 and 950 Ma). Therefore, it seems likely that granulite facies conditions in the Gulen area developed locally in the thermal aureole of the pluton. However, the regional occurrence of Sveconorwegian granulite-facies metamorphism, i.e. also in other parts of the WGR (Engvik et al., 2000; Krabbendam et al., 2000), makes the mechanism of metamorphism and its relations to magmatism speculative.

6.1.4 Caledonian vs. Sveconorwegian reconstructions

Our results confirm that U-Pb zircon geochronology allows to disentangle Sveconorwegian magmatism and migmatization from the effects of Caledonian reworking in the Baltican basement, in accordance with previous studies (Røhr et al., 2013; Kylander-Clark and Hacker 2014; Wiest et al., 2018). The intersection of two orogenic belts poses challenges but it also allows chances to gain insights into the evolution of both orogens.

A remaining challenge is the unequivocal identification of Caledonian versus Sveconorwegian migmatitization in the Baltican basement windows. The spatial distribution of the two generations of migmatites has proven highly variable (Gordon et al., 2013, 2016; Kylander-Clark and Hacker, 2014; Wiest et al., 2021) and remains unclear for large parts of the WGR, due to the lack of high-precision in-situ dating. This is a major drawback for orogenic reconstructions, since migmatites play a crucial role in orogen dynamics (Vanderhaeghe and Teyssier, 2001; Vanderhaeghe, 2012). Similarly, the NE

boundary of Sveconorwegian reworking in the WGR, originally defined by Tucker et al. (1990), is poorly constrained. Furthermore, it is uncertain whether post-1000 Ma granites occur to the north of Nordfjord and the apparent absence of 1500–1000 Ma magmatism and migmatization in most parts of the WGR is an enigmatic issue that hampers reconstructions of the geodynamic setting and tectonic evolution of the Sveconorwegian orogen (Bingen et al., 2005, 2008a; Slagstad et al., 2013).

The complementary erosion levels of the Baltican crust in the Caledonian and Sveconorwegian provinces may provide important insights. In South Norway, mostly the upper parts of the Sveconorwegian orogen are exposed. Deep levels of the Sveconorwegian crust are only exposed in areas that were affected by intense late-/post-orogenic exhumation (Bingen et al., 2006) such as the Rogaland Igneous Complex (Slagstad et al., 2018b) and the Eastern Segment (Viola et al., 2011; Möller et al., 2015; Möller and Andersson, 2018). The Baltican basement windows of the Caledonides expose different sections of the Caledonian orogenic crust, due to the highly variable effects of Devonian post-orogenic collapse (Fossen, 2010). The Hardangerfjord shear zone (Fig. 1c) marks the southern limit of thick-skinned collapse-related deformation (Fossen et al., 2014) and the erosion level exposes consequently high levels of the Caledonian orogen. Due to variable crustal flow, the metamorphic core complexes along the coast of West Norway, in contrast, exhumed different levels of the crust (Andersen et al., 1994; Wiest et al., 2019). The Øygarden Complex, for example, exposes a ca. 10 km vertical (Caledonian) crustal section from localized shearing at upper levels to a Caledonian migmatite dome at the lowest levels (Wiest et al., 2020a). However, these distinct Caledonian structural levels coincide also with distinct Sveconorwegian lithologies, which comprise mostly plutons and supracrustal cover at upper structural levels and dominantly (Sveconorwegian) migmatites at lower levels. Possibly, the intense ductile flow in the WGR north of Nordfjord during Caledonian collapse (Labrousse et al., 2004; Wiest et al., 2021) resulted in the complete removal of the upper Sveconorwegian crust, while exposing the lower crust. This could explain why Sveconorwegian migmatites are abundant while plutons are rare.

Independent of this, our study demonstrates a significant influence of Sveconorwegian tectono-metamorphism on later tectonic episodes. The inferred boundary between Telemarkian and Gothian crust, which corresponds to the northern boundary of SMB magmatism, coincides with the northern Bergen Arcs Shear Zone (Wennberg et al., 1998), a Devonian extensional detachment. This suggests that crustal heterogeneities inherited from the Sveconorwegian orogeny affected the localization of Caledonian shear zones. Similarly, Jakob et al. (2019) suggested that inherited Sveconorwegian lineaments had a control on the development of the segmented pre-Caledonian passive margin of Baltica and thereby the architecture of Caledonian thrust nappes. Furthermore, outside of the Caledonian province, inherited Sveconorwegian structures played an important role for brittle reactivation during Permian-Mesozoic rifting (Sundvoll and Larsen, 1994; Scheiber et al., 2015).

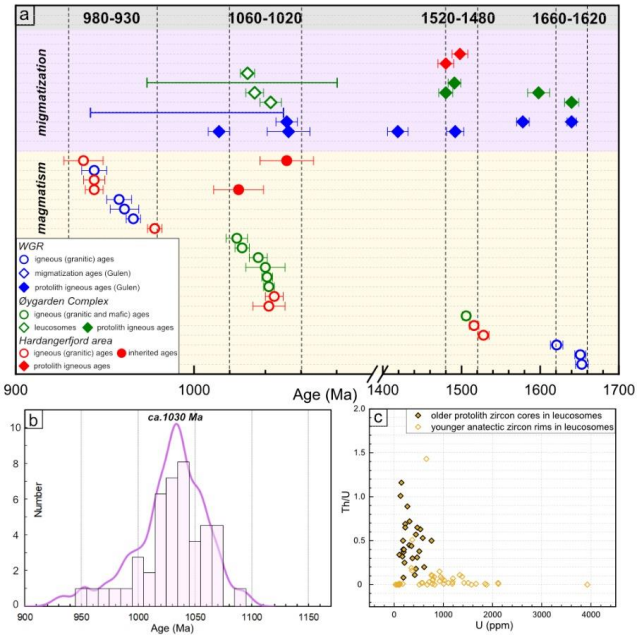

Fig. 5: (a) Summary of magmatic and migmatitic ages in the study areas including ages from Wiest et al. (2018), with dash lines showing the main magmatic periods. The two lines on the top indicate long-lasting or repeated migmatization of samples ØC-03 and GU-02. (b) Histogram and probability distribution of U-Pb ages of zircons from leucosomes; the age peak at ca. 1030 Ma probably indicates the climax of high-grade metamorphism and migmatization; (c) U versus Th/U ratio of dated zircon domains from the leucosomes, showing that older cores and younger mantles/rims have distinct Th/U signatures.

6.2 Proterozoic crustal evolution revealed by U–Pb–Hf–O isotopes

In the recent decade, numerous geochronological and isotopic data of ca. 1.86–0.90 Ga rocks in Fennoscandia, in particular paired zircon U–Pb and Lu–Hf data, have been published (Fig. 8a). This has led to an improved understanding of crustal evolution and tectonics in relation to the amalgamation of supercontinents Columbia/Nuna and Rodinia. However, O isotopic characterization of zircon has been utilized to a much lesser degree so far. Existing combined zircon U–Pb, Lu–Hf and O isotopic data focus on the Telemarkian and Gothian rocks (e.g. Roberts et al., 2013; Petersson et al., 2015), whilst analyses of Sveconorwegian rocks are largely missing. In the following section, we discuss zircon Hf–O isotopic signatures of the two main age groups of ca. 1650–1500 Ma and 1050–930 Ma samples in this study and assess the origin and evolution of the Gothian, Telemarkian and Sveconorwegian rocks.

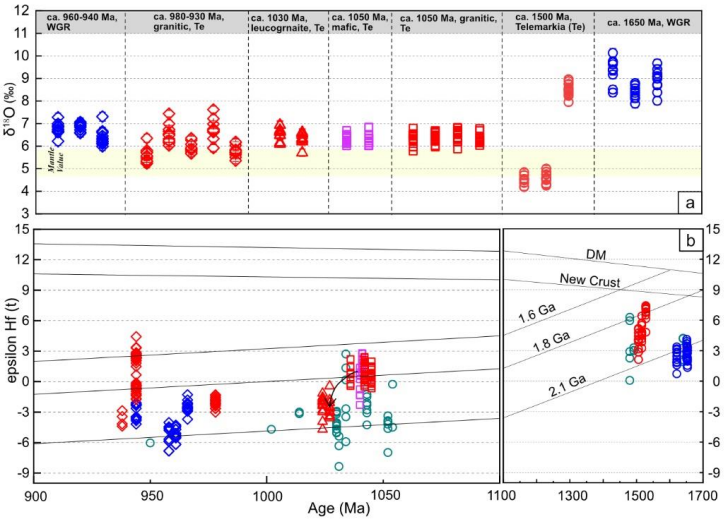

Fig. 6: (a) O isotope composition of the samples in this study, with age, lithologies and locations marked on the top. Te, Telemarkia Unit; (b) Initial epsilon Hf values versus crystallisation ages of samples analysed in this study; depleted mantle (DM) curve is from Griffin et al. (2000) and New Crust curve is from Dhuime et al. (2011). The legend is the same as for (a), and the green open circles indicate the zircons from the leucosomes. The black arrow shows the variation of εHf(t) values from ca. 1050 Ma to ca. 1020 Ma.

6.2.1 1650–1500 Ma Gothian and Telemarkian crust

Three 1650–1600 Ma granitic gneiss samples of the Gothian crust from the WGR define the oldest samples in this study. They generally have radiogenic Hf isotopic compositions with positive εHf(t) values, but the εHf(t) values are >7 units below the DM reservoir vector (Fig. 6b). The Hf isotopic signature, coupled with highly elevated $\delta^{18}O$ values (8–9 ‰, Fig. 6a), is consistent with the involvement of older crust, and/or the addition of sedimentary components during the genesis of these granitic magmas, which were probably derived from inboard of Fennoscandia, such as the Svecofennian (1910–1750 Ma) and post-Svecofennian (1710–1660 Ma) crust.

Compared to the Gothian samples, the Hf isotopic compositions of 1520–1500 Ma tonalitic and granitic samples from the Hardangerfjord area and the Øygarden Complex are more radiogenic with εHf(t) values of +3 to +8 (Fig. 6b), indicating an increasing juvenile input and decreasing crustal reworking. Their O isotopes in this study exhibit bi-modal characteristics, with the $\delta^{18}O$ values of two tonalitic samples in the range of and slightly below the mantle value while that of a granitic sample being significantly high ($\delta^{18}O$ = 8–9‰); the Hf isotopes of the former are slightly more radiogenic than the latter (Fig. 6a). In the adjacent Suldal area to the south, a large spread of Hf and O isotope compositions of 1520–1480 Ma granitoids (Suldal volcanic arc) has been reported with εHf(t) and $\delta^{18}O$ values of +1 to +11 and 6–8‰ respectively; the Hf and O isotopic values have a broadly negative correlation and the samples were interpreted to have derived from a mixture of enriched mantle with moderately

717 elevated $\delta^{18}O$ values and high-$\delta^{18}O$ sedimentary components (Roberts et al., 2013). The O isotope
718 values of two tonalitic gneisses in this study (HCT-11, HCT-13, ca. 4.5‰) are slightly lower than
719 mantle values, indicating a possible assimilation of hydrothermally altered rocks by isotopically light
720 meteoric water during the formation of the tonalitic magmas, which is not uncommon in a subduction-
721 related arc setting (Troch et al., 2020).

722 We compiled the Hf–O isotopic results of our samples with available published data from the
723 Sveconorwegian orogen (Fig. 8). These data clearly show that the Telemarkian and pre-Telemarkian
724 crust (1800–1480 Ma) is mostly characterized by juvenile Hf isotopic compositions with positive εHf(t)
725 values. The post-1600 Ma Gothian and Telemarkian rocks generally have considerably more juvenile
726 Hf isotopic compositions than the Paleoproterozoic crust and varying $\delta^{18}O$ values in a wide range of
727 4.5–9‰, which was probably related to the tectonic switching between advancing and retreating
728 subduction along the long-lived active continental margin of Fennoscandia with more juvenile input
729 and a large volume of sedimentary material involved (Roberts and Slagstad, 2015; Petersson et al.,
730 2015).

731 ***6.2.2 1050–930 Ma Sveconorwegian crust***

732 Although only a small volume of ca. 1050 Ma mafic rocks is exposed in the SMB, a number of previous
733 studies agree that the underplating of mafic magmas could have occurred extensively and constitute an
734 important composition of the lower continental crust in this region (Bybee et al., 2014; Slagstad et al.,
735 2018b; Bingen et al., 2021). These underplated mafic magmas were believed to have provided the heat
736 for the generation of granites, however, their origin and the relationships with coeval granites remain
737 poorly understood due to a lack of geochemical and isotopic constraints. In this study, the ca. 1050 Ma
738 mafic samples (gabbro and amphibolite from Wiest et al., 2018) samples have crust-like Hf–O isotopic
739 compositions with slightly negative to positive εHf(t) (−1 − +3) and moderately elevated $\delta^{18}O$ values
740 (6−6.5‰) (Fig. 7a), indicating a significant involvement of crustal components during magma genesis.
741 Thus, they are not primary melts directly from the depleted mantle but most likely have a mixed origin
742 of continental crust assimilated by mantle-derived magmas. Similar Hf and O isotopic signatures of ca.
743 1050 Ma mafic and and granitic rocks indicate that the mafic magmatism probably provided the source
744 of both heating and material to generate granitic magmas.

745 The Hf–O isotopes therefore indicate that the magma sources of ca. 1050 Ma mafic and granitic rocks
746 incorporated remelting of older continental crust and juvenile inputs, consistent with the interpretation
747 based on their geochemical and isotopic signatures (Bingen et al., 1993; Andersen et al., 2009; Granseth
748 et al., 2021). A mixing model between two endmembers of new crust ($\delta^{18}O$=5.7‰, εHf(t) = +10.2) and
749 1.5 Ga Telemarkia crust ($\delta^{18}O$=7‰, εHf(t) = −4.5) has here been used to estimate the potential
750 contribution of juvenile additions and continental crust (Fig. 7b). The εHf(t) value of the older crust is
751 in line with the Hf isotopic composition of ca. 1030 Ma leucogranite sample ØC-07 (average εHf(t) =

−4.2 ± 0.7), assuming it represents pure crustal melts, and the $\delta^{18}O$ value is consistent with the average lower continental crust. Overall, the modelling results show that ca. 1050 Ma rocks have an isotopic composition of 50% anatectic melts from older crust mixing with a similar proportion of juvenile magmas, which is broadly consistent with the modelling results based on trace element and radioisotope compositions in recent studies (e.g. Granseth et al., 2021). It should be noted however, that the contribution from the older crustal components is probably underestimated, as the Telemarkian crust as a whole has a wide range of isotopic values that cover the isotopic compositions of the Sveconorwegian rocks (Fig. 7b). Overall, the ca. 1050 Ma magmas were most likely derived from the remelting of pre-exsiting crust with juvenile inputs, although it is problematic to precisely constarin the relative proportions of the crustal- and mantle-derived components. The ca. 1030 Ma leucogranites with more evolved Hf isotopic compositions may represent purer crustal melts that derived from a higher proportion of ca. 1.5 Ga Telemarkian crustal components.

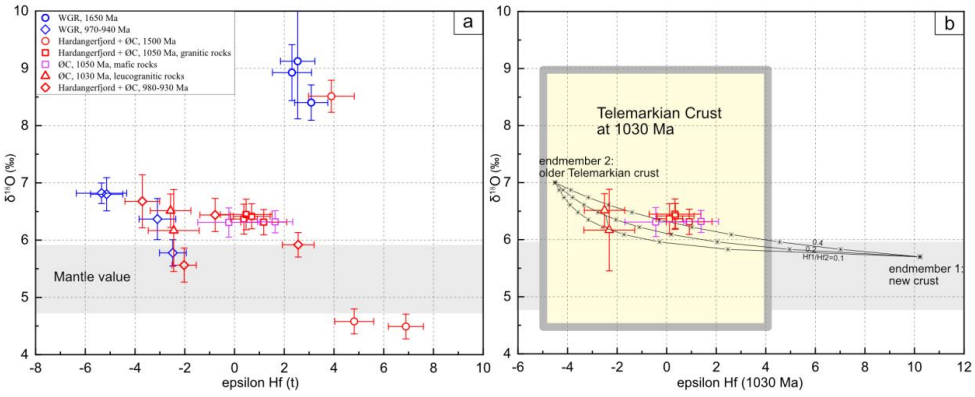

Fig. 7: (a) Initial epsilon Hf versus $\delta^{18}O$ values of all samples in this study; (b) Mixing between a new crustal component (endmember 1) and an older crustal component (endmember 2), showing Hf-O isotopic signatures of ca. 1050−1020 Ma samples (see text for details), with ticks representing 10% mixing. All εHf values of samples and endmembers are recalculated to 1030 Ma. An εHf value of −4.5, which is consistent with the Hf isotopic composition of the ca. 1030 Ma leucogranite sample ØC-07 (average εHf(t) = −4.2 ± 0.7), is assumed for the average Hf isotopic values of ca. 1.5 Ga Telemarkian crust at ca. 1030 Ma. A moderately elevated value of 7‰ is used to represent the average O isotopic compositions of the older crustal endmember. The new crust is assumed to have εHf = +10.2 at ca. 1030 Ma (Dhuime et al., 2011), and its $\delta^{18}O$ value is assumed to be 5.7‰. Hf-concentration ratios between endmembers 1 and 2 are set at 0.1, 0.2 and 0.4 (Rudnick and Gao, 2003). The rectangle shows the Hf and O isotopic range of the Telemarkian crust at ca. 1030 Ma.

In contrast to the N-S trending distribution of the SMB restricted to the Telemarkia Unit, the HBG are sporadically exposed in the Telemarkia, Bamble and Idefjorden lithotectonic units. They range in composition from gabbronorite to granite (55–72 wt.% SiO_2), which is interpreted to reflect extreme fractional crystallization of several batches of basaltic magma (Bogaerts et al., 2003). The HBG suite

was interpreted to be derived from an undepleted to slightly depleted hydrous mafic source that was underplated during previous orogenic events (Bogaerts et al., 2003; Vander Auwera et al., 2003). An alternative interpretation considered granitic magmas as products of mixing of crustal anatectic melts and mafic, mantle-derived magmas (Andersen et al., 2009). In addition, it has been recently proposed that rocks of the HBG suite outside and inside the SMB have different derivations, with the former derived by about 50% remelting of the ca. 1.5 Ga continental crust, while the latter derived from low-degree remelting of the residual continental crust after the extraction of the SMB granitic magmas (Granseth et al., 2020). All of these studies indicate that the source of the HBG (in the SMB) rocks has a complicated and heterogeneous composition, probably involving older and newly underplated mafic crust, residues of continental crust and mantle-derived juvenile magmas. The 980–930 Ma HBG granites in this study show a relatively wide range of Hf isotopic values from –4 to +3 (Fig. 7a), indicating various contributions from multiple mantle- and crust-derived components.

In summary, although the surface expression of ca. 1050 Ma mafic rocks is very limited, it would to some degree produce the parental magmas of the voluminous granitic rocks. These granites were most likely derived from a mixed source of older Telemarkian and relatively juvenile mafic crust. The magma mixing processes could have happened in some sort of area for magma storage at the base of the continental crust, corresponding with the zone where melting, assimilation, storage and homogenization takes place (MASH zone, Hildreth and Moorbath, 1988) or within a deep crustal hot zone (Annen et al., 2006). In such a zone, mafic magmas cause remelting of lower crustal rocks, and the efficient hybridization between crust-derived and juvenile magmas results in ca. 1050 Ma granitic magmas with homogenous isotopic compositions.

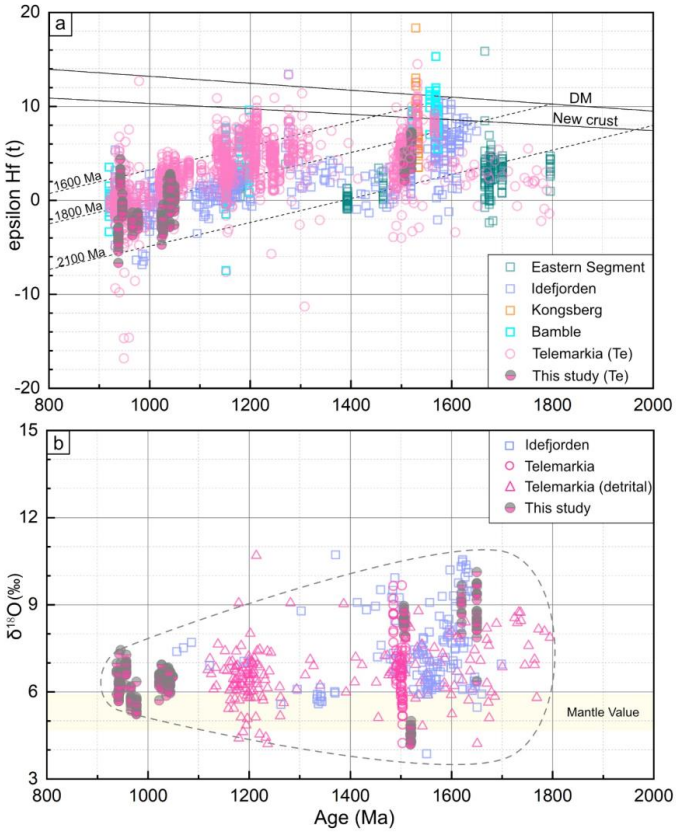

Fig. 8: Compiled Hf (a) and O (b) isotopic data in the Sveconorwegian Orogen (< 1800 Ma). The Hf isotopic data of previous studies are from the data compilation in Granseth et al. (2021), Roberts and Slagstad (2015), Spencer et al. (2014) and Petersson et al. (2015). The O isotopic data are from Roberts et al. (2013), Spencer et al. (2014) and Petersson et al. (2015). The dash line field shows O isotopic variation; Gothian and Telemarkian crust has a wide range of $\delta^{18}O$ values while Sveconorwegian crust mostly shows moderately elevated values.

6.3 Tectonic implications: comparison with typical accretionary margins in Hf–O isotopic composition

The 1050–930 Ma magmatism, which characterizes the Sveconowegian orogenesis in southwest Norway, was interpreted to have happened under a post-collisional extensional environment associated with the delamination and foundering of the lithospheric mantle (e.g. Bingen et al., 2021). An alternative interpretation explained it as subduction-related magmatism that is comparable to arc magmatic activities in cordilleran systems (Coint et al., 2015), with a part of evidence from the arc-like whole-rock and isotopic signatures (Slagstad et al., 2013; Granseth et al., 2020). However, as previous studies pointed out, the geochemical signatures of these granites were largely inherited from the pre-existing Telemarkian crust and this information alone appears to be unable to directly distinguish whether the

granites formed in a subduction- or collision-related setting (e.g. Bingen et al., 2021).

Combined zircon Hf–O isotope compositions of 1050–930 Ma Sveconorwegian magmas reported for the first time in this study provide an opportunity to compare their isotopic signatures with those of typical accretionary orogenies, e.g. those along the Paleo-Pacific margin. The Paleo-Pacific margin developed as a long-lived active continental margin on the southern periphery of Gondwana, forming a series of accretionary orogens along the coast of South America (Andes), West Antarctica and eastern Australia (present coordinates). We compiled the Hf–O isotopic data of magmatic and detrital zircons from the Andes in Argentina and Chile (ca. 300–200 Ma), the Antarctic Peninsula (ca. 300–200 Ma) and the Lachlan and Thomson orogens of the Australian sector (450–400 Ma) (Fig. 9a-c). Irrespective of the spatial and temporal variations of isotopic compositions, $\varepsilon Hf(t)$ and $\delta^{18}O$ values from the three sectors consistently show a marked negative correlation. The common information obtained from their Hf–O isotopic patterns is that sedimentary components with evolved Hf and highly elevated O isotopic values and relatively juvenile magmas with radiogenic isotopes that are close to the values of new crust have been largely incorporated in these arc magmas (Fig. 9a-c). A similar isotopic correlation has also been observed from the ca. 1500 Ma Telemarkian rocks, consistent with their formation in a subduction-related setting (Roberts et al., 2013). In contrast, ca. 1050–930 Ma Sveconorwegian magmas have relatively homogeneous, moderate $\delta^{18}O$ values, and thus their zircon Hf and O isotopic patterns distinguish them from typical arc magmas (Fig. 9d). Considering the limited sampling area in this study, we suggest that more combined Hf–O isotopic studies, especially on the samples from South Norway, are probably required (as one granite sample with high $\delta^{18}O$ values of 11–12‰ was reported by Roberts, 2010). However, the isotopic data reported here are consistent with the geological expressions, as the granitic rocks are mostly I- and A-type, while S-type granites are mostly lacking in the Sveconorwegian (Slagstad et al., 2013; Coint et al., 2015; Granseth et al., 2020).

Overall, presently available Hf–O isotopic data indicate that the 1050–930 Ma Sveconorwegian magmas show little isotopic fingerprint that are expected in an active subduction setting, as their formation witnessed significantly less inputs of sedimentary components and juvenile mantle-derived magmas than arc magmas generated in typical accretionary margins. From this perspective, the 1050–930 Ma Sveconorwegian magmas are not compatible with a supra-subduction setting. A mixed source of older continental crust and juvenile mantle-derived inputs of the Sveconorwegian magmas, as shown by this and a number of previous studies (e.g. Bingen et al., 1993; Andersen et al., 2009; Granseth et al., 2021), is consistent with a collision-related environment. Synchronous emplacement of mafic and granitic rocks (although mafic rocks usually have a limited exposure) is commonly observed in post-collisional settings, such as in the Variscan belt (Couzinié et al., 2016), the Caledonian orogeny in Scotland (Clemens et al., 2009), etc. It has been demonstrated that these magmas originated from a mixed source, very similar to the Sveconorwegian magmas presented here.

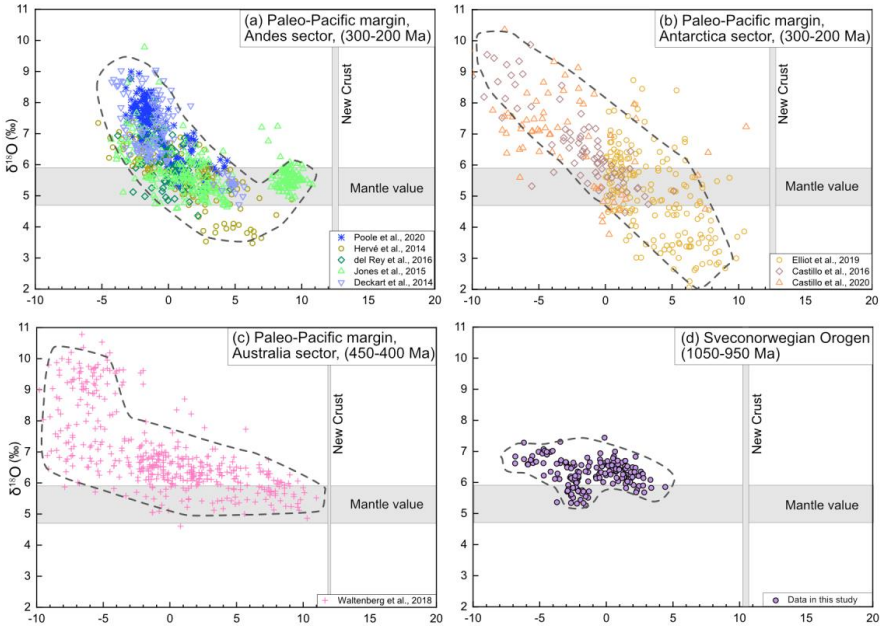

Fig. 9: Initial epsilon Hf values versus $\delta^{18}O$ values of magmatic and detrital zircons from the Paleo-Pacific margin (a-c) and the Sveconorwegian orogen (d). The Sveconorwegian magmas have distinct Hf–O isotopic patterns from the arc magmas along the Paleo-Pacific margin, but it is noted that the Australia sector is comparable to a West-Pacific type margin in contrast to Andean-style orogeny from South America to West Antarctica. The data of the Andes sector are from Deckart et al. (2014), Hervé et al., (2014), Jones et al. (2015), del Rey et al. (2016), Poole et al. (2020), those of Antarctica sector are from Castillo et al. (2016, 2020), Elliot et al. (2019) and those of Australia sector are from Waltenberg et al. (2018). Grey horizontal bars show O isotopic range of mantle-derived magmas, and vertical bars show εHf(t) range of the new crust (Dhuime et al., 2011) at the corresponding age.

6.4 Mesoproterozoic accretionary and collisional orogenesis in the core of Rodinia

In various paleogeographic reconstructions, Laurentia, Amazonia, Baltica and Kalahari constitute the core of the supercontinent Rodinia, where well-preserved remnants of Grenville-age orogenic belts provide a key to understanding their configuration and interactions during Mesoproterozoic times (Li et al., 2008; Merdith et al., 2017; Martin et al., 2020). These Grenville-age belts were largely established on a long-lived accretionary system (ca. 1800–1300 Ma) that developed along the margin of the supercontinent Columbia/Nuna (Columbia hereafter) from Laurentia to Amazonia (Fig. 10d, but see Pisarevsky et al., 2014, who placed Amazonia in a distant position from Laurentia and Baltica), which is associated with the subduction of an exterior ocean to Columbia (Condie, 2013; Roberts, 2013). During the transition from Columbia to Rodinia, the evolution of these three continents appeared to be characterized by the closure of the exterior ocean, and this accretionary margin subsequently turned 'outside in', finally leading to Grenville-age continental collision (e.g. Evans, 2013; Martin et al., 2020). In Laurentia and Baltica, the Hf isotopic compositions of Grenville-age rocks reflect an important

874 contribution of pre-existing crustal components (Fig. 10a, b), typical for continent-continent collisional
875 orogenic systems, where an increasing amount of evolved material is incorporated into melts over time
876 due to crustal thickening (e.g. Spencer et al., 2019).

877 Following Mesoproterozoic accretionary orogeny, it has been well constrained by paleomagnetic data
878 that Baltica had rotated >90° clockwise by ca. 990 Ma with its western margin (present-day coordinates
879 and the same thereafter) broadly facing the margin of Laurentia-Greenland (Cawood and Pisarevsky,
880 2017), but the position of Baltica relative to Laurentia and Amazonia is still debated with various models
881 proposed (see reviews in Bingen et al., 2021). The classical collisional model places the
882 Sveconorwegian orogen facing the northern margin of Amazonia and considers the orogen as the
883 product of continental collision between Baltica and Amazonia with the Putumayo orogen and
884 Oaxaquia in between (Park, 1992; Karlstrom et al., 2001; Bogdanova et al., 2008; Weber et al., 2010;
885 Ibanez-Mejia et al., 2011; Cawood and Pisarevsky, 2017; Ibanez-Mejia, 2020). An alternative view
886 correlates the Sveconorwegian orogen as the opposing collisional margin of the northern Grenville
887 Province in Labrador, mainly based on their comparable ca. 1050 Ma and ca. 950 Ma granitic rocks
888 (Johansson, 2009, 2014). Alternatively, an accretionary model placed Baltica at a position that is
889 relatively distant from Laurentia and Amazonia, and interpreted Sveconorwegian Baltica as a long-term
890 accretionary margin (e.g., Slagstad et al., 2017, 2020). In addition, another model interprets the four
891 western Sveconorwegian lithotectonic units as one plate (exotic to Baltica) that collided with the Eastern
892 Segment (endemic to Baltica) at ca. 990 Ma (Möller and Andersson, 2018). Testing these models is not
893 the aim of this paper. However, as discussed above, the very minor to neglectable involvement of
894 sedimentary components during the formation of ca. 1050–930 Ma Sveconorwegian rocks compared
895 with other typical arc magmas appears to be incompatible with a purely subduction-accretion processes
896 during this time interval.

897 The position of Kalahari in supercontinent Columbia has been poorly constrained due to a lack of well-
898 defined paleomagnetic data, and it was either not considered as a part of Columbia or was placed along
899 the distant periphery of the supercontinent (e.g. Pesonen et al., 2012; Pisarevsky et al., 2014). However,
900 paleomagnetic data show that from Columbia break-up to Rodinia assembly, Kalahari travelled
901 northwards from a high latitude at ca. 1350 Ma until arriving at an equatorial position at ca. 1110 Ma
902 (Fig. 10e, de Kock et al., 2019). Thus, in contrast to Laurentia, Baltica and Amazonia with a long-term
903 juxtaposition from Columbia to Rodinia, Kalahari appeared as an exotic continental block that was
904 incorporated into this 'family' during the amalgamation of Rodinia. During ca. 1350–1110 Ma, the
905 Kalahari margin along the Namaqua-Natal side witnessed multiple periods of arc/back-arc magmatic
906 activities and accretion of oceanic arcs, with both juvenile and rather evolved Hf isotopic signatures
907 indicating a variable contribution of older crustal components (Fig. 10c). Kalahari collided with
908 Laurentia along the Namaqua-Natal margin after rapid southward drift of Laurentia at ca. 1110–1080

Ma (Loewy et al., 2011; Swanson-Hysell et al., 2015, 2019).

It is suggested that core constituents of Rodinia including Laurentia, Amazonia, Baltica and Kalahari were connected by a continuous Grenville-age orogenic belt (Fig. 10e), which probably developed at ca. 1050 Ma. As the archetypal example of the Grenville-age orogens, the Grenville Orogen was constructed as a product of prolonged collision between Amazonia and Laurentia during ca. 1080–980 Ma (Hynes and Rivers, 2010). It probably extended westward through the collision between Kalahari and Laurentia. On its eastern side, the Sveconorwegian Orogen represents the extension of the Grenville Orogen into southwest Baltica, and the orogen most likely formed by collisional interactions of Baltica with Amazonia and/or Laurentia.

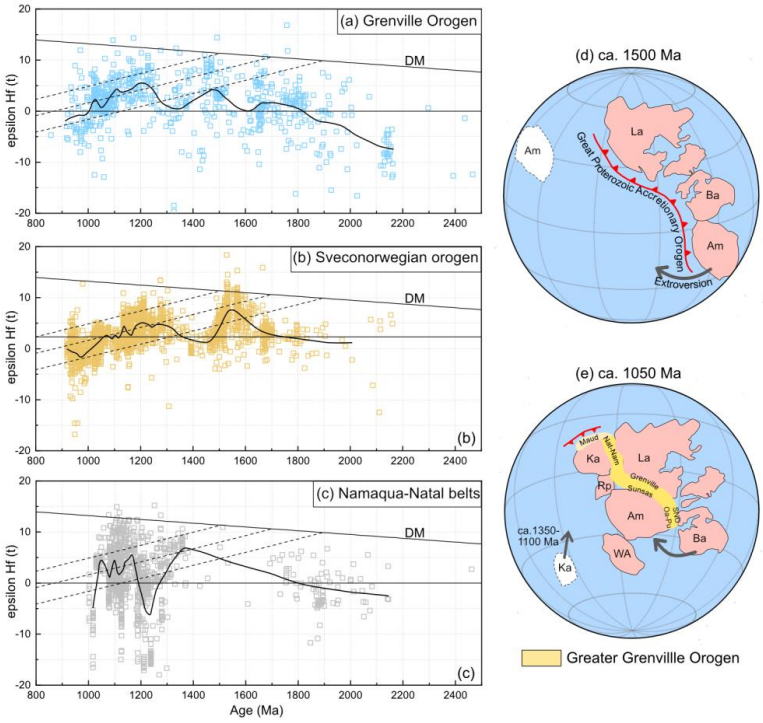

Fig. 10: (a-c) Hf isotopic evolution of the Grenville orogen (a, data from Spencer et al., 2019), of the Sveconorwegian orogen (b, data are the same as Fig. 9), of the Namaqua-Nata belts (c, data from Spencer et al., 2015, Hall et al., 2018 and Martin et al., 2020). The black lines show LOWESS smoothing results; (d) Paleogeographic reconstruction at ca. 1500 Ma (modified after Johansson, 2009; Evans and Mitchell, 2011) with the margins of Laurentia, Baltica and Amazonia as a greater Paleozoic accretionary margin (Condie, 2013). An alternative position of Amazonia that was unconnected with Laurentia-Baltica is also shown (Pisarevsky et al., 2014); (e) Paleogeographic reconstruction at ca. 1050 Ma, showing a possibly continuous Grenville Orogen (after Li et al., 2008, Cawood and Pisarevsky, 2017). Am, Amazonia; Ba, Baltica; Ka, Kalahari; La, Laurentia; Nat-Nam, Natal-Namaqua belts; Oa, Oaxaquia; Pu, Putumayo orogen; RP, Río de la Plata; SNO, Sveconorwegian

928 orogen; WA, West Africa.

Summary and conclusions

Crust with a Sveconorwegian magmatic and metamorphic overprint is described in the Baltican basement of the Caledonides, including the Hardangerfjord area, the Øygarden Complex and the Western Gneiss Region (Gulen and Nordfjord areas). New combined U–Pb, Lu–Hf and O isotopic data show that the crust in the Baltican basement of the southern Scandinavian Caledonides correlates well with the crust exposed in the western Sveconorwegian orogen in southwest Norway, as they have similar geochronological and isotopic characteristics.

1. In the Hardangerfjord area, the crust has a Telemarkian affinity, which was generated at ca. 1520–1480 Ma, probably in a juvenile magmatic arc setting (Suldal volcanic arc). At the northern end of the studied area, the Nordfjord area of the Western Gneiss Region, the crust has Gothian protolith ages, with orthogneiss dated at ca. 1650–1620 Ma and less juvenile isotopic signatures. In between these two areas, within the Øygarden Complex and Gulen domes, the protolith ages are transitional with evidence for both Gothian and Telemarkian ages.

2. Sveconorwegian magmatism includes two main magmatic suites. The ca. 1050–1020 Ma magmatism in the Hardangerfjord area and the Øygarden Complex attests to the northward continuation of the Sirdal Magmatic Belt. Our new data demonstrate that the Sirdal Magmatic Belt is much more extensive than previously thought. It extends for at least 300 km in West Norway, geographically overlapping with the Telemarkian Suldal volcanic arc. The ca. 980–930 Ma granite plutons are found in the Hardangerfjord area and the Western Gneiss Region (Gulen and Nordfjord areas), and are correlated with the hornblende–biotite granite suite exposed in the rest of the Sveconorwegian orogen.

3. The Øygarden Complex and the Gulen dome in southern Western Gneiss Region experienced high-grade metamorphism and migmatization during the Sveconorwegian orogenesis, which occurred predominantly during 1060 and 1020 Ma with a peak at ca. 1030 Ma. It is temporally and spatially related to the formation and emplacement of the Sirdal Magmatic Belt.

4. The northern limit of ca. 1050 Ma magmatic and metamorphic events at the the Øygarden Complex and the Gulen area corresponds to the boundary between Telemarkian and Gothian crust, and these crustal heterogeneities probably controlled the development of Caledonian shear zones.

5. The ca. 1050 Ma granites were most likely derived by melting of both older Telemarkian and juvenile mafic crust. Zircon Hf–O isotopic patterns indicate relatively less involvements of supracrustal (sedimentary) and juvenile material during the formation of ca.1050–930 Ma Sveconorwegian magmas in comparison to typical arc magmas, which makes them appear to be incompatible with a long-term subduction setting.

Collectively, the new data show that the Precambrian crustal architecture and isotopic signatures in the

study area are largely coherent with the Sveconorwegian province that was unaffected by the Caledonian orogeny. A continental collisional setting is favored to interpret the orogenic history of the Sveconorwegian orogen, but specific tectonic models and the configuration of Baltica in relation to Laurentia and Amazonia remain open questions in the context of Rodinia assembly.

Acknowledgements

This study is a part of the PhD project of the first author. It was financially supported by faculty-specific funds and endowments of the Faculty of Mathematics and Natural Sciences, University of Bergen (NO. 814220), and the Research Council of Norway through the funding to The Norwegian Research School on Dynamics and Evolution of Earth and Planets (NO. 249040/F60). C-C. Wang is grateful to the support from the China Scholarship Council. J.D. Wiest acknowledges funding from VISTA – a basic research collaboration between the Norwegian Academy of Science and Letters and Equinor (grant no. 6271). The MC-ICP-MS lab at UJ was funded by NRF-NEP grant 93208, and is supported by DSI-NRF CIMERA. M. A. Elburg acknowledges NRF IFRR funding (No. 119297). We thank Dr. Nick M.W. Roberts and an anonymous referee for their constructive comments and suggestions, which greatly helped to improve the manuscript. This is NordSIM publication #XXX.

Supplementary data to this article can be found online at https://drive.google.com/drive/folders/1FP7Sp_BkZsoczsLFgPoOU6wmiA2YHqya?usp=sharing

977 Table 1 Summary of geochronology and Hf-O isotopic results of magmatic samples in this study

Sample	Longitude (E)	Latitude (N)	Rock types	Main mineral composition	Igneous age (Ma)			εHf (t)	$\delta^{18}O$ (‰)
					concordia age	weighted mean $^{207}Pb/^{206}Pb$ age	weighted mean $^{206}Pb/^{238}U$ age		
Hardangerfjord area									
HCT-11	5.83297	59.93082	Tonalitic gneiss	Qtz + Pl + Amp + Bt + Grt + Chl	1528 ± 7	1516 ± 6	1541 ± 8	6.9 ± 0.7	4.5 ± 0.2
HCT-13	6.20977	59.93102	Tonalitic gneiss	Qtz + Pl + Amp + Bt	1516 ± 6	1509 ± 8	1529 ± 10	4.8 ± 0.8	4.6 ± 0.2
HCT-16	6.07065	60.07829	Granite	Kfs + Qtz + Pl + Bt + Mus + Spn	1042 ± 9	1029 ± 12	1051 ± 8	0.4 ± 0.5	6.4 ± 0.3
HCT-5	6.20556	60.23750	Augen gneiss	Pl + Qtz + Kfs + Amp + Bt + Spn	1045 ± 5	1035 ± 8	1048 ± 5	0.7 ± 0.7	6.4 ± 0.2
HCT-3	6.14859	60.13702	Foliated granite	Qtz + Kfs + Pl + Bt + Mus + Spn + Mnz	978 ± 4	964 ± 8	980 ± 4	–2.0 ± 0.5	5.6 ± 0.3
HCT-14	6.04722	59.99917	Granite	Qtz + Pl (secondary alteration) + Kfs + Bt + Spn + Ep	944 ± 5	914 ± 15	948 ± 5	–0.8 ± 0.6	6.4 ± 0.3
HCT-12	5.82155	59.83664	Foliated granite	Qtz + Kfs + Pl (secondary alteration) + Bt + Mus	944 ± 6	923 ± 13	948 ± 6	2.6 ± 0.6	5.9 ± 0.2
HCT-1	6.55885	60.45515	Granite	Qtz + Pl (secondary alteration) + Kfs + Bt + Mus + Grt + Spn	938 ± 11	937 ± 32	938 ± 12	–3.7 ± 0.7	6.7 ± 0.4
Øygarden Complex									
LYD83-1[a]	5.25992	60.38736	Mylonitic granitic gneiss	Qtz + Pl + Bt + Kfs	1506 ± 5	1501 ± 4	1515 ± 8	3.9 ± 0.9	8.5 ± 0.3
LYD44-1[a]	5.23914	60.37553	Metagabbro	Amp + Opx + pl	1041 ± 3	1035 ± 8	1044 ± 5	1.8 ± 0.6	6.3 ± 0.2
LYD197-1[a]	5.24186	60.37358	Hornblende biotite granite	Kfs + Qtz + Amp + Pl + Bt	1041 ± 3	1039 ± 7	1042 ± 3	1.2 ± 0.9	6.3 ± 0.2
LYD35-1[a]	5.23156	60.37714	Amphibolite	Amp + Pl	1040 ± 11	1026 ± 9	1037 ± 17	–0.2 ±1.3	6.3 ± 0.3
TSS-2	4.99556	60.26667	Augen gneiss	Qtz + Kfs + Pl + Bt + Mus + Ap	1036 ± 5	1036 ± 7	1035 ± 11	0.5 ± 1.0	6.4 ± 0.3
LYD169-1[a]	5.24958	60.36792	Mylonitic granitic gneiss	Qtz + Kfs + Pl + Bt	1027 ± 4	1020 ± 4	1032 ± 5	–2.6 ± 0.8	6.5 ± 0.3
LYD163-1[a]	5.25992	60.38736	Gneissic leucogranite	Kfs + Pl + Qtz + Mus + Bt	1022 ± 11	1022 ± 13	1031 ± 21	–2.4 ± 1.0	6.2 ± 0.7
Western Gneiss Region									
VAH78	6.49285	61.93872	Augen gneiss	Qtz+ Kfs + Pl + Bt + Mus + Ep	1653 ± 8	1648 ± 7	1671 ± 18	2.5 ± 0.7	9.1 ± 1.0
VAH48	5.18452	62.19870	Augen gneiss	Qtz+ Kfs + Pl + Bt + Mus + Ep	1651 ± 7	1649 ± 11	1656 ± 12	3.1 ± 0.7	8.4 ± 0.3
MLM134	5.13059	61.94703	Augen gneiss	Qtz+ Kfs + Pl + Bt + Mus + Ep	1621 ± 8	1624 ± 14	1610 ± 16	2.3 ± 0.8	8.9 ± 0.5
TSG-3	5.03647	60.98648	Foliated granite	Qtz + Kfs + Pl + Bt + Spn + Mnz	966 ± 4	954 ± 9	969 ± 5	–2.5 ± 0.5	5.8 ± 0.2
VAH11	6.96253	61.84878	Foliated granite	Qtz+ Kfs + Pl + Bt + Ap	961 ± 8	939 ± 13	965 ± 8	–5.1 ± 0.6	6.8 ± 0.3

VAH4	6.82158	61.66319	Foliated granite	Qtz+ Kfs + Pl + Bt + Ap + Ep	958 ± 7	939 ± 15	962 ± 7	–5.3 ± 1.0	6.8 ± 0.2
VAH23	5.04299	61.58910	Foliated granite	Qtz+ Kfs + Pl + Bt + Ap	944 ± 7	917 ± 14	950 ± 9	–3.1 ± 0.7	6.4 ± 0.4

978 Samples with superscript 'a' were dated by Wiest et al. (2018). The concordia age is preferred to represent the crystallization age and be used for Hf isotopic calculation.
979 Mineral abbreviations after Whitney and Evans, 2010.
980

981 Table 2 Summary of U-Pb geochronology and Hf isotopic results of leucosome samples in this study

Sample	Longitude (E)	Latitude (N)	Rock types	Mineral composition	Protolith age	Migmatization age	εHf(t) of anatectic zircons
H-01	6.28502	60.15316	Tonalitic leucosome in metatexite	Qtz + Pl + Kfs + Bt + Spn	1498 ± 10 Ma		
H-02	6.37713	60.19363	Tonalitic leucosome in metatexite	Qtz + Pl + Kfs + Bt	ca. 1500 Ma		
ØC-01	4.81128	60.63487	Granitic leucosome in diatexite	Qtz + Kfs + Pl + Bt + Ep	1640 ± 9 Ma	1043 ± 6 Ma	-2.2 ± 1.3
ØC-03	4.91911	60.45208	Tonalitic leucosome in metatexite	Qtz + Pl + Amp + Bt + Spn + Ep	1491 ± 8 Ma	1090–970 Ma	
ØC-05	4.94171	60.48861	Tonalitic leucosome in metatexite	Qtz + Pl + Bt + Mus	ca. 1600 Ma, 1480 ± 9 Ma	1034 ± 5 Ma	-4.0 ± 1.7
ØC-07	4.79851	60.55249	Granitic veins in leucogranite intruding boudinaged amphibolite	Qtz + Kfs + Pl + Bt + Spn + Ep		1030 ± 4 Ma	-4.2 ± 0.7
GU-01	5.09126	60.84787	Granitic leucosome in metatexite	Qtz + Kfs+ Pl + Bt + Ep + Spn	1492 ± 11 Ma, 1419 ± 13 Ma	1053 ± 12 Ma 1014 ± 6 Ma	-2.8 ± 1.5
GU-02	5.06695	60.87438	Granitic leucosome in metatexite	Qtz + Kfs+ Pl + Bt + Mus + Ep +		1050–940 Ma	-6.2 ± 1.4
GU-03	5.02634	60.93123	Granitic leucosome in metatexite	Qtz + Kfs+ Pl + Bt + Ep	ca. 1600 Ma	1052 ± 6 Ma	-4.5 ± 1.3

982

983 Åhäll, K.I. and Larson, S.Å., 2000. Growth-related 1.85–1.55 Ga magmatism in the Baltic Shield; a
984 review addressing the tectonic characteristics of Svecofennian, TIB 1-related, and Gothian events. GFF
985 122, 193–206.

986 Andersen, T.B., Osmundsen, P.T., Jolivet, L., 1994. Deep crustal fabrics and a model for the extensional
987 collapse of the southwest Norwegian Caledonides. Journal of Structural Geology 16, 1191–1203.

988 Andersen, T., Andresen, A., Sylvester, A.G., 2001. Nature and distribution of deep crustal reservoirs in
989 the southwestern part of the Baltic Shield: evidence from Nd, Sr and Pb isotope data on late
990 Sveconorwegian granites. Journal of the Geological Society 158, 253–267.

991 Andersen, T., Griffin, W.L., Pearson, N.J., 2002. Crustal evolution in the SW part of the Baltic Shield:
992 the Hf isotope evidence. Journal of Petrology 43, 1725–1747.

993 Andersen, T., Griffin, W.L., Sylvester, A.G., 2007. Sveconorwegian crustal underplating in
994 southwestern Fennoscandia: LAM-ICPMS U–Pb and Lu–Hf isotope evidence from granites and
995 gneisses in Telemark, southern Norway. Lithos 93, 273–287.

996 Andersen, T., Graham, S., Sylvester, A.G., 2009. The geochemistry, Lu–Hf isotope systematics, and
997 petrogenesis of Late Mesoproterozoic A-type granites in southwestern Fennoscandia. The Canadian
998 Mineralogist 47, 1399–1422.

999 Annen, C., Blundy, J.D., Sparks, R.S.J., 2006. The genesis of intermediate and silicic magmas in deep
1000 crustal hot zones. Journal of Petrology 47, 505–539.

1001 Ashwal, L.D., 1993. Anorthosites. Springer-Verlag, Berlin. 422 pages.

1002 Austrheim, H., Corfu, F., Bryhni, I., Andersen, T.B. 2003. The Proterozoic Hustad igneous complex: a
1003 low strain enclave with a key to the history of the Western Gneiss Region of Norway. Precambrian
1004 Research 120, 149–175.

1005 Beckman, V., Möller, C., Söderlund, U., Corfu, F., Pallon, J., Chamberlain, K.R., 2014. Metamorphic
1006 zircon formation at the transition from gabbro to eclogite in Trollheimen–Surnadalen, Norwegian
1007 Caledonides. Geological Society, London, Special Publication 390, 403–424.

1008 Bergström, U., Stephens, M.B. and Wahlgren, C.H., 2020. Polyphase (1.6–1.5 and 1.1–1.0 Ga)
1009 deformation and metamorphism of Proterozoic (1.7–1.1 Ga) continental crust, Idefjorden terrane,
1010 Sveconorwegian orogen. Geological Society, London, Memoirs, 50, 397–434.

1011 Bingen, B., Demaiffe, D., Hertogen, J., Weis, D. and Michot, J., 1993. K-rich calc-alkaline augen
1012 gneisses of Grenvillian age in SW Norway: mingling of mantle-derived and crustal components. The
1013 Journal of geology 101, 763–778.

1014 Bingen, B., Demaiffe, D., Breemen, O.V., 1998. The 616 Ma old Egersund basaltic dike swarm, SW
1015 Norway, and late Neoproterozoic opening of the Iapetus Ocean. The Journal of Geology 106, 565–574.

1016 Bingen, B., Skår, Ø., Marker, M., Sigmond, E.M., Nordgulen, Ø., Ragnhildstveit, J., Mansfeld, J.,
1017 Tucker, R.D., Liégeois, J.P., 2005. Timing of continental building in the Sveconorwegian orogen, SW
1018 Scandinavia. Norwegian Journal of Geology/Norsk Geologisk Forening, 85.

1019 Bingen, B., Stein, H.J., Bogaerts, M., Bolle, O., Mansfeld, J., 2006. Molybdenite Re–Os dating
1020 constrains gravitational collapse of the Sveconorwegian orogen, SW Scandinavia. Lithos 87, 328–346.

1021 Bingen, B., Nordgulen, Ø., Viola, G., 2008a. A four-phase model for the Sveconorwegian orogeny, SW
1022 Scandinavia. Norwegian Journal of Geology/Norsk Geologisk Forening, 88(1).

1023 Bingen, B., Davis, W.J., Hamilton, M.A., Engvik, A.K., Stein, H.J., Skår, Ø., Nordgulen, Ø., 2008b.
1024 Geochronology of high-grade metamorphism in the Sveconorwegian belt, S. Norway: U-Pb, Th-Pb and
1025 Re-Os data. Norwegian Journal of Geology/Norsk Geologisk Forening, 88(1).

1026 Bingen, B., Andersson, J., Soderlun, U., Moller, C., 2008c. The Mesoproterozoic in the Nordic
1027 countries. Episodes 31, 29.

1028 Bingen, B., Corfu, F., Stein, H.J., Whitehouse, M.J., 2015. U-Pb geochronology of the syn-orogenic
1029 Knaben molybdenum deposits, Sveconorwegian orogen, Norway. Geological Magazine 152, 537–556.

1030 Bingen, B. and Viola, G., 2018. The early-Sveconorwegian orogeny in southern Norway: Tectonic
1031 model involving delamination of the sub-continental lithospheric mantle. Precambrian Research 313,
1032 170–204.

1033 Bingen, B., Viola, G., Möller, C., Vander Auwera, J., Laurent, A., Yi, K., 2021. The Sveconorwegian
1034 orogeny. Gondwana Research 90, 273–313.

1035 Blereau, E., Johnson, T.E., Clark, C., Taylor, R.J., Kinny, P.D., Hand, M., 2017. Reappraising the P–T
1036 evolution of the rogaland–vest agder sector, southwestern Norway. Geoscience Frontiers 8, 1–14.

1037 Bogdanova, S.V., Bingen, B., Gorbatschev, R., Kheraskova, T.N., Kozlov, V.I., Puchkov, V.N., Volozh,
1038 Y.A., 2008. The East European Craton (Baltica) before and during the assembly of Rodinia.
1039 Precambrian Research 160, 23–45.

1040 Bogdanova, S., Gorbatschev, R., Skridlaite, G., Soesoo, A., Taran, L., and Kurlovich, D., 2015, Trans-
1041 Baltic Palaeoproterozoic correlations towards the reconstruction of supercontinent Columbia/Nuna:
1042 Precambrian Research 259, 5–33.

1043 Brueckner, H.K., 2018. The great eclogite debate of the Western Gneiss Region, Norwegian
1044 Caledonides: The in situ crustal v. exotic mantle origin controversy. Journal of Metamorphic Geology
1045 36, 517–527.

1046 Castillo, P., Fanning, C.M., Hervé, F., Lacassie, J.P., 2016. Characterisation and tracing of Permian
1047 magmatism in the south-western segment of the Gondwanan margin; U–Pb age, Lu–Hf and O isotopic
1048 compositions of detrital zircons from metasedimentary complexes of northern Antarctic Peninsula and
1049 western Patagonia. Gondwana Research 36, 1–13.

1050 Castillo, P., Fanning, C.M. and Riley, T.R., 2020. Zircon O and Hf isotopic constraints on the genesis
1051 of Permian–Triassic magmatic and metamorphic rocks in the Antarctic Peninsula and correlations with
1052 Patagonia. Journal of South American Earth Sciences 104, 102848.

1053 Cawood, P.A., McCausland, P.J., Dunning, G.R., 2001. Opening Iapetus: constraints from the
1054 Laurentian margin in Newfoundland. Geological Society of America Bulletin 113, 443–453.

1055 Cawood, P.A. and Pisarevsky, S.A., 2017. Laurentia-Baltica-Amazonia relations during Rodinia
1056 assembly. Precambrian Research 292, 386–397.

1057 Clemens, J.D., Darbyshire, D.P.F. and Flinders, J., 2009. Sources of post-orogenic calcalkaline magmas:
1058 the Arrochar and Garabal Hill–Glen Fyne complexes, Scotland. Lithos 112, 524–542.

1059 Cocks, L.R.M. and Torsvik, T.H., 2005. Baltica from the late Precambrian to mid-Palaeozoic times: the
1060 gain and loss of a terrane's identity. Earth-Science Reviews 72, 39–66.

1061 Coint, N., Slagstad, T., Roberts, N.M.W., Marker, M., Røhr, T., Sørensen, B.E., 2015. The Late
1062 Mesoproterozoic Sirdal Magmatic Belt, SW Norway: relationships between magmatism and
1063 metamorphism and implications for Sveconorwegian orogenesis. Precambrian Research 265, 57–77.

1064 Condie, K.C., 2013. Preservation and recycling of crust during accretionary and collisional phases of
1065 Proterozoic orogens: A bumpy road from Nuna to Rodinia. Geosciences 3, 240–261.

1066 Corfu, F., Andersen, T.B., Gasser, D., 2014a. The Scandinavian Caledonides: main features, conceptual
1067 advances and critical questions. Geological Society, London, Special Publication 390, 9–43.

1068 Corfu, F., Austrheim, H., Ganzhorn, A.C., 2014b. Localized granulite and eclogite facies

metamorphism at Flatraket and Kråkeneset, Western Gneiss Region: U–Pb data and tectonic implications. Geological Society, London, Special Publication 390, 425–442.

Cosca, M.A., Mezger, K., Essene, E.J., 1998. The Baltica-Laurentia connection: Sveconorwegian (Grenvillian) metamorphism, cooling, and unroofing in the Bamble sector, Norway. The Journal of Geology 106, 539–552.

Couzinié, S., Laurent, O., Moyen, J.F., Zeh, A., Bouilhol, P. and Villaros, A., 2016. Post-collisional magmatism: crustal growth not identified by zircon Hf–O isotopes. Earth and Planetary Science Letters 456, 182–195.

Dalziel, I.W., 1997. OVERVIEW: Neoproterozoic-Paleozoic geography and tectonics: Review, hypothesis, environmental speculation. Geological Society of America Bulletin 109, 16–42.

Dalziel, I.W., Mosher, S., Gahagan, L.M., 2000. Laurentia-Kalahari collision and the assembly of Rodinia. The Journal of Geology 108, 499–513.

Deckart, K., Hervé Allamand, F., Fanning, M., Ramírez, V., Calderón, M. and Godoy, E., 2014. U-Pb geochronology and Hf-O isotopes of zircons from the Pennsylvanian Coastal Batholith, south-central Chile. Andean Geology 41, 49–82.

de Kock, M.O., Gumsley, A.P., Klausen, M.B., Söderlund, U., Djeutchou, C., 2019. The Precambrian mafic magmatic record, including large igneous provinces of the Kalahari craton and its constituents: A paleogeographic review. Dyke Swarms of the World: A Modern Perspective, 155–214.

del Rey, A., Deckart, K., Arriagada, C., Martínez, F., 2016. Resolving the paradigm of the late Paleozoic–Triassic Chilean magmatism: Isotopic approach. Gondwana Research 37, 172–181.

Dhuime, B., Hawkesworth, C., Cawood, P., 2011. When continents formed. Science 331, 154–155.

Drüppel, K., Elsäßer, L., Brandt, S., Gerdes, A., 2013. Sveconorwegian mid-crustal ultrahigh-temperature metamorphism in Rogaland, Norway: U–Pb LA-ICP-MS geochronology and pseudosections of sapphirine granulites and associated paragneisses. Journal of Petrology 54, 305–350.

Elliot, D.H., Fanning, C.M., Mukasa, S.B., Millar, I.L., 2019. Hf-and O-isotope data from detrital and granitoid zircons reveal characteristics of the Permian–Triassic magmatic belt along the Antarctic sector of Gondwana. Geosphere 15, 576–604.

Engvik, A.K., Austrheim, H., Andersen, T.B., 2000. Structural, mineralogical and petrophysical effects on deep crustal rocks of fluid- limited polymetamorphism, Western Gneiss Region, Norway. Journal of the Geological Society 157, 121–134.

Engvik, A.K., Bingen, B. and Solli, A., 2016. Localized occurrences of granulite: P–T modeling, U–Pb geochronology and distribution of early-Sveconorwegian high-grade metamorphism in Bamble, South Norway. Lithos 240, 84–103.

Evans, D.A. and Mitchell, R.N., 2011. Assembly and breakup of the core of Paleoproterozoic–Mesoproterozoic supercontinent Nuna. Geology 39, 443–446.

Evans, D.A., 2013. Reconstructing pre-Pangean supercontinents. Bulletin 125, 1735–1751.

Fossen, H., 1992. The Role of Extensional Tectonics in the Caledonides of South Norway. Journal of Structural Geology 14, 1033–1046.

Fossen, H. and Hurich, C.A., 2005. The Hardangerfjord Shear Zone in SW Norway and the North Sea: a large-scale low-angle shear zone in the Caledonian crust. Journal of the Geological Society 162, 675–687.

Fossen, H., 2010. Extensional tectonics in the North Atlantic Caledonides: a regional view. Geological Society, London, Special Publication 335, 767–793.

Fossen, H., Gabrielsen, R.H., Faleide, J.I., Hurich, C.A., 2014. Crustal stretching in the Scandinavian Caledonides as revealed by deep seismic data. Geology 42, 791–794.

Fossen, H., Khani, H.F., Faleide, J.I., Ksienzyk, A.K., Dunlap, W.J., 2016. Post-Caledonian extension in the West Norway–northern North Sea region: the role of structural inheritance. Geological Society, London, Special Publication 439, 465–486.

Gee, D.G., Andréasson, P.G., Lorenz, H., Frei, D., Majka, J., 2015. Detrital zircon signatures of the Baltoscandian margin along the Arctic Circle Caledonides in Sweden: The Sveconorwegian connection. Precambrian Research 265, 40–56.

Glodny, J., Kühn, A., Austrheim, H., 2008. Diffusion versus recrystallization processes in Rb–Sr geochronology: isotopic relics in eclogite facies rocks, Western Gneiss Region, Norway. Geochimica et Cosmochimica Acta 72, 506–525.

Gorbatschev, R. and Bogdanova, S., 1993. Frontiers in the Baltic shield. Precambrian Research 64, 3–21.

Gordon, S.M., Whitney, D.L., Teyssier, C., Fossen, H., 2013. U-Pb dates and trace-element geochemistry of zircon from migmatite, Western Gneiss Region, Norway: Significance for history of partial melting in continental subduction. Lithos 170, 35–53.

Gordon, S.M., Whitney, D.L., Teyssier, C., Fossen, H., Kylander-Clark, A., 2016. Geochronology and geochemistry of zircon from the northern Western Gneiss Region: Insights into the Caledonian tectonic history of western Norway. Lithos 246–247, 134–148.

Griffin, W.L., Pearson, N.J., Belousova, E., Jackson, S.E., van Achterbergh, E., O'Reilly, S.Y., Shee, S.R., 2000. The Hf isotope composition of cratonic mantle: LAM-MCICPMS analysis of zircon megacrysts in kimberlites. Geochimica et Cosmochimica Acta 64, 133–147.

Granseth, A., Slagstad, T., Coint, N., Roberts, N.M., Røhr, T.S., Sørensen, B.E., 2020. Tectonomagmatic evolution of the Sveconorwegian orogen recorded in the chemical and isotopic compositions of 1070–920 Ma granitoids. Precambrian Research, 340, 105527.

Granseth, A., Slagstad, T., Roberts, N.M., Hagen-Peter, G., Kirkland, C.L., Møkkelgjerd, S.H., Røhr, T.S., Coint, N. and Sørensen, B.E., 2021. Multi-isotope tracing of the 1.3–0.9 Ga evolution of Fennoscandia; crustal growth during the Sveconorwegian orogeny. Gondwana Research 91, 31–39.

Hacker, B.R., Andersen, T.B., Johnston, S., Kylander-Clark, A.R., Peterman, E.M., Walsh, E.O., Young, D., 2010. High-temperature deformation during continental-margin subduction & exhumation: The ultrahigh-pressure Western Gneiss Region of Norway. Tectonophysics 480, 149–171.

Hall, W.S., Hitzman, M.W., Kuiper, Y.D., Kylander-Clark, A.R., Holm-Denoma, C.S., Moscati, R.J., Plink-Björklund, P., Enders, M.S., 2018. Igneous and detrital zircon U-Pb and Lu-Hf geochronology of the late Meso-to Neoproterozoic northwest Botswana rift: Maximum depositional age and provenance of the Ghanzi Group, Kalahari Copperbelt, Botswana and Namibia. Precambrian Research 318, 133–155.

Hervé F, Fanning CM, Calderón M, Mpodozis C (2014) Early Permian to Late Triassic batholiths of the Chilean Frontal Cordillera (28°-31°S): SHRIMP U–Pb zircon ages and Lu-Hf and O isotope systematics. Lithos 184–187, 436–446.

Hildreth, W. and Moorbath, S., 1988. Crustal contributions to arc magmatism in the Andes of central Chile. Contributions to mineralogy and petrology 98, 455–489.

Hoffman, P.F., 1991. Did the breakout of Laurentia turn Gondwanaland inside-out?. Science 252, 1409–1412.

Hynes, A. and Rivers, T., 2010. Protracted continental collision—Evidence from the Grenville orogen.

Canadian Journal of Earth Sciences 47, 591–620.

Ibanez-Mejia, M., Ruiz, J., Valencia, V.A., Cardona, A., Gehrels, G.E., Mora, A.R., 2011. The Putumayo Orogen of Amazonia and its implications for Rodinia reconstructions: New U–Pb geochronological insights into the Proterozoic tectonic evolution of northwestern South America. Precambrian Research 191, 58–77.

Ibañez-Mejia, M., 2020. The Putumayo Orogen of Amazonia: A synthesis. In: Gómez, J. & Mateus–Zabala, D. (editors), The Geology of Colombia, Volume 1 Proterozoic–Paleozoic. Servicio Geológico Colombiano, Publicaciones Geológicas Especiales 35, 101–131. Bogotá.

Jakob, J., Andersen, T.B., Kjøll, H.J., 2019. A review and reinterpretation of the architecture of the South and South-Central Scandinavian Caledonides—A magma-poor to magma-rich transition and the significance of the reactivation of rift inherited structures. Earth-Science Reviews 192, 513–528.

Johansson, Å., 2009. Baltica, Amazonia and the SAMBA connection—1000 million years of neighbourhood during the Proterozoic? Precambrian Research 175, 221–234.

Johansson, Å., 2014. From Rodinia to Gondwana with the 'SAMBA' model—a distant view from Baltica towards Amazonia and beyond. Precambrian Research 244, 226–235.

Jones, R.E., Kirstein, L.A., Kasemann, S.A., Dhuime, B., Elliott, T., Litvak, V.D., Alonso, R., Hinton, R., Facility, E.I.M., 2015. Geodynamic controls on the contamination of Cenozoic arc magmas in the southern Central Andes: Insights from the O and Hf isotopic composition of zircon. Geochimica et Cosmochimica Acta 164, 386–402.

Karlstrom, K.E., Åhäll, K.I., Harlan, S.S., Williams, M.L., McLelland, J., Geissman, J.W., 2001. Long-lived (1.8–1.0 Ga) convergent orogen in southern Laurentia, its extensions to Australia and Baltica, and implications for refining Rodinia. Precambrian Research 111, 5–30.

Krabbendam, M., Wain, A., Andersen, T.B., 2000. Pre-Caledonian granulite and gabbro enclaves in the Western Gneiss Region, Norway: indications of incomplete transition at high pressure. Geological Magazine 137, 235–255.

Krogh, T.E., Kamo, S.L., Robinson, P., Terry, M.P., Kwok, K., 2011. U–Pb zircon geochronology of eclogites from the Scandian Orogen, northern Western Gneiss Region, Norway: 14–20 million years between eclogite crystallization and return to amphibolite-facies conditions. Canadian Journal of Earth Sciences 48, 441–472.

Ksienzyk, A.K., Wemmer, K., Jacobs, J., Fossen, H., Schomberg, A.C., Sussenberger, A., Lunsdorf, N.K., Bastesen, E., 2016. Post-Caledonian brittle deformation in the Bergen area, West Norway: results from K-Ar illite fault gouge dating. Norwegian Journal of Geology 96, 275–299.

Kylander-Clark, A.R.C., Hacker, B.R., 2014. Age and significance of felsic dikes from the UHP western gneiss region. Tectonics 33, 2342–2360.

Labrousse, L., Jolivet, L., Agard, P., Hebert, R., Andersen, T.B., 2002. Crustal-scale boudinage and migmatization of gneiss during their exhumation in the UHP Province of Western Norway. Terra Nova 14, 263–270.

Labrousse, L., Jolivet, L., Andersen, T., Agard, P., Hébert, R., Maluski, H., Schärer, U., 2004. Pressure-temperature-time deformation history of the exhumation of ultra-high pressure rocks in the Western Gneiss Region, Norway. Geological Society of America Special Papers 380, 155–183.

Laurent, A.T., Duchene, S., Bingen, B., Bosse, V., Seydoux-Guillaume, A.M., 2018a. Two successive phases of ultrahigh temperature metamorphism in Rogaland, S. Norway: Evidence from Y- in-monazite thermometry. Journal of Metamorphic Geology 36, 1009–1037.

Laurent, A.T., Bingen, B., Duchene, S., Whitehouse, M.J., Seydoux-Guillaume, A.M., Bosse, V., 2018b. Decoding a protracted zircon geochronological record in ultrahigh temperature granulite, and persistence of partial melting in the crust, Rogaland, Norway. Contributions to Mineralogy and Petrology 173, 29.

Li, Z.X., Bogdanova, S.V., Collins, A.S., Davidson, A., De Waele, B., Ernst, R.E., Fitzsimons, I.C.W., Fuck, R.A., Gladkochub, D.P., Jacobs, J., Karlstrom, K.E., Lu, S., Natapov, L.M., Pease, V., Pisarevsky, S.A., Thrane, K., Vernikovsky, V., 2008. Assembly, configuration, and break-up history of Rodinia: a synthesis. Precambrian Research 160, 179–210.

Loewy, S.L., Dalziel, I.W.D., Pisarevsky, S., Connelly, J.N., Tait, J., Hanson, R.E., Bullen, D., 2011. Coats Land crustal block, East Antarctica: A tectonic tracer for Laurentia?. Geology 39, 859–862.

Lorenz, H., Gee, D.G., Larionov, A.N., Majka, J., 2012. The Grenville–Sveconorwegian orogen in the high Arctic. Geological Magazine 149, 875–891.

Martin, E.L., Spencer, C.J., Collins, W.J., Thomas, R.J., Macey, P.H., Roberts, N.M.W., 2020. The core of Rodinia formed by the juxtaposition of opposed retreating and advancing accretionary orogens. Earth-Science Reviews, p.103413.

McLelland, J.M., Selleck, B.W., Bickford, M.E., Tollo, R.P., Bartholomew, M.J., Hibbard, J.P., Karabinos, P.M., 2010. Review of the Proterozoic evolution of the Grenville Province, its Adirondack outlier, and the Mesoproterozoic inliers of the Appalachians. From Rodinia to Pangea: The Lithotectonic Record of the Appalachian Region: Geological Society of America Memoir, 206, 21–49.

Merdith, A.S., Collins, A.S., Williams, S.E., Pisarevsky, S., Foden, J.D., Archibald, D.B., Blades, M.L., Alessio, B.L., Armistead, S., Plavsa, D., Clark, C., 2017. A full-plate global reconstruction of the Neoproterozoic. Gondwana Research 50, 84–134.

Milnes, A., Wennberg, O., Skår, Ø., Koestler, A., 1997. Contraction, extension and timing in the South Norwegian Caledonides: the Sognefjord transect. Geological Society, London, Special Publication 121, 123–148.

Möller, A., O'Brien, P.J., Kennedy, A., Kröner, A., 2002. Polyphase zircon in ultrahigh- temperature granulites (Rogaland, SW Norway): constraints for Pb diffusion in zircon. Journal of metamorphic Geology 20, 727–740.

Möller, C., Andersson, J., Dyck, B., Antal Lundin, I., 2015. Exhumation of an eclogite terrane as a hot migmatitic nappe, Sveconorwegian orogen. Lithos, 226, 147–168.

Möller, C. and Andersson, J., 2018. Metamorphic zoning and behaviour of an underthrusting continental plate. Journal of metamorphic geology 36, 567–589.

Park, R.G., 1992. Plate kinematic history of Baltica during the Middle to Late Proterozoic: a model. Geology 20, 725–728.

Pedersen, S., Andersen, T., Konnerup-Madsen, J. and Griffin, W.L., 2009. Recurrent Mesoproterozoic continental magmatism in south-central Norway. International Journal of Earth Sciences 98, 1151–1171.

Pesonen, L.J., Mertanen, S. and Veikkolainen, T., 2012. Paleo-Mesoproterozoic supercontinents–a paleomagnetic view. Geophysica 48, 5–47.

Petersson, A., Scherstén, A., Bingen, B., Gerdes, A., Whitehouse, M.J., 2015. Mesoproterozoic continental growth: U–Pb–Hf–O zircon record in the Idefjorden terrane, Sveconorwegian Orogen. Precambrian Research 261, 75–95.

Peron-Pinvidic, G. and Osmundsen, P.T., 2020. From orogeny to rifting: insights from the Norwegian 'reactivation phase'. Scientific Reports 10, 14860.

Pisarevsky, S.A., Elming, S.Å., Pesonen, L.J., Li, Z.X., 2014. Mesoproterozoic paleogeography: Supercontinent and beyond. Precambrian Research 244, 207–225.

Poole, G.H., Kemp, A.I., Hagemann, S.G., Fiorentini, M.L., Jeon, H., Williams, I.S., Zappettini, E.O. and Rubinstein, N.A., 2020. The petrogenesis of back-arc magmas, constrained by zircon O and Hf isotopes, in the Frontal Cordillera and Precordillera, Argentina. Contributions to Mineralogy and Petrology 175, 1–21.

Rivers, T., 2008. Assembly and preservation of lower, mid, and upper orogenic crust in the Grenville Province—Implications for the evolution of large hot long-duration orogens. Precambrian Research, 167, 237–259.

Rey, P., Burg, J.-P., Casey, M., 1997. The Scandinavian Caledonides and their relationship to the Variscan belt. Geological Society, London, Special Publication 121, 179–200.

Røhr, T.S., Corfu, F., Austrheim, H., Andersen, T.B., 2004. Sveconorwegian U-Pb zircon and monazite ages of granulite-facies rocks, Hisarøya, Gulen, Western Gneiss Region, Norway. Norwegian Journal of Geology/Norsk Geologisk Forening, 84(4).

Røhr, T.S., Bingen, B., Robinson, P., Reddy, S.M., 2013. Geochronology of Paleoproterozoic augen gneisses in the Western Gneiss Region, Norway: evidence for Sveconorwegian zircon neocrystallization and Caledonian zircon deformation. The Journal of Geology 121, 105–128.

Roberts, N.M.W., 2010. From crystal to crust: the Proterozoic crustal evolution of southwest Norway (Doctoral dissertation, University of Leicester).

Roberts, N.M., Slagstad, T., Parrish, R.R., Norry, M.J., Marker, M., Horstwood, M.S., 2013. Sedimentary recycling in arc magmas: geochemical and U–Pb–Hf–O constraints on the Mesoproterozoic Suldal Arc, SW Norway. Contributions to Mineralogy and Petrology 165, 507–523.

Roberts, N.M., 2013. The boring billion?–Lid tectonics, continental growth and environmental change associated with the Columbia supercontinent. Geoscience Frontiers 4, 681–691.

Roberts, N.M, Slagstad, T., 2015. Continental growth and reworking on the edge of the Columbia and Rodinia supercontinents; 1.86–0.9 Ga accretionary orogeny in southwest Fennoscandia. International Geology Review 57, 1582–1606.

Roffeis, C., Corfu, F., Gabrielsen, R.H., 2013. A Sveconorwegian terrane boundary in the Caledonian Hardanger–Ryfylke Nappe Complex: The lost link between Telemarkia and the Western Gneiss Region? Precambrian Research 228, 20–35.

Roffeis, C. and Corfu, F., 2014. Caledonian nappes of southern Norway and their correlation with Sveconorwegian basement domains. Geological Society, London, Special Publication 390, 193–221.

Schärer, U., Wilmart, E., Duchesne, J.C., 1996. The short duration and anorogenic character of anorthosite magmatism: UPb dating of the Rogaland complex, Norway. Earth and Planetary Science Letters 13, 335–350.

Scheiber, T., Viola, G., Bingen, B., Peters, M., Solli, A. 2015. Multiple reactivation and strain localization along a Proterozoic orogen-scale deformation zone: The Kongsberg-Telemark boundary in southern Norway revisited. Precambrian Research 265, 78–103.

Sigmond, E.M.O., 1998. Geologisk kart over Norge, berggrunnskart Odda, 1:250000. Norges geologiske undersøkelse, Trondheim.

Skår, Ø., Pedersen, R.B., 2003. Relations between granitoid magmatism and migmatization: U–Pb geochronological evidence from the Western Gneiss Complex, Norway. Journal of the Geological Society 160, 935–946.

Slagstad, T., Roberts, N.M., Marker, M., Røhr, T.S., Schiellerup, H., 2013. A non- collisional, accretionary Sveconorwegian orogen. Terra Nova 25, 30–37.

Slagstad, T., Maystrenko, Y., Maupin, V., Gradmann, S., 2018a. An extinct, Late Mesoproterozoic, Sveconorwegian mantle wedge beneath SW Fennoscandia, reflected in seismic tomography and assessed by thermal modelling. Terra Nova 30, 72–77.

Slagstad, T., Roberts, N.M., Coint, N., Høy, I., Sauer, S., Kirkland, C.L., Marker, M., Røhr, T.S., Henderson, I.H., Stormoen, M.A., Skår, Ø., 2018b. Magma-driven, high-grade metamorphism in the Sveconorwegian Province, southwest Norway, during the terminal stages of Fennoscandian Shield evolution. Geosphere 14, 861–882.

Slagstad, T., Roberts, N.M., Kulakov, E., 2017. Linking orogenesis across a supercontinent; the Grenvillian and Sveconorwegian margins on Rodinia. Gondwana Research 44, 109–115.

Slagstad, T., Marker, M., Roberts, N.M., Saalmann, K., Kirkland, C.L., Kulakov, E., Ganerød, M., Røhr, T.S., Møkkelgjerd, S.H., Granseth, A., Sørensen, B.E., 2020. The Sveconorwegian orogeny–reamalgamation of the fragmented southwestern margin of Fennoscandia. Precambrian Research, 105877.

Söderlund, U., Hellström, F.A., Kamo, S.L., 2008. Geochronology of high-pressure mafic granulite dykes in SW Sweden; tracking the P-T-t path of metamorphism using Hf isotopes in zircon and baddeleyite. Journal of Metamorphic Geology 26, 539–560.

Spencer, C.J., Roberts, N.M.W., Cawood, P.A., Hawkesworth, C.J., Prave, A.R., Antonini, A.S.M., Horstwood, M.S.A., 2014. Intermontane basins and bimodal volcanism at the onset of the Sveconorwegian Orogeny, southern Norway. Precambrian Research 252, 107–118.

Spencer, C.J., Kirkland, C.L., Prave, A.R., Strachan, R.A., Pease, V., 2019. Crustal reworking and orogenic styles inferred from zircon Hf isotopes: Proterozoic examples from the North Atlantic region. Geoscience Frontiers 10, 417–424.

Stephens, M.B., 2020. Chapter 8 - Outboard-migrating accretionary orogeny at 1.9–1.8 Ga (Svecokarelian) along a margin to the continent Fennoscandia. Geological Society, London, Memoirs 50, 237–250.

Sundvoll, B., Larsen, B.T., 1994. Architecture and early evolution of the Oslo Rift. Tectonophysics 240, 173–189.

Swanson-Hysell, N.L., Kilian, T.M., Hanson, R.E., 2015, A new grand mean palaeomagnetic pole for the 1.11 Ga Umkondo large igneous province with implications for palaeogeography and the geomagnetic field: Geophysical Journal International 203, 2237–2247.

Swanson-Hysell, N.L., Ramezani, J., Fairchild, L.M., Rose, I.R., 2019. Failed rifting and fast drifting: Midcontinent rift development, Laurentia's rapid motion and the driver of Grenvillian orogenesis. Bulletin 131, 913–940.

Tobi, A.C., Hermans, G.A., Maijer, C., Jansen, J.B.H., 1985. Metamorphic zoning in the high-grade Proterozoic of Rogaland-Vest Agder, SW Norway. In Tobi, A.C. & Touret, J.L. (eds.), The deep Proterozoic crust in the north Atlantic provinces, NATO-ASI C158, 477–497. Reidel, Dordrecht.

Tomkins, H.S., Williams, I.S., Ellis, D.J., 2005. In situ U–Pb dating of zircon formed from retrograde garnet breakdown during decompression in Rogaland, SW Norway. Journal of Metamorphic Geology 23, 201–215.

Torsvik, T.H., Smethurst, M.A., Meert, J.G., Van der Voo, R., McKerrow, W.S., Brasier, M.D., Sturt, B.A. and Walderhaug, H.J., 1996. Continental break-up and collision in the Neoproterozoic and Palaeozoic—a tale of Baltica and Laurentia. Earth-Science Reviews 40, 229–258.

Torske, T., 1982. Structural effects on the Proterozoic Ullensvang Group (West Norway) relatable to forceful emplacement of expanding plutons. Geologische Rundschau 71, 104–119.

Troch, J., Ellis, B.S., Harris, C., Bachmann, O., Bindeman, I.N., 2020. Low-$\delta^{18}O$ silicic magmas on Earth: A review. Earth-Science Reviews, 103299.

Tucker, R. D.; Krogh, T. E.; and Ra°heim, A., 1990. Proterozoic evolution and age-province boundaries in the central part of the Western Gneiss Region, Norway: results of U-Pb dating of accessory minerals from Trondheimsfjord to Geiranger. In Gower, C. F.; Rivers, T.; and Ryan, A. B., eds. Mid-Proterozoic Laurentia- Baltica. Geol. Assoc. Can. Spec. Pap. St. John's, Geological Association of Canada, 149–173.

Vander Auwera, J., Bolle, O., Bingen, B., Liégeois, J.P., Bogaerts, M., Duchesne, J.C., De Waele, B., Longhi, J., 2011. Sveconorwegian massif-type anorthosites and related granitoids result from post-collisional melting of a continental arc root. Earth-Science Reviews 107, 375–397.

Vanderhaeghe, O., Teyssier, C., 2001. Partial melting and flow of orogens. Tectonophysics 342, 451–472.

Vanderhaeghe, O., 2012. The thermal–mechanical evolution of crustal orogenic belts at convergent plate boundaries: A reappraisal of the orogenic cycle. Journal of Geodynamics 56–57, 124–145.

Viola, G., Henderson, I.H.C., Bingen, B., Hendriks, B.W.H., 2011. The Grenvillian–Sveconorwegian orogeny in Fennoscandia: Back-thrusting and extensional shearing along the "Mylonite Zone". Precambrian Research 189, 368–388.

Wain, A., 1997. New evidence for coesite in eclogite and gneisses: Defining an ultrahigh-pressure province in the Western Gneiss region of Norway. Geology 25, 927–930.

Waltenberg, K., Bodorkos, S., Armstrong, R., Fu, B., 2018. Mid-to lower-crustal architecture of the northern Lachlan and southern Thomson orogens: evidence from O–Hf isotopes. Australian Journal of Earth Sciences 65, 1009–1034.

Weber, B., Scherer, E.E., Schulze, C., Valencia, V.A., Montecinos, P., Mezger, K., Ruiz, J., 2010. U–Pb and Lu–Hf isotope systematics of lower crust from central-southern Mexico–Geodynamic significance of Oaxaquia in a Rodinia Realm. Precambrian Research 182, 149–162.

Wennberg, O.P., Milnes, A.G., Winsvold, I., 1998. The northern Bergen Arc Shear Zone - an oblique-lateral ramp in the Devonian extensional detachment system of western Norway. Norsk Geologisk Tidsskrift 78, 169–184.

Whitney, D.L. and Evans, B.W., 2010. Abbreviations for names of rock-forming minerals. American mineralogist 95, 185–187.

Wiest, J.D., Jacobs, J., Ksienzyk, A.K., Fossen, H., 2018. Sveconorwegian vs. Caledonian orogenesis in the eastern Øygarden Complex, SW Norway – Geochronology, structural constraints and tectonic implications. Precambrian Research, 305, 1–18.

Wiest, J.D., Osmundsen, P.T., Jacobs, J., Fossen, H., 2019. Deep crustal flow within post-orogenic metamorphic core complexes – Insights from the southern Western Gneiss Region of Norway Tectonics, 38, 4267–4289.

Wiest, J.D., Fossen, H., Jacobs, J., 2020a. Shear zone evolution during core complex exhumation – Implications for continental detachments. Journal of Structural Geology, 140, 104139.

Wiest, J.D., Wrona, T., Bauck, M.S., Fossen, H., Gawthorpe, R.L., Osmundsen, P.T., Faleide, J.I., 2020b. From Caledonian Collapse to North Sea Rift: The Extended History of a Metamorphic Core Complex. Tectonics, 39, e2020TC006178.

Wiest, J.D., Jacobs, J., Fossen, H., Ganerød, M. & Osmundsen, P.T., 2021. Segmentation of the Caledonian orogenic infrastructure and exhumation of the Western Gneiss Region during transtensional collapse. Journal of the Geological Society, jgs2020-2199, doi: 10.1144/jgs2020-199.

Paper III

Jacobs, J., Mikhalsky, E., Henjes-Kunst, F., Läufer, A., Thomas, R.J., Elburg, M.A., ***Wang, C-C.****, Estrada, S., Skublov, S., 2020. Neoproterozoic geodynamic evolution of easternmost Kalahari: Constraints from U-Pb-Hf-O zircon, Sm-Nd isotope and geochemical data from the Schirmacher Oasis, East Antarctica. Precambrian Research 342, 105553.*

Precambrian Research 342 (2020) 105553

Contents lists available at ScienceDirect

Precambrian Research

journal homepage: www.elsevier.com/locate/precamres

Neoproterozoic geodynamic evolution of easternmost Kalahari: Constraints from U-Pb-Hf-O zircon, Sm-Nd isotope and geochemical data from the Schirmacher Oasis, East Antarctica

J. Jacobs[a,*], E. Mikhalsky[b], F. Henjes-Kunst[c,1], A. Läufer[c], R.J. Thomas[d], M.A. Elburg[e], C.-C. Wang[a], S. Estrada[c], S. Skublov[f,g]

[a] Department of Earth Science, University of Bergen, PB 7803, N-5020 Bergen, Norway
[b] VNIIOkeangeologia, Angliiskii pr. 1, St. Petersburg 190121, Russia
[c] Federal Institute for Geosciences and Natural Resources (BGR), Stilleweg 2, 30655 Hannover, Germany
[d] Council for Geoscience, 3 Oos Street, Bellville, Cape Town 7535, South Africa
[e] Department of Geology, University of Johannesburg, Auckland Park 2006, Johannesburg, South Africa
[f] Institute of Precambrian Geology and Geochronology, Russian Academy of Sciences, Makarova emb. 2, St. Petersburg 199034, Russia
[g] Saint-Petersburg Mining University, 21-st liniya 2, St. Petersburg 199106, Russia

ARTICLE INFO

Keywords:
Dronning Maud Land
Continental arc
Tonian
Rodinia
Extroversion
Zircon
Schirmacher Oasis

ABSTRACT

Late Tonian (ca. 785–760 Ma) granodioritic to granitic orthogneisses of the Schirmacher Oasis region in Dronning Maud Land (DML), East Antarctica, are interpreted as recording an active continental margin setting at the periphery of Kalahari and Rodinia. The rocks probably represent exposures of a significant tectonic province hidden beneath the ice, the erosional remnants of which are recorded as detrital zircons in late Tonian-Cryogenian metasedimentary rocks throughout central and eastern DML, as well as in ice-rafted debris from recent sediments offshore Dronning Maud Land. The orthogneisses have single-stage Sm-Nd model ages of ca. 1.3–1.5 Ga and zircon Hf-signatures ($\varepsilon Hf_t = +2 - +5$), indistinguishable from the adjacent Grenville-age basement rocks of easternmost Kalahari. Their geochemistry suggests that they evolved in the late stages of a continental margin magmatic arc and possibly within a roll-back tectonic framework, suggestive of subduction of relatively old oceanic lithosphere. The eastern Kalahari continental arc is one of a number of continental arcs that characterize the western part of the fragmenting Rodinia and document the supercontinent "turning inside out" after its formation at ca. 1000 Ma and a period of relative tectonic quiescence between ca. 900 and 800 Ma.

The rocks show an ultra-high temperature metamorphic overprint that was accompanied by syn-tectonic magmatism from ca. 650 to 600 Ma. The high temperature metamorphism is interpreted to relate to back-arc extension that also led to major anorthosite magmatism elsewhere, prior to continental collision in the region. The rocks lack the subsequent widespread high-grade metamorphic overprint at ca. 590–500 Ma which occurs in the adjacent regions due to Himalayan-style continental collision along the East African-Antarctic Orogen during Gondwana assembly.

1. Introduction

East Antarctica is transected by Late Neoproterozoic to Early Paleozoic mobile belts, along which the continent was amalgamated during the assembly of Gondwana between ca. 650 and 500 Ma. One of the most important of these mobile belts is the East African-Antarctic Orogen (e.g. Jacobs and Thomas, 2004), a section of which is well exposed along the Dronning Maud Land rift margin escarpment (Figs. 1, 2). The East African-Antarctic Orogen has been shown to be one of the largest Himalayan-style collision orogens on our planet (e.g. Fritz et al., 2013; Jacobs and Thomas, 2004). In Dronning Maud Land (DML), a record of the collision of Kalahari with Indo-Antarctica, along with extensive remnants of the intervening Mozambique Ocean, is well preserved (e.g. Elburg et al., 2015; Jacobs et al., 2015). Several major tectonic lineaments of this orogen can be traced through DML. In the west, the orogenic front of the East African-Antarctic Orogen is

* Corresponding author.
E-mail address: joachim.jacobs@uib.no (J. Jacobs).
[1] Present address: Schubertstr. 10, 30900 Wedemark, Germany.

https://doi.org/10.1016/j.precamres.2019.105553
Received 3 April 2019; Received in revised form 5 November 2019; Accepted 29 November 2019
Available online 17 December 2019

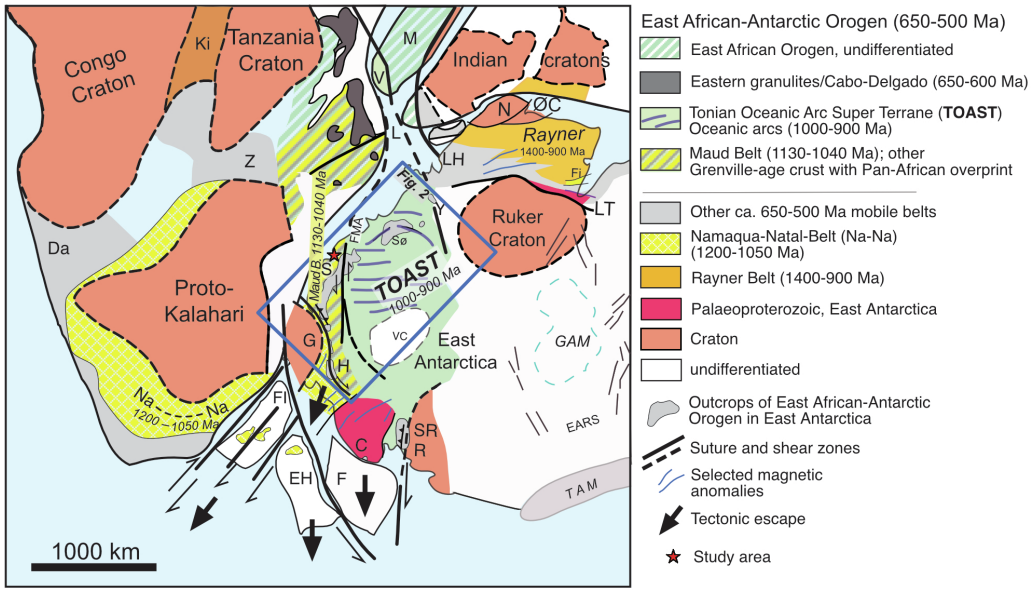

Fig. 1. Location of the study area, Schirmacher Oasis (S) and surrounding nunataks, in central DML and the East African-Antarctic Orogen in its Gondwana context (after Jacobs et al., 2015; Jacobs and Thomas, 2004). The study area is located in the easternmost part of Kalahari and in close proximity to the TOAST to the E. East Antarctica is shown in polar stereographic projection, whereas the adjacent continents are shown schematically. Abbreviation: C – Coats Land, Da – Damara belt, EARS – East Antarctic Rift System: EH – Ellsworth-Haag, F – Filchner block, FI – Falkland Islands, Fi – Fisher Terrane, FMA – Forster Magnetic Anomaly, G – Grunehogna, GAM – Gamburtsev Mts., H – Heimefrontfjella, Ki – Kibaran, L – Lurio Belt, LH – Lützow-Holm Bay, LT – Lambert Terrane, N – Napier Complex, Na-Na – Namaqua-Natal, M – Madagascar, ØC – Øygarden Complex, R – Read Block, S – Schirmacher Oasis, Sø – Sør Rondane, SR – Shackleton Range, TAM – Transantarctic Mts., V – Vohibori, VC – Valkyrie Craton, cryptic (Golynsky et al., 2018), Y – Yamato Mts., Z – Zambesi belt.

represented by the Heimefront Shear Zone (Fig. 2). The Forster Magnetic Anomaly (Riedel et al., 2013), initially interpreted as the main suture zone of the East African-Antarctic Orogen, is now considered to be the eastern margin of Kalahari[2] and the boundary with the Tonian Oceanic Arc Super Terrane (TOAST) (Jacobs et al., 2015) (Figs. 1, 2). The TOAST represents extensive remnants of the Mozambique Ocean, probably in excess of 500,000 km^2 (Ruppel et al., 2018).

The Schirmacher Oasis is the only coastal outcrop in central DML and it lies close to the easternmost margin of Kalahari (e.g. Jacobs et al., 2008), immediately to the north-west of the Forster Magnetic Anomaly (Fig. 2). Its geology and geophysical characteristics appear to be distinct from the Kalahari-type crust farther south in the region (e.g. Baba et al., 2010), suggesting that it may be a key to the better understanding of the complex tectonic history along the eastern margin of Kalahari.

Consequently, we undertook fieldwork in the Schirmacher Oasis area during the austral summers 2010/11 and 2011/12 including some of the poorly studied nunataks to the south (Fig. 3).

We present new U-Pb, Lu-Hf and O isotope and trace-element zircon analyses on all the major zircon-bearing rock units of the region, including detrital zircon analyses from metasedimentary rocks and two glacial moraine samples. Many of the dated samples and additional samples also underwent whole-rock geochemical and Sm-Nd isotope analyses in order to constrain the tectonic setting of the eastern margin of Kalahari.

[2] Kalahari is used here according to Jacobs et al. (2008): It consists of the Archean to Paleoproterozoic Proto-Kalahari core and the surrounding Mesoproterozoic crustal additions. In DML, a fragment of the Archean Proto-Kalahari core is exposed in the east (Grunehogna Craton), whilst the majority of western and central DML is underlain by late Mesoproterozoic crustal additions at the margin of Porto-Kalahari, including the Grenville-age Maud Belt.

2. Geological background and previous work

The Schirmacher Oasis is an ice-free outcrop area with low relief close to the DML coastline measuring about 18 × 4 km (Fig. 3). To the south, a group of scattered small nunataks are also included in this study. The first reconnaissance geological study of the Schirmacher region was undertaken by Soviet geologists (Ravich and Solov'ev, 1966). Subsequently, studies were carried out from the East German, Indian and Russian stations (e.g. Kämpf and Stackebrandt, 1985; Ravikant, 1998; Ravikant et al., 2004; Sengupta, 1988; Sengupta, 1991; Wetzel et al., 1991), as summarized in Bormann and Fritsche (1995). Based on these and our own observations seven metamorphic rock units have been distinguished (Fig. 3). These are:

(1) garnet-leucogneiss and transposed mafic granulite/amphibolite;
(2) mafic granulite/metagabbro/norite;
(3) granitic gneiss (strongly sheared orthopyroxene-bearing gneisses of varying lithology) and partly augen gneiss;
(4) augen gneiss;
(5) banded garnet-biotite gneiss (paragneiss);
(6) metapelite, mainly garnet-biotite-sillimanite gneisses, minor calc-silicates;
(7) syn-kinematic diorite–granodiorite orthogneiss suite, small sheet-like bodies in southern part of the study area.

The rocks of the study area underwent a polyphase Pan-African tectono-metamorphic evolution, characterised by crustal stacking along shallow S- to SSE-dipping (N- to NNW vergent) thrusts (e.g. Kämpf and Stackebrandt, 1985; Sengupta, 1988; Sengupta, 1991; Wetzel et al., 1991). A number of late, NE-trending sinistral and dextral shear zones are associated with zones of ultramylonite.

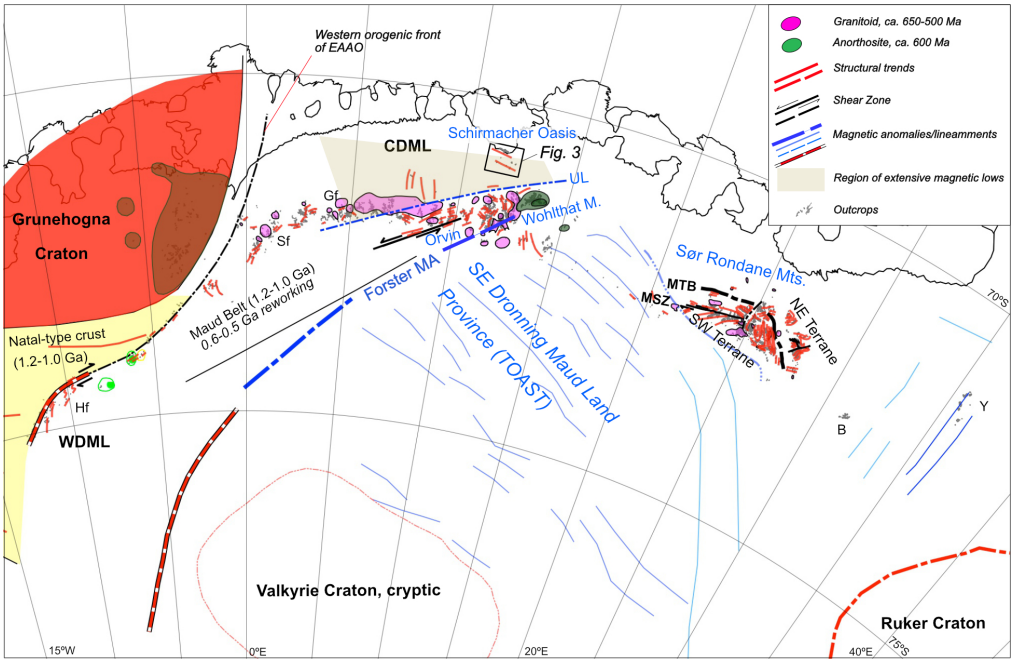

Fig. 2. Location of the Schirmacher Oasis and the regional geology of DML. Magnetic anomalies/lineament and major tectonic boundaries after Mieth et al. (2014), Mieth and Jokat (2014), Jacobs et al. (2015), Ruppel et al. (2015), Jacobs et al. (2017) and Golynsky et al. (2018). The Forster Magnetic Anomaly is considered to be the eastern limit of Kalahari, separating it from TOAST (Jacobs et al., 2015); TOAST is geophysically part of the SE DML Province (Mieth and Jokat, 2014). Abbreviations: B – Belgica Mts., CDML – central Dronning Maud Land, Gf – Gjelsvikfjella, Hf – Heimfrontfjella, MA – Magnetic Anomaly, MSZ – Main Shear Zone, MTB – Main Tectonic Boundary, Sf – Sverdrupfjella, UL – Ulvetanna Lineament, WDML – western Dronning Maud Land, Y – Yamato Mts.

2.1. Previous geochronological studies

Previous geochronological studies in the region are presented in Ravich and Krylov (1963), Grew and Manton (1983), Henjes-Kunst (2004), Ravikant et al. (2004), Ravikant (2006), Ravikant et al. (2007), Baba et al. (2010) and Ravikant et al. (2018). These works revealed that the main high-grade metamorphic imprint occurred at ca. 640–600 Ma and is characterised, at least in part, by UHT metamorphism (sapphirine-orthopyroxene-garnet granulites; Baba et al. (2010)). There is no evidence for high-grade metamorphism after ca. 600 Ma. This contrasts with the mountain range south of the Schirmacher Oasis, between the Orvin and Wohlthat mountains (referred to as the Orvin-Wohlthat Mountains below) (Fig. 2), where the main medium- to high-grade metamorphism had been dated at ca. 590 to 500 Ma and where many units appear to lack metamorphism at ca. 640–600 Ma (e.g. Jacobs et al., 2003b; Jacobs et al., 1998); see compilation in Elburg et al. (2016). Rocks of the Orvin-Wohlthat Mountains include high-pressure granulites (Fig. 2) associated with a clockwise PT path (e.g. Baba et al., 2008; Palmeri et al., 2018).

Whereas the metamorphic history in the Schirmacher region is quite well documented, the protolith ages of the rocks are unclear, a knowledge gap that this paper seeks to address. In the Orvin-Wohlthat Mountains, typical crystallisation ages typically range from ca. 1150 to 1040 Ma (e.g. Jacobs et al., 1998; Jacobs et al., 2003a). In the Schirmacher region, only a few igneous crystallisation ages, ranging from ca. 1000 to 800 Ma, have been reported (e.g. Baba et al., 2010; Rao, 2000). The nature and significance of these Tonian ages is thus far poorly constrained or understood. A Sm-Nd isotope study of mafic granulites from the Schirmacher Oasis gave single-stage Sm-Nd model ages of ca. 1.1–1.35 Ga (Rao, 2000), similar to those reported for the Orvin-Wohlthat Mountains (Jacobs et al., 1998; Mikhalsky et al., 1997).

2.2. Samples and methods

In order to elucidate the temporal tectono-magmatic evolution of this key region at the edge of East Antarctica, our study includes eleven basement samples (six from the Schirmacher Oasis and five from the nunataks to the south) and two moraine samples for geochronological analysis (see Fig. 3 for sample location and Fig. 4 for field photographs). The Schirmacher Oasis samples include two variably sheared augen gneisses from the west, four samples of granite orthogneisses, augen gneisses and a highly foliated garnet-leucogneiss from the east. The five samples from the nunataks to the south include two augen gneisses, two metagranodiorite samples and one metapelitic paragneiss. In addition, two glacial moraine samples from the southern edge of the oasis were analysed in order to characterise the source area to the south, within the glacial catchment. These two samples were treated as detrital samples: batch samples were crushed and zircon-separated (e.g. Jacobs et al., 2017).

Zircons from all thirteen samples were separated with standard separation techniques, including Holman-Wilfley shaking table, magnetic- and heavy-liquid separation. U-Pb zircon SIMS/SHRIMP analyses were carried out at different laboratories: the Nordsim facility (Stockholm, Sweden), the IBERSIMS facility (Granada, Spain), the Centre of Isotopic Research (VSEGEI, St. Petersburg, Russia) and at the John de Laeter Centre at Curtin University (Australia). Two glacial drift samples were analysed by LA-ICPMS at the Senckenberg Naturhistorische Sammlung (Dresden, Germany). Zircon Lu-Hf isotope analyses on five selected samples were carried out on a Nu Plasma II coupled to an ASI 193 nm Excimer laser ablation system at the

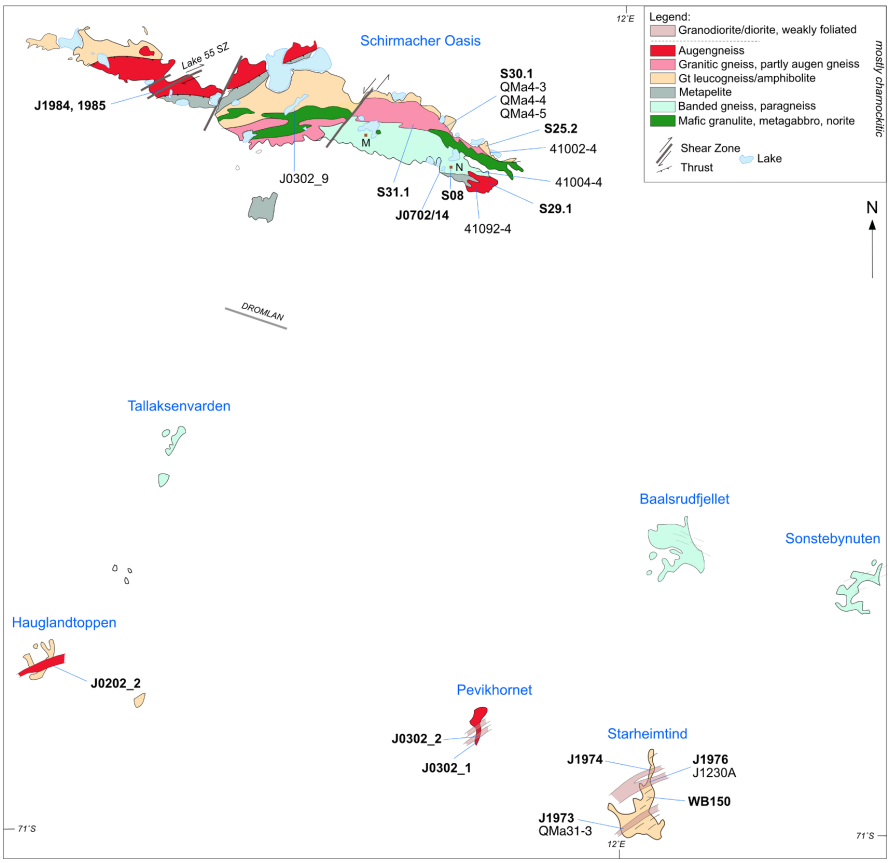

Fig. 3. Geological overview and sample locality map of the Schirmacher Oasis and adjacent nunataks, based on our field mapping, an unpublished geological map by Mikhalsky and Laiba (2010) as well as Ravikant (1998). Sample numbers in bold are U-Pb zircon dated samples. Abbreviations: DROMLAN – airstrip, M – Maitri Station, N – Novolazarevskaya Station, SZ – Shear Zone.

University of Johannesburg (South Africa), following procedures described in Jacobs et al. (2017). Three of the U-Pb zircon-dated samples underwent trace-element analyses on a Cameca IMS-4f ion microprobe at the Yaroslavl' Branch of the Physic-Technological Institute (Russian Academy of Sciences, RAS). Two samples underwent O-isotope analysis at the Nordsim facility. Whole-rock samples of the dated lithologies were analysed for Sm-Nd isotopes at the Federal Institute for Geosciences and Natural Resources (BGR; Hannover, Germany) and at the Institute of Precambrian Geology and Geochronology (IPGG; St. Petersburg, Russia) by standard isotope dilution method and thermal-ionization mass spectrometry. Finally, a representative suite of the dated lithologies including additional samples of those lithologies (Fig. 3) underwent major to trace element analysis by XRF and in part trace element analysis by ICP-MS at the BGR, the VSEGEI and by Actlabs.

Details of the various methods are outlined in Supplementary file A.

3. Results

3.1. Zircon U-Pb-Hf-O isotope and trace-element analyses

Zircon U-Pb-Hf-O isotope and trace-element analyses are given in Supplementary file B, Tables 1–7.

3.1.1. Basement rocks

3.1.1.1. S25.2, Garnet-leucogneiss, Schirmacher Oasis East. This sample is a leucocratic garnet-bearing quartzo-feldspathic layered gneiss. It contains rounded to highly elongate zircons up to 300 µm in length and aspect ratios up to 5. Many zircons are irregularly zoned and resemble metamorphic grains. In cathodoluminescence (CL), clear core-rim relationships are seen (Fig. 5a). Cores often show a broad or oscillatory zoning. Resorption and recrystallization textures are common. The cores often show only thin metamorphic rims. Seventeen spots were analysed in 11 grains focusing on zircon cores.

Six core analyses with variable Th/U form one age group with a concordia age of 1006 ± 22 Ma (MSWD = 1.9). Four further core analyses are from particularly broadly zoned zircon domains, with Th/U ranging from 0.85 to 0.90. These provide a concordia age of 784 ± 14 Ma (MSWD = 1.8). Between these two age groups are three analyses that partly overlap them. Two rim analyses (Th/U ratios 0.62 and 0.78) provide consistent ages of ca. 600 Ma.

The older age group occurs also as small cores within otherwise igneous zircons (analyses 6.1, 6.2). We therefore interpret the older age group as an inherited component within the younger age group of ca. 780 Ma which represents igneous crystallisation. The sample then underwent metamorphism at ca. 600 Ma.

Two ca. 1000 Ma grains with low Th/U of 0.02–0.06, typical for

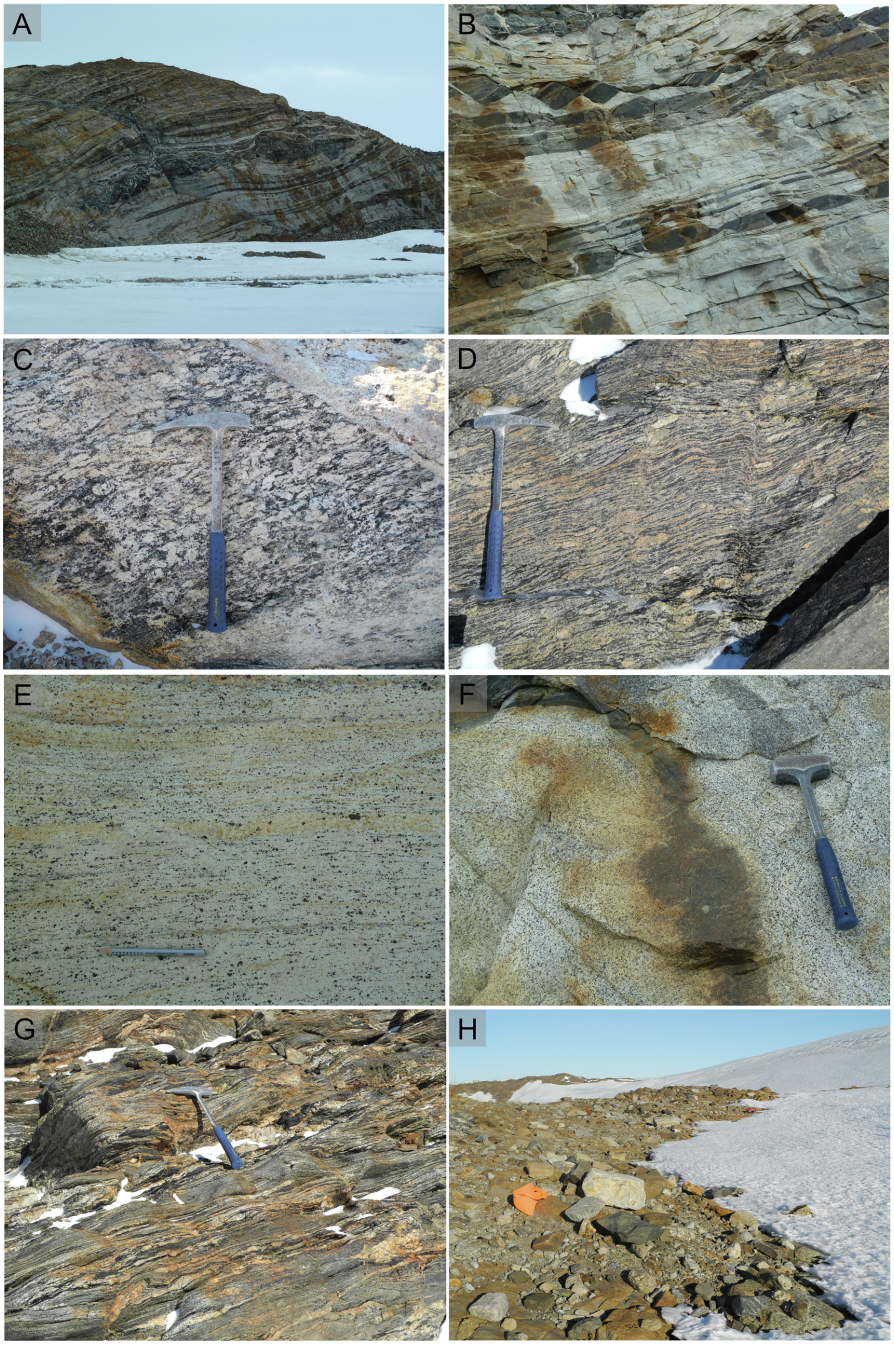

Fig. 4. Selected sample localities and field relationships in the study area. A, B) Highly sheared gt-leucogneisses with boudinaged mafic layers, north-eastern Schirmacher Oasis; C) Late Toninan augen gneiss at Hauglandtoppen (J0202_2), intruded by late-tectonic pegmatite veins; D) Late Tonian highly sheared augen gneiss (J0302_1) at Pekvikhornet; E) Late Tonian leucogneiss with garnet (S25.2), Schirmacher Oasis East; F) Charnockitic leucogneiss; G) Migmatitic paragneiss at Tallaksenvarden; H) Moraine on south-eastern side of Schirmacher Oasis, showing well-rounded boulders and rubble (J0702/14).

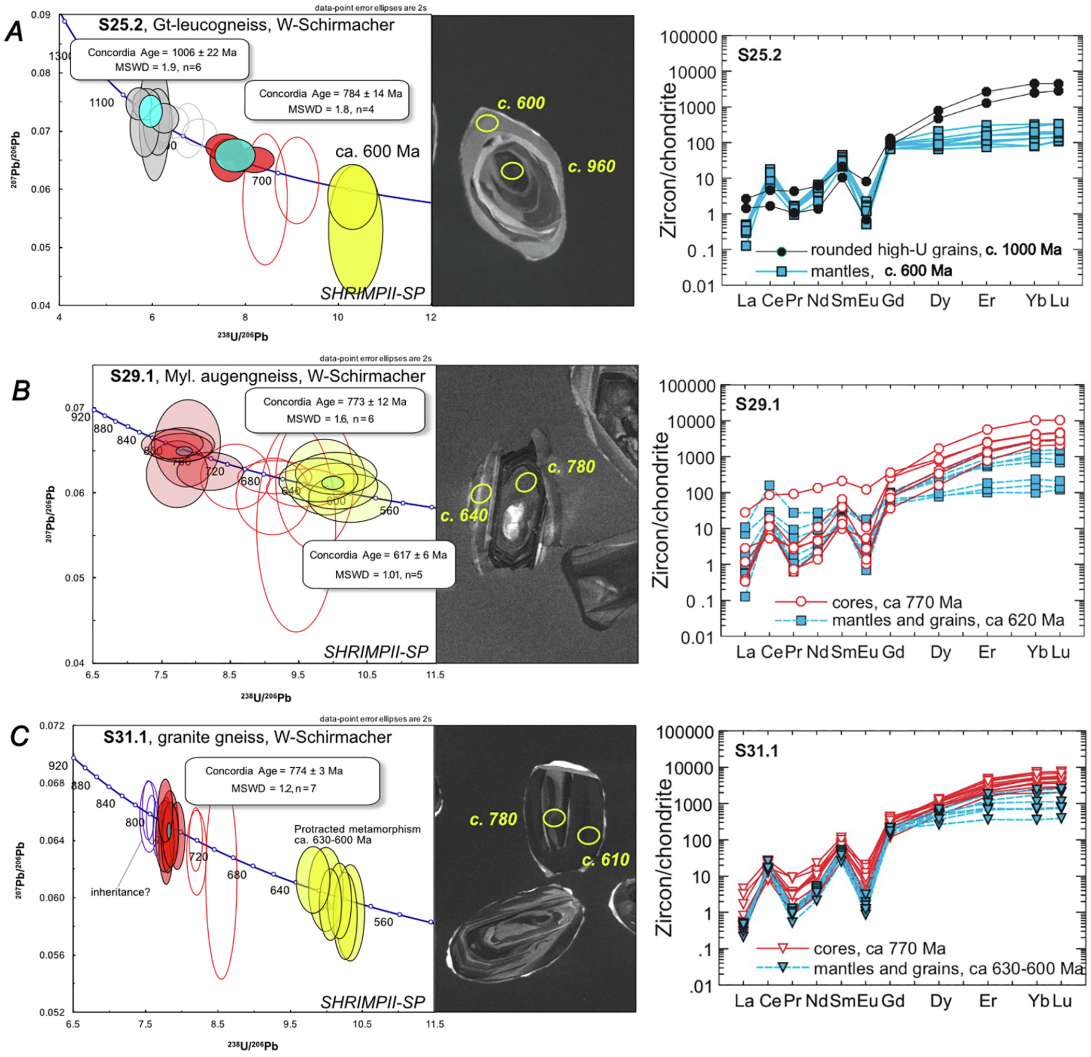

Fig. 5a. U–Pb zircon geochronology and REE distributions of felsic gneisses from Schirmacher Oasis East.

metamorphic zircon growth, show strongly fractionated REE distributions with Lu_N/La_N of about 4500 (Fig. 5a). They have strongly negative Eu anomalies ($Eu/Eu^* = 0.05$) and only minor positive Ce anomalies ($Ce/Ce^* = 2.3$). In their REE patterns, these grains are similar to zircon domains of igneous origin of other investigated samples. It is therefore concluded that the ca. 1000 Ma zircon component in sample S25.2 was inherited from an igneous source that experienced a Grenville-age metamorphic overprint.

Nine analyses from dark grey ca. 620 Ma zircon mantles show very consistent REE distribution spectra and display prominent negative Eu anomalies and positive Ce anomalies with a flat distribution of HREE at about 200–300 chondrite-normalized values (Fig. 5a); Lu_N/Gd_N vary between 1.2 and 3.5. These metamorphic mantles likely crystallized during high-grade metamorphism in the presence of garnet which concentrated HREE and Y.

3.1.1.2. S29.1, Mylonitic augen gneiss, Schirmacher Oasis East. This sample is a mylonitic two-feldspar augen gneiss with perthitic microcline, plagioclase, brown biotite, minor hornblende and garnet with accessory apatite, titanite, zircon and opaque minerals.

The sample yielded rounded to elongated zircons up to 400 µm in length, reaching aspect ratios up to 4. In CL, many zircons show irregular zoning and appear metamorphic in origin (Fig. 5a). A clear core-rim relationship is typically apparent. Cores often show broad or oscillatory zoning, typical of an igneous origin. Resorption and recrystallization features are common. The cores are overgrown by broad structureless rims that have a uniform medium CL-response.

Eighteen spots were analysed in 12 grains (12 cores and 6 rims). The 12 core analyses (U = 572 – 2300 ppm, Th/U = 0.06 – 0.58) show a significant scatter in age between ca. 790 and 630 Ma. However, the six oldest core analyses form a single age group with a concordia age of 773 ± 12 Ma (MSWD = 1.6). The other six core analyses straddle

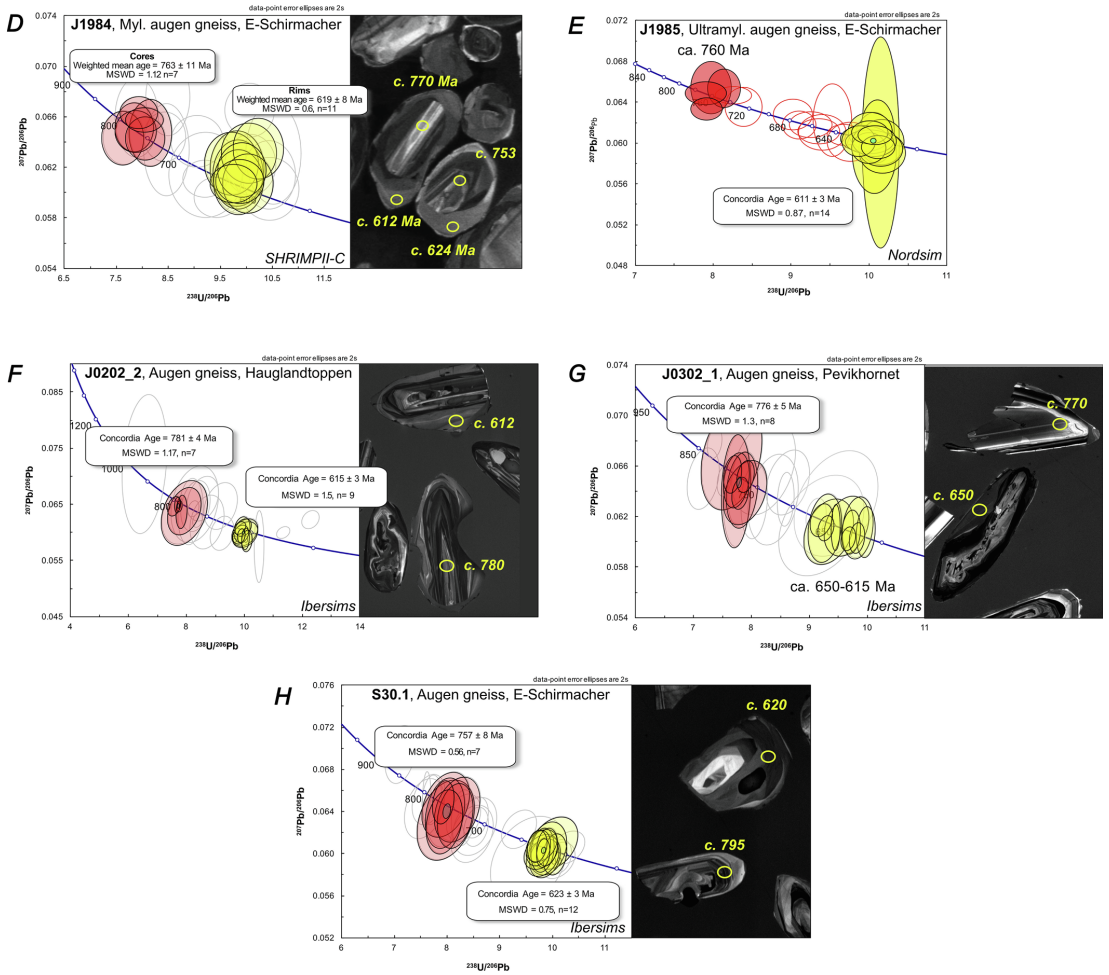

Fig. 5b. U-Pb zircon geochronology of five augen gneisses from various parts of the Schirmacher Oasis and the nunataks to the south.

concordia and the youngest overlap in part with the metamorphic rims. These analyses probably represent zircons that underwent Pb-loss during the metamorphic overprint. Five metamorphic rim analyses have a narrow range in U concentration (350 – 750 ppm) and a narrow range in Th/U (0.27 – 0.31), with a concordia age of 617 ± 6 Ma (MSWD = 1.01).

The age of ca. 770 Ma is interpreted as the crystallization age of the igneous protolith, whilst the rim analyses represent a metamorphic overprint.

The REE patterns of six igneous zircon cores reveal fractionated spectra (Fig. 5a), with variable negative Eu anomalies (on average Eu/Eu* = 0.10), and variable positive Ce anomalies (on average Ce/Ce* = 18). These analyses confirm magmatic protolith compositions. Two other core analyses show gently sloping LREE distributions (Sm_N/La_N = 8.5). These two analyses yielded consistent normalized LREE concentrations and merge into a cluster for HREE. These analyses also show moderate Ce and Eu anomalies and elevated P, Y, and Ca concentrations.

Eight ca. 620 Ma zircon mantles show nearly flat REE distributions (Fig. 5a), but with negative Eu anomalies (Eu/Eu* = 0.2) and variable positive Ce anomalies. Four zircon mantles show strongly fractionated REE spectra and more negative Eu anomalies (Eu/Eu* = 0.12). The mantles probably reflect one prolonged granulite-facies metamorphic episode when garnet was formed at an initial stage (flat REE distribution within inner mantle domains) or two metamorphic episodes close in time but differing in pressure (garnet present or absent; Rubatto, 2002).

3.1.1.3. S31.1, Granite gneiss, Schirmacher Oasis East. The sample consists of perthitic microcline, sericitised plagioclase, quartz, olive-brown biotite, skeletal garnet and accessory apatite and zircon as well as secondary muscovite. It has rounded to elongate zircons up to 500 µm in length, reaching aspect ratios up to 5. In CL, zircons show cores surrounded in part by wide structureless zircon rims with a medium CL response. (Fig. 5a). Cores are mostly oscillatory zoned or show broad simple igneous zoning.

Twenty spots were analysed in 12 grains (14 cores and 6 rims). The 14 core analyses show a significant age scatter from ca. 800 to 710 Ma. Seven analyses from the oscillatory or broadly zoned cores have narrow ranges for U (350 – 650 ppm) and Th/U (0.13–0.35) and form one well-

defined age group with a concordia age of 774 ± 3 Ma (MSWD = 1.2). Four core analyses are slightly older (ca. 800 Ma) and differ in U and Th/U from the ca. 774 Ma cores. These analyses are from either small cores within the oscillatory-zoned zircons, or from other zircons that lack the characteristic oscillatory or broad zoning. Three younger core analyses straddle concordia and probably represent Pb-loss in the course of metamorphic overprint.

The six rim analyses have U of ca. 300–600 ppm and Th/U of 0.05–0.20. Their $^{206}Pb/^{238}U$ ages range from ca. 625 to 596 Ma and have significant scatter with a weighted mean $^{206}Pb/^{238}U$ age of 606 ± 10 Ma (MSWD = 4.9).

The age of ca. 774 Ma is interpreted as the best estimate for the crystallization age of the igneous protolith. Slightly older core ages of ca. 800 Ma probably either represent an earlier stage of igneous activity or inheritance. The rim analyses are interpreted as reflecting protracted metamorphism from ca. 625 to 596 Ma.

The zircon core analyses have a REE distribution characterised by high positive Ce anomalies (Ce/Ce* vary between 3 and 22) and high total LREE abundance (Fig. 5a). The CL-dark zircon mantles (ca. 630–600 Ma) have pronounced positive Ce anomalies (Ce/Ce* = 28) and negative Eu anomalies (Eu/Eu* = 0.02). These spectra overlap for the LREE, but vary for the HREE (Lu_N/Gd_N varies between 2 and 16). The variations in HREE concentrations in zircon mantles most likely reflect the coeval growth of zircon and garnet observed in the rock.

3.1.1.4. J1984, Protomylonitic augen gneiss, Schirmacher Oasis West. Sample J1984 is an augen gneiss with a protomylonitic fabric related to the Lake 55 shear zone (Fig. 3). The sample contains clasts of strongly perthitic K-feldspar and intensely saussuritised plagioclase, surrounded by a ductile matrix of deformed K-feldspar, plagioclase and ribbon quartz. Fine-grained brown biotite formed during retrograde metamorphism and overgrows the foliation.

The sample contains clear inclusion-rich zircons with irregular shapes, including round to elongate and strongly zoned zircons, varying in size between ca. 50 to 250 μm. CL reveals complex internal structures which is characterised by pronounced core – rim relationships (Fig. 5b). Zircon cores usually show clear oscillatory magmatic growth zoning and are in part resorbed.

Thirty spots were analysed, 15 rims and 15 cores. Both core and rim analyses reveal low to moderate U, mostly below 500 ppm. Th/U is variable and not distinctly different in rims and cores. Although the rims have relatively high Th/U, they are likely of metamorphic origin, since the overgrowths have developed fairly isometric shapes typical of granulite-facies zircon growth.

The 15 core analyses have a significant range in $^{206}Pb/^{238}U$ ages, however the older half (n = 7) provide a weighted mean $^{206}Pb/^{238}U$ age of 763 ± 11 Ma (MSWD = 1.12). The younger core analyses mostly straddle the concordia, probably as a result of Pb-loss during a metamorphic overprint. The rim analyses show less scatter and eleven analyses provide a weighted mean $^{206}Pb/^{238}U$ age of 619 ± 8 Ma (MSWD = 0.6). The three youngest analyses show signs of recent Pb-loss.

The age of ca. 760 Ma is the best estimate for formation of the granite protolith, whereas the age of ca. 620 Ma is interpreted to represent metamorphism.

The Hf isotopic composition of the zircons (n = 23) shows very limited variation, in both cores and rims. Epsilon Hf_{763Ma} is + 2.5 ± 0.9 (2σ), and $^{176}Hf/^{177}Hf_{763Ma}$ = 0.282374 ± 0.000026. The two-stage model age (assuming a protolith with $^{176}Lu/^{177}Hf$ = 0.015) is 1.47 Ga (Fig. 6).

$\delta^{18}O$ values range from 5.45 to 7.43 ‰ with a weighted mean of 7.05 ± 0.15 ‰ (MSWD = 1.9).

3.1.1.5. J1985, Ultramylonitic augen gneiss, Schirmacher Oasis West. Sample J1985 is an ultramylonitic augen gneiss from the Lake 55 shear zone (Fig. 3). The sample contains porphyroclasts of strongly perthitic K-feldspar and plagioclase, surrounded by a matrix of plastically deformed K-feldspar, intensely saussuritised plagioclase and quartz ribbons. Late brown fine-grained biotite overgrowths the foliation.

The sample contains transparent inclusion-rich zircons with irregular shapes, including round to elongate and strongly zoned zircons, varying in size between ca. 50 and 200 μm. CL reveals distinct core-rim relationships (Fig. 5b). Many zircon cores show a pronounced oscillatory magmatic growth zoning and partial resorption. Rims vary in size up to ca. 50 vol% of the entire zircon.

This sample was analysed in 29 spots (15 rims and 14 cores). Both core and rim analyses show low to moderate U concentration (100–600 ppm). Th/U ratios are variable, and are slightly lower in the rims.

The 15 core analyses have a significant range in $^{206}Pb/^{238}U$ ages. The oldest four form a single age population with a weighted mean $^{206}Pb/^{238}U$ age of 761 ± 16 Ma (MSWD = 1.4). The remaining core analyses straddle the concordia, probably as a result of Pb-loss during metamorphic overprint. All 15 rim analyses yielded very consistent ages, resulting in a well-defined concordia age of 611 ± 3 Ma (MSWD = 0.87).

The age of ca. 760 Ma is the best estimate for the igneous crystallisation age of the granite protolith and ca. 610 Ma is interpreted to represent a metamorphic overprint.

3.1.1.6. J0202_2, Augen gneiss, Hauglandtoppen. This sample is very coarse-grained and consists of mesoperthite, plagioclase, myrmekite, minor garnet, brown biotite (often skeletal) and accessory apatite and zircon.

The sample contains clear to light brownish elongate and irregular zircons up to 400 μm long with aspect ratios up to 5. Inclusions are common. In CL, zircons show highly resorbed cores, many of which are surrounded by wide metamorphic rims (Fig. 5b). The cores show broad or oscillatory igneous zoning.

Thirty-two spots were analysed, of which 8 are excluded because of discordance and/or high uncertainties. Both rim and core analyses have highly variable U concentrations. Th/U is low in rims (< 0.25), but reaches up to 0.8 in cores.

Fourteen core analyses show significant scatter. Seven analyses give a well-defined concordia age of 781 ± 4 Ma (MSWD = 1.17), the remaining analyses straddle Concordia, or are variably discordant, probably due to ancient/recent Pb-loss. The age of ca. 780 Ma is regarded as the crystallisation age of the granite protolith. Nine out of 10 rim analyses provide a well-defined concordia age of 615 ± 3 Ma (MSWD = 1.5). This age is the best estimate for the high-grade metamorphic overprint of the granite protolith.

Sixteen spots were ablated for Lu-Hf isotopic analysis, the results of which are indistinguishable between cores and rims. The average εHf_{781Ma} is + 4.6 ± 1.4 ($^{176}Hf/^{177}Hf_{781Ma}$ = 0.282424 ± 0.000036), giving a two-stage model age of 1.35 Ga (Fig. 6).

3.1.1.7. J0302_1, Augen gneiss, Pevikhornet. This sample consists of mesoperthite, sericitised plagioclase, myrmekite, quartz, brown biotite, minor titanite, apatite, and opaque minerals.

Zircons are clear to light brownish, stubby to elongate (aspect ratios up to 6) or irregular, up to 400 μm in length. Inclusions are common. CL reveals that the zircon cores have wide, structured, metamorphic rims (Fig. 5b). The cores have broad or oscillatory zoning and are highly resorbed and/or recrystallized along their margins.

Thirty-one spots were analysed (12 rims and 19 cores), one of which has a high error. Both rim and core analyses yielded highly variable U concentrations. Th/U ratios are low in rims (< 0.14) and reach up to 1.13 in cores.

Nineteen core analyses show a significant age scatter. A group of 8 analyses yielded consistent data with a well-defined concordia age of 776 ± 5 Ma (MSWD = 1.3). The younger age "tail" of the core analyses mostly straddles concordia, probably due to Pb-loss during high-

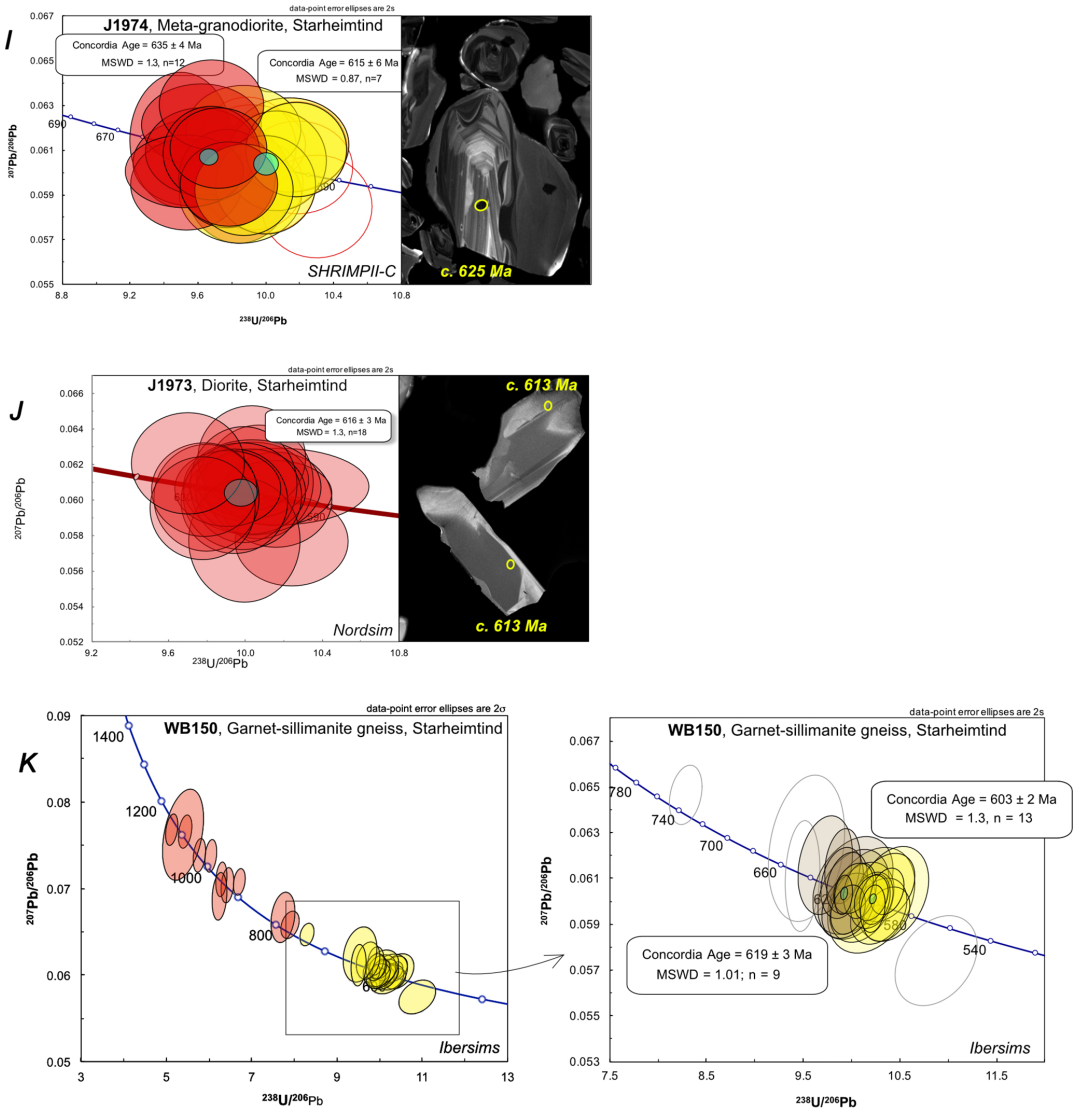

Fig. 5c. I, J). U-Pb zircon geochronology of granodiorite-diorite intrusions from Starheimtind. K) U-Pb zircon geochronology of a metasedimentary country rock from Starheimtind. Detrital zircons scatter between 1150 and 770 Ma; protracted metamorphism between ca. 630–600 Ma or two distinct metamorphic phases at ca. 619 and 603 Ma may be differentiated.

grade metamorphism. The ca. 780 Ma date is regarded as the best estimate for the crystallisation age of the granite protolith.

Twelve rim analyses show a strong and almost uniform scatter in age between 660 and 615 Ma. The seven oldest rim analyses have a weighted mean $^{206}Pb/^{238}U$ age of 651 ± 6 Ma (MSWD = 2.0). However, also the younger ages are reasonably concordant and could indicate continued metamorphism until ca. 615 Ma.

Twenty-three ablations were performed on core and rim areas of 22 grains for Lu-Hf analysis. The results are indistinguishable to those for J0202_02, with εHf_{776Ma} of +4.2 ± 1.4 ($^{176}Hf/^{177}Hf_{776Ma}$ = 0.282413 ± 0.000039), and a two-stage depleted mantle extraction age of 1.37 Ga (Fig. 6).

3.1.1.8. S30.1, Augen gneiss, Schirmacher Oasis East. This sample consists of microcline, plagioclase, quartz, brown biotite, minor olive-green hornblende and skeletal garnet with accessory apatite and zircon. It contains mostly clear, elongate, inclusion-rich, irregular zircons, reaching 400 µm in length. In CL, many zircons have oscillatory or broadly zoned cores, resembling igneous zoning (Fig. 5b). These are overgrown by wide medium-CL rims.

Cores and rims were analysed at 35 spots (18 cores and 17 rims). Twelve rim analyses provide a consistent concordia age of 623 ± 3 Ma (MSWD = 0.75). The 18 core analyses show significantly larger scatter from 850 to 700 Ma. The four oldest analyses are ca. 800 Ma. The main age group of core analyses consists of 7 analyses, which give a

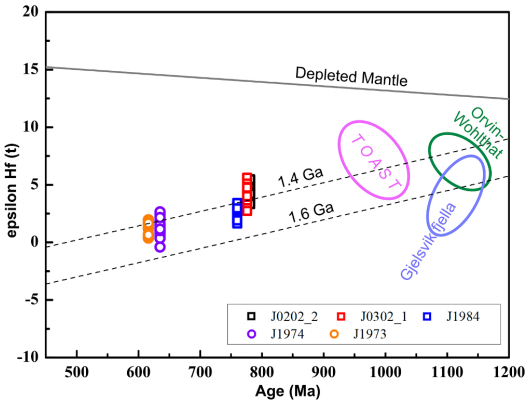

Fig. 6. Epsilon Hf(t) versus zircon age diagram showing zircon data for five of the U-Pb dated samples from study area. The 785–760 Ma age group has slightly positive ε_{Hf} (t) values, straddling the evolution line (1.4 Ga), both across TOAST as well as Grenville-age rocks in the Orvin-Wohlthat Mountains and over the field of Grenville-age rocks in Gjelsvikfjella. Two syn- to late-tectonic igneous rocks (~630 Ma) have a similar Hf isotopic signature. The late Neoproterozoic magmatism has a main derivation from earlier crust, with minor to neglectable input of mantle-derived magmas. The field for TOAST is from Elburg et al. (2015), the field for Grenville-age rocks in the Orvin-Wohlthat Mountains and Gjelsvikfjella is from Wang et al. (2020). The evolution of depleted mantle (DM) is defined with a present-day $^{176}Hf/^{177}Hf = 0.28325$ and $^{176}Lu/^{177}Hf = 0.0384$. Evolution curves of continental crust are calculated by assuming $^{176}Lu/^{177}Hf$ ratio of 0.015. Calculation of ε_{Hf} (t) values is based on the chondritic values of $^{176}Hf/^{177}Hf$ (0.282785) and $^{176}Lu/^{177}Hf$ (0.0336) as reported by Bouvier et al. (2008).

concordia age of 757 ± 8 Ma (MSWD = 0.56).

The age differences of the core analyses are difficult to interpret. They may represent different pulses of igneous activity of the igneous protolith, or the zircon could have undergone different stages or a prolonged period of Pb-loss. The rim analyses are interpreted to represent the high-grade metamorphic overprint.

3.1.1.9. J1974, Granodiorite orthogneiss, Starheimtind. At Starheimtind (Fig. 3), an intensely deformed sequence of garnetiferous metasedimentary rocks is exposed which is intruded by a foliated granodiorite-diorite suite.

Sample J1974 is composed of saussuritised plagioclase, quartz, biotite, K-feldspar and garnet. It contains clear, irregular shaped or equant to elongate zircons up 300 µm in length, with aspect ratios up to 6. Many zircons are intensely cracked preferentially parallel to the prism planes. In CL, clear core-rim relationships are apparent (Fig. 5c). Cores show oscillatory magmatic growth zoning. Some of these cores are resorbed and then overgrown by irregular and, in part, wide, structureless rims. Zircon cores have U-concentrations of ca. 100–300 ppm and rims between ca. 160 and 200 ppm. Th/U in the cores varies between ca. 0.15 and 1.0 and in the rims between ca. 0.03 and 0.3.

The seven rim analyses gave a concordia age of 614 ± 3 Ma (MSWD = 0.87). The 17 core analyses show significant scatter with a weighted mean $^{206}Pb/^{238}U$ age of 626 ± 7 Ma (MSWD = 3.0). If the 5 youngest ages are excluded which yielded ages equal or younger than the rims, the remaining 12 analyses provide a well constrained concordia age of 635 ± 4 Ma (MSWD = 0.57).

The age of ca. 635 Ma is interpreted as the crystallisation age of the granodiorite, whilst the age of ca. 615 Ma is interpreted to date a tectono-metamorphic overprint.

Eighteen spots were ablated for Lu-Hf analyses, giving a homogeneous population with εHf_{635Ma} of +1.3 ± 1.4 ($^{176}Hf/^{177}Hf_{635Ma} = 0.282421 \pm 0.000042$), and a two-stage depleted mantle extraction age of 1.45 Ga (Fig. 6).

$\delta^{18}O$ values range from 8.4 to 10.3 ‰ with a weighted mean of 9.5 ± 0.4 ‰ (MSWD = 13).

3.1.1.10. J1973, Diorite, Starheimtind. This sample from the intrusive suite consists of plagioclase, olive-green amphibole, brown biotite, quartz and apatite, ilmenite, titanite and zircon. It has large (up to 800 µm long) idiomorphic to xenomorphic zircons, containing many inclusions. In CL, the zircons show broad and irregular zoning, and some zircons show resorption (Fig. 5c).

Eighteen analyses were made on 18 grains. All analyses have consistent low U (30–70 ppm) with Th/U ranging from 0.6 to 1.4. All 18 analyses provide a well-constrained concordia age of 616 ± 3 Ma (MSWD = 1.3). This age is interpreted as the crystallisation age of the diorite.

Seventeen spots were ablated for Lu-Hf analyses, giving an average εHf_{616Ma} value of + 1.4 ± 1.0 ($^{176}Hf/^{177}Hf_{616Ma} = 0.282435 \pm 0.000029$), and a two-stage depleted mantle extraction age of 1.43 Ga (Fig. 6).

3.1.1.11. WB150, Garnet-sillimanite gneiss, Starheimtind. This sample represents the metasedimentary country rock to the granodiorite-diorite intrusions. It has large garnet and sillimanite crystals intergrown with microcline, plagioclase, quartz, brown biotite and minor orthopyroxene.

Zircons are clear, anhedral and equant to elongate up to 120 µm in length, with aspect ratios mostly < 2, and some have many inclusions. In CL, zircons show clear core-mantle relations. Many have zoned CL-moderate cores that are surrounded by wide CL-dark mantles. Two types of mantles can be distinguished: a slightly more structured inner mantle with vague patchy zoning and a structureless outer rim.

Thirty-seven spots from 32 grains were analysed (11 cores, 12 inner mantles and 14 outer mantles). All core analyses are concordant and show a broad age scatter between ca. 1150 and 770 Ma with Th/U between 0.04 and 0.5. The 12 analyses of the inner mantle have Th/U varying from 0.02 to 0.1 and have an age range from ca. 730 to 610 Ma. Nine analyses form a tightly constrained age group with a concordia age of 619 ± 3 Ma (MSWD = 1.01). Three analyses yielded ages of ca. 645 Ma (n = 2) and ca. 735 Ma. The age of the outer mantle is well constrained. Thirteen analyses provide a concordia age of 603 ± 2 Ma (MSWD = 1.03).

The zircon cores are interpreted to represent a detrital component. The youngest core date of ca. 770 Ma may be taken as the maximum deposition age of the sedimentary protolith of sample WB150, identical in age with the main igneous age group found in this study. The outer and inner mantles are interpreted to date a two-stage or protracted high-grade metamorphic history at ca. 603 and 619 Ma. Two older rim analyses at ca. 645 Ma may represent a third, less well-defined metamorphic episode and the metamorphic rim dated at ca. 735 Ma may represent a very first metamorphic imprint soon after deposition of the sedimentary protolith.

3.1.2. Glacial moraine samples

Two glacial moraine samples were collected. Sample SE08 is sand collected in immediate proximity of Novolazarevskaya Station and J0702/14 is gravel collected from the southern side of the Schirmacher Oasis, 2 km to the W of Novolazarevskaya Station, at the edge of the ice-sheet. The two samples were individually analysed and because of their similarities then combined; a total of 238 zircons were analysed. Of these, 182 grains yielded concordant ages (< 10% discordant; Fig. 7). Most grains appear to have an igneous origin, as is evident from zoning, grain morphology and Th/U. The largest age peak is at ca. 520 Ma (50%), which has no equivalance to any rocks in the Schirmacher

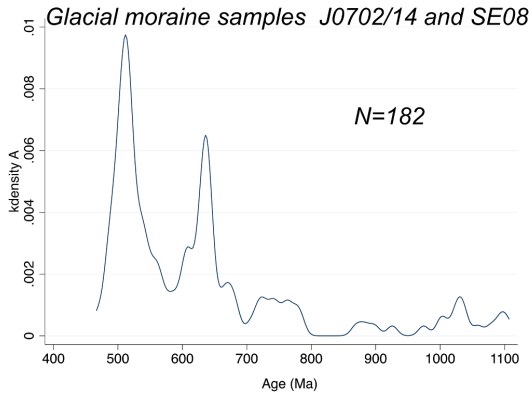

Fig. 7. Kernal density distribution of concordant U-Pb zircon analyses of combined moraine samples J0702/14 and SE08 from south-eastern Schirmacher Oasis. Note that the ca. 785–760 Ma meta-igneous suite of the Schirmacher Oasis is represented by a relatively small and broad age peak, whilst the ca. 520 Ma "Gondwana" peak recorded in this sample is not recorded in the basement samples at Schirmacher.

region and therefore must represent a source to the south. The second largest age peak at ca. 620 Ma mostly relates to late-tectonic intrusions in the nunataks to the south of the Schirmacher Oasis (Fig. 7). The main igneous protolith age of ca. 785–760 Ma of the Schirmacher region is only reflected by a relatively small and broad age peak (10%), indicating that the glacial drift is sourced from south of the Schirmacher Oasis with little local input. Very few ages older than 800 Ma occur (10%) and no pre-Stenian zircons are present.

3.1.3. Summary of zircon U-Pb, Lu-Hf, O isotope and REE analytical results

Eight meta-igneous rocks from the Schirmacher region have igneous crystallisation ages ranging from ca. 785–760 Ma (Fig. 8), of which one sample shows a $\delta^{18}O$ value of 7 ‰. Three of the eight samples show zircon inheritance with age components at ca. 800 and 1000 Ma but no older ages. High-grade metamorphic overprint ranges from 635 to 600 Ma with minor older metamorphic outliers at ca. 650 Ma. The REE patterns of zircon mantles indicate in-situ growth together with garnet at probably medium-P granulite facies conditions. Two meta-diorite-granodiorite samples from Starheimtind have syntectonic igneous crystallisation ages of ca. 635 and 615 Ma, with one sample showing a high $\delta^{18}O$ value of 9 ‰. Another sample shows the same high-grade metamorphic overprint as the other basement samples at ca. 615 Ma.

A paragneiss has detrital age components at ca. 1100, 950 and 800 Ma and shows protracted high-grade metamorphic overprinting from ca. 630 to 600 Ma. Two merged glacial moraine samples have major age peaks at ca. 520 and 630 Ma, which make up ca. 70% of all analysed spots, with no ages older than 1100 Ma.

The zircon Hf isotope data of the five analysed samples are virtually indistinguishable, with two-stage depleted mantle extraction ages of ca. 1.4 Ga (Fig. 6).

3.2. Whole-rock geochemistry and Sm-Nd isotopic composition of igneous lithologies

The results for geochemical analysis of 17 samples from (meta-)igneous lithologies and for Sm-Nd isotopic analysis of 13 samples from mostly (meta-)igneous lithologies are tabulated in Supplementary file C.

3.2.1. 785–760 Ma age group

Meta-igneous rocks of the 785–760 Ma age group have SiO_2 ranging between 61 and 75 wt%, which corresponds to granitoid protolith compositions. According to the classification schemes of Frost et al. (2001), most of the rocks range from alkali-calcic to calcic and are transitional between magnesian and ferroan granitoid types (Fig. 9a,b). On the SiO_2 vs. K_2O diagram, the rocks mostly plot in the high-K calc-alkaline series field, with some samples showing shoshonitic affinity (Fig. 9c). The augen gneisses contain abundant K-feldspar porphyroclasts/blasts suggesting a high-K porphyritic igneous precursor. Samples of the 785–760 Ma age group are slightly peraluminous with ASI indices (molar $Al_2O_3/(CaO + Na_2O + K_2O)$) of ca. 1.0–1.1 (Fig. 9d). In a MORB-normalized trace element diagram, these rocks display a prominent Nb-Ta trough relative to the neighbouring elements and a moderate to strong enrichment of the large-ion lithophile elements typical for igneous rocks formed at an active continental margin or by melting of crustal rocks formed earlier in the same setting (Fig. 9e). The variability in the normalized Th-values is attributed to variations in the amount of high-Th accessory minerals (e.g. allanite, monazite). Negative anomalies for Sr, P, Ti and in part Eu in the normalized multi-element and rare-earth-element diagrams (Fig. 9e, f) are indicative of variable element depletions typical for felsic igneous rocks having experienced fractional crystallization processes.

Meta-igneous rocks of the 785–760 Ma age group show consistent initial Nd isotope composition ($\varepsilon_{Nd}(t)$) values of −0.1 to + 1.6), indicating that they were derived from isotopically very similar magma sources (Fig. 10). The rocks have consistent single-stage Sm-Nd model ages of ca. 1.3 – 1.5 Ga indicative of rather short crustal residence times, consistent with the zircon Hf isotope evidence. The meta-igneous rocks are isotopically largely indistinguishable from those of the SW Terrane of Sør Rondane (single-stage Sm-Nd model ages of c. 0.9–2.1 Ga; Elburg et al., 2015; Kamei et al., 2013; Owada et al., 2013) and of the Orvin-Wohlthat Mountains (1.0-2.2 Ga; Mikhalsky et al., 1997; Jacobs et al., 1998; Jacobs et al., 2015). They are also indistinguishable from metamorphic rocks of the Schirmacher Oasis (1.0–2.1 Ga; Ravikant et al., 2004; Ravikant, 2006; Ravikant et al., 2007; Mikhalsky et al., unpubl. results) and those from western Dronning Maud Land (1.3–2.3 Ga; Arndt et al., 1991; Moyes, 1993; Moyes et al., 1993; Wareham et al., 1998; Grantham et al., 2001; Grosch et al., 2007; Grantham et al., 2008). Only Grenville-age basement rocks exposed on the margin of the Grunehogna Craton in western Dronning Maud Land yielded considerably older single-stage Sm-Nd model ages up to 3.6 Ga (Grosch et al., 2007; Wareham et al., 1998), indicative of the dominance of the adjacent Mesoarchaean cratonic source component.

3.2.2. Ca. 630 Ma age group

Meta-granodiorites/diorites of the ca. 630 Ma age group range in SiO_2 between ca. 52–65 wt%. Like the 785–760 Ma age group, they range from alkali-calcic to calcic series and are transitional between magnesian and ferroan granitoids (Fig. 9a, b). In the SiO_2 vs. K_2O diagram (Fig. 9c), the samples are transitional between the high-K calc-alkaline and the shoshonitic fields with the exception of J1974, which plots at the boundary of the medium to low-K series fields. Their ASI ranges from 0.7 to 1.2 (Fig. 9d). Like the older age group, samples of the ca. 630 Ma age group have high normalized values for the large-ion lithophile elements (e.g. Rb, Ba, K), a negative Nb-Ta anomaly and variable Th values (Fig. 9e). The normalized multi-element and REE diagrams also demonstrate that samples of the ca. 630 Ma group are on average enriched in Nb, Y, and Zr and the light to middle REE compared to the older group (Fig. 9e, f). Again, sample J1974 is distinguished from all other samples by its higher ASI value, normalized multi-element and REE patterns, which for most elements demonstrate a strong enrichment. In addition, zircons from this sample show a significantly higher $\delta^{18}O$ value (9.5 ± 0.4 ‰) than the late Tonian meta-igneous rocks (7.05 ± 0.15 ‰) and mantle values (5.3 ± 0.6 ‰, 2σ; Valley et al., 2005), suggesting a geochemical affinity of this sample to S-type granitic rocks.

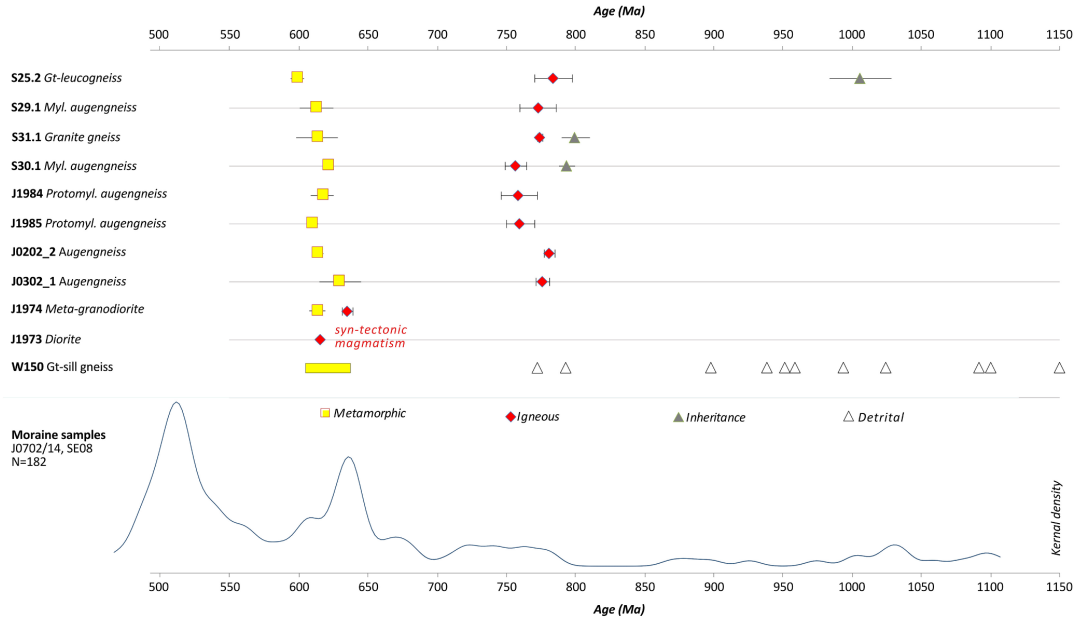

Fig. 8. Summary of the zircon U-Pb geochronological data obtained from the basement outcrops of the Schirmacher region and two glacial moraine samples (bottom).

Sm-Nd isotopic analysis of two samples of the younger age group yielded single-stage model ages of ca. 1.3 – 1.4 Ga and initial ε_{Nd} values of 0 – −1.0 (Fig. 10), within the ranges of the respective values of the older age group.

4. Discussion

4.1. Petrogenetic constraints

Eight, mostly granitic orthogneisses from the Schirmacher region have given late Tonian igneous crystallisation ages of ca. 785–760 Ma, an age group that is uncommon in the Orvin-Wohlthat Mountains to the south. Geochemically, the late Tonian rocks are members of a moderately fractionated felsic high-K igneous suite. The presence of K-feldspar porphyroclasts in augen gneiss at Schirmacher Oasis also favors a plutonic precursor. The classification diagrams of Frost et al. (2001) suggest an origin in a tectonic setting transitional between convergent (subduction-related) and within-plate (anorogenic) environments or by melting of pre-existing rocks formed in such a setting (Fig. 9a, b). A transitional tectonic setting is also evident from the (Y + Nb) versus Rb discrimination diagram of Pearce et al. (1984), where the data points plot around the boundary between the fields of volcanic-arc (VAG) and within-plate granitoids (WPG) (Fig. 11a), which, according to Pearce (1996), is typical for post-collisional granites. Most samples of this age group are also characterised by elevated Ga/Al values typical for A-type granites (Whalen et al., 1987) (Fig. 11b). It is therefore assumed that the protoliths of the ca. 785–760 Ma age group were generated in the late stages of a continental-margin magmatic arc and transitional to a back-arc extensional setting, possibly under conditions of an actively steepening Benioff zone (Morrison, 1980; Müller and Groves, 2019). Alternatively, they could have been generated shortly after subduction roll-back in a distal position to the trench affected by back-arc extension. Such a model has been envisaged, for example, for some of the Miocene granitoids from the Aegean Sea (Altherr and Siebel, 2002; Pe-Piper et al., 2009), which show geochemical similarities to the rocks in our study.

A few similar late Tonian meta-igneous rocks are also reported from the area to the southeast, in the SW Terrane of Sør Rondane (Kamei et al., 2013), which represents a part of the TOAST (Jacobs et al., 2015). However, although coeval and with similar Nd isotope characteristics, the Sør Rondane meta-igneous rocks are classified as low-K tonalites and are interpreted to have formed by slab-melting in an oceanic-arc setting (Kamei et al., 2013), clearly different from the rocks of the Schirmacher study area.

Notwithstanding the above, the latest Mesoproterozoic to early Neoproterozoic basement of the Dronning Maud Land – Sør Rondane crustal province is a potential source for the Tonian Schirmacher granitoids as indicated by overlapping Hf isotopic composition in zircon (Fig. 6) and their whole-rock Nd isotopic composition (Fig. 10), while the involvement of Archean and Paleoproterozoic crustal components of Proto-Kalahari is not indicated by the isotopic composition. The $\delta^{18}O$ value of one sample (J1984, 7.05 ± 0.15 ‰) is slightly higher than zircons crystallized from mantle and mantle-derived magmas (5.3 ± 0.6 ‰, 2σ; Valley et al. (2005)), which may indicate a limited contribution from supracrustal material. This value is comparable to that of the Mesoproterozoic rocks in cDML (Wang et al., 2020), providing further evidence of a derivation from Grenville-age basement.

The geotectonic setting of the ca. 630 Ma meta-igneous rocks is more difficult to define. According to the (Y + Nb) vs. Rb and 10^4Ga/Al vs. Zr discrimination diagrams (Pearce et al., 1984; Whalen et al., 1987), they classify as within-plate or A-type granites (Fig. 10a, b), which is possibly indicative of formation in a syn- to post-collisional geotectonic setting. In the classification diagrams of Frost et al. (2001), samples of the ca. 630 Ma group also plot mostly transitional between anorogenic and continental-margin orogenic igneous suites similar to those of the 785–760 Ma age group (Fig. 9a, b). Based on similar bulk-rock geochemistry and Nd isotope signature, they compare well with the late Neoproterozoic to early Paleozoic (meta-)igneous rocks of the TOAST area (Jacobs et al., 2015; Elburg et al., 2015, 2016) and from the Orvin-Wohlthat Mountains (Jacobs et al., 1998; Markl and Henjes-

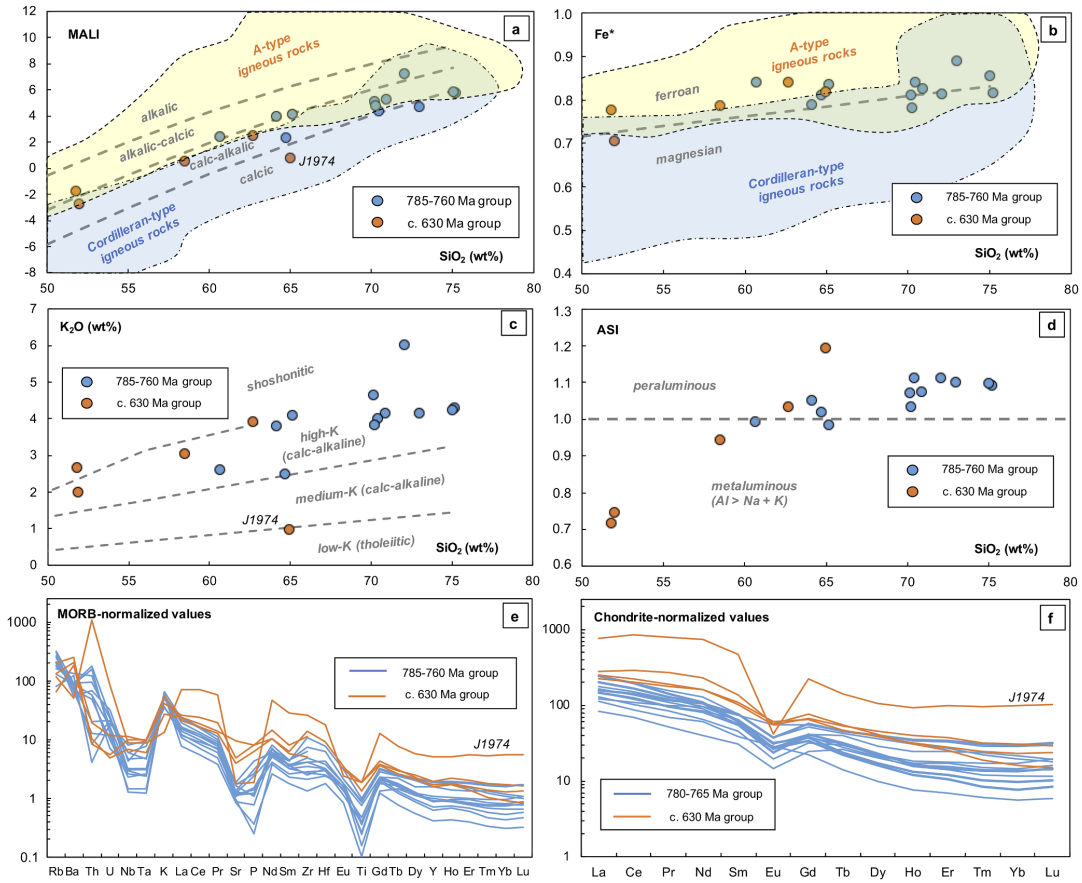

Fig. 9. Geochemical variation diagrams demonstrating the characteristics of the meta-igneous rocks from the Schirmacher area. (a) SiO_2 versus MALI (MALI: $Na_2O + K_2O$-CaO in wt%). Classification between calcic, calc-alkalic, alkalic-calcic and alkaline granitoid types after Frost et al. (2001). (b) SiO_2 versus Fe* (Fe* = $[FeO_{tot}/(FeO_{tot} + MgO)]$). Distinction between magnesian and ferroan granitoid types after Frost et al. (2001). Fields of Cordilleran-type and A-type igneous rocks in (a) and (b) adopted from Frost et al. (2001). (c) SiO_2 versus K_2O for fields of low-K, medium-K, high-K and shoshonitic igneous series after Middlemost (1980). (d) SiO_2 versus ASI (ASI: molar $Al_2O_3/CaO + Na_2O + K_2O$). (e) MORB-normalized multi-element variation diagram (MORB: mid-ocean ridge basalt). (f) Chondrite-normalized REE diagram. MORB and chondrite values from Sun and McDonough (1989).

Kunst, 2004; Roland, 2004). A Palaeoproterozoic to Archean source component as evident from strongly negative initial ε_{Nd} values and Sm-Nd model ages up to 2.6 Ga of early Palaeozoic minettes from the Schirmacher Oasis (Hoch et al., 2001) and of granitoids of cDML and wDML (Moyes et al., 1993; Markl and Henjes-Kunst, 2004) is not found for rocks of the ca. 630 Ma group age of the Schirmacher region (Fig. 10). The Nd and Hf (zircon) isotopic signature of the ca. 630 Ma group is very similar to the 785–760 Ma igneous suite, suggesting derivation from broadly similar sources. As there is no evidence for zircon inheritance, an origin purely by melt generation from pre-existing crustal rocks is unlikely.

The emplacement of the ca. 630 Ma (meta-)igneous rocks was coeval with UHT metamorphism at Schirmacher Oasis, which implies high heat influx from a process such as asthenosphere upwelling. This is consistent with formation of the rocks in an extensional, back-arc type setting where melts were generated at the interface between the hot upper mantle and the lower crust, as previously suggested by Baba et al. (2010). However, the geotectonic setting of the Schirmacher Oasis area ca. 630 Ma ago remains somewhat unclear as there are no exposures of arc-type meta-igneous rocks of appropriate age which could testify to the existence of a somewhat earlier subduction system in the area under investigation.

The rocks of the Schirmacher region show no evidence of the voluminous A-type magmatism which took place between ca. 530 and 490 Ma in neighbouring areas of Dronning Maud Land (Jacobs et al., 1998; Jacobs et al., 2003; Markl and Henjes-Kunst, 2004; Owada et al., 2013 and references therein; Elburg et al., 2015, 2016). One reason could be that the Schirmacher region was isolated from the neighbouring areas as a klippe during the early Pan-African collision.

4.2. Regional and plate tectonic implications

The data from the Schirmacher Oasis show that part of Dronning Maud Land was most likely an active continental margin during late Tonian times. Slab roll-back and back-arc extension in an overall convergent tectonic setting may have played a significant role, possibly indicating subduction of relatively old oceanic lithosphere. Despite the small area of actual outcrop, geophysical data (ADMAP, Golynsky et al.,

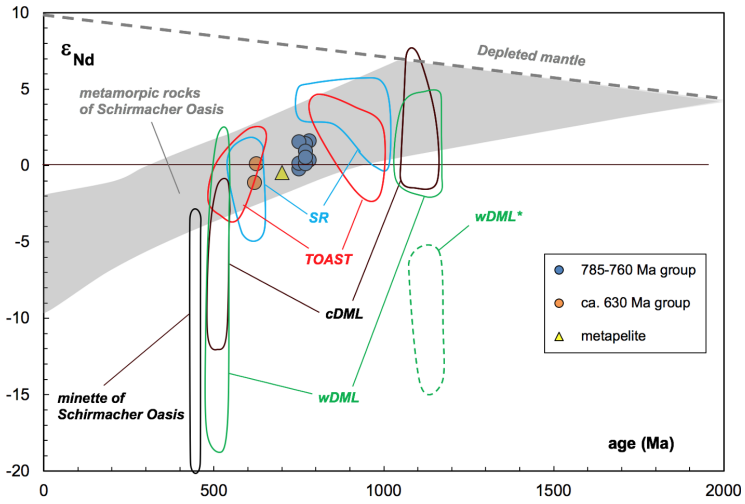

Fig. 10. Initial ε_{Nd} versus age diagram for the samples. The ε_{Nd} versus time array for metamorphic rocks of the Schirmacher Oasis was calculated from Ravikant et al. (2004), Ravikant (2006), Ravikant et al. (2007) and Mikhalsky et al. (unpublished results). For comparison, the respective variation fields for (meta-)igneous rocks of the SW Terrane of Sør Rondane ("SR"): Elburg et al. (2015), Kamei et al. (2013), Owada et al. (2013), of central and south-eastern Dronning Maud Land (cDML, TOAST: Mikhalsky et al. (1997); Jacobs et al. (1998), Hoch et al. (2001), Markl and Henjes-Kunst (2004), Jacobs et al. (2015)) and of western Dronning Maud Land (wDML: Arndt et al. (1991), Moyes (1993), Moyes et al. (1993), Wareham et al. (1998), Grantham et al. (2001), Grosch et al. (2007); wDML*: Grosch et al., 2007; Wareham et al. (1998) are shown. See text for details.

2018) show that the rocks of the Schirmacher region are extensive beneath the ice. The Schirmacher region is characterised by a distinctive low magnetic anomaly that can be traced southwards to the Orvin-Wohlthat Mountains, where it abuts against the Ulvetanna Lineament (Fig. 2), which separates it from Grenville-age rocks of the Orvin-Wohlthat Mountains. The low magnetic anomaly pattern can be traced for ca. 300 km to the W and for ca. 100 km to the east, suggesting that Schirmacher-type lithologies may occupy a total area of ca. 40,000 km^2. A detrital U-Pb age component of ca. 760 Ma is found both within late Tonian to Cryogenian metasedimentary rocks in Dronning Maud Land (e.g. Kitano et al., 2016 and references therein) as well as in ice-rafted debris in recent sediment along the coast line of Dronning Maud Land (Pierce et al., 2014).

Late Tonian igneous crystallisation ages are globally widespread and appear to be largely related to various processes of Rodinia break-up following a period of relative tectonic quiescence between ca. 900 and 800 Ma when Rodinia was stable. These igneous rocks are either related to Rodinia rifting, plume magmatism or to active continental margin magmatism (e.g. Li et al., 2008; Merdith et al., 2017). Whilst arc-related late Tonian rocks are typical for the western part of the disintegrating Rodinia supercontinent, rift related rocks are mostly found in its eastern parts; specifically along the eastern and western margins of Laurentia and its conjugate rift margins (Fig. 12), reflecting the process of Rodinia "turning inside out" (e.g. Dalziel, 1997). In this tectonic scenario, Kalahari lay in a central position and close to the rotation pole of the fragmenting Rodinia supercontinent (Fig. 12).

There are only few other areas in eastern Kalahari that show similar late Tonian arc related rocks, because much of eastern Kalahari is hidden under the thick ice of East Antarctica. However, comparable rocks are reported by Bingen et al. (2007) and Bingen et al. (2009) from north-eastern Mozambique from north of the Lurio Belt.

To the SW of Kalahari at ca. 780 Ma lay the Congo Craton (Fig. 12), the northern side of which acted as an accretionary continental margin during much of the Neoproterozoic, including significant events in late Tonian times, as evidenced from eastern Kenya, Tanzania and northern Mozambique (e.g. Bingen et al., 2009; Fritz et al., 2013; Hauzenberger et al., 2007; Kröner et al., 2000; Meert, 2003; Mole et al., 2018; Möller et al., 1998; Viola et al., 2008). Further W of Congo, the northern side of the Saharan Metacraton (Fig. 12) also records oceanic/continental arc rocks of late Tonian age, e.g. in the Bayuda Block of North Sudan and in

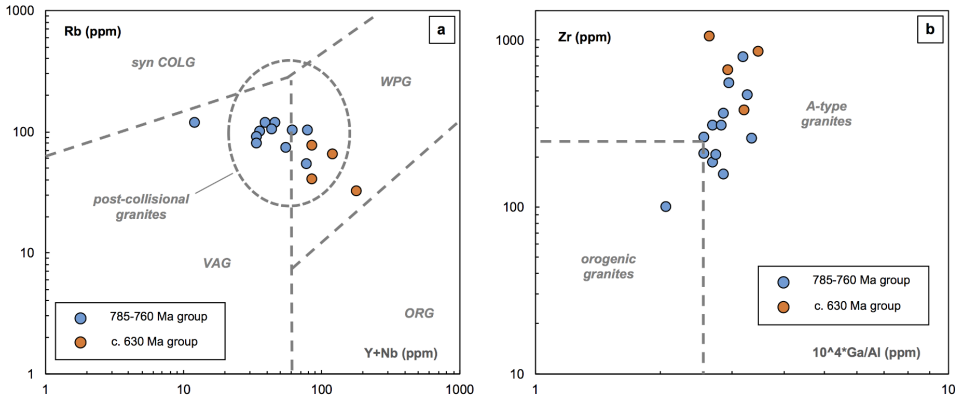

Fig. 11. Geotectonic granitoid discrimination diagrams for the meta-igneous rocks from the Schirmacher area. (a) Y + Nb versus Rb after Pearce et al. (1984) and Pearce (1996); (syn COLG: syn-collisional granites, WPG: within-plate granites, ORG: ocean-ridge granites, VAG: volcanic-arc granites). (b) Ga/Al versus Zr diagram for discriminating between orogenic and anorogenic (A-type) granite types after Whalen et al. (1987). See text for details.

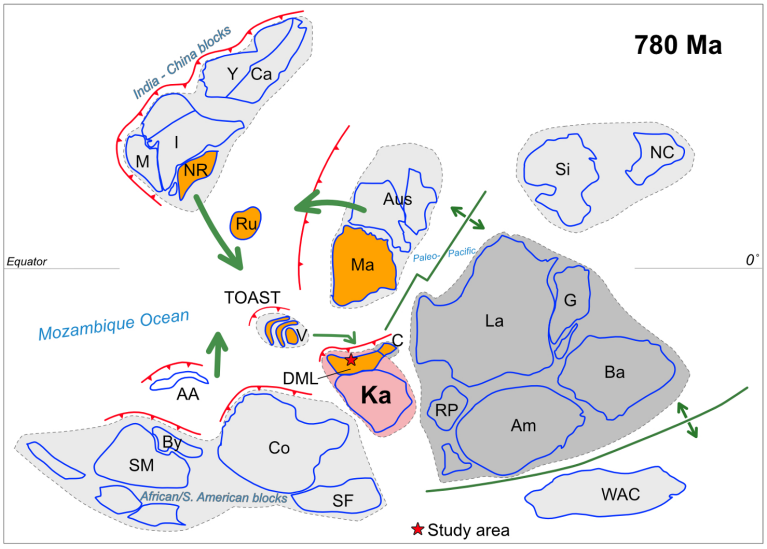

Fig. 12. Continental reconstruction at ca. 780 Ma shortly after the dispersal of Rodinia began (mostly based on Merdith et al. (2017)). Large green arrows indicate generalized time-transgressive plate movement directions of African blocks, an India-China block and the Australia-Mawson block in Tonian-Cryogenian times, culminating later in the amalgamation of Gondwana at ca. 600–500 Ma. In late Tonian times, crustal rocks that form East Antarctica today (orange) were still widely dispersed and only amalgamated during Gondwana assembly ca. 200 Ma later. Whilst the eastern part of Rodinia is largely dominated by rift tectonics (small green arrows) and the growth of the Paleo-Pacific Ocean at the time, western Rodinia is characterised by continental and oceanic arcs, witnessing convergence and destruction of the Mozambique Ocean. Major continental arcs are located in eastern northern Africa, and along an India-China block, as well as along Kalahari (study area indicated as star). Madagascar is placed in the Greater Dharwar model position (e.g. Boger et al., 2014; Tucker et al., 2014) but alternatively could have been shown as part of the Azania microplate within the Mozambique Ocean (not shown; e.g. Collins and Pisarevsky, 2005). Coats Land in East Antarctica represents a piece of Laurentia that had detached from Laurentia after Kalahari rifted from Laurentia shortly after their collision in late Mesoproterozoic times (e.g. Gose et al., 1997; Jacobs et al., 2008; Li et al., 2008). Abbreviations: AA - Afif-Abas Terrane, Am - Amazonia, Aus - Australia, Ba - Baltica, By - Bayuda block, SC - South China, C - Coats Land Block, Ca - Cathaysia, Co - Congo, DML - Dronning Maud Land, G - Greenland, I - India, Ka - Kalahari, La - Laurentia, M - Madagascar, Ma - Mawson, NC - North China, NDML - Nampula-Dronning Maud Land, NR - Napier-Rayner (Antarctica), RP - Rio de la Plata, Ru - Ruker Craton, SF - Sao Francisco, Si - Siberia, SM - Sahara Metacraton, TOAST - Tonian Oceanic Arc Super Terrane, V - Valkyrie Craton, WAC - West African Craton, Y - Yangtze. (For interpretation of the references to colour in this figure legend, the reader is referred to the web version of this article.)

western Ethiopia (e.g. Blades et al., 2015; Fritz et al., 2013; Johnson et al., 2011). Late Tonian arc-related igneous rocks are also well known throughout the Arabian-Nubian-Shield, such as in the Hijaz Terrane, which is composed of a series of juvenile oceanic island arc terranes (e.g. Johnson et al., 2011; Stern, 1994), as well as along the Afif-Abas terrane (Merdith et al., 2017 and ref. therein).

Indo-Antarctica, together with the South China/Yangtze block and possibly Madagascar, record another large active continental margin in late Tonian times in westernmost Rodinia. Remnants of this are preserved as the Imorona-Itsindro Suite in Madagascar (e.g. Archibald et al., 2016; Boger et al., 2014, 2015; Handke et al., 1999; Tucker et al., 2014), which some authors correlate across the Seychelles with the Malani igneous province in Northern India (Bybee et al., 2010). Collins and Windley (2002) showed Madagascar as the separate Azania microcontinent, elsewhere in the Mozambique ocean, separate from India that would have been fringed by a separate active continental margin. In northern Madagascar a Tonian double arc terrane dated at ca. 750 and 715 Ma respectively is preserved in the Bemarivo belt (Thomas et al., 2009). Sri Lanka (Wanni Complex) also has records of I-type granitoids of this age (Kröner et al., 1994, 2013); similarly, in southern India the Madurai Block appears to record an active continental margin setting at this time (e.g. Santosh et al., 2012).

The timing of the late Neoproterozoic UHT metamorphism in the Schirmacher Oasis, recorded by the zircon rims in our samples at ca. 640–600 Ma, is characteristic for the western part of the East African-Antarctic Orogen and appears to correlate with similar high-grade metamorphism in the Cabo Delgado and Nachingwea nappe complexes in northern Mozambique/Tanzania as well as the Eastern Granulites of Tanzania (e.g. Appel et al., 1998; Mole et al., 2018; Möller et al., 2000; Thomas et al., 2016). UHT metamorphism in supercontinent settings are thought to either relate to the formation of back-arc basins (e.g. Brown, 2007) or to the formation of orogenic plateaus (e.g. Fitzsimons, 2016). Our isotopic data do not offer any insights into this issue, but we interpret the metamorphic ages to indicate the continuation of the East African Orogen into this part of East Antarctica.

4.3. Implications for the tectonic setting of Kalahari through time

The Kalahari Craton has undergone protracted episodic growth from its earliest Archean nucleus to its full size by the end of the Mesoproterozoic (Jacobs et al., 2008, and ref. therein), (Fig. 13). That growth took place along different margins over time. Paleoproterozoic crustal additions are recorded from the present-day western side of Proto-Kalahari, and the Limpopo belt stitched the Kaapvaal-Grunehogna and Zimbabwe cratons (e.g. Roering et al., 1992). The eastern margin was probably passive at this time. During the Mesoproterozoic, crustal additions (including juvenile arcs) focused along the southern (Namaqua-Natal orogen) flank, where Kalahari records indentation tectonics with Laurentia forming the major Grenville-age orogens in Laurentia and Kalahari (e.g. Jacobs et al., 1993; Dalziel et al., 2000; Jacobs et al., 2003a; Hanson et al., 2004). The crustal additions also extended north-eastwards into present-day northern Mozambique and SE Tanzania. In the Mesoproterozoic, the north-western part of Kalahari was most likely a passive continental margin (e.g. Becker et al., 2006). During Rodinia break-up in late Tonian times, Kalahari's north-western, western and southwestern edges were largely passive continental margins. However, the tectonic setting of the eastern Kalahari margin in Tonian times has remained unclear so far, because of the prolonged and pervasive later (Pan-African) high-grade tectono-thermal overprinting related to the Himalayan-style East African-Antarctic Orogen at ca. 600–500 Ma. Our data show that the eastern margin of Kalahari was probably the only active one in late Tonian times (i.e. ca. 780 Ma). The main tectonic convergence thus migrated anticlockwise from western Kalahari in the Paleoproterozoic to the southern part in the Mesoproterozoic and finally to eastern Kalahari throughout the Neoproterozoic (Fig. 13). Paleoproterozoic and Mesoproterozoic convergence along the western and southern sides of Proto-Kalahari and Kalahari respectively lasted for a maximum period of about 150–200 Ma, probably with

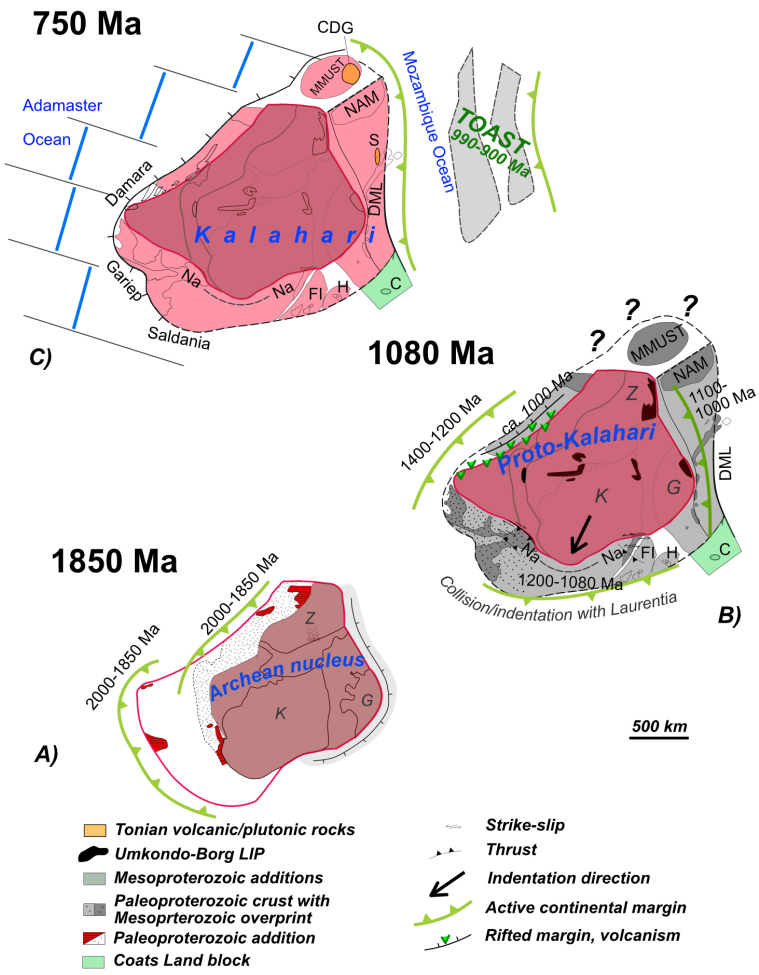

Fig. 13. Tectonic history of Kalahari and its predecessors through time, finally resulting in an active continental margin in eastern Kalahari in Tonian times (modified after Jacobs et al., 2008). A) Archean core of Kalahari, consisting of the Kaapvaal, Grunehogna (East Antarctica) and Zimbabwe cratons. Paleoproterozoic crustal additions on western part of Archean nucleus result in Proto-Kalahari; B) Mesoproterozoic crustal additions are recorded all around Proto-Kalahari, however, the main convergence is along the southern margin of Proto-Kalahari, along the Namaqua-Natal Belt, resulting in indentation tectonics and high-grade metamorphism. C) In late Tonian times, eastern Kalahari is dominated by extension, whilst eastern Kalahari has turned into an active margin. Thus, from the Paleoproterozoic to the Neoproterzoic, the respective active continental margins have moved in an anticlockwise sense from the west to the south and finally to the east. The eastern margin is the collision margin along which the East African-Antarctic Orogen develops in late Neoproterozoic times. Abbreviations: DML – Dronning Maud Land, C – Coats Land block, CGD – Cabo Delgado, G – Grunehogna Craton, K – Kaapvaal Craton, Na–Na – Namaqua-Natal Belt, Nam – Nampula P., MMUST – Marupa-Malawi-Unango south Tanzania terrane, S – Schirmacher region, TOAST – Tonian Oceanic Super Terrane, Z – Zimbabwe Craton.

significant intervening periods of relative quiescence. Convergence along the eastern side of Kalahari probably started immediately after the collision of Kalahari with Laurentia in latest Mesoproterozoic times. The Maud Belt in Dronning Maud Land has traditionally been interpreted as the eastern continuation of the Natal belt into East Antarctica (Groenewald et al., 1991). However, newer studies indicate that the subduction polarity of the former was likely opposite and directed under Proto-Kalahari (e.g. Bauer et al., 2003; Grantham et al., 2011; Mendonides et al., 2015; Wang et al., 2020), rather than away from Proto-Kalahari as in the Natal Belt (e.g. Thomas et al., 1994). It is also likely that the Heimefront Shear Zone in western DML (Fig. 2) separates up to 1200 Ma crust in the west (Natal-type crust) from slightly younger (Maud-type) crust, up to ca. 1150 Ma, in the east (Mendonides et al., 2015). Thus, the collision of Kalahari and Laurentia and the onset of subduction underneath Proto-Kalahari may herald the beginning of long-lived convergence along the eastern margin of Kalahari that successively retreated backwards over time, interrupted by periods of quiescence (Figs. 12,14). Outboard of Kalahari, the Tonian Oceanic Arc Super Terrane (990–900 Ma) of eastern Dronning Maud Land records the early tectonic history of the Mozambique Ocean with the formation of oceanic arcs (Fig. 14). The late Tonian active margin setting of eastern Kalahari that is documented in this study, records renewed subduction underneath eastern Kalahari shortly after the rifting of Rodinia started and a long convergence history of the Mozambique Ocean as a consequence of Rodinia turning "inside out" (Hoffman, 1991; Murphy and Nance, 1991). The eastern margin of Kalahari may thus record the longest convergence history of Kalahari, ca. 400 Ma, that endured from latest Mesoproterozoic to late Neoproterozoic times (Fig. 14). The process culminated in Himalayan-style continental collision from 600 to 500 Ma, which resulted in much of the obliteration of its pre-collisional margin history, and which terminated the supercontinent cycle from Rodinia to Gondwana.

5. Summary and conclusions

Although spatially restricted in outcrop, aerogeophysical data suggest that rocks exposed in the Schirmacher Oasis region are representative of a terrane which is far more extensive and may cover an area of ca. 40,000 km^2 underneath the ice. The rocks exposed are mainly late Tonian granodioritic to granitic rocks with crystallisation ages of ca. 785–760 Ma, an age range that is rare elsewhere in DML and East Antarctica. Tectonically, these rocks are located between the

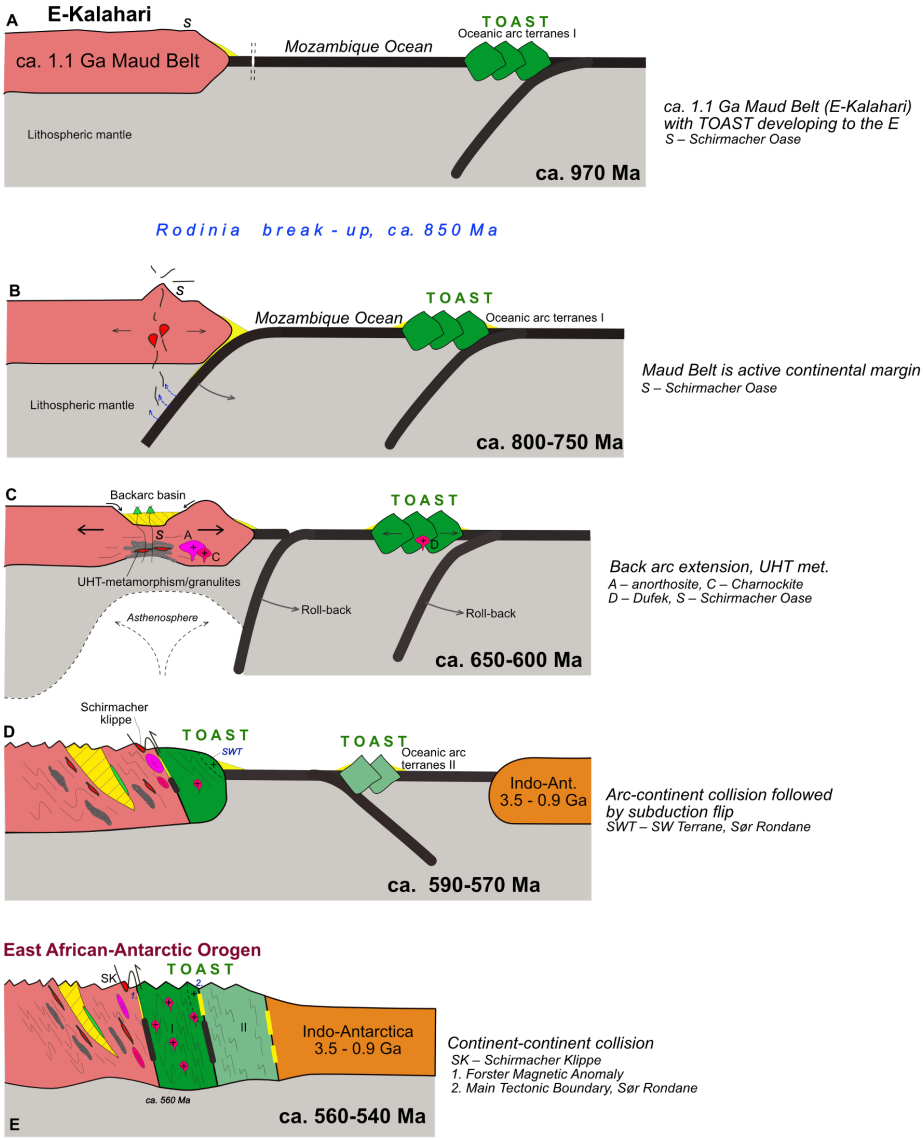

Fig. 14. Neoproterozoic tectonic evolution of the Schirmacher region, illustrated by W-E sketch cross-sections across DML. A) In Tonian times (~970 Ma), the Schirmacher region lies in the Maud Belt of easternmost Kalahari, with the Tonian Oceanic Arc Super Terrane (TOAST) developing in the Mozambique Ocean. E-Kalahari is probably a passive margin in Rodinian times. Rodinia break-up started at ca. 850 Ma that subsequently converted the E-Kalahari margin into an active margin. B) By late Tonian times (785–760 Ma), eastern Kalahari is an active continental margin during which the Schirmacher granitoids were emplaced into the Maud Belt crust. C) In late Cryogenian to early Ediacaran times (650 to 600 Ma), eastern Kalahari is under extension, possibly related to a retreating subduction zone that led to asthenosphere uprise at the continental margin. Extension leads to high-T metamorphism in the Schirmacher region and the intrusion of anorthosites and charnockites in the vicinity of the Orvin-Wohlthat mountains. D) In middle Ediacaran times (590 to 570 Ma), eastern Kalahari records major convergence, possibly related to the collision and accretion of the Tonian Oceanic Arc Super Terrane with the Maud Belt continental margin. However, the Schirmacher region escapes much of this deformation. E) Final amalgamation of East Antarctica at ca. 550 Ma.

boundary of the eastern part of the Kalahari Craton and the western part of the Tonian Oceanic Arc Super Terrane (present day co-ordinates). Geochemically, the late Tonian rocks are interpreted to have evolved in the late stages of the development of a continental magmatic arc, possibly within a subduction roll-back setting. The meta-granitoids of the Schirmacher region have single-stage Sm-Nd model ages of ca. 1.3–1.5 Ga and zircon Hf-isotopic signatures which are very similar to those of the Grenville-age rocks that characterize easternmost Kalahari. Zircon inheritance is found in only one sample in minor amount and never exceeds 1.1 Ga. Zircon of one sample reveals high $\delta^{18}O$ values,

suggesting the involvement of slab-derived sedimentary material. The few detrital zircon data of Neoproterozoic metasedimentary rocks in the Schirmacher region as well as in other parts of central and eastern DML also show a late Tonian age peak, which we interpret as the erosional fingerprint of the continental arc rocks in this region. Two glacial moraine sample show a different range of age peaks than the outcrops, which probably indicates that the material is derived from a glacial catchment source far to the south, probably the Orvin-Wohlthat Mountains.

The study area shows high-grade and ultra-high temperature metamorphic overprinting and syn-tectonic magmatism between ca. 650–600 Ma. No post-600 Ma metamorphism is recorded, in strong contrast to the neighbouring Orvin-Wohlthat Mountains, where the main high-grade metamorphism dated at ca. 590 to 500 Ma follows a clockwise PT-path and where the older metamorphism is not recorded or rare. The Orvin-Wohlthat Mountains do however contain voluminous anorthosite and charnockite magmatism at ca. 600 Ma. 650–600 Ma ultra-high temperature metamorphism and isobaric cooling (Baba et al., 2010) in the study area suggests an evolution in an overall back-arc extensional setting accompanied by asthenosphere upwelling. In contrast, the time from ca. 590 Ma onwards in most of East Antarctica is characterised by orogenic thickening, probably as a result of continental collision along the East African-Antarctic Orogen. The study area has thus escaped the effects of this.

In late Toninan times, Kalahari had a transitional position between eastern (rift dominated, extroverting) and western (converging) parts of Rodinia. At that time, the converging western Rodinia was dominated by ocean consumption and the presence of major continental arcs, the remnants of which are currently preserved along much of East Africa. The late Tonian continental arc in eastern Kalahari is therefore interpreted as a consequence of Rodinia break-up and extroversion. The protracted later collision history along the Late Neoproterozoic/Early Paleozoic East African-Antarctic Orogen has to a large extent obliterated the Tonian continental arc.

Declaration of Competing Interest

The authors declare that they have no known competing financial interests or personal relationships that could have appeared to influence the work reported in this paper.

Acknowledgements

J. Jacobs fieldwork in the Schirmacher region was made possible by the Federal Institute for Geoscience and Natural Resources (BGR) in the austral summers 2010/11 and 2011/12, which has been greatly appreciated. The Alfred-Wegener-Institute for Polar and Marine Research (AWI) provided further logistic support and polar clothing. The hospitality and support at Novolazarevskaya Station is highly acknowledged. J. Jacobs acknowledges funding by the Norwegian Research Council (NFR-NARE).

P. Montero and F. Bea are thanked for help with SHRIMP analyses at the IBERSIMS facility, Granada. N. V. Rodionov is thanked for help at the St. Petersburg SHRIMP laboratory. M. Whitehouse and his team are acknowledged for help at the Nordsim facility, Stockholm. M. Wingate is thanked for support and help at the SHRIMP facility at Curtin. M. Hofmann and A. Gärtner are thanked for zircon LA-ICPMS analyses at the Senckenberg Naturhistorische Sammlung, Dresden. At the BGR, M. Bockrath and S. Gerlach are thanked for analytical assistance and N. Koglin for logistic support. E. Mikhalsky acknowledges funding through the Russian Foundation for Basic Research (grant no. 15-05-02761). Trace elements of zircons were conducted under a state contract No. 0153-2019-0002 (Institute of Precambrian Geology and Geochronology of Russian Academy of Sciences). A. Läufer acknowledges funding through Deutsche Forschungsgemeinschaft (DFG) within the Priority Program SPP 1158 “Antarctic Research with Comparable Investigations in Arctic Sea Ice Areas” (grant LA 1080-9). The LA-MC-ICPMS at UJ was funded by NRF-NEP grant #93208 and is supported by DSI-NRF CIMERA. M.A. Elburg acknowledges funding from NRF IFRR grant 119297. We acknowledge the reviews of two anonymous reviewers. This is Nordsim publication #627. This is a contribution to IGCP 648, Supercontinent Cycles and Global Geodynamics and IGCP 628, The Gondwana Map Project.

Appendix A. Supplementary data

Supplementary data to this article can be found online at https://doi.org/10.1016/j.precamres.2019.105553.

References

Altherr, R., Siebel, W., 2002. I-type plutonism in a continental back-arc setting: Miocene granitoids and monzonites from the central Aegean Sea, Greece. Contrib. Mineral. Petrol. 143 (4), 397–415.

Appel, P., Möller, A., Schenk, V., 1998. High-pressure granulite facies metamorphism in the Pan-African belt of eastern Tanzania: P-T–t evidence against granulite formation by continent collision. J. Metamorph. Geol. 16 (4), 491–509.

Archibald, D.B., Collins, A.S., Foden, J.D., Payne, J.L., Holden, P., Razakamanana, T., De Waele, B., Thomas, R.J., Pitfield, P.E.J., 2016. Genesis of the Tonian Imorona-Itsindro magmatic Suite in central Madagascar: insights from U-Pb, oxygen and hafnium isotopes in zircon. Precambr. Res. 281, 312–337.

Arndt, N.T., Todt, W., Chauvel, C., Tapfer, M., Weber, K., 1991. U-Pb zircon age and Nd isotopic composition of granitoids, charnockites and supracrustal rocks from Heimefrontfjella, Antarctica. Geologische Rundschau 80 (3), 759–777.

Baba, S., Owada, M., Shiraishi, K., 2008. Contrasting metamorphic P-T path between Schirmacher Hills and Mühlig-Hofmannfjella, central Dronning Maud Land, East Antarctica. Geol. Soc. London Spec. Publ. 308, 401–417.

Baba, S., Tomokazu, H., Hiroshi, K., Daniel, J.D., Masaaki, O., Kazuyuki, S., 2010. SHRIMP zircon U-Pb dating of sapphirine-bearing granulite and biotite-hornblende gneiss in the Schirmacher Hills, East Antarctica: implications for Neoproterozoic ultrahigh-temperature metamorphism predating the assembly of Gondwana. J. Geol. 118, 621–639.

Bauer, W., Jacobs, J., Fanning, C.M., Schimdt, R., 2003. Late Mesoproterozoic arc and back-arc volcanism in the Heimefrontfjella (East Antarctica) and implications for the palaeogeography at the southeastern margin of the Kaapvaal-Grunehogna craton. Gondwana Res. 3, 449–465.

Becker, T., Schreiber, U., Kampunzu, A.B., Armstrong, R., 2006. Mesoproterozoic rocks of Namibia and their plate tectonic setting. J. Afr. Earth Sc. 46 (1), 112–140.

Bingen, B., Jacobs, J., Viola, G., Henderson, I.H.C., Skår, Ø., Boyd, R., Thomas, R.J., Solli, A., Key, R.M., Daudi, E.X.F., 2009. Geochronology of the Precambrian crust in the Mozambique belt in NE Mozambique, and implications for Gondwana assembly. Precambr. Res. 170 (3), 231–255.

Bingen, B., Viola, G., Griffin, W.L., Jacobs, J., Boyd, R., Thomas, R.J., Daudi, E.X.F., Henderson, I.H.C., Beyer, E., Skår, Ø., Engvik, A.K., Key, R.M., Solli, A., Sandstad, J.S., Smethurst, M.A., Tveten, E., Bjerkgård, T., Melezhik, V.A., Jamal, D., Smith, R., Hollick, L., Feitio, P., 2007. Crustal architecture of the Mozambique Belt in northeastern Mozambique: perspective from U-Pb geochronology and Lu-Hf isotopes in zircon. 7th International Symposium on Applied Isotope Geochemistry, Stellenbosch.

Blades, M.L., Collins, A.S., Foden, J., Payne, J.L., Xu, X., Alemu, T., Woldetinsae, G., Clark, C., Taylor, R.J.M., 2015. Age and hafnium isotopic evolution of the Didesa and Kemashi Domains, western Ethiopia. Precambr. Res. 270, 267–284.

Boger, S.D., Hirdes, W., Ferreira, C.A.M., Jenett, T., Dallwig, R., Fanning, C.M., 2015. The 580–520 Ma Gondwana suture of Madagascar and its continuation into Antarctica and Africa. Gondwana Res. 28, 1048–1060.

Boger, S.D., Hirdes, W., Ferreira, C.A.M., Schulte, B., Jenett, T., Fanning, C.M., 2014. From passive margin to volcano–sedimentary forearc: the Tonian to Cryogenian evolution of the Anosyen Domain of southeastern Madagascar. Precambr. Res. 247, 159–186.

Bormann, P., Fritsche, D., 1995. The Schirmacher Oasis, Queen Maud Land, East Antarctica, and its surroundings, 289. Perthes, Gotha, p. 448.

Bouvier, A., Vervoort, J.D., Patchett, P.J., 2008. The Lu–Hf and Sm–Nd isotopic composition of CHUR: constraints from unequilibrated chondrites and implications for the bulk composition of terrestrial planets. Earth Planet. Sci. Lett. 273 (1), 48–57.

Brown, M., 2007. Metamorphic conditions in orogenic belts: a record of secular change. Int. Geol. Rev. 49 (3), 193–234.

Bybee, G.M., Ashwal, L.D., Wilson, A.H., 2010. New evidence for a volcanic arc on the western margin of a rifting Rodinia from ultramafic intrusions in the Andriamena region, north-central Madagascar. Earth Planet. Sci. Lett. 293 (1), 42–53.

Collins, A.S., Pisarevsky, S.A., 2005. Amalgamating eastern Gondwana: the evolution of the Circum-Indian Orogens. Earth Sci. Rev. 71 (3), 229–270.

Collins, A.S., Windley, B.F., 2002. The Tectonic Evolution of Central and Northern Madagascar and Its Place in the Final Assembly of Gondwana. J. Geol. 110 (3), 325–339.

Dalziel, I.W.D., 1997. Neoproterozoic-Paleozoic geography and tectonics: review, hypothesis, environmental speculation. GSA Bull. 109 (1), 16–42.

Dalziel, I.W.D., Mosher, S., Gahagan, L.M., 2000. Laurentia-Kalahari collision and the assembly of Rodinia. J. Geology 108, 499–513.

Elburg, M., Jacobs, J., Andersen, T., Clark, C., Läufer, A., Ruppel, A., Krohne, N., Damaske, D., 2015. Early Neoproterozoic metagabbro-tonalite-trondhjemite of Sør Rondane (East Antarctica): implications for supercontinent assembly. Precambr. Res. 259, 189–206.
Elburg, M.A., Andersen, T., Jacobs, J., Läufer, A., Ruppel, A., Krohne, N., Damaske, D., 2016. One hundred fifty million years of intrusive activity in the Sør Rondane mountains (East Antarctica): implications for Gondwana assembly. J. Geol. 124, 1–26.
Fitzsimons, I.C.W., 2016. Pan-African granulites of Madagascar and southern India: Gondwana assembly and parallels with modern Tibet. J. Mineral. Petrol. Sci. 111 (2), 73–88.
Fritz, H., Abdelsalam, M., Ali, K.A., Bingen, B., Collins, A.S., Fowler, A.R., Ghebreab, W., Hauzenberger, C.A., Johnson, P.R., Kusky, T.M., Macey, P., Muhongo, S., Stern, R.J., Viola, G., 2013. Orogen styles in the East African Orogen: a review of the Neoproterozoic to Cambrian tectonic evolution. J. Afr. Earth Sc. 86, 65–106.
Frost, B.R., Barnes, C.G., Collins, W.J., Arculus, R.J., Ellis, D.J., Frost, C.D., 2001. A Geochemical classification for granitic rocks. J. Petrol. 42 (11), 2033–2048.
Golynsky, A.V., Ferraccioli, F., Hong, J.K., Golynsky, D.A., von Frese, R.R.B., Young, D.A., Blankenship, D.D., Holt, J.W., Ivanov, S.V., Kiselev, A.V., Masolov, V.N., Eagles, G., Gohl, K., Jokat, W., Damaske, D., Finn, C., Aitken, A., Bell, R.E., Armadillo, E., Jordan, T.A., Greenbaum, J.S., Bozzo, E., Caneva, G., Forsberg, R., Ghidella, M., Galindo-Zaldivar, J., Bohoyo, F., Martos, Y.M., Nogi, Y., Quartini, E., Kim, H.R., Roberts, J.L., 2018. New magnetic anomaly map of the Antarctic. Geophys. Res. Lett. 45 (13), 6437–6449.
Gose, W.A., Helper, M.A., Connelly, J.N., Hutson, F.E., Dalziel, I.W.D., 1997. Paleomagnetic data and U-Pb isotopic age determinations from Coats Land, Antarctica: implications for late Proterozoic plate reconstructions. J. Geophys. Res. 102, 7887–7902.
Grantham, G.H., Eglington, B.M., Thomas, R.J., Mendonides, P., 2001. The nature of the Grenville-age charnockitic A-type magmatism from the Natal, Namaqua and Maud Belts of southern Africa and western Dronning Maud Land, Antarctica. Mem. Natl. Inst. Polar Res. 55 (Spec. Issue), 59–86.
Grantham, G.H., Macey, P.H., Ingram, B.A., Roberts, M.P., Armstrong, R.A., Hokada, T., Shiraishi, K., Jackscon, C., Bisnath, A., Manhica, A.D.S.T., 2008. Terrane correlation between Antarctica, Mozambique and Sri Lanka; comparisons of geochronology, lithology, structure and metamorphism and possible implications for the geology of southern Africa and Antarctica. Geol. Soc. London Spec. Publ. 308, 91–119.
Grantham, G.H., Manhica, A.D.S.T., Armstrong, R.A., Kruger, F.J., Loubser, M., 2011. New SHRIMP, Rb/Sr and Sm/Nd isotope and whole rock chemical data from central Mozambique and western Dronning Maud Land, Antarctica: implications for the nature of the eastern margin of the Kalahari Craton and the amalgamation of Gondwana. J. Afr. Earth Sc. 59, 74–100.
Grew, E.S., Manton, W.I., 1983. Geochronologic studies in East Antarctica: reconnaissance uranium-thorium-lead data from rocks of the Schirmacher Hills and Mount Stinear. U.S. Ant. J XVIII, 6–8.
Groenewald, P.B., Grantham, G.H., Watkeys, M.K., 1991. Geological evidence for a Proterozoic to Mesozoic link between southeastern Africa and Dronning Maud Land, Antarctica. J. Geol. Soc. 148, 1115–1123.
Grosch, E.G., Bisnath, A., Frimmel, H.E., Board, W.S., 2007. Geochemistry and tectonic setting of mafic rocks in western Dronning Maud Land, East Antarctica: implications for the geodynamic evolution of the Proterozoic Maud Belt. J. Geol. Soc. 164, 465–475.
Handke, M.J., Tucker, R.D., Ashwal, L.D., 1999. Neoproterozoic continental arc magmatism in west-central Madagascar. Geology 27 (4), 351–354.
Hanson, R.E., Crowley, J.L., Bowring, S.A., Ramezani, J., Gose, W.A., Dalziel, I.W.D., Pancake, J.A., Seidel, E.K., Blenkinsop, T.G., Mukwakwami, J., 2004. Coeval large-scale magmatism in the Kalahari and Laurentian cratons during Rodinia assembly. Science 304 (5674), 1126–1129.
Hauzenberger, C.A., Sommer, H., Fritz, H., Bauernhofer, A., Kröner, A., Hoinkes, G., Wallbrecher, E., Thöni, M., 2007. SHRIMP U-Pb zircon and Sm–Nd garnet ages from the granulite-facies basement of SE Kenya: evidence for Neoproterozoic polycyclic assembly of the Mozambique Belt. J. Geol. Soc. 164 (1), 189–201.
Henjes-Kunst, F., 2004. Further evidence for Pan-African polyphase magmatism and metamorphism in Central Dronning Maud Land, East Antarctica, from rocks at Schirmacheroase: a geochronological study. Geol. Jahrb. 96B, 255–291.
Hoch, M., Rehkämper, M., Tobschall, H.J., 2001. Sr, Nd, Pb and O isotopes of minettes from Schirmacher Oasis, East Antarctica: a case of mantle metasomatism involving subducted continental material. J. Petrol. 42, 1387–1400.
Hoffman, P.F., 1991. Did the breakout of Laurentia turn Gondwanaland inside out? Science 252, 1409–1412.
Jacobs, J., Bauer, W., Fanning, C.M., 2003a. New age constraints for Grenville-age metamorphism in western central Dronning Maud Land (East Antarctica), and implications for the palaeogeography of Kalahari in Rodinia. Int. J. Earth Sci. 92, 3031–3315.
Jacobs, J., Elburg, M., Läufer, A., Kleinhanns, I.C., Henjes-Kunst, F., Estrada, S., Ruppel, A.S., Damaske, D., Montero, P., Bea, F., 2015. Two distinct Late Mesoproterozoic/Early Neoproterozoic basement provinces in central/eastern Dronning Maud Land, East Antarctica: the missing link, 15–21°E. Precambr. Res. 265, 249–272.
Jacobs, J., Fanning, C.M., Bauer, W., 2003b. Timing of Grenville-age vs. Pan-African medium- to high grade metamorphism in western Dronning Maud Land (East Antarctica) and significance for correlations in Rodinia and Gondwana. Precambr. Res. 125, 1–20.
Jacobs, J., Fanning, C.M., Henjes-Kunst, F., Olesch, M., Paech, H.-J., 1998. Continuation of the Mozambique Belt into East Antarctica: Grenville-age metamorphism and polyphase Pan-African high-grade events in central Dronning Maud Land. J. Geol. 106, 385–406.
Jacobs, J., Opås, B., Elburg, M.A., Läufer, A., Estrada, S., Ksienzyk, A.K., Damaske, D., Hofmann, M., 2017. Cryptic sub-ice geology revealed by a U-Pb zircon study of glacial till in Dronning Maud Land, East Antarctica. Precambr. Res. 294, 1–14.
Jacobs, J., Pisarevsky, S., Thomas, R.J., Becker, T., 2008. The Kalahari Craton during the assembly and dispersal of Rodinia. Precambr. Res. 160 (1), 142–158.
Jacobs, J., Thomas, R.J., 2004. Himalayan-type indenter-escape tectonics model for the southern part of the late Neoproterozoic–early Paleozoic East African-Antarctic orogen. Geology 32 (8), 721–724.
Jacobs, J., Thomas, R.J., Weber, K., 1993. Accretion and indentation tectonics at the southern edge of the Kaapvaal craton during the Kibaran (Grenville) orogeny. Geology 21, 203–206.
Johnson, P.R., Andresen, A., Collins, A.S., Fowler, A.R., Fritz, H., Ghebreab, W., Kusky, T., Stern, R.J., 2011. Late Cryogenian-Ediacaran history of the Arabian-Nubian Shield: a review of depositional, plutonic, structural, and tectonic events in the closing stages of the northern East African Orogen. J. Afr. Earth Sc. 61 (3), 167–232.
Kamei, A., Horie, K., Owada, M., Yuhara, M., Nakano, N., Osanai, Y., Adachi, T., Hara, Y., Terao, M., Teuchi, S., Shimura, T., Tsukada, K., Hokada, T., Iwata, C., Shiraishi, K., Ishizuka, H., Takahashi, Y., 2013. Late Proterozoic juvenile arc metatonalite and adakitic intrusions in the Sør Rondane Mountains, eastern Dronning Maud Land, Antarctica. Precambr. Res. 234, 47–62.
Kämpf, H., Stackebrandt, W., 1985. Crustal evolution of the Eastern Antarctic craton (Schirmacher Oasis, Dronning Maud Land). Gerlands Beitr. Geophys. 94, 251–258.
Kitano, I., Osanai, Y., Nakano, N., Adachi, T., 2016. Detrital zircon provenances for metamorphic rocks from southern Sør Rondane Mountains, East Antarctica: a new report of Archean to Mesoproterozoic zircons. J. Mineral. Petrol. Sci. 111 (2), 118–128.
Kröner, A., Hegner, E., Collins, A.S., Windley, B.F., Brewer, T.S., Razakamanana, T., Pidgeon, R.T., 2000. Age and Magmatic History of the Antananarivo Block, Central Madagascar, as Derived from Zircon Geochronology and Nd Isotopic Systematics. Am. J. Sci. 300, 251–288.
Kröner, A., Jaeckel, P., 1994. Zircon ages from rocks of the Wanni Complex, SriLanka. J. Geol. Sri Lanka 5, 41–57.
Kröner, A., Rojas-Agramonte, Y., Kehelpannala, K.V.W., Zack, T., Hegner, E., Geng, H.Y., Wong, J., Barth, M., 2013. Age, Nd–Hf isotopes, and geochemistry of the Vijayan Complex of eastern and southern Sri Lanka: A Grenville-age magmatic arc of unknown derivation. Precambr. Res. 234, 288–321.
Li, Z.-X., Bogdanova, S.V., Collins, A.S., Davidson, A., De Waele, B., Ernst, R.E., Fitzsimons, I.C.W., Fuck, R.A., Gladkochub, D.P., Jacobs, J., Karlstrom, K.E., Lu, S., Natapov, L.M., Pease, V., Pisarevsky, S.A., Thrane, K., Vernikovsky, V., 2008. Assembly, configuration, and break-up history of Rodinia: a synthesis. Precambr. Res. 160 (1), 179–210.
Markl, G., Henjes-Kunst, F., 2004. Postkinematic charnockites in Dronning Maud Land, Antarctica: self-retrogression of originally anhydrous rocks by late-magmatic fluids and modeling of their chemical, isotopic and thermal evolution. Geol. Jahrb. Reihe B 96, 139–186.
Meert, J.G., 2003. A synopsis of events related to the assembly of eastern Gondwana. Tectonophysics 362 (1), 1–40.
Mendonides, P., Thomas, R.J., Grantham, G.H., Armstrong, R.A., 2015. Geochronology of emplacement and charnockite formation of the Margate Granite Suite, Natal Metamorphic Province, South Africa: Implications for Natal-Maud belt correlations. Precambr. Res. 265, 189–202.
Merdith, A.S., Collins, A.S., Williams, S.E., Pisarevsky, S., Foden, J.D., Archibald, D.B., Blades, M.L., Alessio, B.L., Armistead, S., Plavsa, D., Clark, C., Müller, R.D., 2017. A full-plate global reconstruction of the Neoproterozoic. Gondwana Res. 50, 84–134.
Mieth, M., Jacobs, J., Ruppel, A., Damaske, D., Läufer, A., Jokat, W., 2014. New detailed aeromagnetic and geological data of eastern Dronning Maud Land: implications for refining the tectonic and structural framework of Sør Rondane, East Antarctica. Precambr. Res. 245, 174–185.
Mieth, M., Jokat, W., 2014. New aeromagnetic view of the geological fabric of southern Dronning Maud Land and Coats Land, East Antarctica. Gondwana Res. 25, 358–367.
Mikhalsky, E.V., Beliatsky, B.V., Savva, E.V., Wetzel, H.-U., Fedorov, L.V., Weiser, T., Hahne, K., 1997. Reconnaissance geochronologic data on polymetamorphic and igneous rocks of the Humboldt Mountains, central Queen Maud Land, East Antarctica. In: Ricci, C.A. (Ed.), The Antarctic Region: Geological Evolution and Processes. Terra Antartica Publication, Siena, pp. 45–53.
Mole, D.R., Barnes, S.J., Taylor, R.J.M., Kinny, P.D., Fritz, H., 2018. A relic of the Mozambique Ocean in south-east Tanzania. Precambr. Res. 305, 386–426.
Möller, A., Mezger, K., Schenk, V., 1998. Crustal age domains and the evolution of the continental crust in the Mozambique Belt of Tanzania: combined Sm–Nd, Rb–Sr, and Pb–Pb isotopic evidence. J. Petrol. 39 (4), 749–783.
Möller, A., Mezger, K., Schenk, V., 2000. U-Pb dating of metamorphic minerals: Pan-African metamorphism and prolonged slow cooling of high pressure granulites in Tanzania, East Africa. Precambr. Res. 104 (3), 123–146.
Morrison, G.W., 1980. Characteristics and tectonic setting of the shoshonite rock association. Lithos 13 (1), 97–108.
Moyes, A.B., 1993. The age and origin of the Jutulsessen granitic gneiss, Gjelsvikfjella, Dronning Maud Land. S. Afr. J. Antarct. Res. 23 (1 & 2), 25–32.
Moyes, A.B., Barton, J.M., Groenewald, P.B., 1993. Late Proterozoic to Early Palaeozoic tectonism in Dronning Maud Land, Antarctica: supercontinental fragmentation and amalgamation. J. Geol. Soc. 150, 833–842.
Müller, D., Groves, D.I., 2019. In: Potassic Igneous Rocks and Associated Gold-Copper Mineralization, fifth ed. Springer-Verlag, Heidelberg, pp. 398.
Murphy, J.B., Nance, R.D., 1991. Supercontinent model for the contrasting character of Late Proterozoic orogenic belts. Geology 19, 469–472.
Owada, M., Kamei, A., Horie, K., Shimura, T., Yuhara, M., Tsukada, K., Osanai, Y., Baba, S., 2013. Magmatic history and evolution of continental lithosphere of the Sør

Rondane Mountains, eastern Dronning Maud Land, East Antarctica. Precambr. Res. 234, 63–84.
Palmeri, R., Godard, G., Di Vincenzo, G., Sandroni, S., Talarico, F., 2018. High-pressure granulite-facies metamorphism in central Dronning Maud Land (East Antarctica): implications for Gondwana assembly. Lithos 300–301, 361–377.
Pe-Piper, G., Piper, D.J.W., Koukouvelas, I., Dolansky, L.M., Kokkalas, S., 2009. Postorogenic shoshonitic rocks and their origin by melting underplated basalts: the Miocene of Limnos, Greece Shoshonites from melting underplated basalt, Greece. GSA Bull. 121 (1–2), 39–54.
Pearce, J.A., 1996. Sources and Settings of Granitic Rocks. Episode 19, 120–125.
Pearce, J.A., Harris, N.B.W., Tindle, A.G., 1984. Trace element discrimination diagrams for the tectonic interpretation of granitic rocks. J. Petrol. 25 (4), 956–983.
Pierce, E.L., Hemming, S.R., Williams, T., van de Flierdt, T., Thomson, S.N., Reiners, P.W., Gehrels, G.E., Brachfeld, S.A., Goldstein, S.L., 2014. A comparison of detrital U-Pb zircon, 40Ar/39Ar hornblende, 40Ar/39Ar biotite ages in marine sediments off East Antarctica: implications for the geology of subglacial terrains and provenance studies. Earth Sci. Rev. 138, 156–178.
Rao, D.R., 2000. Metamorphic evolution of charnockites and felsic gneisses from the Schirmacher Region, East Antarctica. Gondwana Res. 3 (1), 79–89.
Ravich, M.G., Krylov, A., 1963. Absolute ages of rocks from East Antarctica. In: Adie, R.J. (Ed.), Antarctic Geology. North-Holland Publishing Company, Amsterdam,, pp. 579–589.
Ravich, M.G., Solov'ev, D.S., 1966. Geologia i petrologia centralnoi chasti gor Zemli Korolevy Mod [Geology and petrology of the mountains of of central Dronning Maud Land]. Trudy nauchno-issled (Israel program for scientific translations9, Jerusalem, p. 290.
Ravikant, V., 1998. Geological map of the Schirmacher Oasis, central Dronning Maud Land, East Antarctica. Antarctica Division, GSI, Faridabad.
Ravikant, V., 2006. Sm-Nd isotopic evidence for Late Mesoproterozoic metamorphic relics in the East African Orogen from the Schirmacher Oasis, East Antarctica. J. Geol. 114 (5), 615–625.
Ravikant, V., Bühn, B., Pimentel, M., 2018. Zircon U-Pb age constraints for Tonian-early Cryogenian deposition of metasedimentary rocks from the Schirmacher Oasis, East Antarctica: implications for correlations across the Mozambique Ocean. Polar Sci. 18, 39–47.
Ravikant, V., Laux, J., Pimentel, M., 2007. Sm-Nd and U-Pb isotopic constraints for crustal evolution during Late Neoproterozoic from rocks of the Schirmacher Oasis, East Antarctica: geodynamic development coeval with the East African Orogeny. US Geological Survey, Open-File Report, 1047.
Ravikant, V., Rao, Y.B., Gopalan, K., 2004. Schirmacher Oasis as an extension of the Neoproterozoic East African Orogen into Antarctica: new Sm-Nd Isochron Age Constraints. J. Geol. 112 (5), 607–616.
Riedel, S., Jacobs, J., Jokat, W., 2013. Interpretation of new regional aeromagnetic data over Dronning Maud Land (East Antarctica). Tectonophysics 585, 161–171.
Roering, C., van Reenen, D.D., Smit, C.A., Barton, J.M., de Beer, J.H., de Wit, M.J., Stettler, E.H., van Schalkwyk, J.F., Stevens, G., Pretorius, S., 1992. Tectonic model for the evolution of the Limpopo Belt. Precambr. Res. 55 (1), 539–552.
Roland, N., 2004. Pan-African granite–charnockite magmatism in central Dronning Maud Land, East Antarctica: petrography, geochemistry and plate tectonic implications. Geol. Jahrb. Reihe B 96, 187–231.
Rubatto, D., 2002. Zircon trace element geochemistry: partitioning with garnet and the link between U-Pb ages and metamorphism. Chem. Geol. 184 (1), 123–138.
Ruppel, A., Jacobs, J., Eagles, G., Läufer, A., Jokat, W., 2018. New geophysical data from a key region in East Antarctica: estimates for the spatial extent of the Tonian Oceanic Arc Super Terrane (TOAST). Gondwana Res. 59, 97–107.
Ruppel, A.S., Läufer, A., Jacobs, J., Elburg, M., Krohne, N., Damaske, D., Lisker, F., 2015. The Main Shear Zone in Sør Rondane, East Antarctica: implications for the late-Pan-African tectonic evolution of Dronning Maud Land. Tectonics 34 (6), 1290–1305.
Santosh, M., Xiao, W.J., Tsunogae, T., Chetty, T.R.K., Yellappa, T., 2012. The Neoproterozoic subduction complex in southern India: SIMS zircon U-Pb ages and implications for Gondwana assembly. Precambr. Res. 192–195, 190–208.
Sengupta, S., 1988. Precambrian rocks of the Schirmacher range, East Antarctica. Zeitschrift für Geologie Wissenschaften 16, 647–660.
Sengupta, S., 1991. Structural and Petrological Evolution of Basement Rocks in the Schirmacher Hills, Queen Maud Land, East Antarctica. Geological Evolution of Antarctica. Cambridge University Press, pp. 95–97.
Stern, R.J., 1994. Arc-assembly and continental collision in the Neoproterozoic East African Orogen: implications for the consolidation of Gondwanaland. Annu. Rev. Earth Planetary Sci. 22, 319–351.
Sun, S.S., McDonough, W.F., 1989. Chemical and isotopic systematics of oceanic basalts: implications for mantle composition and processes. Geol. Soc. London Spec. Publ. 42 (1), 313–345.
Thomas, R.J., Agenbacht, A.L.D., Cornell, D.H., Moores, J.M., 1994. The Kibaran of southern Africa: tectonic evolution and metallogeny. Ore Geol. Rev. 9, 131–160.
Thomas, R.J., De Waele, B., Schofield, D.I., Goodenough, K.M., Horstwood, M., Tucker, R., Bauer, W., Annells, R., Howard, K., Walsh, G., Rabarimanana, M., Rafahatelo, J.M., Ralison, A.V., Randriamananjara, T., 2009. Geological evolution of the Neoproterozoic Bemarivo Belt, northern Madagascar. Precambr. Res. 172 (3), 279–300.
Thomas, R.J., Spencer, C., Bushi, A.M., Baglow, N., Boniface, N., de Kock, G., Horstwood, M.S.A., Hollick, L., Jacobs, J., Kajara, S., Kamihanda, G., Key, R.M., Maganga, Z., Mbawala, F., McCourt, W., Momburi, P., Moses, F., Mruma, A., Myambilwa, Y., Roberts, N.M.W., Saidi, H., Nyanda, P., Nyoka, K., Millar, I., 2016. Geochronology of the central Tanzania Craton and its southern and eastern orogenic margins. Precambr. Res. 277, 47–67.
Tucker, R.D., Roig, J.Y., Moine, B., Delor, C., Peters, S.G., 2014. A geological synthesis of the Precambrian shield in Madagascar. J. Afr. Earth Sc. 94, 9–30.
Valley, J.W., Lackey, J.S., Cavosie, A.J., Clechenko, C.C., Spicuzza, M.J., Basei, M.A.S., Bindeman, I.N., Ferreira, V.P., Sial, A.N., King, E.M., Peck, W.H., Sinha, A.K., Wei, C.S., 2005. 4.4 billion years of crustal maturation: oxygen isotope ratios of magmatic zircon. Contrib. Miner. Petrol. 150 (6), 561–580.
Viola, G., Henderson, I.H.C., Bingen, B., Thomas, R.J., Smethurst, M.A., de Azavedo, S., 2008. Growth and collapse of a deeply eroded orogen: insights from structural, geophysical, and geochronological constraints on the Pan-African evolution of NE Mozambique. Tectonics 27 (5), 1–31 TC5009.
Wang, C.-C., Jacobs, J., Elburg, M.A., Läufer, A., Thomas, R.J., Elvevold, S., 2020. Grenville-age continental arc magmatism and crustal evolution in central Dronning Maud Land (East Antarctica): zircon geochronological and Hf-O isotopic evidence. Gondwana Res in press.
Wareham, C.D., Pankhurst, R.J., Thomas, R.J., Storey, B.C., Grantham, G.H., Jacobs, J., Eglington, B.M., 1998. Pb, Nd, and Sr isotope mapping of Grenville-age crustal provinces in Rodinia. J. Geol. 106, 647–660.
Wetzel, H.-U., Stackebrandt, W., Hahne, K., 1991. Results on geological mapping in the nunataks area south of the Schirmacher Oasis, East Antarctica. Z. Geol. Wiss. 19, 145–152.
Whalen, J.B., Currie, K.L., Chappell, B.W., 1987. A-type granites: geochemical characteristics, discrimination and petrogenesis. Contrib. Miner. Petrol. 95 (4), 407–419.

Paper IV

***Wang, C-C.**, Jacobs, J., Elburg, M.A., Läufer, A., Elvevold, S., 2020. Late Neoproterozoic–Cambrian magmatism in Dronning Maud Land (East Antarctica): U–Pb zircon geochronology, isotope geochemistry and implications for Gondwana assembly. Precambrian Research 350, 105880.*

Precambrian Research 350 (2020) 105880

Contents lists available at ScienceDirect

Precambrian Research

journal homepage: www.elsevier.com/locate/precamres

Late Neoproterozoic–Cambrian magmatism in Dronning Maud Land (East Antarctica): U–Pb zircon geochronology, isotope geochemistry and implications for Gondwana assembly

Cheng-Cheng Wang[a,*], Joachim Jacobs[a], Marlina A. Elburg[b], Andreas Läufer[c], Synnøve Elvevold[d]

[a] Department of Earth Science, University of Bergen, PB7803, N-5020 Bergen, Norway
[b] Department of Geology, University of Johannesburg, Auckland Park 2006, Johannesburg, South Africa
[c] Federal Institute for Geosciences and Natural Resources (BGR), Stilleweg 2, 30655 Hannover, Germany
[d] Norwegian Polar Institute, Tromsø, Norway

ARTICLE INFO

Keywords:
Zircon U–Pb geochronology
Hf–O isotopes
Kalahari Craton
Gondwana
Continental collision
Crustal evolution

ABSTRACT

Dronning Maud Land (DML) is a key area for the better understanding of the geotectonic history and amalgamation processes of the southern part of Gondwana. Here, we present comprehensive new zircon U–Pb–Hf–O, whole-rock Sm–Nd isotopic and geochemical data for late Neoproterozoic-Cambrian igneous rocks along a profile from central to eastern DML, which provides new insights into the crustal evolution and tectonics of the region. In central DML, magmatism dominantly occurred at 530–485 Ma, with 650–600 Ma charnockite and anorthosite locally distributed at its eastern periphery. In contrast, eastern DML experienced long-term and continuous granitic magmatism from ca. 650 Ma to 500 Ma. In central DML, the 650–600 Ma samples are characterized by highly elevated $\delta^{18}O$ (7.5–9.5‰) associated with slightly negative to positive εHf(t) values (−1 to +3), indicating significant addition of high-$\delta^{18}O$ crustal components, such as sedimentary material at the margin of the Kalahari Craton. Evolved Hf isotopic signatures (εHf(t) = −15 to −6) and moderately elevated O isotopic data ($\delta^{18}O$ = 6–8‰) of the Cambrian granitic rocks from central DML indicate a significant incorporation of the pre-existing, old continental crust. In eastern DML, the suprachondritic Hf–Nd isotope signatures and moderate $\delta^{18}O$ values of the late Neoproterozoic granites (650–550 Ma) from the Sør Rondane Mountains support the view that they mainly originated from crust of the Tonian Oceanic Arc Super Terrane (TOAST). The post-540 Ma granites, however, have more evolved Hf and Nd isotopic compositions, suggesting an increasing involvement of older continental components during Cambrian magmatism. Nd isotopes of the Cambrian granitic rocks in DML display an increasingly more radiogenic composition towards the east with model ages ranging from late Archean to Mesoproterozoic times, which is in line with the isotopic trend of the Precambrian basement in this region. The late Neoproterozoic (> 600 Ma) igneous rocks in central and eastern DML were emplaced in two independent subduction systems, at the periphery of the eastern Kalahari Craton and somewhere within the Mozambique Ocean respectively. The accretion and assembly of the TOAST to the eastern margin of the Kalahari Craton and their collision with surrounding continental blocks was followed by extensive post-collisional magmatism due to delamination tectonics and orogenic collapse in the Cambrian. The late Neoproterozoic–Cambrian igneous rocks in DML thus record an orogenic cycle from subduction-accretion, continental collision to post-collisional process during and after the assembly of Gondwana.

1. Introduction

Late Neoproterozoic – Cambrian times witnessed the transition from the break-up of Rodinia to the amalgamation of Gondwana (e.g., Hoffman, 1991; Li et al., 2008; Merdith et al., 2017). Blocks of East and West Gondwana were sutured along various late Neoproterozoic–early Paleozoic Brasiliano/Pan-African mobile belts including the major East African-Antarctic Orogen (EAAO), the latter of which extends from Saudi Arabia to Mozambique and into Dronning Maud Land (DML) in East Antarctica (Jacobs et al., 1998; Jacobs and Thomas, 2004). The EAAO records first accretionary and then continental collision tectonics during the closure of the Mozambique Ocean from 800 to 500 Ma (Stern, 1994; Meert and Van Der Voo, 1997; Jacobs et al., 2003a, 2020; Meert, 2003; Jacobs and Thomas, 2004; Collins and Pisarevsky, 2005;

* Corresponding author.
E-mail address: Cheng-Cheng.Wang@uib.no (C.-C. Wang).

https://doi.org/10.1016/j.precamres.2020.105880
Received 8 June 2020; Received in revised form 22 July 2020; Accepted 23 July 2020
Available online 28 July 2020

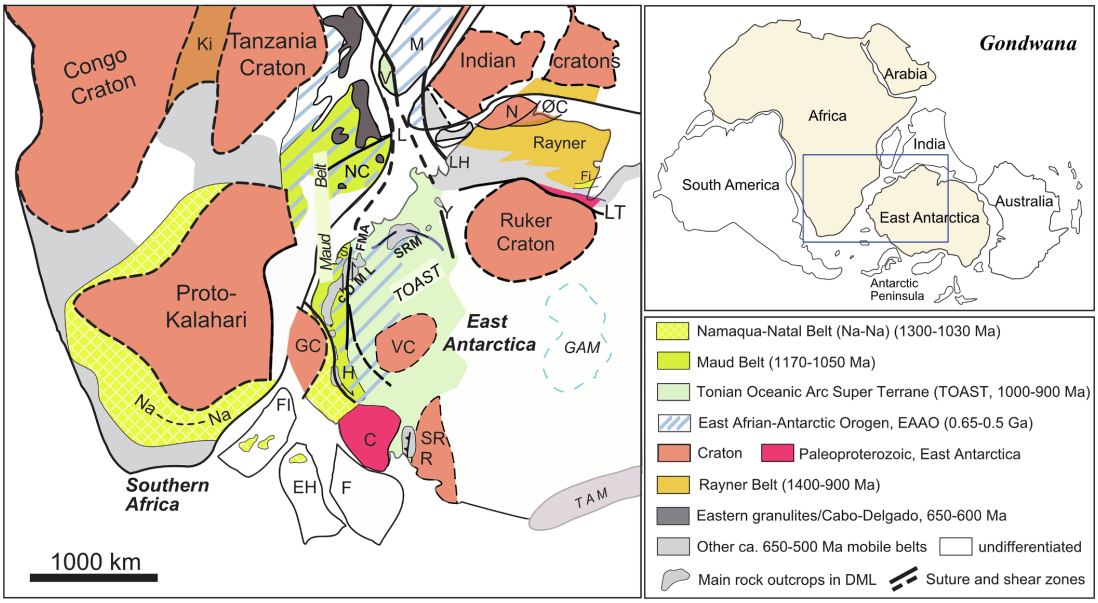

Fig. 1. Location of DML in East Antarctica (after Jacobs et al., 2017) and in Gondwana configuration during Paleo-Mesozoic times (after Gray et al., 2008). Abbreviations: C, Coats Land; cDML, central Dronning Maud Land; EH, Ellsworth-Haag; F, Filchner Block; FI, Falkland Islands; Fi, Fisher Terrane; FMA, Forster Magnetic Anomaly; GAM, Gamburtsev Mountains; GC, Grunehogna Craton; H, Heimefrontfjella; Ki, Kibaran; L, Lurio Belt; LH, Lützow-Holm Bay; LT, Lambert Terrane; M, Madagascar; N, Napier Complex; NC, Nampula Complex; Na–Na, Namaqua–Natal Belt; ØC, Øygarden Complex; R, Read Block; S, Schirmacher Oasis; SR, Shackleton Range; SRM, Sør Rondane Mountains; TAM, Transantarctic Mountains; V, Vohibori; VC, Valkyrie Craton; Y, Yamato Mountains.

Bingen et al., 2009; Fritz et al., 2013; Mole et al., 2018). The southern part of the EAAO in DML records multiple episodes of magmatism and high-grade metamorphism from ca. 650 to 500 Ma (e.g., Jacobs et al., 2008a; Osanai et al., 2013; Elburg et al., 2016), which provides a key to understanding the amalgamation history of this region. Within Gondwana, western-central DML was attached to the eastern margin of the Kalahari Craton with the Grenville-age Maud Belt constituting the main basement (Groenewald et al., 1995; Jacobs et al., 2008b), while eastern DML is dominated by exotic 1000–900 Ma juvenile oceanic arcs (Tonian Oceanic Arc Super Terrane, TOAST, Jacobs et al., 2015) that were accreted onto the Kalahari Craton during the assembly of Gondwana (Fig. 1).

Igneous rocks generated during East African-Antarctic orogenesis provide important information on the crustal and tectonic evolution associated with subduction, accretion and collision processes. Particularly, the cessation of major orogenic events is marked by widespread post-collisional magmatism throughout almost the entire orogen (e.g., Küster and Harms, 1998; Stern, 2002; Veevers, 2007). In the southern part of the EAAO, voluminous Cambrian granites in Mozambique, Madagascar and East Antarctica (Jacobs et al., 2008a; Bingen et al., 2009; Goodenough et al., 2010; Archibald et al., 2019) are attributed to post-collisional delamination tectonics, followed by orogenic collapse (Jacobs et al., 2008a; Viola et al., 2008; Ueda et al., 2012). In western and central DML, Pan-African igneous rocks are dominated by 530–485 Ma post-collisional granites, syenites, charnockites and subordinate mafic rocks (Jacobs et al., 2008a). This magmatism is preceded by ca. 610–600 Ma anorthosite and charnockite magmatism in the easternmost part of central DML – at the eastern margin of the Kalahari Craton (Jacobs et al., 1998). Eastern DML in contrast, witnessed almost continuous granitic magmatism from 650 to 500 Ma (Elburg et al., 2016). Elucidating the formation and tectonic setting of late Neoproterozoic to Cambrian igneous rocks in DML is critical for the better understanding of the orogenic processes and evolution associated with the amalgamation of Gondwana in the southern part of the EAAO.

In this contribution, we present the first comprehensive U–Pb–Hf–O zircon data set and additional whole-rock Sm–Nd isotope and geochemistry data of late Neoproterozoic to Cambrian igneous rocks, along an E-W trending profile of the DML mountains. The new data provide new constraints on the age, origin and evolution of mostly granitic rocks across the eastern margin of the Kalahari Craton and into the TOAST. Based on compiled new and published data, we investigate the spatial and temporal variations in isotopic composition and evolution along our profile, and relate this to crustal evolution and tectonic setting during closure of the Mozambique Ocean and the amalgamation of Gondwana in this key region of East Antarctica.

2. Geological background

The Jurassic rift margin escarpment of DML resulted in an approximately 1500 km long mountain range that offers a unique cross section through the southern part of the EAAO (Fig. 1), in an area that is otherwise largely ice-covered. Three major tectonic domains can be differentiated. In the west, the EAAO has reworked the easternmost part of the Kalahari Craton; the western orogenic front of the orogen is a major transcurrent shear zone, exposed in Heimefrontfjella. In the east, the EAAO has overprinted Indo-Antarctic crust, with a less well defined orogenic front. In between these two major blocks with African and Indo-Antarctic affinities lies the TOAST (Jacobs et al., 2015), interpreted as a remnant of the Mozambique Ocean, comparable to the Arabian-Nubian Shield. The contact of the easternmost Kalahari Craton with the TOAST is marked by the Forster Magnetic Anomaly that appears to be collinear with the South Orvin Shear Zone (Fig. 2). The Forster Magnetic Anomaly can be traced underneath the ice for a considerable distance to the south. The eastern boundary of the TOAST is ill-defined and is probably somewhere close to the Yamato Mountains

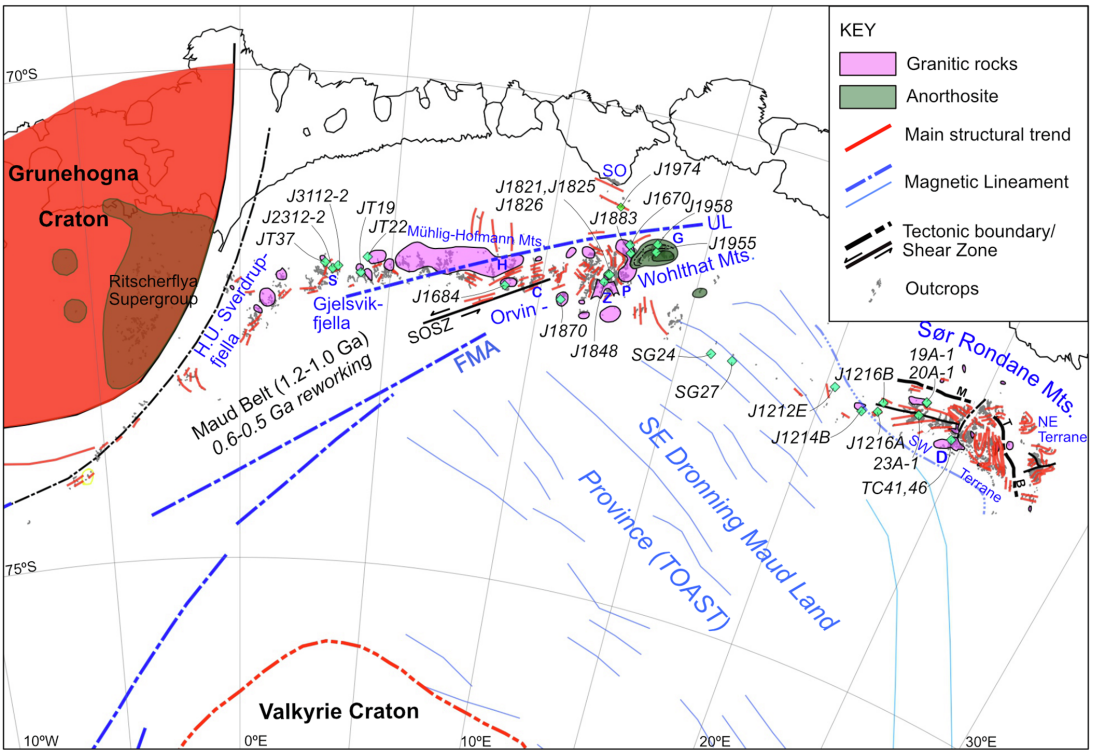

Fig. 2. Geological overview map of the study area and sample localities in central and eastern DML. Abbreviations: C, Conrad mountain; D, mount Dufek; FMA, Forster Magnetic Anomaly; G, Grubergebirge; H, Holtedahlfjella; MTB, Main Tectonic Boundary; P, Petermannketten; S, mount Stabben; SO, Schirmacher Oasis; SOSZ, South Orvin Shear Zone; TOAST, Tonian Oceanic Arc Super Terrane; UL, Ulvetanna Lineament; Z, mount Zwiesel.

(Ruppel et al., 2018). To the south of the DML mountains, a cryptic craton, the Valkyrie Craton, may limit the southern extent of the TOAST (Jacobs et al., 2015; Golynsky et al., 2018) (Fig. 2). Our granitic samples provide a cross section from the easternmost Kalahari Craton into the TOAST, but do not cover the easternmost part of the orogen with an Indo-Antarctic affinity.

2.1. Western-central DML

In western and central DML, the tectonically reworked margin of the easternmost Kalahari Craton is exposed. The region includes the Archean Grunehogna Craton, which was interpreted as part of the Kalahari Craton before the breakup of Gondwana (Groenewald et al., 1995; Jones et al., 2003; Marschall et al., 2010). It is surrounded by the eastern extension of the late Mesoproterozoic Natal Belt to the south and the Maud Belt to the east (Fig. 2). The Maud Belt is largely exposed between H.U. Sverdrupfjella in the west and the Orvin-Wohlthat mountains in the east. It is interpreted as a major Grenville-age continental arc that formed at the periphery of Proto-Kalahari and Rodina (e.g., Marschall et al., 2013; Wang et al., 2020). The Mesoproterozoic basement of the Maud Belt in western and central DML is dominated by (meta-) volcanic and intrusive rocks formed between 1170 and 1090 Ma, which are intruded by 1090–1050 Ma A-type granite sheets and plutons accompanied by amphibolite to granulite facies metamorphism (Jacobs et al., 2003a, 2003b; Paulsson and Austrheim, 2003; Board et al., 2005; Bisnath et al., 2006; Grantham et al., 2011). Hf and Nd isotopes of the Grenville-age basement exhibit an obvious variation from the west to east, with H.U. Sverdrupfjella showing significantly negative epsilon values and Archean model ages, while Gjelsvikfjeik and the Orvin-Wohlthat Mountains have Paleoproterozoic to Mesoproterozoic model ages. This indicates the large involvement of older cratonic crust in the west and successively more juvenile rocks towards the east (Wang et al., 2020).

After a period of tectonic quiescence, renewed continental arc magmatism commenced at ca. 780 Ma, as is evident from the Schirmacher Oasis (Jacobs et al., 2020). The Maud Belt has thereafter been tectonically reworked at amphibolite- to granulite-facies grade during East African-Antarctic orogenesis between ca. 650 and 500 Ma (Moyes et al., 1993a; Groenewald et al., 1995; Moyes and Groenewald, 1996; Board et al., 2005; Pant et al., 2013; Pauly et al., 2016). Protracted late Neoproterozoic/early Paleozoic tectono-metamorphism is recorded in metamorphic zircon rims at 600 Ma, 580–550 Ma and 530–515 Ma (e.g., Jacobs et al., 1998; Baba et al., 2015; Wang et al., 2020). The late Neoproterozoic (650–600 Ma) UHT metamorphism (peak conditions: 950–1050 °C, 0.9–1.0 GPa, Baba et al., 2006, 2010) and syn-tectonic magmatism may relate to a period of back-arc extension of the eastern Kalahari Craton (Baba et al., 2010; Jacobs et al., 2020). During this stage, anorthosite and charnockite magmatism is recorded in the easternmost part of central DML (Grubergebirge). Subsequently, at ca. 580–550 Ma, western-central DML experienced crustal thickening with peak metamorphism reaching (eclogite)granulite-facies (> 900 °C, 1.5 GPa) (Pauly et al., 2016; Palmeri et al., 2018) followed by isothermal decompression, constituting a clockwise P-T path (Colombo and Talarico, 2004; Bisnath and Frimmel, 2005; Baba et al., 2008; Elvevold and Engvik, 2013; Pauly et al., 2016; Palmeri et al., 2018; Elvevold et al., 2020). This was interpreted as a result of

Table 1
Summary of analysed samples from central and eastern DML in this study.

Sample	Latitude (S)	Longitude (E)	Rock types	Main mineral composition	Zircon characterization	Th, U concentration and Th/U ratio of concordant igneous analyses	Igneous age (Ma) (# of conc. igneous analyses/ # of total)	Inherited ages (Ma)	εHf(t)	Model age (Ga)	$\delta^{18}O$ (‰)
Gjelsvikfjella, central DML (530–485 Ma)											
2312–2[1]	−72.000373	3.088794	Lamprophyre dyke	Pl, Kfs, Bt, Qtz			ca. 525		−2.4 ± 1.6		5.8 ± 0.7
JT19[a]	−72.024676	4.025192	Charnockite	Opx, Amp, Pl, Kfs, Qtz	subhedral to euhedral, 100–250 μm, oscillatory zoning	40–170, 130–520, 0.3–0.4	500 ± 3 (13/14)		−7.1 ± 1.6	1.83–1.99	6.8 ± 0.5
JT22[a]	−71.861973	4.215732	Granite	Kfs, Qtz, Pl	subhedral to euhedral, 200–300 μm, oscillatory zoning	60–700, 110–1750, 0.1–1.8	499 ± 4	ca. 1080	−12.2 ± 2.0	2.06–2.36	6.3 ± 0.6
3112–2[1]	−71.969864	3.263118	Granite	Kfs, Pl, Bt, Qtz			487 ± 4		−8.7 ± 1.3	1.94–2.04	6.3 ± 0.9
JT37[a]	−71.941944	2.826667	Gabbro (Stabben)	Bt, Amp, Pl, Cpx	small, irregular, weak zoning	50–170, 50–230, 0.9–1.5	483 ± 4 (8/10)	ca. 1090	−12.7 ± 2.1	2.07–2.39	6.8 ± 0.4
Orvin-Wohlthat Mountains, central DML (530–485 Ma)											
J1826[b]	−71.690620	12.145744	Gabbro	Amp, Bt, Pl, Qtz, Cpx	euhedral, up to 500 μm, oscillatory zoning	40–430, 90–380, 0.5–1.1	524 ± 2 (16/21)		−3.0 ± 0.9		8.0 ± 0.4
J1870[2]	−72.038188	10.721204	Charnockite	Pl, Kfs, Qtz, Opx, Amp, Bt			501 ± 7		−6.9 ± 1.4	1.81–1.93	7.4 ± 0.5
J1670[2]	−71.352218	12.575029	Granite	Kfs, Pl, Qtz, Amp			499 ± 4		−7.4 ± 1.4	1.81–1.93	7.4 ± 0.4
J1821[c]	−71.689233	12.099042	Charnockite	Opx, Pl, Qtz	oscillatory zoning		514 ± 5 (39/52)	ca. 1068, 600			
J1825[c]	−71.689233	12.099042	Syenite	Kfs, Pl, Bt, Amp	oscillatory zoning		494 ± 6 (15/23)	ca. 1058, 600			
J1684[c]	−71.991797	8.816522	Granite	Kfs, Qtz, Pl, Bt, Amp	oscillatory zoning		486 ± 7 (16/23)	ca. 1065, 610			
Orvin-Wohlthat Mountains, central DML (650–600 Ma)											
J1883[b]	−71.431244	12.659893	Charnockite	Pl, Qtz, Kfs, Opx, Bt, Amp	subhedral or irregular, 150–250 μm, oscillatory zoned cores- srructureless rims	20–90, 70–250, 0.3–0.5	645 ± 6 (8/29)		+1.2 ± 1.1	1.38–1.52	8.8 ± 0.3
J1848[b]	−71.775703	12.010605	Gt-gneiss	Kfs, Pl, Qtz, Bt, Grt	a mixture of large (700 μm) and smaller zircons (generally between 200 and 350 μm), oscillatory zoned cores-srructureless mantle and rims	50–130, 170–430, 0.3–0.5	636 ± 7 (5/33)		+1.1 ± 1.4	1.43–1.53	8.4 ± 0.6
J1886[3]	−71.431244	12.659893	Charnockite	Pl, Qtz, Kfs, Opx, Amp			608 ± 9		+0.6 ± 1.5	1.41–1.58	8.5 ± 0.7
J1955[3]	−71.364170	13.449743	anorthosite	Pl, Opx, Amp, Qtz			600 ± 12		+0.9 ± 1.6	1.38–1.57	7.9 ± 0.4
J1958[3]	−71.282666	13.436036	anorthosite	Pl, Opx, Amp, Qtz			583 ± 7		+0.5 ± 1.6	1.43–1.57	8.5 ± 0.7
SE DML											
SG 27[4]	−72.234169	16.774981	Granodiorite	Pl, Kfs, Qtz, Bt, Amp			532 ± 5	ca. 730	−0.4 ± 0.9	1.46–1.53	7.5 ± 0.9
SG 24[4]	−72.223950	16.027433	Granite	Kfs, Pl, Qtz, Bt			503 ± 5		−2.0 ± 1.6	1.48–1.65	7.9 ± 1.3
SRM, eastern DML											
J1212E[4]	−72.150050	20.321083	Amphibole gneiss	Qtz, Pl, Kfs, Bt, Amp, Ms			925 ± 11		+5.5 ± 1.7	1.35–1.54	6.6 ± 0.5
TC46[b]	−72.195043	23.650854	Dufek Granite	Kfs, Pl, Qtz, Bt	Subhedral to euhedral, 200–400 μm, oscillatory zoned cores and thin, CL-dark rims	210–600, 380–1000, 0.3–0.9	606 ± 1 (6/20)				
TC41[b]	−72.196507	24.593602	Dufek Granite	Kfs, Pl, Qtz, Bt	Subhedral to euhedral, 150–300 μm, oscillatory zoned cores and CL-dark, structureless rims	100–150, 100–300, 0.3–0.7	588 ± 4 (7/22)		+3.0 ± 2.0	1.21–1.41	6.5 ± 0.8
J1214B[4]	−72.284683	21.435233	Granite	Kfs, Pl, Qtz, Amp, Bt			557 ± 2		+1.0 ± 2.2	1.32–1.48	6.1 ± 0.8
J1216B[4]	−72.121600	22.018700	Quartz-monzonite	Kfs, Pl, Qtz, Bt			555 ± 4	ca. 600, 750, 850	−0.5 ± 5.2	1.36–1.59	6.7 ± 1.5

(*continued on next page*)

Table 1 (*continued*)

Sample	Latitude (S)	Longitude (E)	Rock types	Main mineral composition	Zircon characterization	Th, U concentration and Th/U ratio of concordant igneous analyses	Igneous age (Ma) (# of conc. igneous analyses/ # of total)	Inherited ages (Ma)	εHf(t)	Model age (Ga)	$\delta^{18}O$ (‰)
23A-1[a]	−72.100100	23.269733	Granite	Kfs, Pl, Qtz, Bt	Euhedral, 200–300 μm, oscillatory zoning	100–600, 200–800, 0.3–0.9	555 ± 4 (8/10)	ca. 620	+1.0 ± 0.7	1.35–1.46	7.2 ± 0.8
J1216A[4]	−72.228930	21.953620	Granite	Kfs, Pl, Qtz, Bt			534 ± 4		+0.1 ± 1.0	1.36–1.53	6.4 ± 0.6
20A-1[a]	−71.946691	23.344872	Granite	Kfs, Pl, Qtz, Bt	Euhedral, 300–400 μm, oscillatory zoning	30–170, 120–540, 0.3–0.5	524 ± 3 (9/12)		−3.2 ± 1.6	1.49–1.73	6.6 ± 0.8
19A-1[a]	−71.954113	23.349175	Granite	Kfs, Pl, Qtz, Bt	Euhedral, 300–400 μm, oscillatory zoning	40–170, 130–520, 0.3–0.4	521 ± 2 (13/15)		−2.5 ± 1.5	1.54–1.68	6.7 ± 0.6

Samples in each region are ordered by age. The samples with superscript a and b are newly dated samples in this study, a-SIMS, b-SHRIMP; c-LA-ICP-MS (Suliman, 2011).
1 – Jacobs et al., 2003a, 2 – Jacobs et al., 2008a, 3 – Jacobs et al., 1998, 4 – Jacobs et al., 2015, all are SHRIMP ages; Mineral abbreviations from Whitney and Evans (2010).

continental collision between the Kalahari Craton and other crustal terranes. Accompanying high-grade metamorphism, the Mesoproterozoic basement has also experienced migmatisation, but major synchronous granitic plutons have not been recognized thus far. In Cambrian times, orogenic collapse and extensional tectonics led to the emplacement of large volumes of late-tectonic igneous rocks at ca. 530–485 Ma, including charnockites, syenites, granites and gabbros (Jacobs et al., 1998, Jacobs et al., 2003a, 2003b, Jacobs et al., 2008a, Jacobs et al., 2008b).

Thus, late Neoproterozoic–Cambrian igneous rocks in western-central DML were mainly emplaced in two periods at ca. 650–600 Ma and at ca. 530–485 Ma. The continental collision stage is characterized by migmatites and granulites and lacks significant volumes of *syn*-tectonic plutonic rocks, whereas the Cambrian orogenic collapse stage provides the by far largest volumes of granitoids in this part of the EAAO.

2.2. Eastern DML

A recent aerogeophysical survey over eastern DML has revealed an extensive tectonic block (SE DML province, Fig. 2), characterised by low amplitude, elongate, NW-SE trending magnetic anomalies (Mieth et al., 2014). It is dominated by a distinct suite of gabbro-tonalite-trondhjemite-granodiorites (GTTG) dated at ca. 1000–900 Ma (e.g., Jacobs et al., 2015), which are tectonically interleaved with volcano-sedimentary rocks. The GTTGs are interpreted as juvenile oceanic arc crust, based on their geochemistry, juvenile Sm–Nd and zircon Hf-signature, as well as the lack of older inheritance (Kamei et al., 2013; Elburg et al., 2015; Jacobs et al., 2015). The volcano-sedimentary rocks include marbles, calcsilicates, garnet-sillimanite gneisses, graphite schists and heterogeneous quartzo-feldspathic gneisses, interpreted as a meta-volcano-sedimentary sequence of the Mozambique Ocean (Elburg et al., 2015; Jacobs et al., 2015; Kamei et al., 2013). Detrital zircons of the metasedimentary rocks show very limited pre-Tonian provenance (Kitano et al., 2016), in line with the juvenile characteristic of this region. The GTTGs and the associated volcano-sedimentary rocks together form the TOAST (Jacobs et al., 2015). The formation of the TOAST is probably related to the amalgamation of a number of oceanic island arcs during late Neoproterozoic times (Baba et al., 2013; Ruppel et al., in press). The latest geophysical investigations show that the TOAST may extend into the Belgica and Yamato mountains towards the east, and thus represents a significant region with a size of over 500,000 km^2, sandwiched between the Kalahari Craton in the west and an Indo-Antarctic craton in the east (Ruppel et al., 2018).

The tectonically reworked TOAST is exposed in the Sør Rondane Mountains (SRM), where it shows various degrees of tectono-metamorphism, dated at ca. 650–500 Ma, and ranging from granulite facies to greenschist facies (e.g., Osanai et al., 2013). The SRM has been divided into two terranes with different late Neoproterozoic to Cambrian metamorphic histories, the Northeast (NE) and the Southwest (SW) Terrane (Osanai et al., 2013), with the boundary defined as the 'Main Tectonic Boundary' (Fig. 2). The SW Terrane is characterized by a counterclockwise P–T path with isothermal compression at the initial stage of metamorphism and retrograde isobaric cooling, while the NE Terrane yield a clockwise P–T path with decompression and cooling processes (Adachi et al., 2013; Baba et al., 2013; Osanai et al., 2013). The peak granulite facies metamorphism was dated at 650–600 Ma and interpreted as a result of the overthrusting of the NE Terrane over the SW Terrane (Adachi et al., 2013; Osanai et al., 2013). The subsequent 590–530 Ma thermal events were attributed to continental collision between the Kalahari Craton and Indo-Antarctica (Shiraishi et al, 2008; Boger, 2011; Osanai et al., 2013). At least four phases of late Neoproterozoic–Cambrian magmatic activities have been identified in the SRM. The oldest Ediacaran magmatic activity is represented by the granitic magmatism in the Dufek area and the reported ages range from ca. 640 Ma to 620 Ma (Li et al., 2006; Elburg et al., 2016), followed by a suite of 570–550 Ma garnet-leucogneisses, granite sheets and minette

dykes (Shiraishi et al., 2008; Owada et al., 2013; Elburg et al., 2016). The ca. 530 Ma granites are distributed across the SW Terrane from west to east (Elburg et al., 2016), while the latest magmatism occurred at 510–500 Ma, producing mafic and granitic intrusions (Owada et al., 2008; Elburg et al., 2016).

3. Samples and analytical methods

The samples in this study were collected during four expeditions between 1995 and 2018. The core of this study consists of 27 granitic and gabbro samples that were collected from Gjelsvikfjella in the west, across the Orvin-Wohlthat Mountains (central DML) to the SRM (eastern DML) in the east (Fig. 2, Table 1). The combined U–Pb–Hf–O zircon results constitute a W-E oriented isotopic profile across the reworked eastern margin of the Kalahari Craton and a significant part of the tectono-thermally reworked part of the TOAST. Our study utilized in part samples from previous studies, for which U–Pb zircon data were already available (Jacobs et al., 1998, Jacobs et al., 2003a, 2015, Suliman, 2011). All Hf–O zircon data of this study are new.

Moreover, whole-rock Sm–Nd isotope analyses have been conducted on 34 granitic samples from central and eastern DML. They include three dated samples from the SRM, eastern DML, whilst the other 31 granitic samples (samples of Roland, 2004) from the Orvin-Wohlthat Mountains of central DML are undated. As the late voluminous granitic rocks in central DML are all Cambrian in age (Jacobs et al., 2008a and dating results in this study), it is inferred that the latter samples have igneous crystallization ages between ca. 515–485 Ma.

Detailed analytical methods are provided in Supplementary File A.

3.1. Zircon U–Pb dating and Hf–O isotopes

Optical (reflected and transmitted light) and cathodoluminescence (CL) images were taken on zircons prior to U–Pb analyses to reveal the internal textures and to guide the selection of analysis spots. U–Pb, Lu–Hf and O isotopic analyses were mostly performed on the same spot or from the same growth domain.

Zircon U–Pb dating on most samples from central DML was carried out using the Sensitive High Resolution Ion Microprobe (SHRIMP) at the IBERSIMS Laboratory, University of Granada, Spain. Three samples were dated by LA-ICP-MS at the University of Bergen. Four samples from eastern DML were analysed using a CAMECA IMS-1280 instrument at the NordSIM facility, Stockholm Museum of Natural History (Sweden). For most samples, we report ^{204}Pb-corrected ages, while ^{208}Pb-corrected ages are used for samples with low Th and U concentrations. Weighted mean ages and group concordia ages are calculated with Isoplot (Version 4.15; Ludwig, 2011). All errors are reported at the 2σ-level. Oxygen isotope ratios of zircon grains were measured at the NordSIM and IBERSIMS laboratories. Prior to O-ion microprobe analysis, the U–Pb analysis spots were removed from the zircons by polishing, followed by recoating with ~30 nm gold. The values of average δ^{18}O values are reported as mean ± 2 standard deviation (S.D.).

Lu–Hf isotopes were measured at the University of Johannesburg, using an ASI 265 Resonetics 193 nm Excimer laser ablation system coupled to a Nu Plasma II multi-collector ICPMS. For calculation of the epsilon Hf, the chondritic uniform reservoir (CHUR) was used as recommended by Bouvier et al. (2008) (^{176}Lu/^{177}Hf and ^{176}Hf/^{177}Hf of 0.0336 and 0.282785, respectively), and a decay constant of 1.867×10^{-11} (Scherer et al., 2001; Söderlund et al., 2004). The calculation of model ages is based on the depleted mantle source values of Griffin et al. (2000) with present-day ^{176}Hf/^{177}Hf = 0.28325 and ^{176}Lu/^{177}Hf = 0.0384. Initial ^{176}Hf/^{177}Hf and εHf values for all analysed zircon domains were calculated using the respective interpreted crystallization age of each sample. The values of average εHf(t) and ^{176}Hf/^{177}Hf$_{(i)}$ for each sample are reported as mean ± 2 S.D.

3.2. Whole-rock Sm–Nd isotope and geochemistry

Sm–Nd isotope data were acquired at the University of Bergen, Norway and the University of Tübingen, Germany. Calculation of the Sm–Nd model parameter εNd(t) is based on ^{143}Nd/^{144}Nd = 0.512638 and ^{147}Sm/^{144}Nd = 0.1967 for a CHUR reference ('chondritic uniform reservoir', Jacobsen and Wasserburg, 1980). Single-stage depleted-mantle model ages (T_{DM}) were calculated assuming ^{143}Nd/^{144}Nd = 0.51315 and ^{147}Sm/^{144}Nd = 0.2137 for the present-day depleted-mantle reservoir and a linear Sm/Nd evolution trough time. Whole-rock element analyses were conducted at the University of Johannesburg, South Africa and the University of Tübingen, Germany.

4. Results

Detailed zircon U–Pb dating and Hf–O isotopic data are provided in Supplementary File B, and whole-rock geochemical and Sm–Nd isotopic data are presented in Supplementary File C. A summary of key sample information and U–Pb–Hf–O results in this study are summarized in Table 1.

4.1. Zircon U–Pb geochronology of samples from central DML

4.1.1. Late Neoproterozoic (650–630 Ma) samples

Two samples from the Petermannketten, including one charnockitic gneiss (J1883) and one garnet-bearing granitic gneiss (J1848), have late Neoproterozoic igneous crystallization ages (Fig. 3). Most zircons from these two samples are characterized by core-(mantle)-rim structures (Fig. 3b, d). The cores display clear oscillatory zoning and high Th/U ratios between 0.3 and 0.5, and thus are interpreted as igneous zircons. In contrast, the rims are invariably CL-dark, structureless and have low Th/U ratios (< 0.1), consistent with the characteristics of metamorphic zircons. As for sample J1883, twenty-nine analyses were conducted on 27 grains, including 23 oscillatory-zoned domains and 6 rims. Eight core analyses define a concordia age of 645 ± 6 Ma (MSWD = 1.18), which is interpreted as the igneous crystallization age of igneous protolith; many other core analyses are discordant due to Pb-loss. Five rim analyses define a common concordia age of 592 ± 8 Ma (MSWD = 0.94), which is interpreted as the time of metamorphic overprint (Fig. 3a). Similarly, the igneous crystallization age of sample J1848 is determined by 5 core analyses, which give a well-constrained concordia age of 628 ± 7 Ma (MSWD = 1.14) (Fig. 3c). Eighteen rims and three cores, which show no zoning but with similar ages than the rims, yield a common concordia age of 562 ± 3 Ma (MSWD = 1.3), which is interpreted as the timing of high-grade metamorphic overprint. In addition, three core analyses are (nearly) concordant at ca. 680 Ma, probably representing zircon inheritance.

4.1.2. Cambrian (530–485 Ma) samples

This sample group includes two gabbros and five granitic samples from Gjelsvikfjella and the Orvin-Wohlthat Mountains (Table 1). Most zircon grains of the individual samples have typical euhedral to subhedral shapes with sizes between ca. 150 and 450 μm, and their internal structure shows mostly simple oscillatory zoning, interpreted as magmatic growth zoning. Gabbro sample JT 37 is one of the westernmost samples (mount Stabben) of this study. Eight concordant analyses provide a concordia age of 483 ± 4 Ma (MSWD = 0.79) (Fig. 4a), which is slightly younger than the associated Stabben syenite (500 ± 8 Ma, Paulsson and Austrheim, 2003). Two granitic samples from Gjelsvikfjella yield concordia ages of 500 ± 3 Ma (n = 14, MSWD = 0.81) (charnockite, JT19) and 499 ± 4 Ma (n = 9, MSWD = 1.07) (granite JT22) respectively (Fig. 4b, c). These ages indicate a pulse of Cambrian gabbroic and granitic magmatism between 500 and 485 Ma in Gjelsvikfjella. Further east, granite sample J1684 has an igneous crystallization age of 486 ± 7 Ma (n = 16, MSWD = 0.83) (Fig. 4d). Further east at mount Zwiesel, the igneous

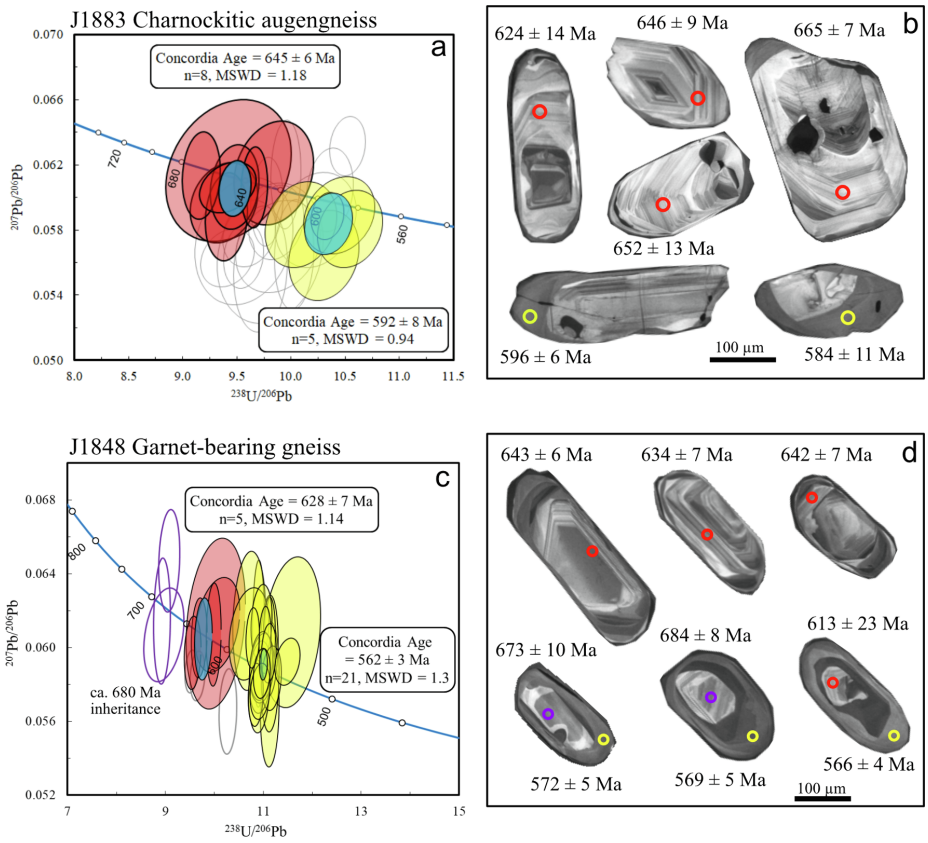

Fig. 3. U–Pb Tera-Wasserburg diagram and CL images of two late Neoproterozoic granitic samples from central DML. In the Tera-Wasserburg diagrams, red and yellow filled ellipses indicate concordant igneous and metamorphic zircons respectively with concordia ellipse in blue. The grey ellipses indicate discordant zircon analyses and purple ones are inherited zircons; CL images show core (red) – rim (yellow) structures, representing igeous crystallization and metamorphic domains respectively. (For interpretation of the references to colour in this figure legend, the reader is referred to the web version of this article.)

crystallization ages of three gabbroic and granitic samples range from ca. 525 Ma to ca. 495 Ma (Fig. 4e–g). The age of the gabbro sample (J1826, 524 ± 2 Ma, n = 17, MSWD = 1.3) is within error of the published ages in this region (521 ± 6 and 527 ± 5 Ma, Jacobs et al., 2003a, 2003b), defining the oldest late-tectonic age in this study. Two granitic samples from this region have younger igneous crystallization ages of 514 ± 5 Ma (charnockite J1821, n = 39, MSWD = 0.50) and 494 ± 6 Ma (syenite J1825, n = 15, MSWD = 0.56). Precambrian inheritance is revealed by a few samples, including Grenville-age (1090–1060 Ma) and late Neoproterozoic (610–600 Ma) ages.

4.2. Zircon U–Pb geochronology of granites from eastern DML

Five new granite samples were dated from the SW Terrane of the SRM, including two granites from mount Dufek and three from adjacent regions to the west. In CL, the zircon grains of two Dufek granites (TC-46, TC-41) are dominated by oscillatory-zoned cores surrounded by dark and structureless rims. In sample TC-46, all analyses were conducted on cores, which define two concordia age groups at 612 ± 2 Ma (n = 7, MSWD = 0.37) and 606 ± 1 Ma (n = 6, MSWD = 1.4) respectively. This may indicate a progressive zircon crystallization over a period of several millions of years. The weighted mean age (607 ± 2 Ma, MSWD = 3.4) agrees within error with the second concordia age group (Fig. 5a). Therefore, the latter concordia age is used here to represent the closest approximation of the crystallization age of the Dufek granite. The zircon core and rim analyses of sample TC-41 show a significant scatter from ca. 600 to 550 Ma. Seven oldest concordant analyses, including 5 cores and 2 rims, give a concordia age of 588 ± 4 Ma (MSWD = 1.5) (Fig. 5b), which is interpreted as the crystallization age of this sample. Five concordant rims define a concordia age of 579 ± 4 Ma (MSWD = 1.2). These rim analyses generally have higher U (1800–4100 ppm) and lower Th/U (ca. 0.1) than the core analyses (U < 350 ppm, Th/U = 0.4–0.7), and they are thus interpreted as metamorphic rims; the age probably represents the timing of a later thermal event postdating granite crystallisation. The U–Pb isotopic system of some cores with high U (500–5000 ppm) and lower Th/U (0.2), may have been reset during a second subsequent thermal event, with a young concordant age group providing a concordia age of 547 ± 2 Ma (n = 5, MSWD = 0.95).

Zircon grains from the remaining three granite samples (23A-1, 20–1, 19A-1) generally have typical igneous zircons with oscillatory zoning. Their U–Pb data define their igneous crystallisation ages at 555 ± 4 Ma (n = 8, MSWD = 1.3), 524 ± 3 Ma (n = 9, MSWD = 0.99) and 521 ± 2 Ma (n = 13, MSWD = 0.70) (Fig. 5c-e) respectively. Ediacaran inheritance of ca. 620 Ma is present in one of the samples (Fig. 5c).

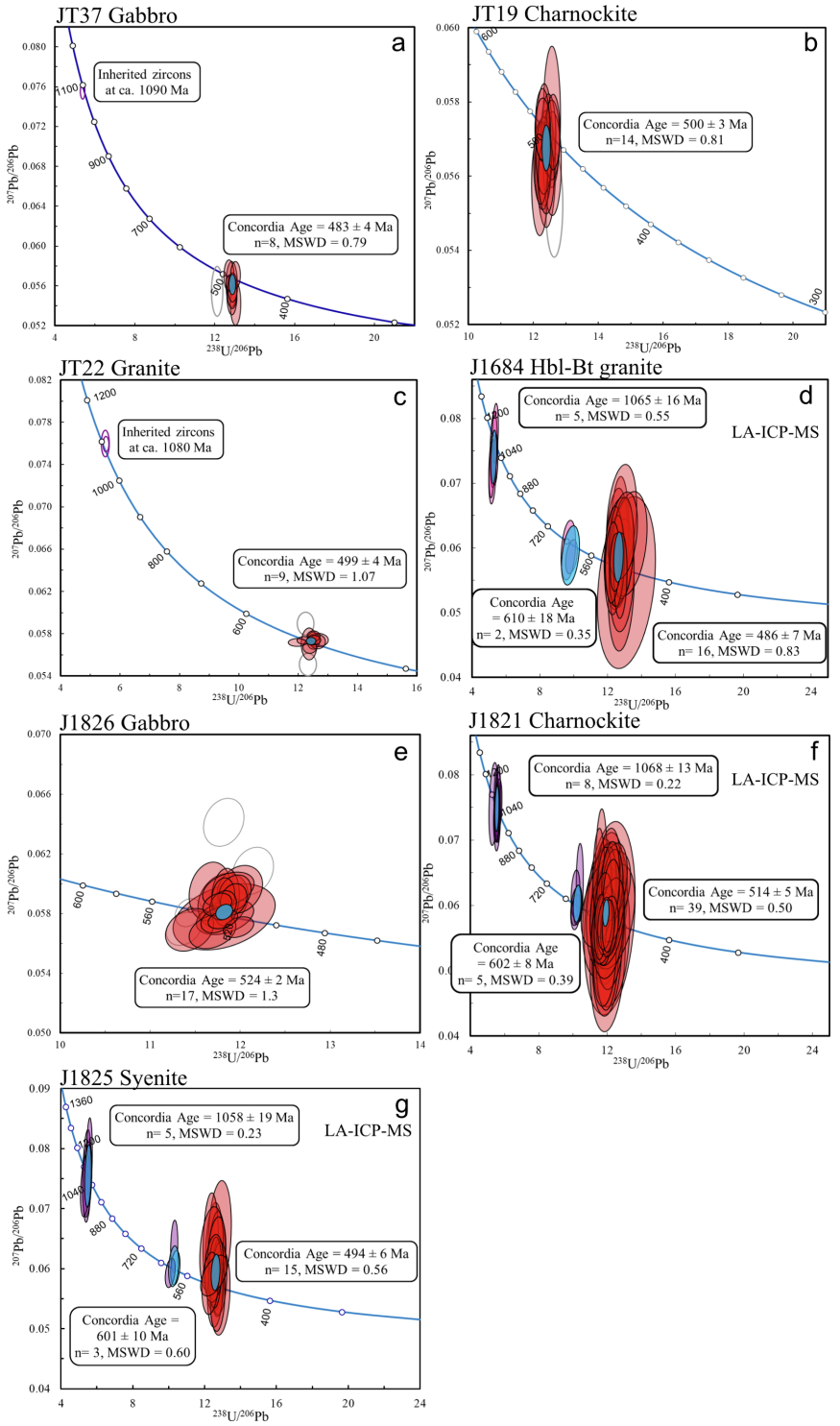

(caption on next page)

Fig. 4. U–Pb Tera-Wasserburg diagram of the Cambrian samples from central DML. The colour coding is the same as in Fig. 3. The dating data of three samples analysed by LA-ICP-MS are from Suliman (2011). CL images for each sample can be found in Supplementary File B.

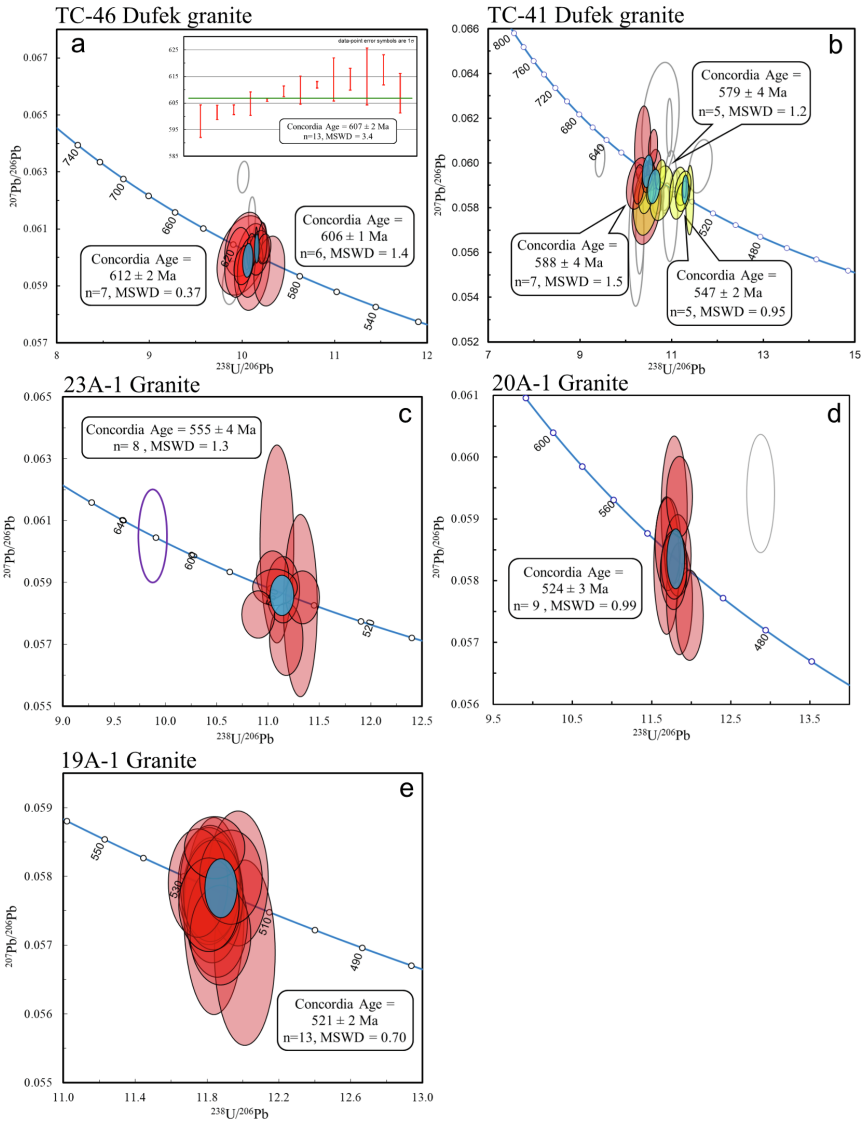

Fig. 5. U–Pb Tera-Wasserburg diagram of the granite samples from eastern DML. The colour coding is the same as in Fig. 3. CL images for each sample can be found in Supplementary File B.

4.3. Major and trace elements

The geochemical characteristics are illustrated in Fig. 6. The granitic rocks from central DML have overall moderate to high silica (SiO_2 = 60–71 wt%), mostly plotting in the quartz monzonite and granite fields on the TAS diagram (Fig. 6a). They have alkali contents ($Na_2O + K_2O$) of 6.0–10.9 wt%, and the modified alkali–lime index of Frost et al. (2001), MALI, varies from 1.05 to 9.06; the samples therefore plot in alkaline and alkali-calcic fields (Fig. 6b). In the K_2O versus SiO_2 diagram, most samples plot in the shoshonitic field, whereas a few display high-K affinities (Fig. 6c). They are generally metaluminous to slightly peraluminous with molar $Al_2O_3/(CaO + Na_2O + K_2O)$ ratios of 0.83–1.09 (Fig. 6e). The Fe-index ($FeO^*/(FeO^* + MgO)$) ranges from 0.75 to 0.85, which demonstrates their ferroan character (Fig. 6d). In the A-type granite discrimination diagram, both quartz monzonite and granite samples show high

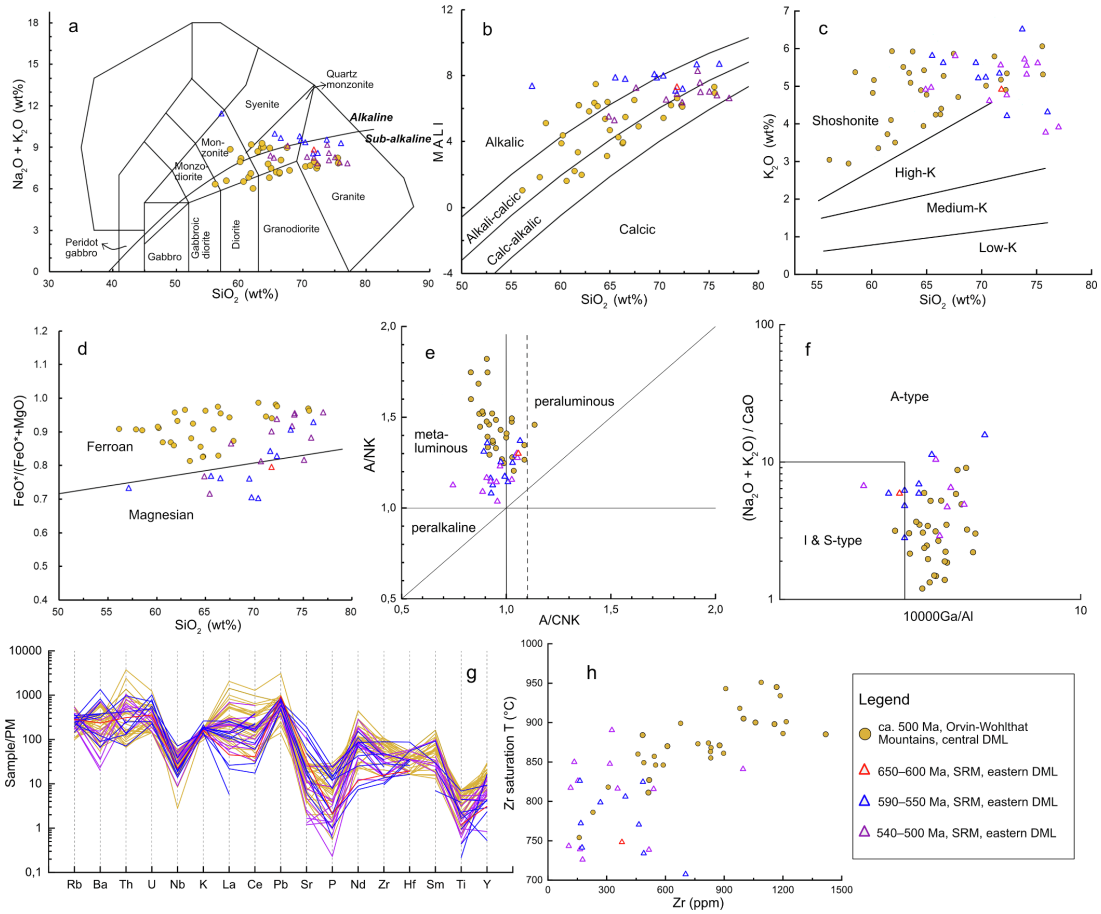

Fig. 6. Geochemical characterisation of late-Neoproterozoic to Cambrian granitic rocks from DML. (a) Discrimination diagram from Middlemost (1994), grey dividing line between alkaline and subalkaline series is from Irvine and Baragar (1971); (b) MALI (modified alkaline lime index, $Na_2O + K_2O$-CaO, wt%) versus SiO_2 diagram of Frost et al. (2001) represents the range varying from alkalic to moderate alkali-calcic to calc-alkalic field of studied samples; (c) SiO_2-K_2O diagram (after Gill, 1981); (d) Fe-index vs. wt% SiO_2 (Frost et al., 2001), showing that most samples plot in the field of ferroan granite; (e) Aluminum saturation index (ASI) plot of Maniar and Piccoli (1989), (Al/Na + K) and (Al/Ca + Na + K) are defined as molecular ratios; (f) 10^4*Ga/Al vs ($Na_2O + K_2O$)/CaO diagram after Whalen et al. (1987) to identify A-type granites from S-or I-type; (g) Primary mantle (PM) normalized trace element spider patterns; (h) Zr vs. Zr saturation temperature diagram, the equation follows Boehnke et al. (2013).

$10^4 * Ga/Al$ (> 2.6), pointing to A-type granites (Whalen et al., 1987) (Fig. 6f). On the primitive mantle-normalized spidergram, all samples are characterized by positive anomalies of Rb, Th, U and LREE (La, Ce, Nd, Sm) as well as Pb, but negative anomalies in Sr, Nb, P and Ti (Fig. 6g). Most samples have a zircon-saturation temperature over 800–850 °C (Fig. 6h).

The granitic samples from SRM are overall similar to the central DML samples in major element composition, and most of them have a geochemical affinity to metaluminous, alkaline to alkali-calcic, ferroan A-type granite; however, a significant subgroup displays a magnesian character and contains lower alkali contents. Generally, the Cambrian samples (540–500 Ma) have a higher SiO_2 and lower alkali concentration than the older 590–550 samples. The trace element concentration and patterns are similar with the central DML samples. Their zircon-saturation temperatures are commonly lower than 850 °C (Fig. 6h).

4.4. Zircon Hf–O isotopic composition

Zircon O and Hf isotopic results are illustrated in Figs. 7 and 8 respectively. The 645–600 Ma charnockites (J1883 and J1886) and anorthosite samples (J1955 and J1958) from the eastern Orvin-Wohlthat Mountains have homogeneous zircon Hf–O isotopic compositions. They are characterized by enriched heavy O isotopic composition with $\delta^{18}O$ values between 8‰ and 9‰ (Fig. 7a); εHf(t) values are mostly neutral with averages between + 0.7 and + 1.4. Zircons grains from a garnet-gneiss sample dated at 636 Ma (J1848) have a similar Hf–O isotopic signature, with εHf(t) values yielding an average of + 1.0 ± 1.4 and $\delta^{18}O$ value of 8–9‰.

The 530 – 485 Ma mafic and granitic samples from the western part of central DML in Gjelsvikfjella (JT19, JT22, 3112–2, 2312–2, JT37) have an average of mantle-like and mildly higher $\delta^{18}O$ values of 5.7–6.5‰ (Fig. 7a). One lamprophyre dyke (2312–2) has unradiogenic εHf(t) values of −4.1—0.9, while the other four samples have

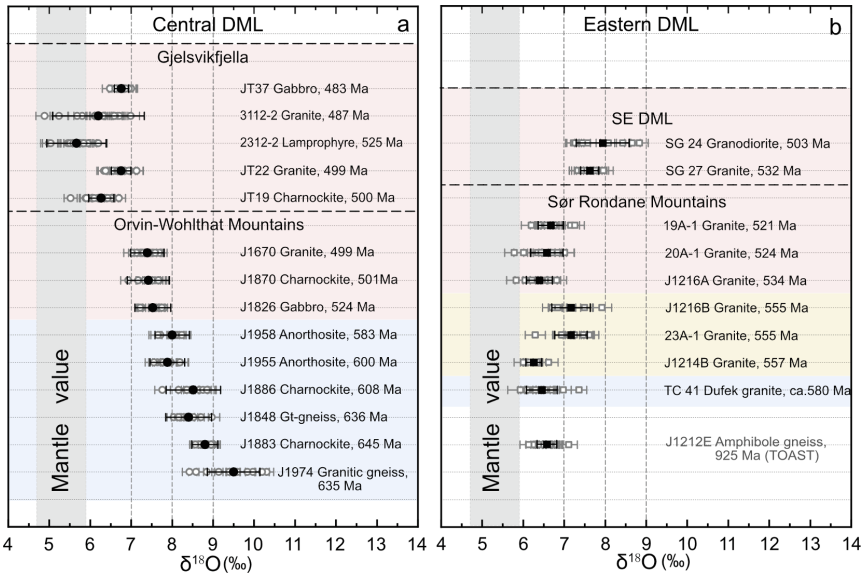

Fig. 7. Zircon oxygen isotope values of 650–485 Ma samples and one ca. 925 Ma (TOAST) sample from central and eastern DML. The grey symbols show individual spot values, whilst the black ones show average values for each sample. Mantle values are 5.3 ± 0.6‰, 2σ (Valley et al., 1998). Light blue, yellow and red colours show > 580 Ma, 570–550 Ma and 530–485 Ma samples respectively. (For interpretation of the references to colour in this figure legend, the reader is referred to the web version of this article.)

significantly evolved Hf isotopic compositions with average εHf(t) of −12 to −7. Similarly, the ca. 500 Ma granitic rocks (J1870, J1670) from the Orvin-Wohlthat Mountains display more evolved Hf isotopic composition with εHf(t) values of −8.8 to −5.6 than the ca. 525 Ma gabbro (J1826, εHf(t) = −3.7 to −1.7) (Fig. 8a), while their $\delta^{18}O$ values are generally moderately elevated at 7.0–8.0‰.

One amphibolite gneiss (J1212E, ca. 925 Ma) of the TOAST and nine granites (610–500 Ma) have been analysed for their zircon Hf and O isotopic compositions. The older TOAST sample has moderately elevated $\delta^{18}O$ values of 6–7‰ and juvenile Hf isotopic compositions (εHf(t) values at ca. + 5.5). Oxygen isotopic compositions of the granites appear to be unrelated to the igneous ages, but largely controlled by their location. Seven granite samples from the SRM mostly have moderate $\delta^{18}O$ values of 6–7‰, but two granites from SE DML have higher $\delta^{18}O$ values between 7 and 9‰ (Fig. 7b). Their Hf isotopes exhibit an obvious variation from Ediacaran to Cambrian times, with the older pre-540 Ma granites showing positive εHf(t) values while the Cambrian granites having negative εHf(t) values of −5 to −1 (Fig. 8b).

4.5. Whole-rock Sm–Nd isotopic composition

Sm–Nd isotopic data of the Cambrian granitic samples from central DML are presented in Table 3, Supplementary File C and are illustrated in Fig. 11b. As ca. 500 Ma marks the most voluminous granitic magmatism in central DML (compiled data in Table 4 of Supplementary File B), this age is used in this study for the calculation of initial Nd isotopic values. Overall, initial εNd values are strongly to moderately unradiogenic with values ranging from −14 to −3, and model ages (T_{DM}) show a wide range from Paleoproterozoic to Mesoproterozoic times (2.1–1.4 Ga). In contrast, the granites from SRM have slightly negative to positive εNd(t) values and younger model ages at ca. 1.2 Ga (Fig. 11b).

5. Discussion

5.1. Late Neoproterozoic to Cambrian geochronological framework of DML

5.1.1. Central DML

The new U–Pb zircon data of this study, together with compiled published geochronological results, provide a refined temporal framework for the late Neoproterozoic to Cambrian magmatic activity in DML. The magmatic and metamorphic ages have been compiled and plotted in Fig. 9, in order to show and compare the distribution of different age groups. Two new igneous crystallization ages of ca. 645 Ma and 630 Ma are obtained from one charnockite augengneiss (J1883) and one garnet gneiss (J1848), which represent the oldest known Neoproterozoic magmatism in central DML (except the Schirmacher Oasis). Subsequently, 610–600 Ma anorthosite and charnockite were emplaced in the Grubergebirge, the easternmost exposures of central DML (Jacobs et al., 1998). The 650–600 Ma charnockite and anorthosite magmatism is accompanied by high-grade metamorphism up to (U)HT-HP granulite facies (Baba et al., 2010). The emplacement of Cambrian magmatic rocks in central DML post-dates 590–560 Ma high-grade metamorphism and migmatization (Jacobs et al., 1998; Pauly et al., 2016), which occurred across almost the entire region (Fig. 9). The reported magmatic ages in this period are rare, possibly in part due to sampling bias, and lack of availability of dated migmatitic rocks from areas such as Gjelsvikfjella. Cambrian magmatism (530–485 Ma) produced a series of granitic rocks, gabbros and mafic dykes across central and western DML. The granitic rocks are exposed throughout central DML, while the gabbro occurrences are relatively small, with the largest massif located at mount Zwiesel, eastern part of the Orvin-Wohlthat Mountains. The oldest post-collisional rocks so far dated is a meta-diorite from central Conrad (530 Ma, Jacobs et al., 2003a), almost synchronous with the gabbro intrusions at mount Zwiesel, which were dated at ca. 525 Ma (this study; Jacobs et al., 2003b). Subsequently, voluminous magmatism, which generated charnockites (J1821, 514 Ma), syenite (512 Ma), anorthosite (506 Ma)

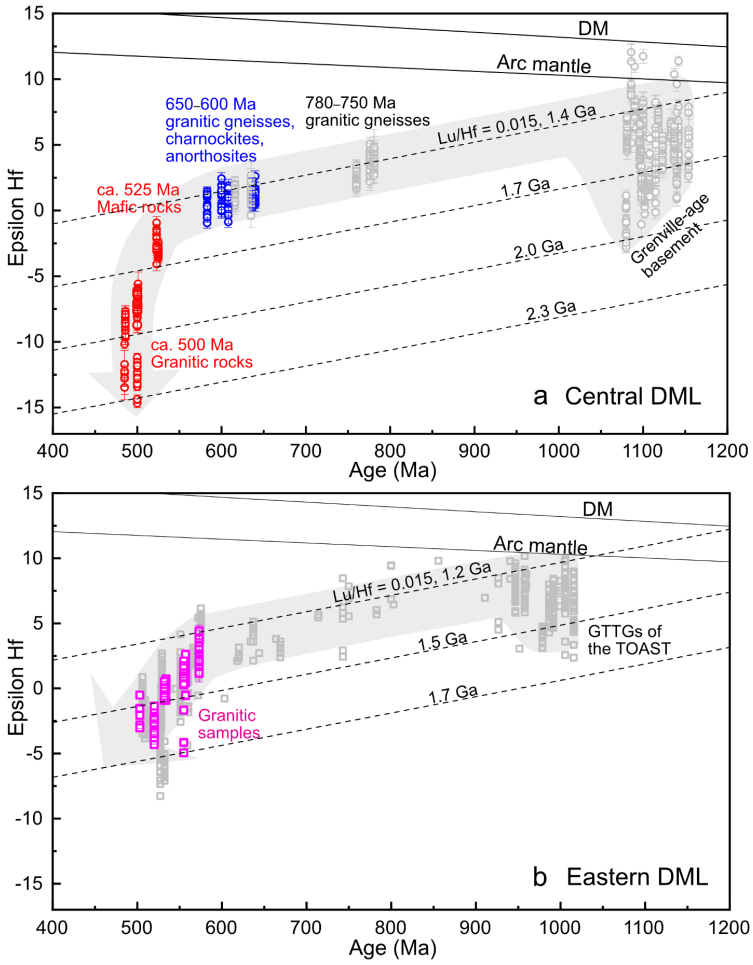

Fig. 8. Time versus εHf(t) plot of samples from central DML (a) and eastern DML (b). The evolution curve of arc mantle is from Dhuime et al. (2011). The Cambrian mafic and granitic rocks from central DML have an evolved Hf isotopic composition. Moreover, εHf(t) values of granitic rocks are significantly lower than mafic rocks. The granites from eastern DML are overall more radiogenic than those from central DML, but show an evolution that negatively deviates from the evolution array of 1.2 Ga crust. The light grey fields show the isotopic trends from the Meso-Neoproterozoic to the Cambrian. The grey samples in (a) show the Hf isotopes of Grenville-age basement in central DML (Wang et al., 2020) and 780–630 Ma gneisses from the Schirmacher Oasis (Jacobs et al., 2020); the grey samples in (b) show the Hf isotopes of 1000–900 Ma TOAST rocks, 650–500 Ma SRM granites as well as the scattered inherited zircons therein (Elburg et al., 2015, 2016).

(Mikhalsky et al., 1997), granites and minor gabbros (500–485 Ma, this study and Jacobs et al., 2008a), accompanied by high-grade metamorphism and anataxis, occurred at 515–485 Ma. These ages thus define an overall continuous period of post-collisional magmatism in central DML from 530 to 485 Ma, accompanied by widespread metamorphism that affected the entire region of western-central DML as very commonly recorded by zircon rims and felsic leucosomes in migmatites.

The Cambrian granitic samples have usually very minor zircon inheritance. Inheritance-poor granitic magmas are usually generated under large heat input into the crust (Miller et al., 2003), which is consistent with the high zircon saturation temperature observed in the central DML samples (Fig. 6h). However, the limited Precambrian inheritance in 515–485 Ma samples in this study appears to differ in the western and eastern parts of central DML. Only older, i.e. ca. 1090–1080 Ma, inherited ages were recorded by the granite and gabbro samples (JT22 and JT37) in Gjelsvikfjella, whereas the inherited zircons from the Orvin-Wohlthat Mountains (J1821, J1825 and J1684) show both Grenville-age (1070–1060 Ma) and late Neoproterozoic (610–600 Ma) ages. The 615–600 Ma crust appears to have comprised an important composition of continental crust in the eastern part of central DML and contributed to the formation of Cambrian magmas. The ages of Cambrian magmatic activities also exhibit a spatial variation from west to east. The reported ages in Gjelsvikfjella are mostly around or younger than 500 Ma (Paulsson and Austrheim, 2003; Jacobs et al., 2003a, 2003b; Bisnath et al., 2006), except one older age at ca. 523 Ma obtained from a lamprophyre dyke (Jacobs et al., 2003a). Similarly, in H.U. Sverdrupfjella, western DML, the granite intrusions were dated at ca. 490–470 Ma (Grantham et al., 2011; Pauly et al., 2016) and older ages have not been reported so far. In contrast, the earlier-stage (530–510 Ma) mafic and granitic magmatism appears to be restricted to the east of the Ulvetanna Lineament.

5.1.2. Eastern DML

The granitic magmatism in the SRM lasted from Neoproterozoic to Cambrian times over a period of approximately 150 Myr with main pulses at 650–600 Ma, 580–550 Ma, ca. 530 Ma, 510–500 Ma, while post-500 Ma zircon U-Pb ages have not been reported so far (Elburg et al., 2016). The 650–600 Ma and 580–550 Ma events correspond to two main metamorphic episodes identified from elsewhere in this region, while 530–500 Ma thermal events are less prominent than in western-central DML. Pre-600 Ma magmatism in the SRM is represented

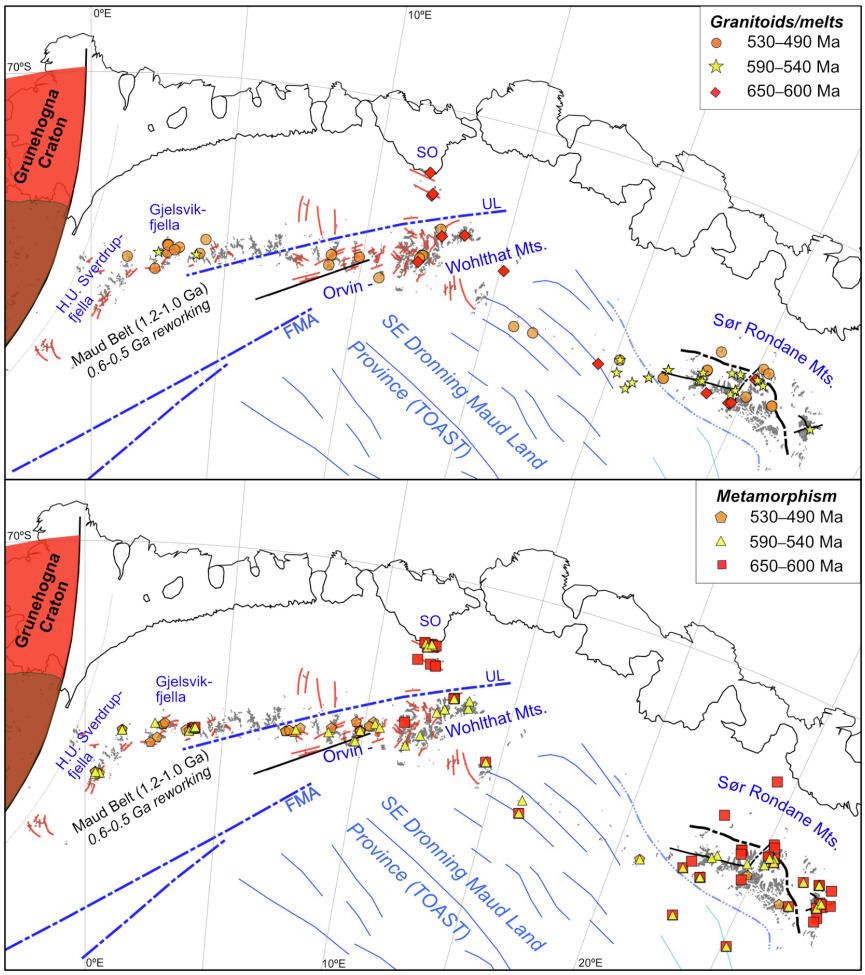

Fig. 9. Distribution of different magmatic and metamorphic age groups in DML. The detailed data list and sources are provided in Tables 4 and 5, Supplementary File B. The abbreviations are the same as in Fig. 2.

by the Dufek granite in the SW Terrane, while combined new and previous data show that the granites in this area have a prolonged magmatic history with a broad range of ages at ca. 640 Ma (Elburg et al., 2016), ca. 620 Ma (Li et al., 2006), ca. 610 Ma to ca. 590 Ma (this study). The 580–550 Ma magma activity is characterized by bimodal magmatism, producing granites and minettes (Owada et al., 2013; Elburg et al., 2016). Neoproterozoic inheritance of 1000–900 Ma and 800–700 Ma are present (Elburg et al., 2016).

5.2. Isotopic and geochemical perspective on magmatism in central DML

5.2.1. Late Neoproterozoic charnockite and anorthosite

Charnockites and anorthosites are mainly exposed in the easternmost part of the Orvin-Wohlthat Mountains (Fig. 2), and they commonly have significantly enriched (heavy) O isotopic compositions ($\delta^{18}O$ = 7.5–9.5‰) and slightly negative to positive $\varepsilon Hf(t)$ values (−1 to +3). This implies that a considerable amount of older supracrustal material was most likely recycled into the 650–600 Ma magmas. Although some studies proposed that anorthosites are impossible to derive from purely crustal sources (e.g., Ashwal and Bybee, 2017), mantle-derived magmas are frequently contaminated by crustal components to various degrees during magma ascent. Enriched heavy O isotopes in anorthosites have been interpreted to be obtained from the assimilation of crustal components, or enriched sub-continental lithospheric mantle, or both. For example, Peck et al. (2010) reported 1.3 Ga Grenvillian anorthosites with high magmatic $\delta^{18}O$ (whole rock) values of 8–11‰ and attributed this to the involvement of oceanic crust during subduction; Heinonen et al. (2015) presented high $\delta^{18}O_{zrn}$ values (6.3–7.8‰) of 1.64 Ga Fennoscandian anorthosite that could be derived from the metasomatised subcontinental lithospheric mantle with a higher $\delta^{18}O$ value than the depleted mantle. In this study, it is possible that the mantle had been metasomatised by heavy $\delta^{18}O$ flux, which usually derived from the subducted oceanic slab, and contributed to enriched Hf and heavy O isotopic signatures of the 650–600 Ma charnockite-anorthosite magmas. However, the metasomatised mantle alone appears unable to produce a high enough shift in oxygen isotope as observed in this study (Eiler et al., 2000; Harris et al., 2015). An alternative explanation is that significant amounts of high $\delta^{18}O$

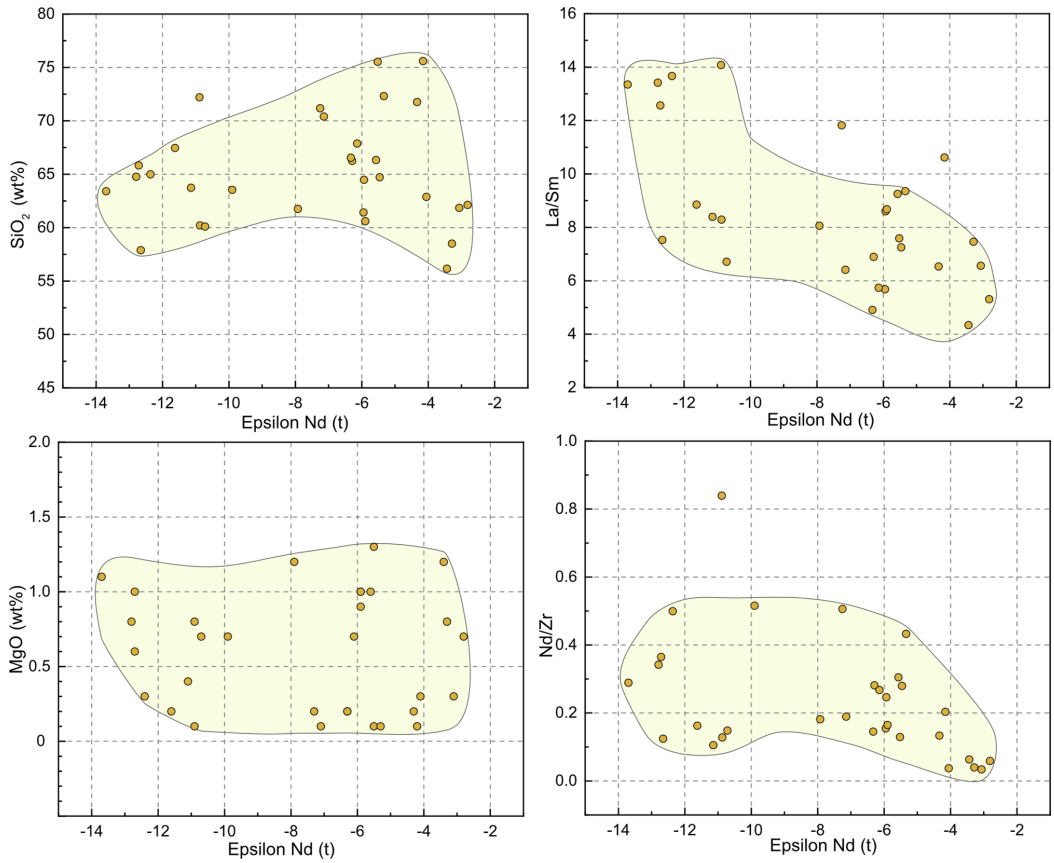

Fig. 10. Initial εNd values versus SiO_2, MgO, La/Sm and Nd/Zr of Cambrian granitic samples from the Orvin-Wohlthat Mountains (central DML). The light yellow fields show the range of the majority of the analysed samples. (For interpretation of the references to colour in this figure legend, the reader is referred to the web version of this article.)

sedimentary material from the overlying crust were involved in 650–600 Ma magmas, and these sediments were originally from the subducted oceanic slab and attached to the lower crust of the eastern margin of the Kalahari Craton by subduction undeplating (Von Huene and Scholl, 1991). It is thus preferred here that high $\delta^{18}O$ crustal material played an important role in the formation of charnockite and anorthosite magmas, while the input of mantle-derived magma is uncertain, since its isotopic composition remains ambiguous.

5.2.2. Cambrian granitic and mafic rocks

The 515–485 Ma quartz monzonite and granite samples in central DML generally show metaluminous and ferroan-potassic signatures (Fig. 6d, e). They have high incompatible trace element contents such as LREE, Zr and Nb, and plot in the field of A-type granites in the discrimination diagrams (Fig. 6f). Most samples have a zircon-saturation temperature over 850 °C (Fig. 6h), in line with the formation condition of typical A-type granites. The granitic rocks with these characteristics in major and trace element composition are classified as “ferro-potassic” (Fe-K) granitoids, which are generally formed during late- and post-collisional orogenic events (Sylvester, 1989; Ferré et al., 1998; Laurent et al., 2014). However, their source composition, specifically the respective contribution from the mantle and crust-derived components, varies in different orogenic systems. Most studies ascribe its origin to the re-melting of pre-existing continental crust, either juvenile or old crust (e.g., Tagne-Kamga, 2003; Duchesne et al., 2010), while a derivation from metasomatised mantle with varying degrees of crustal contamination has also been proposed to interpret the petrogenesis of the late-Archean granitoids (e.g., Laurent et al., 2014).

The 500–485 Ma granitic samples from Gjelsvikfjella and the Orvin-Wohlthat Mountains in central DML show significantly evolved Hf isotopic compositions (Fig. 8a). The εHf(t) values of the samples from the latter region range from −10 to −5, corresponding to two-stage model ages between 2.0 and 1.8 Ga, while Hf isotopic compositions of some Gjelsvikfjella samples are more evolved with εHf(t) values of −15 to −10 (Fig. 11d). One ca. 485 Ma gabbro (JT37) from Gjelsvikfjella has similarly unradiogenic Hf isotopic values (−14 to −11) with the granitic rocks in this region. Their clear difference from 525 Ma mafic rocks in Hf isotopic composition indicates that the granitic and mafic rocks were derived from different sources, precluding the possibility that the granites were formed by the fractional crystallization of the mafic magmas. Furthermore, the paucity of mafic enclaves indicates that mafic additions and interaction with granitic magmas must have been insignificant, and the presence of Grenville-age and Neoproterozoic inherited zircons supports a large contribution from older continental crust. Some Gjelsvikfjella samples have even lower εHf(t) values than the extrapolated Hf isotope values of the Grenville-age

basement at ca. 500 Ma (Fig. 8a). This probably indicates an additional contribution of continental material that is isotopically more evolved than Grenville-age basement in this region, such as the Paleoproterozoic to Archean crust underlying the Kalahari Craton at its eastern side (Marschall et al., 2013; Wang et al., 2020). This indicates that older crust at the margin of the Kalahari Craton played a vital role in the genesis of the Cambrian post-collisional granitic magmas. Major element geochemistry of high-silica ferroan, calc-alkalic to alkali-calcic signatures of most samples indicate they were likely derived from anhydrous melting of intermediate metaigneous rocks under reducing conditions (Frost and Frost, 2008).

The ca. 500 Ma granitic samples from Gjelsvikfjella and the Orvin-Wohlthat Mountains show a clear difference in O isotopic signatures. The former is characterized by $\delta^{18}O$ values close to the mantle range, while the latter has higher $\delta^{18}O$ values at 7.0–8.0‰ (Fig. 7a). Their O isotopic compositions reflect an inheritance from the Grenville-age basement in these two regions, as the O isotopic composition of the Grenville-age crust is generally mantle-like (5.5–6.0‰) in Gjelsvikfjella, whereas it is moderately higher than mantle value in the Orvin-Wohlthat Mountains (Wang et al., 2020).

The Nd isotope values of > 40 granitic samples from central DML show a wide range from −14 to −3 with Nd model ages (T_{DM}) ranging from 2.1 to 1.4 Ga (Fig. 11b). In the εNd(t) vs. SiO_2 and trace element ratio diagrams (Fig. 10), the εNd(t) values appear to be broadly positively correlated to SiO_2 and negtively correlated to La/Sm, but no obvious correlation with other major elements and trace element ratios, such as MgO and Nd/Zr, is observed. This indicates that a simple two-endmember mixing model seems to be inappropriate to interpret the generation of granitic magmas here. Overall, the Cambrian granitic rocks probably derived from a mixture of multiple Precambrian crustal components, and the heterogeneous crustal compositions varied in different regions of central DML. For example, samples from the Conrad mountain, in the western part of the Orvin-Wohlthat Mountains, show significantly evolved Nd isotopic compositions with initial εNd values lower than −10 (Table 3 of Supplementary File C), more enriched than the recalculated Nd isotopic compositions of the Grenville-age basement to 500 Ma (Fig. 11b). In contrast, Holtedahlfjella samples generally have εNd(t) values of −6–-4, which are in the range of the εNd(t) values of the Grenville-age basement at ca. 500 Ma (Fig. 11b). The complexity of the continental crust in central DML is also revealed by isotopic compositions of the Grenville-age basement rocks, as they exhibit both juvenile and highly evolved Hf and Nd isotopes, indicating the co-existence of juvenile Mesoproterozoic crust and older crustal components (Wang et al., 2020).

The ca. 525 Ma gabbro and lamprophyre dyke (J1826, 2312–2) yield a more radiogenic Hf isotopic composition than ca. 500 Ma granitic samples but with negative εHf(t) values of −4– −2, which can be explained either as their primitive melts derived from an enriched mantle source (lithospheric mantle metasomatized by recycled crustal materials) or melts derived from the depleted (asthenospheric) mantle with significant crustal contamination. These samples (SiO_2 = 43–50%) are enriched in compatible elements (Fe, Mg, Cr, Ni), and have a low content of incompatible elements (K_2O, HFSE, LREE), which makes the first explanation more likely although crustal contamination cannot be excluded. This is consistent with a previous study (Owada et al., 2008) that interpreted similarly-aged lamprophyre and lamproite rocks in the Mühlig-Hofmann Mountains to have derived from the enriched mantle. In addition, enriched Sr–Nd–Pb–O isotopic compositions of ca. 455 Ma minettes from the Schirmacher Oasis also indicate the existence of metasomatized lithospheric mantle beneath central DML (Hoch et al., 2001), although when and how mantle enrichment took place remains uncertain. Recent modelling reveals that post-collisional (ultra)mafic magmatism largely originated from a mantle source, which, however, is often not reflected by Hf–O isotopic compositions, since even a small proportion (10–20%) of continental material or melts/fluids generated from them interacting with the mantle would drive Hf isotopic composition to a crust-like signature and also O isotope above the mantle value (Couzinié et al., 2016). Therefore, we prefer to interpret the ca. 525 Ma mafic magmas to have been derived from an enriched mantle source that most likely acquired its enriched isotopic composition during the Precambrian subduction events.

In summary, the isotopic and geochemical data presented here support the view that 515–485 Ma granitic rocks in central DML were largely derived from the remelting of pre-existing continental crust, while the ca. 525 Ma mafic magmas, which have more radiogenic Hf isotopes, most likely derived from an enriched mantle source that was metasomatised by earlier subduction processes. This is typical for postorogenic and post-collisional magmatism (Bonin, 2004).

5.3. Isotopic signatures of granites in eastern DML

The Hf and Nd isotopes of 650–500 Ma granites from the SRM exhibit overall more juvenile signatures than synchronous samples from central DML (Fig. 11b, c). Their εHf(t) values are dominantly between −5 and + 5 (this study; Elburg et al., 2016), and the array of them, especially for the pre-540 Ma samples, broadly follows the evolution trend of GTTGs of the TOAST (Fig. 8b). They mostly have εNd(t) values of −3 to +2 and late Mesoproterozoic Nd model ages, in contrast to the significantly negtive εNd(t) values and Archean to Paleoproterozoic model ages of most central DML samples (Fig. 11b). The $\delta^{18}O$ values are mostly between 6 and 7‰, more 'mantle-like' than samples from the eastern part of central DML (Fig. 7b). These differences in Hf–Nd–O isotopes are closely related to the varying isotopic signatures of the Precambrian basement from west to east. Compared to the Grenville-age basement in western-central DML (Fig. 8a), the TOAST rocks overall have more homogeneous and juvenile Hf isotopic compositions with most εHf(t) values of + 5 to +10 (Fig. 8b), and an average of mildly elevated $\delta^{18}O$ value at around 6.5‰ (sample J1212E, Fig. 7b).

Hf and Nd isotopic compositions as well as whole-rock geochemistry of the granites in eastern DML show a variation from late Neoproterozoic to Cambrian times. The Ediacaran samples generally have suprachondritic Hf and Nd isotope signatures, while the post-540 Ma granites have a more evolved radiogenic isotopic composition with negative εHf(t) and εNd(t) values (Fig. 11b and c). The initial εHf values of ca. 600–500 Ma granites in this study display a trend that gradually decreases and deviates from the secular evolution of TOAST crust (Fig. 8b), and a similar isotopic pattern is also revealed by Elburg et al. (2016). This can be interpreted as the increasing involvement of pre-existing, old continental material, especially for the post-540 Ma samples. In addition, a higher SiO_2 concentration and lower alkalic geochemistry as well as higher zircon saturation temperatures observed in Cambrian rocks compared to older samples (Fig. 6a–c, h) is consistent with the formation of the former by remelting more continental material. It is not excluded that juvenile input may have played a considerable role in the formation of the late Neoproterozoic granites, its contribution, however, diminished in Cambrian times.

The 570–550 Ma igneous activity in the SRM produced coeval lamprophyre dykes, minettes and syenites (Lunckeryggen) at ca. 560 Ma, which have evolved Nd isotopic composition (εNd(t) values around 0) and have been interpreted as derived from an enriched mantle (Li et al., 2003, 2006; Owada et al., 2008, Owada et al., 2013). These rocks were further interpreted to have formed under an extensional setting with an elevated geothermal gradient due to the upwelling of the asthenosphere and thinning of the lithosphere (Owada et al., 2013). In this study, however, high silica concentration, neutral εHf(t) and mildly elevated $\delta^{18}O$ values (7%) of 560–555 Ma samples (Fig. 7) suggest that these granitic magmas contain significant involvement of crustal components of the TOAST. The relevant post-530 Ma samples are distributed across SE DML and the SW Terrane of the SRM, and a broad trend that the εHf(t) values are more unradiogenic from west to east was revelaed by Elburg et al. (2016). In this study, two granites from SE DML yield higher $\delta^{18}O$ values (7.5–8‰) than samples from the

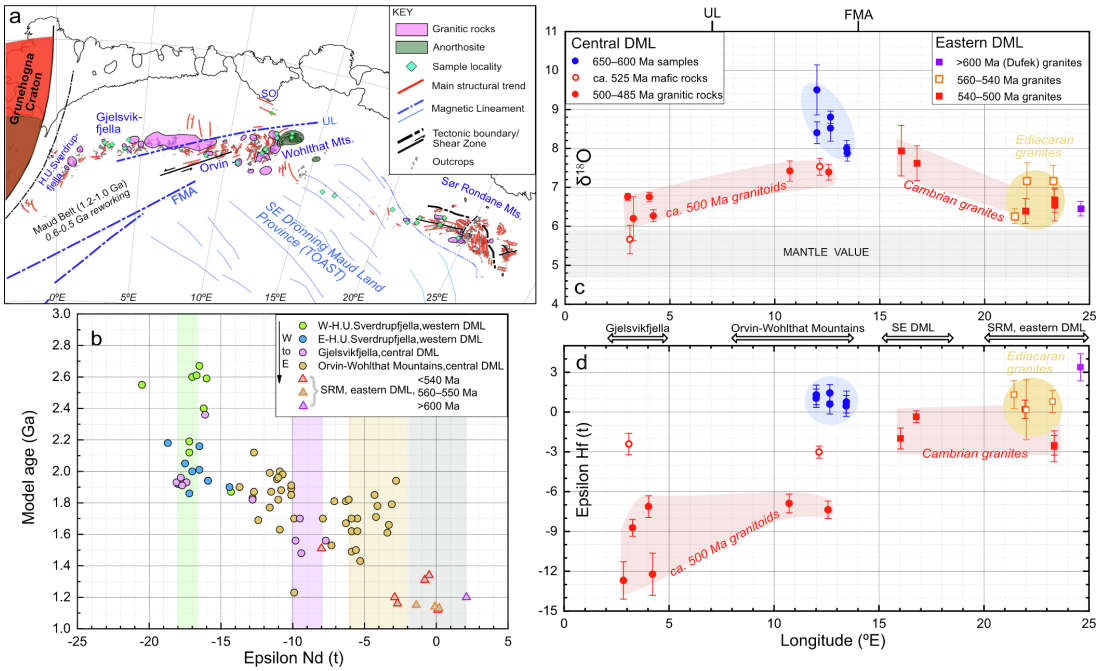

Fig. 11. (a) Geological overview map of DML and sampled Hf-O isotopic profile along the DML mountain range; (b) Nd model ages versus initial epsilon values of Cambrian granitic samples from H.U. Sverdrupfjella (western DML) across central DML to SRM (Table 3 in Supplementary File C). The Nd isotopic data of H.U. Sverdrupfjella, Gjelsvikfjella and the Orvin-Wohlthat Mountains are from Moyes (1993), Moyes et al. (1993b), Paulsson and Austrheim (2003), Markl and Henjes-Kunst (2004), Grantham et al. (2019) and this study; the Nd isotopic data of eastern DML are from Jacobs et al. (2015) and this study; the light green, purple yellow and gray bars indicate the range of εNd(t) values of the Precambrian basement in H.U. Sverdrupfjella, Gjelsvikfjella, the Orvin-Wohlthat Moutains and eastern DML respectively when calculated at Cambrian times (Table 4 in Supplementary File C); Sm-Nd isotopic data of basement rocks are from Moyes (1993), Wareham et al. (1998), Paulsson and Austrheim (2003), Jacobs et al. (1998), Kamei et al. (2013), Jacobs et al. (2015) and Elburg et al. (2015); (c,d) O and Hf isotopic composition and variation from Gjelsvikfjella to SRM, see text for detailed explanations. (For interpretation of the references to colour in this figure legend, the reader is referred to the web version of this article.)

SRM (< 7‰) (Fig. 11c). The varied Hf and O isotopes of the Cambrian granites in eastern DML probably indicate different source regions of old continental components, which could be from the Kalahari Craton, Indo-Antarctica or the Valkyrie Craton (Fig. 2).

5.4. Tectonic evolution in DML during Gondwana assembly

Our new zircon U–Pb–Hf–O and whole-rock Nd isotopic data provide detailed insights into the protracted tectonic processes of two major crustal domains, western-central DML and eastern DML that are separated by the Forster Magnetic Anomaly. Western-central DML is underlain by Grenville-age basement, whilst eastern DML is underlain by the TOAST. In late Neoproterozoic times, the two crustal domains largely record different crustal evolutions, whilst from ca. 590 Ma onwards the geological processes overall record a common tectono-metamorphic history, reflected by commonly extensive high-grade metamorphism, migmatisation and granitic magmatism (Fig. 9).

In western-central DML, evidence for a retreating accretionary continental margin comes from 650 to 600 Ma charnockites, anorthosites and granodiorites at the eastern periphery of the Kalahari Craton, close to the Forster Magnetic Anomaly. These igneous rocks commonly have highly elevated O (8–9‰) and radiogenic Hf isotopic compositions (εHf(t) = 0 to +2), distinct from the significantly unradiogenic Hf and mantle-like to moderately high O isotopic values of the later Cambrian granitic rocks (Fig. 11c, d). This demonstrates that the sources they were derived from are different. The 650–600 Ma magmas most likely involved significant amounts of high $\delta^{18}O$ sedimentary components at the eastern margin of the Kalahari Craton. The eastern margin of the Kalahari Craton has been an active continental margin in the Neoproterozoic, such as during late Tonian times, at ca. 785–760 Ma (e.g., Jacobs et al., 2020). The eastern Kalahari Craton margin repeatedly changed from an advancing to a retreating continental margin and vice verca during the Neoproterozoic. The ca. 650 Ma charnockite magmatism (J1883, this study) is accompanied by UHT metamorphism (950–1050 °C, 0.9–1.0 GPa, Baba et al., 2006, 2010) in the Schirmacher Oasis, probably indicating subduction roll-back and a back-arc environment (e.g., Baba et al., 2010; Jacobs et al., 2020). The formation of 610–600 Ma anorthosites, charnockites and granodiorites accompanied by high-grade metamorphism recorded by metamorphic zircon rims (Jacobs et al., 2020 and unpublished data) may relate to the inversion of the back-arc basin.

In western-central DML, the Nd isotopic compositions of Cambrian granitic rocks exhibit a clear spatial variation from H.U. Sverdrupfjella (western DML) to the Orvin-Wohlthat Mountains (central DML) (Fig. 11b), indicating that the composition and/or proportion of involved crustal components have varied significantly. The westernmost part of western DML (western H.U. Sverdrupfjella) is characterised by Archean Nd model ages of 2.7–2.5 Ga, while samples from eastern H.U. Sverdrupfjella and Gjelsvikfjella mostly yield Paleoproterozoic model ages. Further east, Nd model ages of samples from the Orvin-Wohlthat Mountains have a wide range from 2.1 to 1.4 Ga. The trend that Nd isotopes are increasingly more radiogenic towards the east (towards the

margin of the Kalahari Craton) is consistent with the regional trends of the Hf and Nd isotope signatures of the Grenville-age basement (Wang et al., 2020), although the Nd isotopic compositions of part of the Cambrian intrusions in central DML appear to be more enriched than those of the Grenville-age basement calculated at Cambrian times (Fig. 11b). In contrast, the ca. 525 Ma mafic magmas (garbbros and lamprophyres), which have more juvenile Hf isotopic signatures than the voluminous ca. 500 Ma granitic rocks, are most likely derived from an enriched mantle source. This magma formation mechanism supports the tectonic process proposed by previous studies, that the delamination of an orogenic root removed part of the lithospheric mantle and induced extensive melting in the upper lithospheric mantle and in the continental crust, producing large-scale post-collisional magmatism (Jacobs et al., 2003b, 2008). The magmas that gave rise to the restricted ca. 525 Ma mafic rocks in central DML probably formed at the start of lithosphere mantle delamination, while the widespread post-collisional magmatism that re-melted the overlying continental crust occurred subsequently at ca. 500 Ma.

In eastern DML, the Ediacaran-Cambrian granites have unsurprisingly more radiogenic Hf–Nd isotopic compositions (Fig. 11b, d), as the Tonian basement in eastern DML (TOAST) is more juvenile than the Grenville-age crust in central DML (Fig. 8). The radioactive isotope composition of the granites from eastern DML is characterised by a dramatic decrease in Hf and Nd isotopic values of Cambrian granites compared with older samples, which indicates the increased involvement of evolved continental material after 540 Ma. The juvenile Hf isotopes of the 640–600 Ma Dufek granites indicate that the TOAST was rather isolated in the Mozambique Ocean with very limited input of old continental crustal in early Ediacaran times. It clearly developed on an independent subduction system than the synchronous subduction system at the periphery of the eastern Kalahari Craton. The subduction system that affected the TOAST was contractional as evident by the overthrusting of the NE Terrane onto the SW Terrane in the SRM (e.g., Adachi et al., 2013). The increasing input of older crustal components after ca. 540 Ma suggests that the TOAST had become wedged between adjacent older cratons latest by Cambrian times. The subsequent delamination and orogenic collapse, which mainly happened in central DML, also influenced eastern DML to some extent and resulted in the Cambrian magmatism.

Western-central and eastern DML obviously underwent different crustal evolutions before ca. 590 Ma and were not joint by that time. However, subsequent 590–550 Ma high-grade metamorphism and migmatisation is widespread and quite uniform across entire DML (Fig. 9), including the Lützow-Holm Bay to the east (Tsunogae et al., 2014, 2015). This tectono-metamorphic episode most likely represents the main period of crustal thickening in the southern part of the EAAO, during which various cratons and terranes, including the Kalahari Craton, the TOAST, Indo-Antarctica and probably the Valkyrie Craton finally amalgamated (Fig. 12). This scenario is consistent with the tectonic evolution in the central EAAO. Recent work on the 580–540 Ma high-grade metamorphism such as in Madagascar and south India suggests that the intervening Mozambique Ocean were not completely closed until ca. 550 Ma or even later (Armistead et al., 2020; Boger et al., 2015; Yeshanew et al., 2017; Clark et al., 2020). Thus, in late Neoproterozoic times, DML is dominated by E-W oriented (present coordinates) convergent tectonics that led to the final closure of the Mozambique Ocean at the transition from Neoproterozoic to Cambrian times. Post-collisional delamination and collapse caused widespread magmatism and associated metamorphism in an overall extensional setting. The late Neoproterozoic to Cambrian rocks in DML thus record an orogenic cycle from subduction-accretion, continental collision to post-collisional process during and after the assembly of Gondwana.

6. Summary and conclusions

DML preserves an extensive record of late Neoproterozoic–Cambrian magmatic and metamorphic activity associated with the closure of the Mozambique Ocean and the assembly of Gondwana. New and compiled published geochronology data indicate that central and eastern DML have distinct magmatic and metamorphic history and probably did not join before ca. 590–550 Ma. In late Neoproterozoic times (ca. 650–600 Ma), central DML formed a retreating accretionary continental margin along the eastern Kalahari Craton with extensive records of anorthosite and charnockite magmatism and accompanied UHT metamorphism. In contrast, eastern DML records granite magmatism, crustal stacking and associated granulite facies metamorphism at the same time that probably resulted from the collision of the TOAST with the Valkyrie Craton. Common pervasive tectono-metamorphism of central and eastern DML is recorded from ca. 590 Ma onwards, although the associated magmatic record differs somewhat in the two broadly different regions. Whilst eastern DML records long-term and continuous magmatism from ca. 650 to 500 Ma, central DML is dominated by voluminous late-tectonic magmatism between ca. 530–485 Ma.

The 650–600 Ma anorthosite and charnockite samples in easternmost central DML (eastern periphery of the Kalahari Craton) have slightly positive εHf(t) (0 to +2) and heavy $\delta^{18}O$ values (8–9‰), indicating a large involvement of high $\delta^{18}O$ crustal components. The reason for this is likely that the long-term active continental margin setting of the easternmost Kalahari Craton allowed for the addition of sedimentary material. The initial Cambrian magmatism in central DML is marked by mafic magmas at ca. 525 Ma, followed by very voluminous granitic magmas across the entire region at ca. 515–485 Ma. The granitic rocks generally have enriched Hf isotopic compositions with εHf(t) values of −10 to −6 and mildly elevated $\delta^{18}O$ values. Their Nd isotopes show a regional variation towards radiogenic values from west to east, with model ages varying from the Archean to Mesoproterozoic, which is consistent with the isotopic trend of the Grenville-age crust in this region. As such, the Cambrian granitic magmas are interpreted to have mainly derived from the re-melting of pre-existing continental crust.

Compared to the Cambrian granitic rocks from central DML, the late Neoproterozoic-Cambrian granites from the SRM of eastern DML have more juvenile Hf isotopic compositions associated with O values closer to the mantle range, which points to a distinct source, most likely the TOAST crust. The 640–600 Ma granites in eastern DML (Dufek granites) have more juvenile Hf and Nd isotopic compositions than the post-540 Ma granites, indicating that the TOAST crust was in the vicinity of, and probably had been sandwiched in between, other continental fragments by Cambrian times. The increasingly negative εHf(t) values in the Cambrian are interpreted to document the change in tectonic setting from subduction accretion to continental collisions.

Therefore, the first detailed zircon U–Pb–Hf–O and new whole-rock Nd isotopic data of late Neoproterozoic to Cambrian igneous rocks in western-central and eastern DML provide a significantly improved understanding of the tectonic setting that led to the amalgamation of DML and East Antarctica. It is significant to note that the eastern margin of Kalahari and the TOAST developed on two independent subduction systems in late Neoproterozoic times. The accretion and assembly of the TOAST to the Kalahari Craton and collision with surrounding continental blocks (i.e. Indo-Antarctica and Valkyrie Craton) probably happened in late Ediacaran times, which marks the closure of the Mozambique Ocean and the amalgamation of Gondwana. Subsequently, DML was affected by extensive post-collisional magmatism due to delamination tectonics and orogenic collapse in Cambrian times, resulting in voluminous A-type granitic rocks, which generally have crustal characteristics as revealed by their isotopic and geochemical signatures.

CRediT authorship contribution statement

Cheng-Cheng Wang: Conceptualization, Methodology, Formal analysis, Investigation, Writing - original draft, Writing - review & editing, Visualization, Funding acquisition. **Joachim Jacobs:**

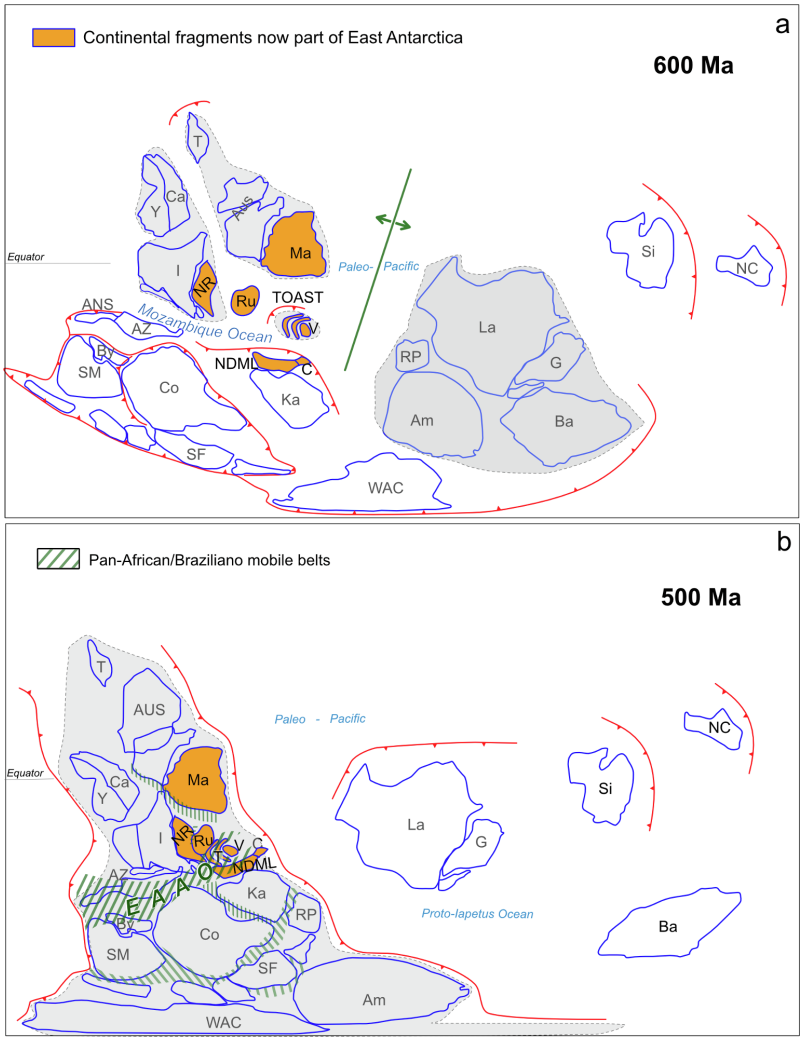

Fig. 12. Continental reconstructions at 600 and 500 Ma, indicating the various East Antarctic continental fragments (orange) with African, Australian, Indian and Laurentian heritage as well as juvenile crust such as the TOAST that joined during the assembly of Gondwana (based and modified after Merdith et al., 2017). a) By 600 Ma the Paleo-Pacific was still expanding, whilst the Mozambique Ocean was near to closure. Different parts of DML are characterized by different subduction zone systems, probably no continental collision so far. b) By 500 Ma, Gondwana had assembled along a network of Pan-African/Braziliano mobile belts, of which the East African-Antarctic Orogen (EAAO) appears to be one of the major ones, stretching from the Arabian Nubian Shield, along East Africa into East Antarctica. In DML, the best age estimate for continental collision between the Kalahari Carton, the TOAST, the Ruker Craton and an Indo-Antarctic block is ca. 590–550 Ma. Abbreviations: Am, Amazonia; Aus, Australia; AZ, Azania; Ba, Baltica; By, Bayuda block; SC, South China; C, Coats Land Block; Ca, Cathaysia; Co, Congo; G, Greenland; I, India; Ka, Kalahari; La, Laurentia; M, Madagascar; Ma, Mawson; NC, North China; NDML, Nampula-Dronning Maud Land (western-central); NR, Napier-Rayner (Antarctica); RP, Rio de la Plata; Ru, Ruker Craton, SF, Sao Francisco; Si, Siberia; SM, Sahara Metacraton; TOAST, Tonian Oceanic Arc Super Terrane; V, Valkyrie Craton; WAC, West African Craton; Y, Yangtze. (For interpretation of the references to colour in this figure legend, the reader is referred to the web version of this article.)

Conceptualization, Investigation, Resources, Writing - review & editing, Visualization, Supervision, Project administration, Funding acquisition. **Marlina A. Elburg:** Investigation, Writing - review & editing, Funding acquisition. **Andreas Läufer:** Writing - review & editing, Funding acquisition. **Synnøve Elvevold:** Resources, Writing - review & editing.

Declaration of Competing Interest

The authors declare that they have no known competing financial interests or personal relationships that could have appeared to influence the work reported in this paper.

Acknowledgements

This work was financially supported by faculty-specific funds and endowments of the Faculty of Mathematics and Natural Sciences, University of Bergen (NO. 812378), and was partly supported by the Research Council of Norway through the funding to The Norwegian Research School on Dynamics and Evolution of Earth and Planets (NO. 249040/F60). C-C. Wang is grateful to the support from the China Scholarship Council. J. Jacobs thanks for continued field support of the Alfred-Wegener Institute Helmhotz Centre of Polar and Marine Research (AWI), Bremerhaven, the Federal Institute for Geosciences and Natural Resources (BGR), Hannover and the Norwegian Polar Institute, Tromsø. N.W. Roland is thanked for providing samples from central DML for Sm–Nd isotopic analyses. We thank I.C. Kleinhanns for providing unpublished major and trace element (eastern DML) and Sm–Nd isotope data (central and eastern DML). We thank M. Whitehouse and his team for their help with SIMS zircon U–Pb–O isotopic analyses, P. Montero and F. Bea for their help with SHRIMP U–Pb–O analyses. The MC-ICP-MS lab at UJ was funded by NRF-NEP grant 93208, and is supported by DSI-NRF CIMERA. M. A. Elburg acknowledges NRF IFRR funding (No. 119297). Two anonymous reviewers are thanked for their constructive and insightful comments that greatly improved the quality of the manuscript. We thank editor V. Pease for her efficient handling of this paper. This is IBERSIMS

publication #73 and NORDSIM publication #654.

Appendix A. Supplementary data

Supplementary data to this article can be found online at https://doi.org/10.1016/j.precamres.2020.105880.

References

Adachi, T., Osanai, Y., Hokada, T., Nakano, N., Baba, S., Toyoshima, T., 2013. Timing of metamorphism in the central Sør Rondane Mountains, eastern Dronning Maud Land, East Antarctica: Constrains from SHRIMP zircon and EPMA monazite dating. Precambr. Res. 234, 136–160.

Archibald, D.B., Collins, A.S., Foden, J.D., Payne, J.L., Holden, P., Razakamanana, T., 2019. Late syn-to post-collisional magmatism in Madagascar: The genesis of the Ambalavao and Maevarano Suites. Geosci. Front. 10, 2063–2084.

Armistead, S.E., Collins, A.S., Redaa, A., Jepson, G., Gillespie, J., Gilbert, S., Blades, M.L., Foden, J.D., Razakamanana, T., 2020. Structural evolution and medium-temperature thermochronology of central Madagascar: Implications for Gondwana amalgamation. J. Geol. Soc.

Ashwal, L.D., Bybee, G.M., 2017. Crustal evolution and the temporality of anorthosites. Earth Sci. Rev. 173, 307–330.

Baba, S., Owada, M., Grew, E.S., Shiraishi, K., 2006. Sapphirine granulite from Schirmacher Hills, central Dronning Maud Land. In: Fütterer, D.K., Damaske, D., Kleinschmidt, G., Miller, H., Tessensohn, F. (Eds.), Antarctic Contributions to Global Earth Science. Springer, Berlin, pp. 37–44.

Baba, S., Owada, M., Shiraishi, K., 2008. Contrasting metamorphic P-T path between Schirmacher Hills and Mühlig-Hofmannfjella, central Dronning Maud Land, East Antarctica. Geological Society, London, Special Publication 308, 401–417.

Baba, S., Hokada, T., Kaiden, H., Dunkley, D.J., Owada, M., Shiraishi, K., 2010. SHRIMP zircon U-Pb dating of sapphirine-bearing granulite and biotite-hornblende gneiss in the Schirmacher Hills, east Antarctica: Implications for Neoproterozoic ultrahigh-temperature metamorphism predating the assembly of Gondwana. J. Geol. 118, 621–639.

Baba, S., Osanai, Y., Nakano, N., Owada, M., Hokada, T., Horie, K., Adachi, T., Toyoshima, T., 2013. Counterclockwise P-T path and isobaric cooling of metapelites from Brattnipene, Sør Rondane Mountains, East Antarctica: Implications for a tectonothermal event at the proto-Gondwana margin. Precambr. Res. 234, 210–228.

Baba, S., Horie, K., Hokada, T., Owada, M., Adachi, T., Shiraishi, K., 2015. Multiple collisions in the East African-Antarctica Orogen: Constraints from timing of metamorphism in the Filchnerfjella and Hochlinfjellet terranes in central Dronning Maud Land. J. Geol. 123, 55–77.

Bingen, B., Jacobs, J., Viola, G., Henderson, I.H.C., Skår, Ø., Boyd, R., Thomas, R.J., Solli, A., Key, R.M., Daudi, E.X.F., 2009. Geochronology of the Precambrian crust in the Mozambique belt in NE Mozambique, and implications for Gondwana assembly. Precambr. Res. 170, 231–255.

Bisnath, A., Frimmel, H.E., 2005. Metamorphic evolution of the Maud Belt: P-T–t path for high-grade gneisses in Gjelsvikfjella, Dronning Maud Land, East Antarctica. J. Afr. Earth Sci. 43, 505–524.

Bisnath, A., Frimmel, H.E., Armstrong, R.A., Board, W.S., 2006. Tectono-thermal evolution of the Maud Belt: new SHRIMP U-Pb zircon data from Gjelsvikfjella, Dronning Maud land, East Antarctica. Precambr. Res. 150, 95–121.

Boehnke, P., Watson, E.B., Trail, D., Harrison, T.M., Schmitt, A.K., 2013. Zircon saturation re-revisited. Chem. Geol. 351, 324–334.

Boger, S.D., 2011. Antarctica – Before and after Gondwana. Gondwana Res. 19, 335–371.

Boger, S.D., Hirdes, W., Ferreira, C.A.M., Jenett, T., Dallwig, R., Fanning, C.M., 2015. The 580–520 Ma Gondwana suture of Madagascar and its continuation into Antarctica and Africa. Gondwana Res. 28, 1048–1060.

Board, W.S., Frimmel, H.E., Armstrong, R.A., 2005. Pan-African tectonism in the western Maud Belt: P-T–t path for high-grade gneisses in the H.U. Sverdrupfjella, East Antarctica. J. Petrol. 46, 671–699.

Bonin, B., 2004. Do coeval mafic and felsic magmas in post-collisional to withinplate regimes necessarily imply two contrasting, mantle and crustal, sources? A review. Lithos 78, 1–24.

Bouvier, A., Vervoort, J.D., Patchett, P.J., 2008. The Lu–Hf and Sm–Nd isotopic composition of CHUR: constraints from unequilibrated chondrites and implications for the bulk composition of terrestrial planets. Earth Planet. Sci. Lett. 273, 48–57.

Clark, C., Collins, A.S., Taylor, R.J., Hand, M., 2020. Isotopic systematics of zircon indicate an African affinity for the rocks of southernmost India. Sci. Rep. 10, 1–12.

Collins, A.S., Pisarevsky, S.A., 2005. Amalgamating eastern Gondwana: The evolution of the Circum-Indian Orogens. Earth-Sci. Rev. 71, 229–270.

Colombo, F., Talarico, F., 2004. Regional metamorphism in the high-grade basement of central Dronning Maud Land, East Antarctica. Geologisches Jahrbuch, Reihe B 96, 7–47.

Couzinié, S., Laurent, O., Moyen, J.F., Zeh, A., Bouilhol, P., Villaros, A., 2016. Post-collisional magmatism: Crustal growth not identified by zircon Hf–O isotopes. Earth Planet. Sci. Lett. 456, 182–195.

Dhuime, B., Hawkesworth, C., Cawood, P., 2011. When continents formed. Science 331, 154–155.

Duchesne, J.C., Martin, H., Baginski, B., Wiszniewska, J., Vander, A.J., 2010. The origin of ferroan-potassic A-type granitoids: The case of the hornblende-biotite granite suite of the Mesoproterozoic Mazury complex, northeastern Poland. Can. Mineral. 48, 947–968.

Eiler, J.M., Crawford, A., Elliott, T.I.M., Farley, K.A., Valley, J.W., Stolper, E.M., 2000. Oxygen isotope geochemistry of oceanic-arc lavas. J. Petrol. 41, 229–256.

Elburg, M., Jacobs, J., Andersen, T., Clark, C., Läufer, A., Ruppel, A., Krohne, N., Damaske, D., 2015. Early Neoproterozoic metagabbro-tonalite-trondhjemite of Sør Rondane (East Antarctica): implications for supercontinent assembly. Precambr. Res. 259, 189–206.

Elburg, M.A., Andersen, T., Jacobs, J., Läufer, A., Ruppel, A., Krohne, N., Damaske, D., 2016. One hundred fifty million years of intrusive activity in the Sør Rondane Mountains (East Antarctica): Implications for Gondwana assembly. J. Geol. 124, 1–26.

Elvevold, S., Engvik, A.K., 2013. Pan-African decompressional P-T path recorded by granulites from central Dronning Maud Land, Antarctica. Mineral. Petrol. 107, 651–664.

Elvevold, S., Engvik, A.K., Abu-Alam, T.S., Myhre, P.I., Corfu, F., 2020. Prolonged high-grade metamorphism of supracrustal gneisses from Mühlig-Hofmannfjella, central Dronning Maud Land (East Antarctica). Precambr. Res. 339, 105618.

Ferré, E.C., Caby, R., Peucat, J.J., Capdevila, R., Monié, P., 1998. Pan-African, post-collisional, ferro-potassic granite and quartz–monzonite plutons of Eastern Nigeria. Lithos 45, 255–279.

Fritz, H., Abdelsalam, M., Ali, K.A., Bingen, B., Collins, A.S., Fowler, A.R., Ghebreab, W., Hauzenberger, C.A., Johnson, P.R., Kusky, T.M., Macey, P., 2013. Orogen styles in the East African Orogen: A review of the Neoproterozoic to Cambrian tectonic evolution. J. Afr. Earth Sc. 86, 65–106.

Frost, B.R., Barnes, C.G., Collins, W.J., Arculus, R.J., Ellis, D.J., Frost, C.D., 2001. A geochemical classification for granitic rocks. J. Petrol. 42, 2033–2048.

Frost, B.R., Frost, C.D., 2008. A geochemical classification for feldspathic igneous rocks. J. Petrol. 49, 1955–1969.

Gill, J.B., 1981. Orogenic Andesites and Plate Tectonics. Springer Verlag, New York.

Golynsky, A.V., Ferraccioli, F., Hong, J.K., Golynsky, D.A., von Frese, R.R.B., Young, D.A., Blankenship, D.D., Holt, J.W., Ivanov, S.V., Kiselev, A.V., Masolov, V.N., 2018. New magnetic anomaly map of the Antarctic. Geophys. Res. Lett. 45, 6437–6449.

Goodenough, K.M., Thomas, R.J., De Waele, B., Key, R.M., Schofield, D.I., Bauer, W., Tucker, R.D., Rafahatelo, J.M., Rabarimanana, M., Ralison, A.V., Randriamananjara, T., 2010. Post-collisional magmatism in the central East African Orogen: The Maevarano Suite of north Madagascar. Lithos 116, 18–34.

Grantham, G.H., Manhica, A.D.S.T., Armstrong, R.A., Kruger, F.J., Loubser, M., 2011. New SHRIMP, Rb/Sr and Sm/Nd isotope and whole rock chemical data from central Mozambique and western Dronning Maud Land, Antarctica: Implications for the nature of the eastern margin of the Kalahari Craton and the amalgamation of Gondwana. J. Afr. Earth Sc. 59, 74–100.

Grantham, G.H., Kramers, J.D., Eglington, B., Burger, E.P., 2019. The Ediacarian-Cambrian uplift history of western Dronning Maud Land: New ^{40}Ar-^{39}Ar and Sr/Nd data from Sverdrupfjella and Kirwanveggen, the source of the Urfjell Group and tectonic evolution of Dronning Maud Land within the Kuunga Orogeny and Gondwana amalgamation. Precambr. Res. 333, 105444.

Gray, D.R., Foster, D.A., Meert, J.G., Goscombe, B.D., Armstrong, R., Trouw, R.A.J., Passchier, C.W., 2008. A Damara orogen perspective on the assembly of southwestern Gondwana. Geological Society, London, Special Publication 294, 257–278.

Griffin, W.L., Pearson, N.J., Belousova, E., Jackson, S.E., van Achterbergh, E., O'Reilly, S.Y., Shee, S.R., 2000. The Hf isotope composition of cratonic mantle: LAM-MC-ICPMS analysis of zircon megacrysts in kimberlites. Geochim. Cosmochim. Acta 64, 133–147.

Groenewald, P.B., Moyes, A.B., Grantham, G.H., Krynauw, J.R., 1995. East Antarctic crustal evolution: Geological constraints and modelling in western Dronning Maud Land, East Antarctica. Precambr. Res. 75, 231–250.

Harris, C., Le Roux, P., Cochrane, R., Martin, L., Duncan, A.R., Marsh, J.S., Le Roex, A.P., Class, C., 2015. The oxygen isotope composition of Karoo and Etendeka picrites: High δ18O mantle or crustal contamination? Contrib. Miner. Petrol. 170, 1–24.

Heinonen, A., Andersen, T., Rämö, O.T., Whitehouse, M., 2015. The source of Proterozoic anorthosite and rapakivi granite magmatism: Evidence from combined in situ Hf–O isotopes of zircon in the Ahvenisto complex, southeastern Finland. J. Geol. Soc. 172, 103–112.

Hoch, M., Rehkämper, M., Tobschall, H.J., 2001. Sr, Nd, Pb and O isotopes of minettes from Schirmacher Oasis, East Antarctica: A case of mantle metasomatism involving subducted continental material. J. Petrol. 42, 1387–1400.

Hoffman, J.P., 1991. Did the breakout of Laurentia turn Gondwanaland inside-out. Science 252501, 1409–1412.

Irvine, T.N.J., Baragar, W.R.A.F., 1971. A guide to the chemical classification of the common volcanic rocks. Canada J. Earth Sci. 8, 523–548.

Jacobs, J., Fanning, C.M., Henjes-Kunst, F., Olesch, M., Paech, H.J., 1998. Continuation of the Mozambique Belt into East Antarctica: Grenville age metamorphism and polyphase Pan-African high grade events in Central Dronning Maud Land. J. Geol. 106, 385–406.

Jacobs, J., Bauer, W., Fanning, C.M., 2003a. Late Neoproterozoic/Early Palaeozoic events in central Dronning Maud Land and significance for the southern extension of the East African Orogen into East Antarctica. Precambr. Res. 126, 27–53.

Jacobs, J., Klemd, R., Fanning, C.M., Bauer, W., Colombo, F., 2003b. Extensional collapse of the late Neoproterozoic-early Palaeozoic East African-Antarctic Orogen in central Dronning Maud Land, East Antarctica. Geological Society, London, Special Publication 206, 271–287.

Jacobs, J., Thomas, R.J., 2004. Himalayan-type indenter-escape tectonics model for the southern part of the late Neoproterozoic–early Paleozoic East African-Antarctic orogen. Geology 32, 721–724.

Jacobs, J., Bingen, B., Thomas, R.J., Bauer, W., Wingate, M.T., Feitio, P., 2008a. Early Palaeozoic orogenic collapse and voluminous late-tectonic magmatism in Dronning Maud Land and Mozambique: insights into the partially delaminated orogenic root of

the East African-Antarctic Orogen? Geological Society, London, Special Publication 308, 69–90.
Jacobs, J., Pisarevsky, S., Thomas, R.J., Becker, T., 2008b. The Kalahari Craton during the assembly and dispersal of Rodinia. Precambr. Res. 160, 142–158.
Jacobs, J., Elburg, M., Läufer, A., Kleinhanns, I.C., Henjes-Kunst, F., Estrada, S., Ruppel, A.S., Damaske, D., Montero, P., Bea, F., 2015. Two distinct Late Mesoproterozoic/Early Neoproterozoic basement provinces in central/eastern Dronning Maud Land, East Antarctica: The missing link, 15–21°E. Precambr. Res. 265, 249–272.
Jacobs, J., Opås, B., Elburg, M.A., Läufer, A., Estrada, S., Ksienzyk, A.K., Damaske, D., Hofmann, M., 2017. Cryptic sub-ice geology revealed by a U-Pb zircon study of glacial till in Dronning Maud Land, East Antarctica. Precambr. Res. 294, 1–14.
Jacobs, J., Mikhalsky, E., Henjes-Kunst, F., Läufer, A., Thomas, R.J., Elburg, M.A., Wang, C.C., Estrada, S., Skublov, G., 2020. Neoproterozoic geodynamic evolution of easternmost Kalahari: Constraints from U-Pb-Hf-O zircon, Sm-Nd isotope and geochemical data from the Schirmacher Oasis East Antarctica. Precambr. Res. 342, 105553.
Jacobsen, S.B., Wasserburg, G.J., 1980. Sm-Nd isotopic evolution of chondrites. Earth Planet. Sci. Lett. 50, 139–155.
Jones, D.L., Bates, M.P., Li, Z.X., Corner, B., Hodgkinson, G., 2003. Palaeomagnetic results from the ca. 1130 Ma Borgmassivet intrusions in the Ahlmannryggen region of Dronning Maud Land, Antarctica, and tectonic implications. Tectonophysics 375, 247–260.
Kamei, A., Horie, K., Owada, M., Yuhara, M., Nakano, N., Osanai, Y., Adachi, T., Hara, Y., Terao, M., Teuchi, S., Shimura, T., 2013. Late Proterozoic juvenile arc metatonalite and adakitic intrusions in the Sør Rondane Mountains, eastern Dronning Maud Land, Antarctica. Precambr. Res. 234, 47–62.
Kitano, I., Osanai, Y., Nakano, N., Adachi, T., 2016. Detrital zircon provenances for metamorphic rocks from southern Sør Rondane Mountains, East Antarctica: A new report of Archean to Mesoproterozoic zircons. J. Mineral. Petrol. Sci. 111, 118–128.
Küster, D., Harms, U., 1998. Post-collisional potassic granitoids from the southern and northwestern parts of the Late Neoproterozoic East African Orogen: A review. Lithos 45, 177–195.
Laurent, O., Rapopo, M., Stevens, G., Moyen, J.-F., Martin, H., Doucelance, R., Bosq, C., 2014. Contrasting petrogenesis of Mg–K and Fe–K granitoids and implications for post-collisional magmatism: case study from the Late-Archean Matok pluton (Pietersburg block, South Africa). Lithos 196–197, 131–149.
Li, Z.L., Tainosho, Y., Kimura, J.I., Shiraishi, K., Owada, M., 2003. Pan-African alkali granitoids from the Sør Rondane Mountains, East Antarctica. Gondwana Res. 6, 595–605.
Li, Z.L., Du, Z.M., Yang, S.F., Chen, H.L., Song, B., Liu, D.Y., 2006. First report of zircon SHRIMP U-Pb dating from the Dufek granite in the Sør Rondane Mountains, East Antarctica. J. Zhejiang Univ.-SCIENCE A 7, 315–319.
Li, Z.X., Bogdanova, S.V., Collins, A.S., Davidson, A., DeWaele, B., Ernst, R.E., Fitzsimons, I.C.W., Fuck, R.A., Gladkochub, D.P., Jacobs, J., Karlstrom, K.E., Lu, S., Natapov, L.M., Pease, V., Pisarevsky, S.A., Thrane, K., Vernikovsky, V., 2008. Assembly, configuration, and break- up history of Rodinia: a synthesis. Precambr. Res. 160, 179–210.
Ludwig, K.R., 2011. A Geochronological Toolkit for Microsoft Excel. Berkeley Geochronol. Centre Special Publications Version 4, 1.
Maniar, P.D., Piccoli, P.M., 1989. Tectonic discrimination of granitoids. Geol. Soc. Am. Bull. 101, 635–643.
Markl, G., Henjes-Kunst, F., 2004. Magmatic conditions of formation and autometasomatism of post-kinematic charnockites in central dronning maud Land, East Antarctica: A model of magmatic evolution. Geologisches Jahrbuch, Reihe B 96, 139–185.
Marschall, H.R., Hawkesworth, C.J., Storey, C.D., Dhuime, B., Leat, P.T., Meyer, H.P., Tamm-Buckle, S., 2010. The Annandagstoppane Granite, East Antarctica: evidence for Archaean intracrustal recycling in the Kaapvaal-Grunehogna Craton from zircon O and Hf isotopes. J. Petrol. 51, 2277–2301.
Marschall, H.R., Hawkesworth, C.J., Leat, P.T., 2013. Mesoproterozoic subduction under the eastern edge of the Kalahari-Grunehogna Craton preceding Rodinia assembly: The Ritscherflya detrital zircon record, Ahlmannryggen (Dronning Maud Land, Antarctica). Precambr. Res. 236, 31–45.
Meert, J.G., Van Der Voo, R., 1997. The assembly of Gondwana 800–550 Ma. J. Geodyn. 23, 223–235.
Meert, J.G., 2003. A synopsis of events related to the assembly of eastern Gondwana. Tectonophysics 362, 1–40.
Merdith, A.S., Collins, A.S., Williams, S.E., Pisarevsky, S., Foden, J.D., Archibald, D.B., Blades, M.L., Alessio, B.L., Armistead, S., Plavsa, D., Clark, C., 2017. A full-plate global reconstruction of the Neoproterozoic. Gondwana Res. 50, 84–134.
Middlemost, E.A., 1994. Naming materials in the magma/igneous rock system. Earth Sci. Rev. 37, 215–224.
Mieth, M., Jacobs, J., Ruppel, A., Damaske, D., Läufer, A., Jokat, W., 2014. New detailed aeromagnetic and geological data of eastern Dronning Maud Land: Implications for refining the tectonic and structural framework of Sør Rondane, East Antarctica. Precambr. Res. 245, 174–185.
Mikhalsky, E.V., Beliatsky, B.V., Savva, E.V., Wetzel, H.U., Fedorov, L.V., Weiser, T.I., Hahne, K., 1997. Reconnaissance geochronologic data on polymetamorphic and igneous rocks of the Humboldt Mountains, central Queen Maud Land, East Antarctica. Antarctic Region: Geological Evol. Process. 45, 53.
Miller, C.F., McDowell, S.M., Mapes, R.W., 2003. Hot and cold granites? Implications of zircon saturation temperatures and preservation of inheritance. Geology 31, 529–532.
Mole, D.R., Barnes, S.J., Taylor, R.J., Kinny, P.D., Fritz, H., 2018. A relic of the Mozambique Ocean in south-east Tanzania. Precambr. Res. 305, 386–426.
Moyes, A.B., Barton, J.M., Groenewald, P.B., 1993a. Late Proterozoic to early Palaeozoic tectonism in Dronning Maud Land, Antarctica: Supercontinental fragmentation and amalgamation. J. Geol. Soc. 150, 833–842.
Moyes, A.B., Groenewald, P.B., Brown, R.W., 1993b. Isotopic constraints on the age and origin of the Brattskarvet intrusive suite, Dronning Maud Land, Antarctica. Chem. Geol. 106, 453–466.
Moyes, 1993. The age and origin of the Jutulsessen granitic gneiss, Gjelsvikfjella, Dronning Maud Land. South Afr. J. Antarctic Res. 23, 25–32.
Moyes, A.B., Groenewald, P.B., 1996. Isotopic constraints on Pan-African metamorphism in Dronning Maud Land, Antarctica. Chem. Geol. 129, 247–256.
Osanai, Y., Nogi, Y., Baba, S., Nakano, N., Adachi, T., Hokada, T., Toyoshima, T., Owada, M., Satish-Kumar, M., Kamei, A., Kitano, I., 2013. Geologic evolution of the Sør Rondane Mountains, East Antarctica: Collision tectonics proposed based on metamorphic processes and magnetic anomalies. Precambr. Res. 234, 8–29.
Owada, M., Baba, S., Osanai, Y., Kagami, H., 2008. Geochemistry of post-kinematic mafic dykes from central to eastern Dronning Maud Land, East Antarctica: Evidence for a Pan-African suture in Dronning Maud Land. Geological Society, London, Special Publication 308, 235–252.
Owada, M., Kamei, A., Horie, K., Shimura, T., Yuhara, M., Tsukada, K., Osanai, Y., Baba, S., 2013. Magmatic history and evolution of continental lithosphere of the Sør Rondane Mountains, eastern Dronning Maud Land, East Antarctica. Precambr. Res. 234, 63–84.
Palmeri, R., Godard, G., Di Vincenzo, G., Sandroni, S., Talarico, F.M., 2018. High-pressure granulite-facies metamorphism in central Dronning Maud Land (East Antarctica): implications for Gondwana assembly. Lithos 300, 361–377.
Pant, N.C., Kundu, A., D'Souza, M.J., Saikia, A., 2013. Petrology of the Neoproterozoic granulites from Central Dronning Maud Land, East Antarctica – Implications for southward extension of East African Orogen (EAO). Precambr. Res. 227, 389–408.
Paulsson, O., Austrheim, H., 2003. A geochronological and geochemical study of rocks from Gjelsvikfjella, Dronning Maud Land, Antarctica – Implications for Mesoproterozoic correlations and assembly of Gondwana. Precambr. Res. 125, 113–138.
Pauly, J., Marschall, H.R., Meyer, H.P., Chatterjee, N., Monteleone, B., 2016. Prolonged Ediacaran-Cambrian metamorphic history and short-lived high-pressure granulite-facies metamorphism in the HU Sverdrupfjella, Dronning Maud Land (East Antarctica): evidence for continental collision during Gondwana assembly. J. Petrol. 57, 185–228.
Peck, W.H., Clechenko, C.C., Hamilton, M.A., Valley, J.W., 2010. Oxygen isotopes in the Grenville and Nain AMCG suites: Regional aspects of the crustal component in massif anorthosites. Can. Mineral. 48, 763–786.
Roland, N.W., 2004. Pan-African granite-charnockite magmatism in central Dronning Maud Land, East Antarctica: Petrography, geochemistry and plate tectonic implications. Geologisches Jahrbuch, Reihe B 96, 187–232.
Ruppel, A., Jacobs, J., Eagles, G., Läufer, A., Jokat, W., 2018. New geophysical data from a key region in East Antarctica: Estimates for the spatial extent of the Tonian Oceanic Arc Super Terrane (TOAST). Gondwana Res. 59, 97–107.
Ruppel A., Jacobs, J., Läufer, A., Ratschbacher, L., Pfänder, J.A., Sonntag, B-L., Krasniqi, K., Elburg, M., Krohne, N., Damaske, D., Lisker, F., Protracted late Neoproterozic – early Palaeozoic deformation and cooling history of Sør Rondane, East Antarctica, from 40Ar/39Ar and U–Pb geochronology. Geological Magazine, in press, https://doi.org/10.1017/S0016756820000746.
Scherer, E., Münker, C., Mezger, K., 2001. Calibration of the lutetium-hafnium clock. Science 293, 683–687.
Shiraishi, K., Dunkley, D.J., Hokada, T., Fanning, C.M., Kagami, H., Hamamoto, T., 2008. Geochronological constraints on the Late Proterozoic to Cambrian crustal evolution of eastern Dronning Maud Land, East Antarctica: A synthesis of SHRIMP U-Pb age and Nd model age data. Geological Society, London, Special Publication 308, 21–67.
Söderlund, U., Patchett, P.J., Vervoort, J.D., Isachsen, C.E., 2004. The ^{176}Lu decay constant determined by Lu–Hf and U-Pb isotope systematics of Precambrian mafic intrusions. Earth Planet. Sci. Lett. 219, 311–324.
Stern, R.J., 1994. Arc assembly and continental collision in the Neoproterozoic East African Orogen: Implications for consolidation of Gondwanaland. Annu. Rev. Earth Planet. Sci. 22, 319–351.
Stern, R.J., 2002. Crustal evolution in the East African Orogen: A neodymium isotopic perspective. J. Afr. Earth Sc. 34, 109–117.
Suliman, A.E., 2011. Geochronology and tectonic setting of voluminous granitoids and related rocks and associated extensional structures in Dronning Maud Land (East Antarctica). Master thesis. University of Bergen, Bergen Norway.
Sylvester, P.J., 1989. Post-collisional alkaline granites. J. Geol. 97, 261–280.
Tagne-Kamga, G., 2003. Petrogenesis of the Neoproterozoic Ngondo Plutonic complex (Cameroon, west central Africa): A case of late-collisional ferro-potassic magmatism. J. Afr. Earth Sci. 36, 149–171.
Tsunogae, T., Dunkley, D.J., Horie, K., Endo, T., Miyamoto, T., Kato, M., 2014. Petrology and SHRIMP zircon geochronology of granulites from Vesleknausen, Lützow-Holm Complex, East Antarctica: Neoarchean magmatism and Neoproterozoic high-grade metamorphism. Geosci. Front. 5, 167–182.
Tsunogae, T., Yang, Q.Y., Santosh, M., 2015. Early Neoproterozoic arc magmatism in the Lützow-Holm Complex, East Antarctica: petrology, geochemistry, zircon U-Pb geochronology and Lu–Hf isotopes and tectonic implications. Precambr. Res. 266, 467–489.
Ueda, K., Jacobs, J., Thomas, R.J., Kosler, J., Horstwood, M.S., Wartho, J.A., Jourdan, F., Emmel, B., Matola, R., 2012. Postcollisional high-grade metamorphism, orogenic collapse, and differential cooling of the East African Orogen of northeast Mozambique. J. Geol. 120, 507–530.
Valley, J.W., Kinny, P.D., Schulze, D.J., Spicuzza, M.J., 1998. Zircon megacrysts from kimberlite: Oxygen isotope variability among mantle melts. Contrib. Miner. Petrol. 133, 1–11.
Veevers, J.J., 2007. Pan-Gondwanaland post-collisional extension marked by 650–500

Ma alkaline rocks and carbonatites and related detrital zircons: A review. Earth Sci. Rev. 83, 1–47.
Viola, G., Henderson, I.H.C., Bingen, B., Thomas, R.J., Smethurst, M.D., De Azavedo, S., 2008. Growth and collapse of a deeply eroded orogen: Insights from structural, geophysical, and geochronological constraints on the Pan-African evolution of NE Mozambique. Tectonics 27, TC5009.
Von Huene, R., Scholl, D.W., 1991. Observations at convergent margins concerning sediment subduction, subduction erosion, and the growth of continental crust. Rev. Geophys. 29, 279–316.
Wang, C.C., Jacobs, J., Elburg, M.A., Läufer, A., Thomas, R.J., Elvevold, S., 2020. Grenville-age continental arc magmatism and crustal evolution in central Dronning Maud Land (East Antarctica): Zircon geochronological and Hf-O isotopic evidence. Gondwana Res. 82, 108–127.
Wareham, C.D., Pankhurst, R.J., Thomas, R.J., Storey, B.C., Grantham, G.H., Jacobs, J., Eglington, B.M., 1998. Pb, Nd, and Sr isotope mapping of Grenville-age crustal provinces in Rodinia. J. Geol. 106, 647–660.
Whalen, J.B., Currie, K.L., Chappell, B.W., 1987. A-type granites: Geochemical characteristics, discrimination and petrogenesis. Contrib. Miner. Petrol. 95, 407–419.
Whitney, D.L., Evans, B.W., 2010. Abbreviations for names of rock-forming minerals. Am. Mineral. 95, 185–187.
Yeshanew, F.G., Pease, V., Abdelsalam, M.G., Whitehouse, M.J., 2017. Zircon U-Pb ages, $\delta^{18}O$ and whole-rock Nd isotopic compositions of the Dire Dawa Precambrian basement, eastern Ethiopia: Implications for the assembly of Gondwana. J. Geol. Soc. 174, 142–156.

Graphic design: Communication Division, UiB / Print: Skipnes Kommunikasjon AS

uib.no

ISBN: 9788230860427 (print)
9788230860861 (PDF)